UILU-ENG-78-2025

CIVIL ENGINEERING STUDIES
STRUCTURAL RESEARCH SERIES NO. 457

ANALYSIS OF REINFORCED CONCRETE FRAME-WALL STRUCTURES FOR STRONG MOTION EARTHQUAKES

By
KATSUHIKO EMORI
and
WILLIAM C. SCHNOBRICH

A Report on a Research Project
Sponsored by
THE NATIONAL SCIENCE FOUNDATION
Research Grant ENV 74-22962

UNIVERSITY OF ILLINOIS
at URBANA-CHAMPAIGN
URBANA, ILLINOIS
DECEMBER 1978

BIBLIOGRAPHIC DATA SHEET	1. Report No. UILU-ENG 78-2025	2.	3. Recipient's Accession No. PB291995
4. Title and Subtitle: Analysis of Reinforced Concrete Frame-Wall Structures for Strong Motion Earthquakes			5. Report Date: December, 1978 6.
7. Author(s): Katsuhiko Emori and William C. Schnobrich			8. Performing Organization Rept. No. SRS 457
9. Performing Organization Name and Address: University of Illinois at Urbana-Champaign, Urbana, Illinois 61801			10. Project/Task/Work Unit No. 11. Contract/Grant No. ENV 7422962
12. Sponsoring Organization Name and Address: National Science Foundation, Washington, D.C. 20013			13. Type of Report & Period Covered 14.

15. Supplementary Notes

16. Abstracts

The nonlinear response and failure mechanism of reinforced concrete frame-wall systems are investigated through mechanical models for both dynamic loads and static loads.

Three mechanical models: a concentrated spring model, a multiple spring model, and a layered model, which take into account inelastic behavior of a reinforced concrete cantilever beam, are presented. Ten story reinforced concrete frame-wall structures are investigated. The stiffness characteristics of each constituent member are determined through one of the mechanical models by its inelastic properties or by a hysteresis model. The procedure of a load increment analysis is used for a static loading case. The equations of motion are solved by a step by step integration procedure for a dynamic loading case. Computed results are compared with experimental results.

17. Key Words and Document Analysis. 17a. Descriptors

Nonlinear dynamic analysis, Earthquake engineering, Hysteresis loops, Equations of motion, Reinforced Concrete, Rigid Frames

17b. Identifiers/Open-Ended Terms

17c. COSATI Field/Group

18. Availability Statement: Release Unlimited	19. Security Class (This Report) UNCLASSIFIED	21. No. of Pages 206
	20. Security Class (This Page) UNCLASSIFIED	22. Price A10-A01

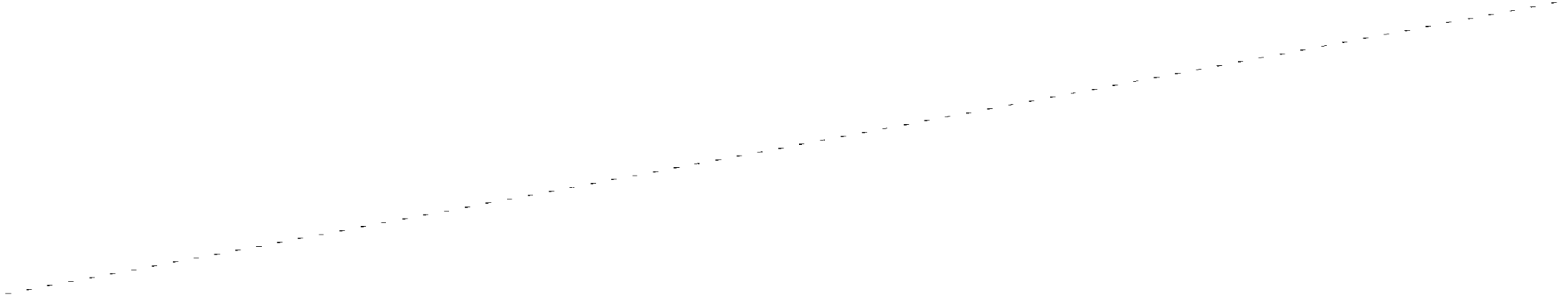

ACKNOWLEDGMENT

The writers would like to express their special gratitude to Professor Mete A. Sozen of the University of Illinois for his invaluable comments and help.

Deep appreciation is also due Dr. T. Takayanagi and Mr. D. A. Abrams, former and current research assistants at the University of Illinois for providing the authors with information from their analytical and experimental studies.

The numerical calculations were performed on the CYBER 175 System of the Computing Services Office of the University of Illinois. The work was supported by U. S. National Science Foundation Grant No. ENV 7422962. The support is gratefully acknowledged.

TABLE OF CONTENTS

CHAPTER		Page
1	INTRODUCTION	1
	1.1 Introductory Remarks	1
	1.2 Review of Previous Research	2
	1.3 Object and Scope	5
2	STRUCTURAL SYSTEM AND MECHANICAL MODELS	8
	2.1 Structural System	8
	2.2 An Analytical Model for Frame-Wall Structures	8
	2.3 Mechanical Models for Structural Components	9
3	FORCE-DEFORMATION RELATIONSHIPS FOR CANTILEVER BEAM MODELS	13
	3.1 Introductory Remarks	13
	3.2 Concentrated Spring Model and Multiple Spring Model	14
	3.3 Layered Model	22
	3.4 Additional Considerations for Each Model	26
4	ANALYTICAL PROCEDURE	31
	4.1 Introductory Remarks	31
	4.2 Basic Assumptions	32
	4.3 Analytical Models	32
	4.4 Structural Stiffness Matrix	42
	4.5 Static Analysis	45
	4.6 Dynamic Analysis	46
5	HYSTERESIS RULES AND NUMERICAL EXAMPLES	54
	5.1 Introductory Remarks	54
	5.2 Degrading Trilinear Hysteresis Rule	54
	5.3 Comparison of Computed Hysteresis Loop with Experimental Results	58
	5.4 Effect of Axial Load	59
6.	COMPUTED RESULTS	61
	6.1 Introductory Remarks	61
	6.2 Static Analysis	62
	6.3 Dynamic Analysis	66
	6.4 Effect of Changing Axial Load at the Base of the Exterior Columns	73

Page

7 SUMMARY AND CONCLUSIONS ---------- 78

7.1 Summary ---------- 78
7.2 Conclusions ---------- 79
7.3 Recommendations for Further Studies ---------- 80

LIST OF REFERENCES ---------- 82

APPENDIX

A DETAILS OF STIFFNESS MATRICES ----------190

B COMPUTER PROGRAM FOR NONLINEAR RESPONSE ANALYSIS
OF REINFORCED CONCRETE FRAME-WALL STRUCTURES ----------199

C NOTATION ----------203

LIST OF TABLES

Table		Page
2.1	REINFORCING SCHEDULES FOR THE STRUCTURES OF FW-1 AND FW-2	86
5.1	ASSUMED CHARACTERISTICS OF A CANTILEVER BEAM SPECIMEN FOR HYSTERESIS LOOP STUDY (FIG. 5.3)	87
5.2	ASSUMED CHARACTERISTICS OF A BEAM-COLUMN JOINT SPECIMEN FOR LOAD-DISPLACEMENT RELATIONSHIP STUDY (FIG. 5.5)	88
5.3	ASSUMED CHARACTERISTICS OF A CANTILEVER WALL SPECIMEN FOR LOAD-DISPLACEMENT RELATIONSHIP STUDY	90
6.1	SUMMARY OF ASSUMED ANALYTICAL CONDITIONS FOR NUMERICAL EXAMPLES	93
6.2	ASSUMED MATERIAL PROPERTIES FOR FRAME-WALL STRUCTURES	95
6.3	CONFIGURATIONS OF THE STRUCTURES FW-1 AND FW-2	96
6.4	STIFFNESS PROPERTIES OF CONSTITUENT MEMBERS OF THE STRUCTURES FW-1 AND FW-2	97
6.5	MODE SHAPES AND FREQUENCIES OF THE STRUCTURES FW-1 AND FW-2	101
6.6	MAXIMUM RESPONSES OF FRAME-WALL STRUCTURES	103
6.7	PROPERTIES OF LAYERED MODEL USED FOR THE STRUCTURE FW-2	109

LIST OF FIGURES

Figure		Page
2.1	REINFORCED CONCRETE FRAME-WALL TEST STRUCTURE	110
2.2	REINFORCEMENT DETAILS OF STRUCTURAL COMPONENTS	111
2.3	DEFORMATION MODES OF FRAME-WALL STRUCTURES	113
2.4	CURVATURE DISTRIBUTION ALONG A CANTILEVER BEAM	114
2.5	MECHANICAL MODELS USED IN INVESTIGATION	115
3.1	IDEALIZED STRESS-STRAIN RELATIONSHIPS FOR CONCRETE AND STEEL FOR THE CONCENTRATED SPRING AND MULTIPLE SPRING MODELS	116
3.2	DISTRIBUTIONS OF STRESS AND STRAIN OVER A CROSS SECTION	117
3.3	IDEALIZED MOMENT-CURVATURE RELATIONSHIP USED FOR THE CONCENTRATED SPRING MODEL	118
3.4	IDEALIZED MOMENT-ROTATION RELATIONSHIP USED FOR THE CONCENTRATED SPRING MODEL	118
3.5	IDEALIZED MOMENT-CURVATURE RELATIONSHIP FOR EACH SPRING OF THE MULTIPLE SPRING MODEL	119
3.6	IDEALIZED STRESS-STRAIN RELATIONSHIPS USED WITH THE LAYERED MODEL	120
3.7	DISTRIBUTIONS OF STRESS AND STRAIN OVER A CROSS SECTION OF THE LAYERED MODEL	121
3.8	INSTANTANEOUS MOMENT-CURVATURE RELATIONSHIPS FOR THE LAYERED SECTION OF THE LAYERED MODEL	122
3.9	BOND SLIP MECHANISM	123
3.10	COMPARISON OF COMPUTED BOND SLIP WITH EXPERIMENTAL DATA	124
3.11	TYPICAL LOAD-DISPLACEMENT CURVES FOR INELASTIC ANALYSIS	125
4.1	DEFORMED SHAPES OF A CONCENTRATED SPRING MODEL AND AN EQUIVALENT SIMPLE BEAM MODEL	126
4.2	TYPICAL MEMBERS IN GLOBAL COORDINATES SYSTEM	127
4.3	MULTIPLE SPRING MODEL	128
4.4	APPLICATION OF THE LAYERED MODEL TO 1ST STORY EXTERIOR COLUMNS	129

Figure		Page
4.5	GLOBAL COORDINATES: DISPLACEMENTS OF THE i-th AND i-1-th STORIES OF THE STRUCTURE	130
5.1	HYSTERESIS MODEL 1 (TAKEDA MODEL)	131
5.2	HYSTERESIS MODEL 2	132
5.3	COMPUTED MOMENT-ROTATION RELATIONSHIPS OF A CANTILEVER BEAM USING HYSTERESIS MODEL 2	133
5.4	FORCE-DISPLACEMENT RELATIONSHIPS OF A CANTILEVER BEAM	134
5.5	FORCE-DISPLACEMENT RELATIONSHIPS OF BEAM-COLUMN JOINTS	137
5.6	ASSUMED AXIAL LOADS USED IN COLUMN MEMBERS WHEN ESTABLISHING HYSTERESIS RULES	138
6.1	BASE SHEAR-TOP DISPLACEMENT RELATIONSHIPS OF THE STRUCTURES UNDER MONOTONICALLY INCREASING EXTERNAL LOAD	139
6.2	MOMENT DISTRIBUTION PATTERNS AT THE COLLAPSE LOAD (FW-2)	140
6.3	REDISTRIBUTION OF BASE SHEAR BETWEEN WALL AND COLUMNS OF STRUCTURE FW-1 UNDER MONOTONICALLY INCREASING LOAD	142
6.4	REDISTRIBUTION OF BASE SHEAR BETWEEN WALL AND COLUMNS OF STRUCTURE FW-2 UNDER MONOTONICALLY INCREASING LOAD	143
6.5	COLLAPSE MECHANISM FOR STRUCTURE FW-1 UNDER STATIC TRIANGULAR LATERAL LOADING	144
6.6	COLLAPSE MECHANISM FOR STRUCTURE FW-2 UNDER STATIC TRIANGULAR LATERAL LOADING	145
6.7	BASE ACCELERATION WAVEFORMS AS OBSERVED IN TESTS AND COMPARISON WITH THOSE USED FOR RESPONSE ANALYSIS	146
6.8	MODE SHAPES OF STRUCTURE FW-1	147
6.9	MODE SHAPES OF STRUCTURE FW-2	148
6.10	RESPONSE WAVEFORMS FOR STRUCTURE FW-1, RUN-1	149
6.11	RESPONSE WAVEFORMS FOR STRUCTURE FW-1, RUN-3	154
6.12	RESPONSE WAVEFORMS FOR STRUCTURE FW-2, RUN-1	156
6.13	RESPONSE WAVEFORMS FOR STRUCTURE FW-2, RUN-2	162

Figure Page

6.14 RESPONSE WAVEFORMS FOR STRUCTURE FW-2, RUN-2 USING HYSTERESIS MODELS 1 AND 2 ---------- 167

6.15 MOMENT-ROTATION RELATIONSHIPS OF THE FLEXURAL SPRING AT THE 5TH LEVEL LEFT EXTERIOR BEAM ---------- 169

6.16 MOMENT-ROTATION RELATIONSHIPS OF THE FLEXURAL SPRING USING HYSTERESIS MODELS 1 AND 2 AT THE 5TH LEVEL LEFT EXTERIOR BEAM ---------- 171

6.17 MOMENT-ROTATION RELATIONSHIPS OF A FLEXURAL SPRING AT THE BASE OF THE LEFT COLUMN ---------- 172

6.18 MOMENT-CURVATURE RELATIONSHIPS OF THE FLEXURAL SPRING AT THE BASE ELEMENT OF THE WALL ---------- 174

6.19 BASE OVERTURNING MOMENT VS. TOP-STORY DISPLACEMENT RELATIONSHIPS OF THE STRUCTURES ---------- 175

6.20 RESPONSE WAVEFORMS FOR AXIAL FORCE AT THE BASE OF THE LEFT COLUMN ---------- 177

6.21 COMPUTED STRUCTURAL YIELD PATTERNS (STRUCTURE FW-1, RUN-1) ----- 179

6.22 OBSERVED CRACK PATTERNS IN STRUCTURE FW-2, RUN-2 ---------- 183

6.23 BASE SHEAR VS. TOP-STORY DISPLACEMENT RELATIONSHIPS OF STRUCTURE FW-2 USING CONCENTRATED SPRING MODEL AND LAYERED MODEL ---------- 184

6.24 MOMENT-CURVATURE RELATIONSHIPS OF THE LAYERED SECTION AT THE BASE OF THE COLUMNS ---------- 185

6.25 LOADING PATH AT THE BASE OF THE EXTERIOR COLUMNS ---------- 186

6.26 BASE SHEAR VS. TOP-STORY DISPLACEMENT RELATIONSHIPS OF STRUCTURE FW-2 USING CONCENTRATED SPRING MODEL AND LAYERED MODEL FOR SINGLE CYCLE OF LOADING ---------- 187

6.27 MOMENT-CURVATURE RELATIONSHIPS OF THE LAYERED SECTION AT THE BASE OF THE COLUMNS FOR SINGLE CYCLE OF LOADING --------- 188

6.28 BEHAVIOR OF THE LAYERED SECTION AT THE BASE OF THE COLUMNS FOR SINGLE CYCLE OF LOADING ---------- 189

B.1 FLOW DIAGRAM OF COMPUTER PROGRAM FOR NONLINEAR RESPONSE ANALYSIS OF REINFORCED CONCRETE FRAME-WALL SYSTEMS ---------- 200

CHAPTER 1

INTRODUCTION

1.1 Introductory Remarks

When designing reinforced concrete structures, one important aspect to be decided is the insurance of an adequate stiffness to resist lateral forces caused by such events as earthquakes, winds, or blast loadings. The forces associated with these events can produce high stresses and induce vibration, etc. Reinforced concrete shear walls, which have a high inplane stiffness, are often used to economically provide the necessary resistance to such horizontal forces. Columns also resist horizontal forces, but their contribution, depending on their stiffness, is normally much smaller than that which would be provided by walls. Also nonlinear characteristics of column type members relative to those of wall types tend to further degrade their contribution.

Recent studies of damage caused by strong earthquakes indicate that the significant inelastic deformation to reinforced concrete structural components has to be taken into consideration when designing a reinforced concrete structure. For a proper structure, it is desirable that such inelastic action should take place first in the beams in order to prevent collapse of the structure. The inelastic behavior of reinforced concrete structures in an earthquake environment has been the objective of extensive investigation over the past decade[3,13,30], but there are aspects that are still not fully

understood. In analyzing reinforced concrete structures in the inelastic range, many phenomena arise which have to be taken into consideration, such as cracking, crushing of concrete, yielding, strain hardening of reinforcing steel, and bond slip, to name a few. These characteristics make the analysis complicated.

In this study, the analysis of idealized reinforced concrete plane frame-wall structures will be treated on the basis of certain assumptions such as the substitute frame structure, fixed inflection point locations in members, concentrated mass at each floor level, etc. These assumptions are made to simplify the analysis while not markedly affecting its accuracy. The study presented is limited to plane structures of laboratory test specimens.

1.2 Review of Previous Research

When analyzing a reinforced concrete structural system deformed beyond its elastic range, it is obviously very important to choose an idealized element model suitable to represent the inelastic behavior of the reinforced concrete member components. Many different approaches which take into account material and geometric nonlinearities have been reported in the literature. Several of the more successful models are discribed below.

Giberson[15] proposed a concentrated spring model for column and beam elements. His model consists of a linearly elastic member with a spring attached at each end. These springs take account of any nonlinear characteristics that occur within the members. This model for nonlinear analysis was applied to reinforced concrete multi-story

structures. This model is versatile since the spring at each end can have different curvilinear or bilinear hysteretic characteristics. Otani's[34] combined two cantilever beam model with nonlinear springs, belongs to the class of concentrated spring models. Concentrated spring models are effective for the antisymmetric moment distributions with fixed inflection points. Otani's model also demonstrates good agreement between analytical and test results.

Benuska[10] presented a two-component model with the members divided into two imaginary parallel elements. There is an elastic element to represent the linear phase and an elasto-plastic element to represent a yielding characteristic. This model was applied to a nonlinear analysis of a 20-story open frame structure.

Takizawa[45] assumed the distribution of flexural rigidity along a member element to be that of a parabolic function. This distribution is used in the determination of the member flexibility matrix. The inflection point is not fixed in this model. This model has been applied to the nonlinear analysis of a 3-story reinforced concrete frame structure.

Takayanagi[42] has presented a multiple spring beam model for analyzing wall members. This model divides the member into several subelements along its longitudinal axis. Each subelement has a uniform flexural rigidity which changes based on the hysteresis loop appropriate to each subelement. This model is effective for a distribution of moment whose inflection point can lie outside of the element.

A somewhat different approach to analyzing inelastic behavior of reinforced concrete members is the layering concept. This can be a very

effective tool. In this approach the cross section is divided into a number of layers. Each layer has material behavior characteristics which depend on the stress-strain curve of its material in its current state of deformation. The stress resultants for a cross section are then obtained by integrating or summing the layer contributions.

Park et al[24,36,37] investigated the stress-strain behavior of concrete under cyclic loading by this method and showed that the layer method can cope with the complex stress distributions due to cyclic loading. Aktan[5] and Karlsson[23] have studied, with such a procedure, the moment-curvature relationships of reinforced concrete columns subjected to load reversals. They have obtained satisfactory agreement between calculated and measured relationships. As an iteration scheme is used in the above mentioned layering method when calculating moment-curvature relationships of a member, this method has the disadvantage of requiring a large amount of computation time.

Hand[17] also applied a layering method to reinforced concrete plates and shells and suggested it would be a valuable tool for determining structural behavior in the intermediate region between the elastic and limit states.

The finite element method in the form of plane stress analysis has been applied to inelastic analyses of reinforced concrete structures[4,38,41]. Such two-dimensional analyses have been a satisfactory tool for inelastic analyses of some isolated wall components. However, the computational effort involved can be substantial so that the use of plane stress elements for wall panels of multistory structures would be practical only in very unusual

circumstances.

Yuzugullu[51] investigated the behavior of a shear wall frame system for monotonic, increasing load. Darwin[12] analyzed reinforced concrete shear panels under cyclic loading. They both obtained good correlation with experimental results. However, such a finite element analysis requires quite a large number of elements if the local stress distribution is important. Therefore this approach is costly, maybe too much so, for use on large scale reinforced concrete structural systems such as those being investigated in this study. The finite element analysis still has a very promising future but on more limited problems.

1.3 Object and Scope

The objective of this study is to investigate analytically the nonlinear seismic behavior of reinforced concrete frame-wall structures and with that analysis to trace the development of a failure mechanism for these structures.

First of all, three types of mechanical models : a concentrated spring beam model, a multiple spring beam model, and a layered beam model, which can take into account both the linear and the nonlinear behavior of such reinforced concrete cantilever beams are presented. To describe the nonlinear behavior of the reinforced concrete cantilever beams, a numerical procedure is presented for computing moments, curvatures and deflections. The selection of the analytical models, which is to be used to analyze the structure, depends upon the physical loading condition that exists.

In order to establish the force-deflection relations of the

structure, a beam-column component and a single shear wall of the structure are investigated. In this respect, for each constituent member: beams, columns, and the wall, a degrading trilinear hysteresis loop is adopted. But this hysteresis loop does not include any pinching effect which might occur in the structural components being tested. A second new hysteresis rule is therefore presented. This hysteresis rule was developed primarily for application to the beam members in this structure.

Finally, the frame-wall structure is modelled as a system which has a concentrated spring model for the beam and column elements and a multiple spring beam model for the wall elements. A layered model is applied to the first story exterior columns of the structure only when the effect of changing axial force is investigated. Furthermore in this phase, a substitute-frame system has been chosen as the frame subsystem model because the structure being modelled has a geometrical symmetry aspect while the frame is subjected to antisymmetrical loading. This substitute frame system described in Chapter 2 reduces significantly the computation time.

The instantaneous nonlinear characteristics of the structure being investigated are estimated and the failure processes of each constituent member under a strong earthquake motion are traced by numerically integrating the equations of motion in a step by step method.

A computer program is developed to carry out the numerical calculations of the analysis. The computed results are discussed and compared with the available test results.

This study is a continuation of the work which was initiated by Otani[34] for the reinforced concrete frame structures, and followed by Takayanagi[42] for the coupled shear wall structures.

CHAPTER 2

STRUCTURAL SYSTEM AND MECHANICAL MODELS

2.1 Structural System

The test structure(Fig.2.1) to be analyzed consists of two-ten story, three bay frames surrounding a slender shear wall. The shear wall is placed at the center of the structure in the plan. It was the intention that the wall not be subjected to gravity load. Thus the wall is joined to the frames with connections that transmit only horizontal motion. It is assumed that each floor diaphragm is displaced in its horizontal plane as a rigid body. All elements of each frame undergo the same horizontal motion at each story level. A total floor weight including story weight of the structure is considered lumped at each floor level. The structure is considered to be fixed at the base. A "weak beam-strong column" design was made for lateral load resistance for the framed structure. The details of the structural components are shown in Fig.2.2. The reinforcing schedule for the structures is tabulated in Table 2.1.

2.2 An Analytical Model for Frame-Wall Structures

A simplified approximate procedure is adopted for the analysis of this frame-wall structure. The frame structure is a symmetrical rectangular frame which is being investigated for the case of antisymmetrical loadings. Therefore the contraflexure point of the beam, which is approximately at the center of the beam length, is

assumed to be a roller joint. The symmetrical placement of a shear wall in the structure allows the structure to respond still in a planar manner. Therefore the entire system is idealized as a plane structure composed of two systems as shown in Fig.2.3. One of these systems is an isolated shear wall. The second system is a substitute frame structure which models the two parallel-rigid frames as a frame substructure. The substitute frame structure system consists of two exterior frames and one interior frame. In defining the stiffness characteristics, each exterior frame and the interior frame of the substitute frame structure represent two exterior parts and four interior parts of the actual frame structure, respectively.

The shear wall is treated as a vertical cantilever beam which is subjected only to horizontal loading. With the diaphragms assumed rigid in their own planes, all the frames and the shear wall sway by the same amount at each floor level. Each of the structural components: frames, walls etc., is attached by links to the adjacent components at each floor level.

2.3 Mechanical Models for Structural Components

When a reinforced concrete cantilever beam is loaded into the inelastic range, its end rotation and tip deflection can be computed from the distribution of curvatures along the beam by means of the moment-area method. The cantilever beam containing flexural cracks has its moment diagram and the distribution of curvatures along this member as shown in Fig.2.4[24,46]. For computational purposes, this actual distribution of curvatures is simplified into three types of shapes of

distribution of curvatures as shown in Fig.2.5. The corresponding mechanical models are also shown in the figure. These three types of mechanical models, therefore, can take into account nonlinear behavior of a reinforced concrete cantilever beam.

The concentrated spring model is the one which Otani[32] developed based on inelastic action of a cantilever beam. This model consists of a flexible elastic line element and a nonlinear rotational spring at the end of the cantilever beam as shown in Fig.2.5(a). The curvature distribution along the beam, such as that which might occur at ultimate moment, as well as an idealized curvature distribution used with this model are shown in Fig.2.5(a). The nonlinear rotational spring can take care of the hatched portion of the idealized curvature assumed to exist along the beam. This model is quite suitable for the beam members of this structure being investigated since the moment distribution of the fixed-hinged beam member is exactly the same as that of the cantilever beam. This model is also applicable to the column members since the point of contraflexure can be assumed practically at the center of the column length during its response even though the contraflexure point of the upper columns shifts downwards while that of the lower columns of the frame structure shifts upwards from the center of the column story height.

The multiple spring model is the one studied by Takayanagi[42]. This is a line element model and is composed of a number of segments, each of which handles independently both the linear and the nonlinear action as springs. This model as well as the assumed curvature distribution along the beam are shown in Fig.2.5(b). This multiple

spring model is applicable to wall members which are exposed to a more general moment distribution than is the case for the beams and columns of the frame. The centroid of each segment is used as the control point for the determination of the nonlinear properties of that segment. All interior or segment nodal points are condensed out of the element stiffness matrix before it is used in the analysis of the complete structure. Therefore only story level displacements remain in the structural stiffness matrix as used. The line element model is considered to be more reasonable than a plane stress finite element model especially for a slender shear wall.

The layered model shown in Fig.2.5(c) is a modification or alteration of the concentrated spring model. Instead of the nonlinear rotational spring being in the form of a concentrated spring, a layered cross section of length, Lp, is assigned at the end of the cantilever beam and connected to an elastic line element. Lp is an inelastic length as shown in Fig.2.5(c). The inelastic flexural action of the cantilever beam is calculated explicitly by the layered method which is derived from an overall moment-curvature relation reflecting the various stages of material behavior of concrete and steel in the layered section [17,49]. This model has the advantage that the layered concept can take care of the change of flexural rigidity due to both a change in the moment and a change in the axial force. This model is suitable to the case where the exterior lower level columns are subjected to a significant change in the axial force during cyclic loadings.

These mechanical models are applied to the reinforced concrete frame-wall structures. It should be kept in mind that this analytical

work on nonlinear response of reinforced concrete frame-wall structures is based on the flexural yielding capacity of the reinforced concrete cantilever beam members.

CHAPTER 3

FORCE-DEFORMATION RELATIONSHIPS FOR CANTILEVER BEAM MODELS

3.1 Introductory Remarks

The process of inelastic structural analysis includes the choice of mechanical models, the establishment of force-deformation relationships of mechanical models, and then the application of the mechanical models to the structure. This chapter describes the force-deformation relationships of these mechanical models.

Idealized stress-strain relationships for concrete and steel are constructed in order that the three mechanical models can have a common basic shape for each concrete and steel. Then these idealized stress-strain relationships for concrete and steel are used in order to construct inelastic force-deformation relationships for each mechanical model. Small aggregate concrete and plain annealed wire steel are used in this study. The mechanical properties for this concrete and steel are described in detail in Ref.[2].

For the concentrated spring model, the force-deformation relationship is obtained from the idealized quarter-cycle moment-curvature relationship of the type shown in Fig.3.3. Then this force-deformation relationship is used as the primary curve in the development of the hysteresis rule. The inelastic deformation in later stages can be obtained from direct application of the hysteresis rules.

For a multiple spring model, a modified EI (flexural rigidity) approach is used in each spring. An idealized quarter cycle

moment-curvature relationship is used as the primary curve for the hysteresis rule. The modified EI to be used at each subsequent load increment is obtained in turn from the developed hysteresis rules.

For a layered model, the modified EI approach is again used at the layered section. An overall moment-curvature relationship is assumed. It includes the changing axial load effect as well as the cyclic loading effect which reflect directly the various stages of material behavior.

3.2 Concentrated Spring Model and Multiple Spring Model

3.2.1 Stress-Strain Relationship for Concrete

The stress-strain relationship for concrete is constructed from a parabola combined with a straight line as proposed by Hognestad[21]. The various branches of these defining relationships are:

$$
\begin{aligned}
f_c &= 0 && \varepsilon_c \le \varepsilon_t \\
f_c &= f'_c\left[2\left(\frac{\varepsilon_c}{\varepsilon_o}\right) - \left(\frac{\varepsilon_c}{\varepsilon_o}\right)^2\right] && \varepsilon_t \le \varepsilon_c \le \varepsilon_o \\
f_c &= f'_c[1 - Z(\varepsilon_c - \varepsilon_o)] && \varepsilon_o < \varepsilon_c
\end{aligned}
\qquad (3.1)
$$

and

$$\varepsilon_t = \varepsilon_o[1 - (1 - f_t/f'_c)^{1/2}]$$

where

f_c = stress of concrete

f'_c = compressive uniaxial strength of concrete

f_t = tensile strength of concrete, $0.5\sqrt{f'_c}$, (Mpa)

ε_c = strain of concrete

ε_o = strain at which f'_c is attained

ε_t = strain at which f_t is attained

Z = constant which defines the desending slope of the stress-strain curve, assumed to be 100 [34]

The proposed curve is shown in Fig.3.1(a).

3.2.2 Stress-Strain Relationship for Steel

A piecewise linear stress-strain relationship is adopted for the reinforcing steel.

$$\begin{aligned} f_s &= E_s\varepsilon_s && \varepsilon_s \leq \varepsilon_y \\ f_s &= f_y && \varepsilon_y \leq \varepsilon_s \leq \varepsilon_{sh} \\ f_s &= f_y + E_{sh}(\varepsilon_s - \varepsilon_{sh}) && \varepsilon_{sh} \leq \varepsilon_s \leq \varepsilon_u \\ f_s &= f_u && \varepsilon_u \leq \varepsilon_s \end{aligned} \qquad (3.2)$$

where

f_s = stress of steel

f_y = yield stress of steel

f_u = ultimate stress of steel

ε_s = strain of steel

ε_y = strain at which f_y is attained

ε_{sh} = strain at which strain hardening commences

ε_u = strain at which f_u is attained

E_s = modulus of elasticity of steel

E_{sh} = modulus to define stiffness in strain hardening range

The yield stress, f_y, and ultimate stress, f_u, are obtained by averaging the results from a number of coupon samples taken from the wire[2]. The proposed stress-strain curve for the steel is that described in Ref.[42] and shown in Fig.3.1(b).

3.2.3 Moment-Curvature Relationship of a Section

Based on the idealized stress-strain properties of concrete and reinforcing steel just described, a moment-curvature relationship can be constructed. The relationship is based on the geometry of the section and on the assumption of linear variation of strain through the depth as shown in Fig.3.2. The strains and curvature are related through the well known equations as follows:

$$\begin{aligned} \phi &= \varepsilon_c/c \\ &= \varepsilon_s'/(c - d') \\ &= \varepsilon_s/(d - c) \end{aligned} \tag{3.3}$$

where

ϕ = curvature

ε_c = concrete strain at the extreme compressive fiber

ε_s', ε_s = strain in the compressive, tensile steel, respectively

d', d = distance from the extreme compressive fiber to the center of compressive, tensile steel, respectively

c = depth of the neutral axis

From equilibrium conditions for the section, we have the following expressions.

$$N = \int_{-c'}^{c} f_c b\,dx + A_s' f_s' - A_s f_s \tag{3.4}$$

$$C_c = \int_{-c'}^{c} f_c b x\,dx \tag{3.5}$$

$$M = C_c(C_p - \gamma C) + A_s' f_s'(C_p - d') + A_s f_s(d - C_p)$$

where

f_s', f_s = stress of the compressive,tensile steel, respectively

b = width of the cross section

A_s', A_s = area of the compressive,tensile steel, respectively

N = axial load acting on the section

C_c = concrete compression force

C_p, γC = distance from the extreme compression fiber to centroid of axial load, concrete compression force, respectively

c' = distance from the neutral axis to the point of the maximum tensile stress of the concrete

M = bending moment about centroid of axial load

x = distance from the neutral axis

Using Eqs.(3.1) and (3.2), the stresses f_c, f_s, and f_s' can be determined for given strains ε_c,ε_s, and ε_s', respectively. The location of the neutral axis denoted by, c, can be obtained with given ε_c and N from Eqs.(3.3) and (3.4) using an iteration method. The moment M and curvature ϕ can be calculated from Eqs.(3.3) and (3.5)

Flexural cracking at a cross section is assumed to occur when the stress at the extreme tension fiber of the section reaches the tensile strength of the concrete. The flexural cracking moment M_c is computed using simple bending theory as follows:

$$M_c = \frac{I_g}{y_t}\left(f_t + \frac{N}{A}\right) \tag{3.6}$$

where

N = axial force on a section , compression positive

A = area of a cross section

I_g = moment of inertia of a gross section

y_t = distance from neutral axis of the section to extreme fiber in tension

Flexural yielding is defined as the point at which the tensile reinforcement reaches its yield strain. If the tensile reinforcement is arranged in several layers,yielding will occur gradually starting at the outer layer of the tension reinforcement and proceeding to the layer closest to the neutral axis of the section. Because the hysteresis relationship requires a definite value for the yield moment, yield moment M_y is defined as the moment corresponding to the development of a yield strain at the centroid of the reinforcement working in tension.

3.2.4 Idealized Moment Curvature Relationships for a Concentrated Spring Model

Using the three values of moment: cracking, yielding, and ultimate, the moment-curvature relationship is idealized by three straight lines as follows[34],(Fig.3.3):

$$\begin{aligned} \phi &= \frac{M}{EI} && M \leq M_c \\ \phi &= \frac{\phi_y}{M_y} \cdot M && M_c \leq M \leq M_y \\ \phi &= \phi_y \left[1 + \frac{1}{EI_y}\left(\frac{M}{M_y} - 1\right)\right], && M_y \leq M \end{aligned} \tag{3.7}$$

and

$$EI_y = \frac{M_u - M_y}{\phi_u - \phi_y} \cdot \frac{\phi_y}{y}$$

where

EI = initial flexural rigidity

M = bending moment

M_c, M_y, M_u = cracking, yielding, ultimate moment, respectively

ϕ = curvature

ϕ_c, ϕ_y, ϕ_u = curvature at cracking, yielding, ultimate, respectively

3.2.5 Rotation due to Inelastic Flexural Action Based on Idealized Moment-Curvature Relationships for a Concentrated Spring Model

Displacement at the free end of a cantilever beam is calculated from the curvature distribution along member length. With the load effectively concentrated at the free end, the bending moment can be assumed to be distributed linearly. The free end displacement D(M) can be expressed as follows[34]:

$$
\begin{aligned}
D(M) &= \frac{L^2 M}{3EI} && M \leq M_c \\
D(M) &= \frac{L^2}{3}\left[1 - \alpha^3\right) \phi_y \frac{M}{M_y} + \alpha^2 \phi_c] && M_c \leq M < M_y \\
D(M_y) &= \frac{L^2}{3}\left[\left(1 - \alpha_y^3\right) \phi_y + \alpha_y^2 \phi_c\right] && M = M_y \\
D(M) &= \frac{L^2}{6}[(2+\beta)(1-\beta)\{\beta + \frac{1}{EI_y}(1-\beta)\} \\
&\quad + \beta(1+\beta) - 2\alpha^3] \frac{\phi_y}{\beta} + \frac{L^2}{3}\alpha^2\phi_c && M_y < M \\
D(M_u) &= \frac{L^2}{6}[(2+\beta_u)(1-\beta_u)\{\beta_u + \frac{1}{EI_y}(1-\beta_u)\} \\
&\quad + \beta_u(1+\beta_u) - 2\alpha_u^3] \frac{\phi_y}{\beta_u} + \frac{L^2}{3}\alpha_u^2\phi_c && M = M_u
\end{aligned}
\qquad (3.8)
$$

where

L = length of the cantilever beam

$$\alpha = \frac{M_c}{M}$$

$$\alpha_y = \frac{M_c}{M_y}$$

$$\alpha_u = \frac{M_c}{M_u} \qquad (3.9)$$

$$\beta = \frac{M_y}{M}$$

$$\beta_u = \frac{M_y}{M_u}$$

Average rotation of the cantilever beam is

$$\theta = \frac{D(M)}{L} \qquad (3.10)$$

Slopes in the three stages of the idealized trilinear moment-displacement relationship are expressed as follows:

$$SD_1 = \frac{M_c}{D(M_c)} \qquad 0 \leq M \leq M_c$$

$$SD_2 = \frac{M_y - M_c}{D(M_y) - D(M_c)} \qquad M_c \leq M \leq M_y \qquad (3.11)$$

$$SD_3 = \frac{M_u - M_y}{D(M_u) - D(M_y)} \qquad M_y < M$$

where

instantaneous stiffness of the concentrated spring model of unit length (Fig.3.4)

The incremental rotation of the cantilever beam can be expressed by the instantaneous rotational stiffness

$$\Delta\theta = \frac{L}{SD_i} \cdot \Delta M \tag{3.12}$$

where

$\Delta\theta$ = incremental rotation of a cantilever beam

ΔM = increment of external moment at the fixed end of a cantilever beam

L = length of a cantilever beam

The idealized moment-rotation relationships obtained are shown in Fig.3.4 and are used as the primary curve for the hysteresis rule.

3.2.6 Force-Displacement Relationship for a Multiple Spring Model

This model is composed of a series of segments. Each segment can be subjected to a different level of nonlinearity. The instantaneous flexural stiffness of each segment is derived from the stress resultants existing at the centroid of each segment. Forces vary but properties are constant.

Flexural rigidities (slope) can be defined for each segment[42].

$$\phi = \frac{M}{EI_i}$$

$$EI_1 = \frac{M_c}{\phi_c} \qquad M \leq M_c$$

$$EI_2 = \frac{M_y - M_c}{\phi_y - \phi_c} \qquad M_c \leq M \leq M_y \tag{3.13}$$

$$EI_3 = \frac{M_u - M_y}{\phi_u - \phi_y} \qquad M_y \leq M$$

where

EI_1, EI_2, EI_3 = flexural rigidity before cracking, from cracking to yielding, and after yielding, respectively

The idealized moment-curvature relationship built from three straight lines is shown in Fig.3.5 for the multiple spring model.

3.3 Layered Model

The cross section in the inelastic zone (fixed end portion) of a cantilever beam is divided into layers of equal thickness. For each layer, the concrete inside the stirrup is considered as confined while that outside is taken as unconfined. The length, Lp, of the inelastic zone is arbitrary, say Lp= o.5*(depth of beam). The depth to each layer of steel and the area of steel at that level are also specified.

3.3.1 Stress-Strain Relationship for Concrete

The tensile stress of concrete is now neglected. This is because this simplification is needed for the iteration procedure in this model and this modification does not affect the overall stiffness characteristics of this model. With a monotonically increasing load capacity, the stress-strain curve for the compressed concrete follows the previously proposed shape in Eq.3.1(a) for both confined and unconfined concrete. Thus the three analytical cantilever beam models can have a common basic shape. The unconfined concrete, however, provides no contribution at strains greater than $\varepsilon_{cu} = 0.004$.

Because of the nature of the problem the analysis is required to

predict unloading from an inelastic state and subsequent reloading back into that inelastic range. The shape of the model curve for the above case is assumed to be based on the values of ε_e , strain on the envelope curve (Fig.3.6(a)) at which unloading starts, and ε_n, the plastic strain remaining after all load has been released [12,39]. Values for these strains are related by the following equation which was developed experimentally by Karsan and Jirsa [22].

$$\frac{\varepsilon_n}{\varepsilon_{cu}} = 0.145\left(\frac{\varepsilon_e}{\varepsilon_{cu}}\right)^2 + 0.13\left(\frac{\varepsilon_e}{\varepsilon_{cu}}\right) \qquad (3.14)$$

With ε_e established, a linear equation is used for unloading from the ε_e point on the envelope curve passing toward the ε_n point. Subsequent reloading to ε_e follows back on the same line. This equation is

$$f_c = \frac{f_{en}}{\varepsilon_e - \varepsilon_n}(\varepsilon_c - \varepsilon_n) \qquad (3.15)$$

where

f_{en} = concrete stress at which the concrete strain is ε_e

This rule is shown in Fig.3.6(a).

3.3.2 Stress-Strain Relationship for Steel

For simplicity a bilinear stress-strain relationship and hardening rule have been assumed. The Bauschinger effect is not consiered. Such bilinear behavior with strain hardening representation for the general loading case is reasonable when detailed test data are

not available. The strain hardening stiffness E_y is the slope of the line between the yield point and the point at which the ultimate strength is attained on the primary stress-strain curve. This rule is shown in Fig.3.6(b).

3.3.3 Moment Curvature Relationships for a Layered Section

Assuming a linear strain distribution through the depth of the layered cross section, values of curvature and the position of neutral axis define the strains at the center lines of each concrete and steel layer (Fig.3.7). These two quantities are determined by an iterative process using the Newton-Raphson method to satisfy the equilibrium conditions[16].

$$N = C_c + C_s' - T$$
$$M = T(d - C_p) + C_s'(C_p - d') + C_c(C_p - \gamma C) \tag{3.16}$$

where

C_c = concrete compression force

C_s' = steel compression force

T = steel tension force

C_p = distance from the extreme compression fiber to centroid of axial load

γC = distance from the extreme compression fiber to centroid of concrete compressive force

As the external axial force can be changing within each load increment, the moment M_i becomes a function of the axial force N_i as

well as the curvature ϕ_i as follows:

$$M_i = m(\phi_i, N_i)$$

The instantaneous flexural rigidity EI_i of the layered section can be expressed as (Fig.3.8)

$$EI_i = \frac{\Delta M_i}{\Delta \phi_i} \tag{3.17}$$

where

$$\Delta M_i = M_i - M_{i-1} = m(\phi_i, N_i) - m(\phi_{i-1}, N_{i-1})$$
$$\Delta \phi_i = \phi_i - \phi_{i-1} \tag{3.18}$$

The effect of changing axial force on the instantaneous flexural rigidity EI_i is included in the ΔM_i term. The secondary bending moment created from both axial force and member deflection is not taken into account. The nonlinearity of axial rigidity EA_i is also neglected.

3.3.4 Moment-Rotation Relationship for a Layered Model

Displacement D(M) at the free end of a cantilever beam is calculated from the curvature distribution along its length.

$$D(M) = \int_0^L (\phi(x))\ x\ dx \tag{3.19}$$

where

$$\phi(x) = \frac{M(x)}{EI} \qquad 0 \leq x \leq L - L_p$$
$$\phi(x) = \frac{M(x)}{EI_i} \qquad L - L_p \leq x \leq L \tag{3.20}$$

L_p is the length of the inelastic zone at the fixed end of the cantilever beam. $\phi(x)$ is the curvature as a function of the distance x from the free end of the cantilever beam. The moment M(x) along the beam is linear because applied loads are assumed to be concentrated at the free end of the cantilever beam. The end rotation is then computed as,

$$\theta = \frac{D(M)}{L} \tag{3.21}$$

The incremental rotation $\Delta\theta$ of the layered model can be expressed by the instantaneous rotational flexibility f_L similar to Eq.3.12.

$$\Delta\theta = f_L \cdot \Delta M \tag{3.22}$$

This is used to obtain the member stiffness later.

3.4 Additional Considerations for Each Model

3.4.1 Shear Deformation

Because of the uncertainty regarding inelastic shear deformations of reinforced concrete members, such shear deformations are calculated from an elastic shear deformation multiplied by a reduction factor $\alpha = 0.5$. This factor takes account of the effect of nonlinear deformation by simply reducing the uncracked shear stiffness[1]. The shear rigidity is then assumed to remain constant throughout the whole process. Shear modulus is computed from the equation, $E_c/(2(1+\mu))$ with $\mu = 1/6$, where is Poisson's ratio.

3.4.2 Rotation due to Bond Slippage of Embedded Steel

Rotation due to the slip of the tensile reinforcement along its embedded length must be taken into account. In order to formulate a flexibility due to bond slippage, the following assumptions are made (Fig.3.9).

1. Bond stress is constant along the embedded length of the reinforcement.
2. The reinforcement embedment length is sufficient to provide the maximum tensile stress.
3. The steel stress decreases linearly with distance in from the beam or column face.

Then the development length L and the elongations ΔL of the reinforcement are obtained as [26,34],

$$L = \frac{A_s f_s}{\pi D u}$$

$$\Delta L = \frac{L f_s}{2E_s} = \frac{1}{8}\frac{D}{E_s u} f_s^2 \qquad f_s \le f_y \qquad (3.23)$$

$$\Delta L = \frac{f_y^2 L}{2 f_s E_s} + \left(1 - \frac{f_y}{f_s}\right)\left(\frac{f_y}{E_s} + \frac{f_s - f_y}{2E_y}\right) L, \qquad f_y \le f_s$$

$$= \frac{D}{4u}\left[\frac{f_y}{E_s}\left(f_s - \frac{f_y}{2}\right) + \frac{(f_s - f_y)^2}{2E_y}\right]$$

where

A_s = cross sectional area of the tensile reinforcement

f_s = stress of the reinforcement at the face of column or beam

D = diameter of a reinforcing bar

u = average bond stress, $0.5\sqrt{f'_c}$ (f'_c :Mpa) for plain wire

gages[14]

E_s = Young's modulus of the reinforcement

E_y = inelastic modulus of the reinforcement after yielding

f_y = yield stress of the reinforcement

Because the stress in reinforcement after yielding does not differ markedly from the value at yield, the equation for the elongation can be written in a single simple form.

$$\Delta L = \frac{1}{8} \cdot \frac{D}{E_s u} f_s^2 = \frac{D E_s}{8u} \varepsilon_s^2 \tag{3.24}$$

The elongation due to bond slippage is a function of steel stress or steel strain as seen in Eq.3.24. In Figure 3.10 Eq.3.24 is compared with experimental results obtained by Wight[49] where average bond stress, u, is assumed to be $1.17\sqrt{f'_c}$ (Mpa) for No.6 deformed bars, E =200000 (Mpa), f'_c =34.5 (Mpa), and area of a bar A_s=284 (MM**2).

Assuming that the rotation axis due to slippage of the tensile reinforcement is at the level of compressive reinforcement and that the stress in the tensile reinforcement is proportional to the moment, the moment-rotation relationship can be expressed as follows:

$$\frac{f_s}{M} = \frac{f_y}{M_y} \tag{3.25}$$

Then

$$R(M) = \frac{L}{d - d'}$$

$$= \frac{1}{8} \frac{D}{E_s u} \left(\frac{f_y}{M_y}\right)^2 \cdot \frac{M^2}{d - d'} \tag{3.26}$$

where

f_s, f_y = acting stress and yielding stress of the tensile reinforcement at the section where bond slippage is considered, respectively

M, M_y = acting moment and yielding moment at the section where bond slippage is considered, respectively

$R(M)$ = rotation due to the slip

d, d' = depth of the tensile reinforcement and the compressive reinforcement, respectively

The rotation $R(M)$ due to bar slip is seen to be a quadratic function of the acting moment M.

The idealized moment-rotation relationship can be obtained from Eq.3.26 in any form, the original curve itself, a bilinear modification curve, or a trilinear modification curve.

For the trilinear modification curve, the flexibilities in the three stages of the idealized trilinear moment-rotation relationships are defined as,

$$f_b(M) = \frac{R(M_c)}{M_c} \qquad M \leq M_c$$

$$f_b(M) = \frac{R(M_y) - R(M_c)}{M_y - M_c} \qquad M_c \leq M \leq M_y \qquad (3.27)$$

$$f_b(M) = \frac{R(M_u) - R(M_y)}{M_u - M_y} \qquad M_y \leq M$$

where

$R(M_c)$, $R(M_y)$, $R(M_u)$ = rotation at which the cracking, the yielding and the ultimate moment is developed, respectively

$f_b(M)$ = flexibility due to the bond slippage of tensile reinforcement

The flexibility $f_b(M)$ is then used as a part of the instantaneous moment-rotation relationship of a rotational spring as

$$\Delta\theta = f_b(M) \cdot \Delta M \tag{3.28}$$

3.4.3 Assumptions for Inelastic Analysis

Generally, when inelastic analysis is made, stiffness characteristics of constituent members of a structure are examined. Figures 3.11(a) and (b) show the typical load-displacement curves which appear in inelastic analyses of members. In both cases, there is no difficulty in proceeding with a load increment analysis technique for inelastic analysis where the instantaneous stiffnesses of the members are always positive regardless of loading or unloading conditions. Figures 3.11(c) and (d) also show types of load-displacement curves which one could encounter in inelastic analysis. These are a decreasing slope phenomenon and snap-through phenomenon in stiffness characteristics. The instantaneous stiffness becomes negative due to severe loss in the load carrying capacity of constituent members and would lead to erroneous results in the behavior of the structure. Special consideration is given to modify these phenomenon. The negative instantaneous stiffness is replaced by a small positve one for that purpose.

CHAPTER 4

ANALYTICAL PROCEDURE

4.1 Introductory Remarks

This chapter describes a method of inelastic analysis for reinforced concrete frame-wall structures subjected to static loads and to dynamic base excitations.

Three mechanical methods are developed and introduced to study the behavior of the constituent members of the structure. The members are studied as a cantilever beam action. The three mechanical models : a concentrated spring model, a multiple spring model, and a layered model, are each applied to the constituent members of the frame-wall structure taking into account their specific stiffness characteristics during inelastic behavior. The concentrated spring model is intended for primary application to the frame elements : column members and beam members. The multiple spring model is to be applied to the wall elements. The layered model would be applied only to the exterior column members of the first story of the structure to incorporate the effect of variation of column axial force.

The structural stiffnesses are constructed from each constituent member stiffness. These stiffnesses are then used to construct the nonlinear response history and failure mechanisms of frame-wall systems subjected to static and to dynamic loadings. Trilinear degrading hysteresis rules such as a Takeda model or a modified Takeda model are chosen to represent the behavior characteristics of each constituent

member. The equations of motion analytically describing the system are then solved by a step-by-step procedure of the Newmark β method [31].

4.2 Basic Assumptions

In this section the basic assumptions used in the analysis of the frame-wall structures are presented. These basic assumptions are,

1. Torsional effects are neglected. Thus the analysis is limited to planar frame-wall systems.
2. A substitute frame system is adopted to simplify and economize in modeling a frame substructure.
3. Every member in this substitute structure is represented as a massless line member considered to act along its centroidal axis.
4. Geometric nonlinearities are assumed insignificant and are thus neglected in the analysis.
5. The structure is assumed to be fixed to a rigid foundation at the base.
6. The mass of the structure is assumed to be concentrated at the floor levels.
7. Axial deformations of beam members, internal column members and wall members are ignored.
8. The shear deformations that occur in a joint core are neglected.
9. In the incremental force method the stiffness of each constituent member of the structure is assumed constant within the force interval. Residuals or overshoots are applied to the next increment.

4.3 Analytical Models

4.3.1 The Concentrated Spring Model

The concentrated spring model is a cantilever beam with the

addition of a rotational spring inserted at the fixed end as described previously. Instead of analyzing this model, however, a simple beam which is constructed with a flexible portion over the interior of the member and two concentrated rotational springs placed at each end is analyzed. This replacement is possible because a simple beam can be formed from a combination of two concentrated spring cantilever models. The resulting simple beam model can be used extensively. In order for this simple beam to be applied to frame-wall structures, rigid portions have to be added at both ends as well. The configurations of a simple beam as well as a concentrated spring model are shown in Fig.4.1. The rotational springs take account of the beam end rotations due to bond slippage of the embeded reinforcing steel at the point A' in the Fig.4.1 as well as the normal inelastic flexural action over the beam length. The flexibility matrix for the simple beam which is combined with two concentrated spring models, can be calculated by simply adding the flexibilities of the rotational springs to those due to flexural and shearing actions in the flexible element. The instantaneous flexibility matrix relating the incremental external moments to the incremental rotations are expressed as:

$$\begin{Bmatrix} \Delta\theta'_A \\ \Delta\theta'_B \end{Bmatrix} = [F] \begin{Bmatrix} \Delta M'_A \\ \Delta M'_B \end{Bmatrix} \tag{4.1}$$

where

$\Delta\theta'_A$, $\Delta\theta'_B$ = incremental rotations at the ends A', B' of a flexural line element, respectively

$[F]$ = the instantaneous flexibility matrix

$\Delta M'_A$, $\Delta M'_B$ = incremental moments applied at the ends A',B' of a flexural line element, respectively

The instantaneous flexibility matrix appearing in Eq.(4.1) can be expressed in the following form[18,42].

$$[F] = \begin{bmatrix} f_1 + f(M'_A), & f_2 \\ f_2 , & f_1 + f(M'_B) \end{bmatrix} \tag{4.2}$$

where

$$f_1 = \frac{\ell}{3EI} + \frac{1}{\alpha kAG\ell}$$

$$f_2 = -\frac{\ell}{6EI} + \frac{1}{\alpha kAG\ell} \tag{4.3}$$

kAG = shear rigidity, k is a shape factor for shear deformation

α = 0.5, reduction fator (Sec.3.4.1)

ℓ = length of the flexible element

EI = elastic flexural rigidity of the cross section of the flexible element

$f(M'_A), f(M'_B)$ = the rotational flexibilities resulting from bond slip, inelastic action over the beam length, ℓ, at the ends A' and B', respectively

An instantaneous stiffness matrix can be obtained by inverting the instantaneous flexibility matrix of Eq.(4.2), Thus

$$[K] = [F]^{-1} = \begin{bmatrix} K_{11} & K_{12} \\ K_{21} & K_{22} \end{bmatrix} \tag{4.4}$$

If axial deformation is also taken into account,

$$\begin{Bmatrix} \Delta M'_A \\ \Delta M'_B \\ \Delta N' \end{Bmatrix} = \begin{bmatrix} K_{11} & K_{12} & 0 \\ K_{21} & K_{22} & 0 \\ 0 & 0 & K_{33} \end{bmatrix} \begin{Bmatrix} \Delta\theta'_A \\ \Delta\theta'_B \\ \Delta\varepsilon' \end{Bmatrix} \tag{4.5}$$

Incremental forces ΔM_A, ΔM_B, ΔN and the incremental deformations $\Delta\theta_A$, $\Delta\theta_B$, $\Delta\varepsilon$, at the ends of the rigid portions are related to the incremental forces $\Delta M_A'$, $\Delta M_B'$, $\Delta N'$ and the inremental deformations $\Delta\theta_A'$, $\Delta\theta_B'$, $\Delta\varepsilon'$ at the ends of the flexible element through a transformation matrix T as,

$$\begin{Bmatrix} \Delta M_A \\ \Delta M_B \\ \Delta N \end{Bmatrix} = T^T \begin{Bmatrix} \Delta M_A' \\ \Delta M_B' \\ \Delta N' \end{Bmatrix} \tag{4.6}$$

$$\begin{Bmatrix} \Delta\theta_A' \\ \Delta\theta_B' \\ \Delta\varepsilon' \end{Bmatrix} = T \begin{Bmatrix} \Delta\theta_A \\ \Delta\theta_B \\ \Delta\varepsilon \end{Bmatrix}$$

where

T^T = the transpose of the matrix T

$$T = T^T = \begin{bmatrix} 1+\lambda & \lambda & 0 \\ \lambda & 1+\lambda & 0 \\ 0 & 0 & 1 \end{bmatrix} \tag{4.7}$$

λ is the ratio of the length of a rigid portion to that of a flexible element. The instantaneous moment-rotation relationship of the simple beam with rigid portions at both ends can be expressed by combining Eqs.(4.4),(4.5) and (4.6),

$$\begin{Bmatrix} \Delta M_A \\ \Delta M_B \\ \Delta N \end{Bmatrix} = T^T \cdot K \cdot T \begin{Bmatrix} \Delta\theta_A \\ \Delta\theta_B \\ \Delta\varepsilon \end{Bmatrix} \tag{4.8}$$

The forces and the displacements of the simple beam model in local coordinates are related to the corresponding quantities in global coordinates by the transformation matrix C,

$$\underset{\text{(Local)}}{\begin{Bmatrix} \Delta\theta_A \\ \Delta\theta_B \\ \Delta\varepsilon \end{Bmatrix}} = C \underset{\text{(Global)}}{\begin{Bmatrix} \Delta u_A \\ \Delta v_A \\ \Delta w_A \\ \Delta u_B \\ \Delta v_B \\ \Delta w_B \end{Bmatrix}}, \underset{\text{(Global)}}{\begin{Bmatrix} \Delta P_A \\ \Delta V_A \\ \Delta M_A \\ \Delta P_B \\ \Delta V_B \\ \Delta M_B \end{Bmatrix}} = C^T \underset{\text{(Local)}}{\begin{Bmatrix} \Delta M_A \\ \Delta M_B \\ \Delta N \end{Bmatrix}} \tag{4.9}$$

where

setting $L = (1 + 2\lambda)\,\ell$

$$C = \left[\begin{array}{ccc:ccc} 0 & 1/L & 1 & 0 & -1/L & 0 \\ 0 & 1/L & 0 & 0 & -1/L & 1 \\ -1 & 0 & 0 & 1 & 0 & 0 \end{array}\right], \text{ for horizontal members}$$

$$C = \left|\begin{array}{ccc:ccc} -1/L & 0 & 1 & 1/L & 0 & 0 \\ -1/L & 0 & 0 & 1/L & 0 & 1 \\ 0 & -1 & 0 & 0 & 1 & 0 \end{array}\right|, \text{ for vertical members} \tag{4.10}$$

where

$(\Delta u_A, \Delta v_A, \Delta w_A, \Delta u_B, \Delta v_B, \Delta w_B)$ and $(\Delta P_A, \Delta V_A, \Delta M_A, \Delta P_B, \Delta V_B, \Delta M_B)$ are the displacements and forces expressed in global coordinates as shown in Fig.4.2. By combining Eqs.(4.8),(4.9) and (4.10), the instantaneous force-displacement relationship of a member is expressed in global coordinates by:

$$\begin{Bmatrix} \Delta P_A \\ \Delta V_A \\ \Delta M_A \\ \Delta P_B \\ \Delta V_B \\ \Delta M_B \end{Bmatrix} = K_m \begin{Bmatrix} \Delta u_A \\ \Delta v_A \\ \Delta w_A \\ \Delta u_B \\ \Delta v_B \\ \Delta w_B \end{Bmatrix} \tag{4.11}$$

where

$$K_m = C^T \cdot T^T \cdot K \cdot T \cdot C \tag{4.12}$$

K_m is a member stiffness matrix in global coordinates. The K_m is described in Appendix A. This member stiffness matrix is used to construct the structural stiffness matrix of the structure in the usual manner.

4.3.2 The Multiple Spring Model

The multiple spring model is considered to be built up from several subelements along its length. The subelements need not

necessarily be equal in length. The model looks like a single chain of subelements joined together in series to form the member. Each subelement may have different values of inelastic properties depending on the level or magnitude of forces to which it is subjected and on properties of the member which the subelement models. These properties however are assumed to be constant over the length of each subelement. Any moment-curvature relation can be assigned to each short segment. Figure 4.3(b) shows the assumed flexural rigidities as well as the moment distribution along the length of a cantilever beam.

The method of analysis with this model uses the flexibility matrix of each subelement in conjunction with transfer matrices. Figure 4.3(a) shows this model in which the joints are numbered sequentially from left to right. Because, as used, the multiple spring model has loads applied only at story levels, that model is discussed here as a cantilever beam subjected to forces applied only at the tip and not subjected to any external forces applied within the span length, L, of the cantilever beam.

The flexibility matrix of the cantilever beam can be derived as follows: According to Fig.4.3(a),

$$[F_{ab}] = \sum_{j} E_{jb}^{T} \cdot F_{ij} \cdot E_{jb} = \begin{bmatrix} F_1 & 0 & 0 \\ 0 & F_2 & F_3 \\ 0 & F_3 & F_4 \end{bmatrix} \qquad (4.13)$$

where

$[F_{ab}]$ = flexibility matrix of the cantilever beam ab.

F_{ij} = flexibility matrix of the element ij.

E_{jb} = transformation matrix of element jb.

and

$$F_{ij} = \begin{bmatrix} \frac{\ell_i}{EA_i} & 0 & 0 \\ 0 & \frac{\ell_i^3}{3EI_i} + \frac{\ell_i}{\alpha k GA_i} & -\frac{\ell_i^2}{2EI_i} \\ 0 & -\frac{\ell_i^2}{2EI_i} & \frac{\ell_i}{EI_i} \end{bmatrix} \tag{4.14}$$

and

$$E_{jb} = \begin{bmatrix} 1 & 0 & 0 \\ 0 & 1 & 0 \\ 0 & -\sum_{k=j}^{b} \ell_k & 1 \end{bmatrix} \tag{4.15}$$

$$L = \sum_{k=1}^{b} \ell_k \tag{4.16}$$

where

L = length of the cantilever beam

ℓ_k = length of the k-th subelement of the cantilever beam

EA_i, kGA_i, EI_i = instantaneous equivalent axial, shear, and flexural rigidity of the i-th subelement of the cantilever beam

As the external forces $\{P_b\}$ are applied only at the tip of the cantilever, the displacements are obtained by the following equation

$$\{U_b\} = [F_{ab}] \cdot \{P_b\}$$

$$\{U_b\} = \begin{Bmatrix} u_b \\ v_b \\ \theta_b \end{Bmatrix}, \quad \{P_b\} = \begin{Bmatrix} P_b \\ V_b \\ M_b \end{Bmatrix} \tag{4.17}$$

where

$\{U_b\}$ = displacement vector at the tip of the cantilever beam

$\{P_b\}$ = applied force vector at the tip of the cantilever beam

In order to achieve an inelastic analysis of the cantilever beam, incremental member end forces are applied in order to be able to trace the behavior of material nonlinearity. Thus Eq.(4.17) is written in incrmental form

$$\{\Delta U_b\} = [F_{ab}] \cdot \{\Delta P_b\} \tag{4.18}$$

where

$\{\Delta U_b\}$ = incremental displacement vector at the tip of the cantilever beam

$\{\Delta P_b\}$ = incremental applied force vector at the tip of the cantilever beam

$[F_{ab}]$ = incremental flexibility matrix of the cantilever beam

In the application of this model to general structures, a member stiffness matrix has to be obtained. This stiffness matrix $[K_{bb}]$ of the cantilever beam is obtained by inverting the flexibility matrix$[F_{ab}]$.

$$[K_{bb}] = [F_{ab}]^{-1} = \begin{bmatrix} K_1 & 0 & 0 \\ 0 & K_2 & K_3 \\ 0 & K_3 & K_4 \end{bmatrix} \tag{4.19}$$

The stiffness matrix of an individual member can be obtained as follows:

$$[K_{ab}] = \begin{bmatrix} E_{ab}K_{bb}E_{ab}^T & -E_{ab}K_{bb} \\ -K_{bb}E_{ab}^T & K_{bb} \end{bmatrix} \tag{4.20}$$

The member end forces are related to the member end displacements through the member stiffness matrix $[K_{ab}]$ in the incremental form as follows:

$$\begin{Bmatrix} \Delta P_a \\ \Delta V_a \\ \Delta M_a \\ \Delta P_b \\ \Delta V_b \\ \Delta M_b \end{Bmatrix} = [K_{ab}] \begin{Bmatrix} \Delta u_a \\ \Delta v_a \\ \Delta \theta_a \\ \Delta u_b \\ \Delta v_b \\ \Delta \theta_b \end{Bmatrix} \tag{4.21}$$

In the global coordinates, using transformation matrix c,

$$\begin{Bmatrix} \Delta P_A \\ \Delta V_A \\ \Delta M_A \\ \Delta P_B \\ \Delta V_B \\ \Delta M_B \end{Bmatrix} = K_m \begin{Bmatrix} \Delta u_A \\ \Delta v_A \\ \Delta \theta_A \\ \Delta u_B \\ \Delta v_B \\ \Delta \theta_B \end{Bmatrix} \tag{4.22}$$

$$K_m = C^T K_{ab} C \tag{4.23}$$

where

for vertical members

$$C = \left[\begin{array}{ccc:ccc} 0 & 1 & 0 & & & \\ -1 & 0 & 0 & & 0 & \\ 0 & 0 & 1 & & & \\ \hdashline & & & 0 & 1 & 0 \\ & 0 & & -1 & 0 & 0 \\ & & & 0 & 0 & 1 \end{array}\right],$$

for horizontal members

$$C = \left[\begin{array}{ccc:ccc} 1 & 0 & 0 & & & \\ 0 & 1 & 0 & & 0 & \\ 0 & 0 & 1 & & & \\ \hdashline & & & 1 & 0 & 0 \\ & 0 & & 0 & 1 & 0 \\ & & & 0 & 0 & 1 \end{array}\right]$$

This member stiffness matrix K_m is used to construct the structural stiffness matrix of the structure again in the normal fashion.

4.3.3 Layered Model

The layered model is a cantilever beam with a layered section of length Lp of inelastic zone at the fixed end as described previously. The layered model is used in the first story exterior columns of the frame structure in combination with the concentrated spring model. It is shown in Fig.4.4. The analytical procedure is similar to the case of the concentrated spring model. The instantaneous flexibility matrix corresponding to Eq.(4.2) is,

$$[F] = \begin{bmatrix} f_1 + f(M_A) & , & f_2 \\ f_2 & , & f_{LM} \end{bmatrix} \tag{4.24}$$

where

$$f_{LM} = f_L + \frac{1}{\alpha k GAL} \cdot \quad (f_L: \text{Eq. } 3.22)$$

The counterflexure point is assumed to be at the center of the column length, the effect of inelastic action of f_1 on the coupling term of f_2 can be ignored. The member stiffness matrix obtained from Eqs.(4.4)-(4.12) is applied to the structural stiffness matrix.

4.4 Structural Stiffness Matrix

The structural stiffness matrix of the frame-wall system is developed by combining all member stiffness matrices into story

stiffness matrices and then condensing out a number of the degrees of freedom so that only horizontal story movements appear in the final form of the equations.

4.4.1 Story Stiffness Matrix

The i-th story stiffness matrix of the frame-wall structure is developed as follows:

$$[K_i] = A^T \cdot \begin{bmatrix} K_{c1} & & & \\ & K_{c2} & 0 & 0 \\ & & K_{c3} & \\ & & & K_{b1} \\ & 0 & & \\ & & K_{b2} & 0 \\ & & & K_{b3} \\ & 0 & 0 & K_w \end{bmatrix} \cdot A \qquad (4.25)$$

where

K_{cj}, K_{bj}, K_w are the column, the beam and the wall member stiffness matrices in global coordinates as shown in Fig.4.5. A is the connectivity matrix and shown in appendix A.

4.4.2 Assembled Stiffness Matrix

The full-size structural stiffness matrix is accomplished by summing the story stiffness matrices, $[K_i]$, in proper order. The force-displacement relation of a structure is then expressed in the form.

$$\begin{Bmatrix} F_F \\ F_w \\ \hline F_H \end{Bmatrix} = \left[\begin{array}{cc:c} A_1 & 0 & R_1 \\ 0 & A_2 & R_2 \\ \hdashline R_1^T & R_2^T & E \end{array}\right] \begin{Bmatrix} D_F \\ D_w \\ \hline D_H \end{Bmatrix} \tag{4.26}$$

where

$\{F_F\}$, $\{D_F\}$ = force, displacement vector of frame term

$\{F_w\}$, $\{D_w\}$ = force, displacement vector of wall term

$\{F_H\}$, $\{D_H\}$ = holizontal force, displacement vector

The details of Eq.(4.26) are described in Appendix A.

Only external lateral loads are considered in this study. Thus external vertical forces and moments at joints of a structure are assumed to be zero.

$$\begin{Bmatrix} F_F \\ F_w \\ \hline F_H \end{Bmatrix} = \begin{Bmatrix} 0 \\ 0 \\ \hline F_H \end{Bmatrix} \tag{4.27}$$

Static condensation of the vertical displacements and rotations yields

$$\{F_H\} = \left[E - [R_1^T R_2^T] \left[\begin{array}{c:c} A_1 & 0 \\ \hdashline 0 & A_2 \end{array}\right]^{-1} \begin{Bmatrix} R_1 \\ R_2 \end{Bmatrix} \right] \cdot \{D_H\}$$

$$= [E - (R_1^T A_1^{-1} R_1 + R_2^T A_2^{-1} R_2)] \{D_H\} \tag{4.28}$$

$$= [K_H] \cdot \{D_H\}$$

In incremental form this equation is rewrthis equationten as:

$$\{\Delta F_H\} = [K_H] \cdot \{\Delta D_H\} \tag{4.29}$$

where

$$[K_H] = \left[E - R_1^T A_1^{-1} R_1 + R_2^T A_2^{-1} R_2\right] \tag{4.30}$$

$[K_H]$ = the reduced structural stiffness matrix of size, number of stories by number of stories

Eq.(4.29) is solved for lateral displacements from a given set of lateral load and a known instantaneous structural stiffness.

$$\{\Delta D_H\} = [K_H]^{-1} \{\Delta F_H\} \tag{4.31}$$

4.5 Static Analysis

The frame-wall structure is analyzed under several increments of load which may be either a monotonically increasing load or a cyclic load.

Load increments are applied to each story level of the structure. The load distribution shape over the height of the structure is arbitrary. But it is assumed that the load distribution shape does not change during the loading process. During each load increment, the structure is assumed to behave linearly. The structure's stiffness matrix is reconstructed or reevaluated following each load increment in accordance with the hysteresis rules for the concentrated spring model and the multiple spring model or in accordance with the nonlinear behavior of the material model selected for the layered model. Any unbalance or excess force that developes within an increment is applied

as a load to the next increment. This force correction procedure is an adaptation of the Initial Stress Method. As the iteration scheme is not used, the load increment should be chosen to be small enough to avoid significant residual forces.

4.6 Dynamic Analysis

A step-by-step numerical integration (time-history) procedure is used to solve the equations of motion for the dynamic analysis of the frame-wall structure. The earthquake time history is divided into a number of small time incrments. The incremental response values are obtained using the structural properties at the beginning of the time step. The solution advances in a step-by-step manner using a series of linear systems with changing stiffness properties.

4.6.1 The Equations of Motion

The equations of motion in terms of the relative displacements of the mass points can be written in an incremental form as follows,

$$[M]\{\Delta\ddot{x}\} + [c]\{\Delta\dot{x}\} + [K_H]\{\Delta x\} = -[M] \cdot \{\Delta\ddot{Y}\} \qquad (4.32)$$

where

$[M]$ = diagonal story mass matrix

$[c]$ = damping matrix

$[K_H]$ = structural stiffness matrix which is evaluated at the end of the previous time step

$\{\Delta\ddot{x}\},\{\Delta\dot{x}\},\{\Delta x\}$ = relative incremental story acceleration, story velocity, and story displacement vector, respectively

$\{\Delta\ddot{Y}\}$ = base acceleration vector

4.6.2 Mass Matrix

The lumped mass concept is assumed in the analysis. All of the mass of the structure is assumed to be concentrated at the story levels of the structure. Members or elements are considered as massless line elements. Thus the mass matrix is expressed as,

$$[M] = \begin{bmatrix} m_1 & & & 0 \\ & \ddots & & \\ & & m_i & \\ & & & \ddots \\ 0 & & & m_n \end{bmatrix} \qquad (4.33)$$

where

$[M]$ = a diagonal mass matrix of order n by n

m_i = lumped mass at each story

n = number of story

The dynamic analysis of a consistent mass system generally requires more computational effort than a lumped mass system does. This is because the lumped mass matrix is diagonal, while the consistent mass matrix has many off-diagonal terms (mass coupling). Another reason is that the rotational degrees of freedom can be eliminated from a lumped mass analysis by static condensation, whereas all rotational and translational degrees of freedom are included in a consistent mass analysis[11].

4.6.3 Damping Matrix

The viscous type of damping is used in this study for mathematical simplicity. The damping matrix is expressed as a linear combination of the stiffness and mass matrices.

$$[C] = C_1[M] + C_2[K_H] \qquad (4.34)$$

where

$[C]$ = viscous damping matrix

C_1, C_2 = the constant multipliers

The constant multipliers C_1, C_2 are related to the damping ratio for any mode k by,

$$\lambda_k = \frac{C_1}{2w_k} + \frac{C_2 \cdot w_k}{2} \tag{4.35}$$

where

w_k = the circular frequency of the k-th mode

λ_k = damping factor of the k-th mode

In a direct integration solution, C_1 and C_2 may be chosen to provide a specified damping ratio at two selected frequencies. Alternately, it is often more convenient to specify $\lambda_k = \bar{\lambda}$ for a given frequency $w_k = \bar{w}$ on the basis of test data or field observations.

Then i-th $C_1 = 2\bar{\lambda}\bar{w}$

and

$$C_2 = \frac{2\bar{\lambda}}{\bar{w}} \tag{4.36}$$

$[C]$ can be evaluated from Eq.(4.34). A damping matrix proportional to just the stiffness matrix is used in this study.

$$[C] = C_2 \cdot [K_H] \tag{4.37}$$

It is effective in reducing the amount of high frequency components in the structure's response[42].

The initial stiffness matrix denoted by $[K_H]$ in Eq.(4.37) is used in the analysis. This means that the damping matrix remains unchanged during any inelastic structural response. Overestimations due to usage of the initial stiffness matrix is acceptable because the damping effect should be expected to become larger when any inelastic action is occurring in the structure.

4.6.4 Numerical Solution of Equations of Motion

Assuming that the properties of the structure do not change within two time steps, the equations of motion(Eq.4.32) can be solved numerically by an explicit or an implicit method. In this study an implicit method is used since the bandwidth of the stiffness matrix is small and an iteration procedure is not needed.

Applying the implicit form of the Newmark Beta method[31], the incremental acceleration $\{\Delta\ddot{X}\}$ and the incremental velocity $\{\Delta\dot{X}\}$ can be expressed in terms of the incremental displacement $\{\Delta X\}$ and quantities, $\{\dot{X}\}$, and $\{\ddot{X}\}$ at the end of the previous time step.

$$\{\Delta\dot{x}\} = \frac{1}{2\beta\Delta t}\{\Delta x\} - \frac{1}{2\beta}\{\dot{x}\} - (\frac{1}{4\beta} - 1)\,\Delta t\,\{\ddot{x}\} \qquad (4.38)$$

$$\{\Delta\ddot{x}\} = \frac{1}{\beta(\Delta t)^2}\{\Delta x\} - \frac{1}{\beta\Delta t}\{\dot{x}\} - \frac{1}{2\beta}\{\ddot{x}\} \qquad (4.39)$$

where

t = time interval

β = a constant which indicates the variation of acceleration in a time interval (β =1/4 is chosen).

$\{\dot{x}\}$ = relative story velocity vector at the end of the previous time step

$\{\ddot{X}\}$ = relative story acceleration vector at the end of the previous time step

Substituting Eqs.(4.38) and (4.39) into Eq.(4.32), the incremental story displacement vector can be obtained as

$$[A] \cdot \{\Delta x\} = \{B\} \tag{4.40}$$

$$\{\Delta x\} = [A]^{-1} \{B\} \tag{4.41}$$

where

$\{\Delta x\}$ = the incremental story displacement vector

$$[A] = [K_H] + \frac{1}{\beta \Delta t^2} [M] + \frac{1}{2\beta \Delta t} [C] \tag{4.42}$$

$$\{B\} = \left\{ \frac{1}{\beta \Delta t} [M] + \frac{1}{2\beta} [C] \right\} \{\dot{x}\}$$

$$+ \left\{ \frac{1}{2\beta} [M] + \Delta t \left(\frac{1}{4\beta} - 1 \right) [C] \right\} \{\ddot{x}\} - [M]\{\Delta \ddot{Y}\} \tag{4.43}$$

$[A]$,$\{B\}$ are defined as the dynamic stiffness matrix and the dynamic load matrix of the structure, respectively. The equations can be solved by Gaussian elimination or other decomposition procedure such as the Choleski method. Once the incremental relative displacement vector has been obtained,the incremental relative velocities are calculated from Eq.(4.38). The incremental relative accelerations are calculated from Eq.(4.32) based on the current structural properties, $[C]$ and $[K_H]$.

$$\{\Delta \ddot{x}\} = - [M]^{-1} \left[[C]\{\Delta \dot{x}\} + [K_H]\{\Delta x\} + [M]\{\Delta \ddot{Y}\} \right] \tag{4.44}$$

The acceleration response is very sensitive to changes in the stiffness properties of the structure. Therefore Equation (4.44) instead of Eq.(4.39) is used to calculate the incremental relative accelerations. More accurate results can be obtained by computing the incremental accelerations based on the updated structural properties rather than the previous ones[41]. The structural story displacements, joint rotations and so forth at the end of the time increment are equal to the response quantities at the beginning of the time increment plus the calculated changes in the response quantities.

In the numerical solution of the equations of motion, the cost of an analysis relates directly to the size of the time step which has to be used for stability and accuracy[50].

Bathe[8] investigated stability limits, amplitude decay and period elongation in the dynamic response based on simple linear systems.

Weeks[48] concluded that the characteristics of operators such as Newmark's β method or Wilson's θ method [31,50], carry over essentially unchanged from the linear to the nonlinear case if time increments small enough to adequately trace the response are used and if equilibrium is satisfied at each step.

McNamara[28] recommended that even though the nature of nonlinear analysis does not lend itself easily to rigid conclusions, the time increment of the solution must be relatively small and certainly less than 1/100 to 1/200 of the solution period.

Furthermore, from another aspect it should be noted that the higher frequencies of a lumped parameter system are always in error when

compared to the continuous problem. It should also be noted that as the earthquake excitation components with periods smaller than about 0.05 sec. generally are not accurately recorded, there is very little justification to include the response in these higher frequencies in the analysis. Therefore in the nonlinear analysis of complex structures, many high frequency modes do not contribute appreciably to the response.

With these sugestions described above, the Newmark's method with $\beta = 1/4$ is chosen in this study. This method is known to be unconditionably stable in linear applications. As a time increment $\Delta t = 0.0004$ sec. is chosen for the analysis of the equations of motion with constant instantaneous structural stiffness $[K_H]$. This time step corresponds to $\Delta t/T_1 = 1/500$, $\Delta t/T_2 = 1/140$, $\Delta t/T_3 = 1/70$ where T_1 is the fundamental period of the structure and so on. In every ten time increments, which corresponds to $\Delta t = 0.004$, the constant instantaneous structural stiffness is replaced by an updated one calculated from the updated member stiffnesses. This numerical technique allows an acceptable and econonical solution.

4.6.5 Residual Forces

During the response calculation of the equations of motion an overshoot may result because of the assumed moment-curvature relationships used for the structural elements. The excess moments are detected at each element level by comparing the calculated moment from the equations of motion with the moment obtained from the hysteresis loop. A numerical iteration procedure for the overshooting forces, when yielding occurs within the time interval, is not applied in this study

since it needs more computation time and a numerical iteration within the time interval does not always yield a true solution for the case of dynamic problems anyway. Therefore a correction is made only in the moment at the joint at element level. The residual moment at each joint is applied to the subsequent time step.

CHAPTER 5

HYSTERESIS RULES AND NUMERICAL EXAMPLES

5.1 Introductory Remarks

When using either the concentrated spring model or the multiple spring model, hysteresis rules have to be created in order to trace the inelastic behavior of these models. Two hysteresis rules are adopted in this study. The first hysteresis model used is that proposed by Takeda[44]. The second hysteresis model used is a modified Takeda model which takes account of the pinching action and bond deterioration in beam-column joints. The second hysteresis model is applied to the beam members of this structure. This is only necessary in the case of very large excitation from the earthquake motions. This is observed from the results of experimental studies of reinforced concrete beam-column joints under large load reversals[25].

5.2 Degrading Trilinear Hysteresis Rule

5.2.1 Hysteresis Model 1

The degrading trilinear hysteresis rule of the Takeda model is in common usage to represent the inelastic behavior of reinforced concrete members. With this model the moment-rotation relationship of a cantilever flexural element is defined as shown in Fig.5.1.

A trilinear primary curve is defined by three points: a concrete cracking point, a steel yielding point, and a concrete ultimate point. This primary curve is assumed to be symmetric about its origin. This rule changes its unloading stiffness according to the following

mathematical expression.

$$K_u = K_o \left(\frac{D_y}{D_m} \right)^a \qquad (5.1)$$

where

K_u = new unloading stiffness

K_o = primary stiffness of hysteresis rule

D_y = yield deflection

D_m = maximum deflection attained in the direction of the loading

a = constant (0.5 is used in this study)

The reloading curve basically aims at the previous maximum point on the primary curve in that direction. In this study the hysteresis model 1 is used to define the moment – rotation relationship of the rotation spring of the concentrated spring model and the moment-curvature relationship of each spring of the multiple spring model. The hysteresis model 1 is applicable to those cases where the member fails in a dominantly flexure mode. Shear failure, pinching action or bond deterioration are not considered in this hysteresis rule.

5.2.2 Hysteresis model 2

Hysteresis model 1 had to be modified in order to deal with the effect of pinching action and bond deterioration that appears in the behavior of beam-column joints under large load reversals.

Through analytical models, Lybas[27] investigated the mechanism of slip of the reinforcement in the beam-pier joint for the coupled shear wall structure. But here the mathematical hysteresis rule is created just from the results of experimental observation[25].

Hysteresis model 2 is defined as follows(Fig.5.2). If the maximum rotation(displacement) never exceeds the yielding points, the hysteresis rule is exactly the same as hysteresis model 1. Once the maximum rotation (displacement) goes beyond the yield point, then for the next one-half cycle during unloading and reloading, moment-rotation relations behave according to an assumed cubic function (Fig.5.2).

$$M = a(D^3 - D_0^3) \tag{5.2}$$

where

M = moment variable

D = displacement variable

D_0 = displacement value on the x coordinate which is obtained by using the slope of K_u in Eq.(5.1)

a = coefficient

The coefficient "a" of the cubic function Eq.(5.2) can be determined by requiring that this function passes through the known points $A(D_1, M_1)$, $B(D_0, 0)$, and the assumed point $E(-D_1, -M_1)$. The position of the point E is assumed symmetric about the origin with respect to the point A, as indicated in Fig.5.2. In lieu of this function a simplification made up of three straight lines : AB, BD and DE, is used as the hysteresis loop of model 2. Key points of this model are $C(0, -aD_0^3)$ and $D(-D_0, -2aD_0^3)$ in addition to the points A, B and E. If unloading and the subsequent reloading occur at some point , say a point F, whose position is still of the same sign in displacement as the previous maximum unloading point A, then the hysteresis behavior is assumed to follow along a line FG whose slope is K_u and then a line GA which aims at the maximum point A

directly. If unloading and the subsequent reloading occur from a point F' whose position is now of opposite sign in displacement from the previous maximum unloading point A, then the hysteresis rules follow along a line F'G' whose slope is K_u and follows the cubic function rule from the point G' to the point A. In this case the coefficient "a" is obtained from the assumption that Eq.(5.2) passes through the assumed negative maximum point E, G' and A. The points $A(D_1,M_1)$ and $E(-D_1,-M_1)$ are the current maximum positive and negative displacement points experienced by the member during all previous cycles respectively.

Using the hysteresis model 2 in the concentrated spring model, numerical computations are performed to obtain the moment-rotation relationship of a cantilever beam. The assumed specimen has a length of 152.4 MM. and a rectangular cross section of (38 MM. x 38 MM.) with 2-3No.13G wire as reinforcing. The assumed material and cross sectional properties are similar to those of the middle level exterior beams of the structure FW-2 (Table 6.2). The stiffness characteristics are listed in Table 5.2. At first, regularly increasing five cycle loading is applied to the free end of the cantilever beam. Second, irregular eight cycle loading is applied to the free end of the beam. Computed moment-rotation relationships for both cases are shown in Fig.5.3. The hysteresis model 2 can numerically produce the pinching action (including the effect of bar pull-out due to bond deterioration) in both cases.

5 5.3 Comparison of Computed Hysteresis Loops with Experimental Results s

5.3.1 Force-Displacement Relationship of a Deep Beam

The three mechanical models described in the previous chapters are applied to a cantilever deep beam (wall) to trace the force-displacement curves for the wall. The assumed specimen has a length of 686 MM. and a rectangular cross section of (38 MM. x 203 MM.) with 2-2No.2G wire as reinforcing. The assumed material and cross sectional properties are listed in Table 5.3. The computed stiffness characteristics are also listed in Table 5.3. The hysteresis model 1 is used in the concentrated spring model and the multiple spring model. The computed force-displacement curves for the free end of the cantilever beam are compared with experimental values[2] as shown in Figs.5.4(a),(b), and (c). The primary intent of this comparison is to obtain a basic feeling for the applicability of the three mechanical models to the reinforced concrete cantilever beam in so far as representing the force-displacement relations of that beam. The agreement between the computed values from each mechanical model and the experimentally obtained results is seen.

5.3.2 Force-Displacement Relationship of a Beam-Column Joint

The two hysteresis models just discussed are compared to the experimental results obtained for a beam-column joint. These tests were performed for multi-cycles of loading. The assumed data on the material characteristics used in the analysis of the beam-column joint is taken from the FW-2 structure. For convenience this data is retabulated in Table 5.2. The comparison is illustrated in Fig.5.4, showing variations

of top lateral loading force versus top level deflection. The experimental results are represented by the broken line. Figure 5.5 shows that hysteresis model 2 fits quite effectively with the experimental results. But it should be noted that the test was conducted in the range of very large deformations. Although it is not illustrated, hysteresis model 1 also is effective as long as the range of response is limited to that of small deformations of beam-column joints.

5.4 Effect of Axial Load

A reinforced concrete section typically is weakened in its flexural strength when it is also under the influence of axial tension. Yielding of the tensile reinforcement limits its flexural strength. On the other hand moderate axial compression has a positive effect on moment capacity[7,20,40].

For beam members it can be assumed that the axial force is zero. For the wall members it is reasonable to assume that the axial force is also zero even though the wall members are subjected to their own dead load. This is normally a very small value. For the column members each column is subjected to an axial load which changes during the earthquake motion. The curves of the moment-curvature relations for each story column vary depending upon its axial force. However, for the sake of simplicity it is assumed that the axial force remains constant during the earthquake motion. Furthermore the structure is divided into three zones of constant values for the axial force. This subdivision is accomplished based on judgement assigning each story column to the group

with axial force near its dead load. This assignment is shown in Fig.5.6.

The effect of axial load on inelastic behavior of the structure was also investigated by using the layered model to model the first story exterior columns. The computed results achieved are presented in Chapter 6.

CHAPTER 6

COMPUTED RESULTS

6.1 Introductory Remarks

To demonstrate the applicability and flexibility of the proposed models, a series of numerical examples are presented. The examples presented in this study are of two types, the structure with a strong wall referred to as FW-1 and the structure with a weak wall referred to as FW-2. The main difference between the strong wall and the weak wall is the amount of steel reinforcement used in the wall. The vertical reinforcement is concentrated in two small bundles located in the outer two edges of the wall as shown in Fig.2.2. In order to study the behavioral characteristics of the frame-wall structures FW-1 and FW-2, static analyses are first made. Following these preliminary studies, dynamic analyses are made for these structures subjecting them to the first three seconds of the base accelerations obtained from experimental tests[2]. A third investigation into the effect of changing the axial load on the first story exterior columns is also made. The numerical examples thus computed are listed in Table 6.1. The computed results are compared with experimental results obtained by Abrams[2].

Material properties assumed for the models are listed in Table 6.2. The cross-sectional properties of the constituent members of the models are shown in Figs.2.1 and 2.2. The configurations of the models are listed in Table 6.3. The stiffness properties of these constituent members are calculated by the procedures described in Chapter 3. These

calculated stiffness properties are listed in Table 6.4. The structure type FW-2 is the main specimen to be investigated in this study.

6.2 Static Analysis

It is assumed that both structures are subjected to a first-mode (triangular) loading because the first mode is considered to be the major contributor to the response that would occur under dynamic loads. The static load is applied to the structures: FW-1 and FW-2, in small increments with the same distribution pattern of triangular load shape. The load increment used in this investigation is selected as 1/50 of the maximum anticipated static load(max. base shear of 24.5 KN.. This corresponds to top lateral load of 4.45 KN..)

6.2.1 Base Shear-Top Story Displacement Relationship

Curves depicting base shear versus tenth-level displacement calculated for FW-1 and FW-2 are shown in Fig.6.1. A curve for FW-1 neglecting the steel bar slip effect in the beam-column joints is also shown in that figure. The overall behavior of these structures can be seen from this figure. Cracking starts at about the same loading levels for all three cases. For the FW-1 strucrure, the first yielding of the beams is initiated at a base shear of 14.5 KN. followed by yielding of the wall at the base. After yielding at the base of the wall, (at a base shear of 18.1 KN.), a marked change in the structural stiffness occurs. The structure, however, maintains its resisting system against further load increase due to the strain hardening assumption in the hysteresis. Neglecting steel bar slip in the beam-column joints

produces a stiffer curve as expected. For the FW-2 structure, the wall yields first (at a base shear of 10.3 KN.) followed by the beam members (at a base shear of 12.3 KN.). An elastic curve is also shown in Fig.6.1 for comparison purposes with the three other curves.

6.2.2 Moment Distribution Patterns

Moment distribution patterns in all members of FW-2 are shown in Fig.6.2 for the load level initiating yielding at the column base(at a base shear of 14.7 KN.). The two patterns shown are for first the case where the structure remained elastic and then for the inelastic case. Comparison of the two patterns shows that the change due to reduced flexural rigidity of the wall member allows the upper portion of the wall to keep more flexural moment whereas the lower portion of the wall retains a lesser flexural moment as compared with that from an elastic analysis. The point of contraflexure of the wall shifts downward in the inelastic moment distribution pattern. Except for the first and the second level columns, the point of contraflexure is seen to remain near the center of the member.

6.2.3 Redistribution of Base Shear between a Wall and Columns.

A redistribution of base shear occurs between the wall and the various columns as the load increases on structures FW-1 and FW-2. The results of the investigation are shown in Figs.6.3 and 6.4. The distribution of base shear varies depending upon the nonlinear characteristics of the constituent members during the loading process. In the elastic stage of the FW-1 structure, the wall is subjected to 84

per cent of the base shear. When cracking in the wall is initiated and is followed in the beams and columns, the wall's share declines from 84 per cent to 79 per cent of the base shear. Initially the wall's contribution to the base shear is almost constant and more than 80 per cent of all the shear until the wall yields at the base. Following yielding at the base in the wall, a rapid shift of the base shear in the wall to that in the column members occurs until those column members reach yield at the base.

In the FW-2 structure, the wall is subjected to 78 per cent of the base shear in the elastic stage. Then part of that shear from the wall is transferred to the column members when cracking is initiated in wall. Distribution of base shear in the wall changes from the 78 per cent of the elastic stage to 68 per cent when the wall yields at the base. There is then an accelerated decline down to 32 per cent at which time the base of columns yield. The wall of the FW-2 structure transfers its shear gradually to the column members during the loading process.

6.2.4 Collapse Mechanism

The sequence of formation of the collapse mechanisms for FW-1 and FW-2 is presented in Figs.6.5 and 6.6 for the monotonically increasing load. A triangular lateral load distribution is assumed. When a bending moment exceeds the yield moment capacity at the end of any constituent member, a yield hinge is assigned to that end. This is shown as darkened zones in Figs.6.5 and 6.6.

In the FW-1 structure with its strong wall, the first yield

hinges appear at the end of the 4-th level beams. This occurs at 30/50 (60 per cent) of the assumed maximum lateral load(max. base shear 24.5 KN.). Then yield hinges form sequentially in the beams toward the upper levels of the structure. After the formation of the 6-th set of yield hinges in the beam members, the segment nearest the base of the wall starts yielding from the base portion. However, the yield zone of the wall does not propagate significantly. At the same time the remaining beam members also yield. The final failure of the structure occurs when the first story columns yielded at the base at a load of 41/50 (82 per cent) of the assumed maximum load(assumed maximum base shear = 24.5 KN.).

In the FW-2 structure with its weak wall, the segment of the wall nearest the base starts yielding first at a load of 21/50 (42 per cent) of the assumed maximum load. Then various beam members form hinges. Yielding of the beams begins at the intermediate levels and proceeds further into the lower and upper levels. Finally when the first story column members yield at the base at 30/50 (60 per cent) of the assumed maximum load(24.5 KN.), the structure forms a mechanism. The yield zone in the wall has propagated to a higher portion of the wall than was the case for FW-1.

6.2.5 Comparison of the Structure FW-1 and FW-2

The structure FW-1 with its strong wall, yielded at a higher load and has the higher ultimate strength, as to be expected, compared to the FW-2 structure(Fig.6.1). Base shear-top story displacement of FW-1 approaches more nearly an elastic-plastic diagram whereas that of FW-2

draws a more curved shape. In FW-1, the behavior of the wall dominates markedly the overall behavior of the structure. In FW-2, this is not so true. After the collapse mechanism has been formed, however, the structure does not lose its resisting capability against further load increases because of the assumption of strain hardening in the hysteresis rule. As seen in Fig.6.5 and 6.6, the yield zone in the weak wall is more fully developed than that of a strong wall.

6.3 Dynamic Analysis

Next nonlinear dynamic response analyses for the FW-1 structure and for the FW-2 structure were made. A total of five different cases of response-history analyses were carried out. These cases are for two different levels of accelerations for FW-1 and two different levels of accelerations and one variation on the hysteresis model for FW-2. The analytical method is described in Chapter 4. A summary of numerical examples including the assumed analytical conditions is listed in Table 6.1. The purpose herein is to investigate analytically the general response phenomenon of a reinforced concrete frame-wall structure.

6.3.1 Base Motion

The base acceleration records used for the analysis in this study are those base motions measured in the structures tested on the earthquake simulator. The original waveforms of input base motions for the experimental tests are the acceleration signals of the El Centro (1940) NS component. The original time axis is compressed by a factor of 2.5 and the amplitudes of acceleration are modified depending upon

the purpose of the model tests[2]. The duration of the earthquake is an important factor. However only the first 3.0 seconds of recorded base motions are used in this study. This is justified because the maximum responses and most of the damage to the structures are expected to take place within those 3.0 seconds. The waveforms of these observed base motions as well as those of the digitalized input base motion for response calculation are shown in Fig.6.7. The maximum accelerations of the base motions used for each analysis are listed in Table 6.1.

6.3.2 Modal Properties of the Structures

Modal properties associated with the first three vibration modes of FW-1 and FW-2 are computed before and after the runs. These properties are listed in Table 6.5 and are also shown in Figs.6.8 and 6.9. The mode shapes of both the FW-1 and FW-2 structures are quite similar. The mode shapes are not significantly changed during the dynamic tests. Because of the structural damage occurring during the earthquake motions, the fundamental frequency is reduced after run-3(max. acc.= 2.41G) for FW-1 to 50 per cent of its initial fundamental value and reduced to less than 40 per cent of the initial fundamental frequency after run-2(max. acc.=0.92G) for FW-2.

6.3.3 Calculated Response

The numerical integration of the equations of motion is carried out with the time increment of 0.0004 seconds (Newmark =1/4). Response values are recorded at every 10 numerical time integration points(at every 0.004 seconds). The calculated response waveforms are compared

with the observed response waveforms for each structure for each run. Selected results for run-1 on FW-1 with a maximum input base acceleration of 0.49G are shown in Fig.6.10. Maximum output response values for these cases are listed in Table 6.6. The results for run-3 on FW-1 with a maximum input base acceleration of 2.41G are shown in Fig.6.11.

For FW-1 run-1, the agreement obtained between computed waveforms and the observed experimental ones is seen to be quite close on each of the response waveforms of story shears, base overturning moment, accelerations, displacements and shear forces on walls. But a slight elongation of the fundamental period is observed in this comparison.

For FW-1 run-3, similar reasonable agreement between the analytical and the experimental results can be seen in Fig.6.11. These agreements exist even though a rather strong earthquake with a maximum base acceleration of 2.41G has been used. The elongation of the fundamental period is not observed in this comparison.

The results for FW-2 run-1 with maximum input base acceleration of 0.49G and for FW-2 run-2 with maximum input base acceleration of 0.92G are shown in Figs.6.12 and 6.13. In both cases the agreement existing between the computed and experimental waveforms is excellent. No period elongation can be seen in these cases either. The analytical scheme does trend to produce smaller response values than observed in the experimental tests. The response waveforms of displacements, shears and base overturning moment are relatively smooth and governed by the first mode component. The response waveforms of acceleration show the effect of some higher mode components. The agreement between the

experimental and the calculated curves is satisfactory. The analytical method can estimate the acceleration, the displacement, the shear and the overturning moment in each story of the structure at each time increment regardless of both the base input values and wall characteristics in the structure.

6.3.4 Effects of the Pinching Action of the Beam-Column Joints

The pinching action, including the slipping effect of the steel bars due to bond deterioration described in Chapter 5, experimentally appears in the characteristics of beam-column joints under large load reversals or after a number of lower amplitude load cycles. These effects of the pinching action on the maximum responses and response waveforms of the structure are investigated. The hysteresis model 2 described in Chapter 5 is assigned to the beam member springs in the beam-column joints of FW-2 for run-2. There appears to be little sensitivity due to pinching action in the response analysis. This is because the behavior of the wall dominates the behavior of the structure and the wall behaves without pinching action. Pinching action of beam-column joints produces slightly larger displacements and slightly smaller accelerations, shear forces and overturning moments in the response of FW-2 run-2. A detailed comparison of maximum response data with and without pinching action in the beam-column joints of the structure can be seen in Table 6.6. The response waveforms compared with those without pinching action are also shown in Fig.6.14.

6.3.5 Moment-Rotation Relationship for the Flexural Spring of a Beam

The response-history of the moment-rotation relationship for the flexural spring of a beam is studied. The flexural spring selected for study is the one at the left end of the exterior beam at the fifth level. The elastic deformation occurring along the beam length is included in the value of rotation. Results for four test runs(FW-1 run-1 and run-3, FW-2 run-1 and run-2) are shown in Fig.6.15. The flexural spring of the beam experiences two yield excursions on the negative side for FW-1 run-1(max. input acc.=0.55G) and FW-2 run-1 (max. input acc.=0.49G) whereas the flexural spring of the beam experiences yielding in both directions for FW-1 run-3 and FW-2 run-2. Once beyond yielding, the spring stiffness is reduced in proportion to the yielding value for all cases. Note the area enclosed by the curve represents the energy dissipation.

The large difference in the appearance of the hysteresis curves for springs with and without pinching action can be seen in Fig.6.16 (FW-2 run-2). Large rotation of the spring is seen when consideration of pinching action is included. Although this difference in the characteristics of the hysteresis curves exists, its effect on the overall behavior is minimal as noted in section 6.3.4.

6.3.6 Moment-Rotation Relationship of a Flexural Spring of a Column

The response-history of the moment-rotation relationship of a flexural spring at the base of the left exterior column is shown in Fig.6.17. Only the spring for FW-1 run-3 experiences yielding and that

only on the negative side. The remaining three cases experience cracking but no yielding on either side.

6.3.7 Moment-Curvature Relationship of a Wall Segment

The response-history of the moment-curvature relationship for the base of the wall segment is shown in Fig.6.18. Only a limited number of yield excursions are seen with these occurring both sides. The reduced stiffness of the wall of FW-1 remains stiffer than that of the wall of FW-2 throughout the test.

6.3.8 Base Moment-Top Story Displacement Relationship

The base moment-top story displacement relationships of both structures are shown in Fig.6.19. The overall structural response history during the dynamic motion is seen in these figures. Softening of the stiffness of each structure is seen in all cases because of the effect of inelastic action in the constituent members. The relatively narrower width of loop in the FW-1 run-1 can be seen compared with FW-2 runs 1 and 2.

6.3.9 Response Waveforms of the Axial Force of the Column at the Base

Response waveforms of the axial force at the base of the left column are recorded during the earthquake motions and are shown in Fig.6.20. These response waveforms are obtained with the use of the concentrated spring model for that column member. The first mode component dominates these response waveforms. The load axis is seen to

be shifted by the dead load of 5.5 KN. At the base the column's axial force varies within an envelope bounded by a maximum compression force of about 15 KN. This is the value at which the beams from every level have formed yield hinges. The lower bound is a minimum force(tension) of about -2.0 KN.

6.3.10 Structural Yield Patterns

Inelastic hinge locations calculated during the earthquake base motions are illustrated in Fig.6.21 for four cases(FW-1 runs 1 and 3, FW-2 runs 1 and 2). The sequences of yielding and the time when yielding occurs in the constituent members of the structure are also shown in these figures.

The columns of these structures do not yield throughout the runs(FW-1 run-1, FW-2 runs 1 and 2). However for FW-1 run-3(max. input base acc.=2.41G), yield action was initiated at the base of the columns. By contrast yielding hinges are distributed fairly uniformly at the ends of the beams throughout almost all of the levels. This is because the structure is designed with weak beams and strong columns.

For FW-2 run-2(max. input base acc.=0.49G), all the yielding of the various members is initiated within the first 0.9 seconds. For the rest of the cases(FW-1 runs 1 and 3, FW-2 run-1), all yielding occurs during the first 2.0 seconds. Inelastic action of the wall can be seen to propagate some from the base toward the upper segments.

For the FW-1 run-3(max. input base acc.=2.41G), the structure forms a collapse mechanism when the first story columns yield at the time t=1.421 seconds. Also the wall at the base is severly damaged by

this time. The whole portion of the first story wall can be seen to be yielding. All columns but the ones belonging to the first story prove to be strong enough to avoid any significant yielding. The structure is still capable of sustaining the additional forces applied to the structural system because of the assumption of the strain hardening hysteresis rule in each model as seen in the static case. Finally the experimentally observed cracking patterns of FW-2 run-2 is presented from reference,[2] in Fig.6.22.

6.4 Effect of Changing Axial Load at the Base of the Exterior Columns

It is important to check axial loads of the column members induced by the earthquake motion. These loads might be critical in the exterior columns of slender structures. The exterior columns can play an important role in the behavior of a system when the variation of axial forces and axial deformations are included. The layered model is used herein to study in a quantitative sense the change in the axial force on the bending moment resisting mechanism of the column members. This is done for both monotonically increasing loading and for the single cycle loading. The layered model is applied to both first story exterior column members of the structure. The concentrated spring model is used for the remaining frame members and the multiple spring model is used for wall members. The general trends of the axial force-bending moment resisting mechanism at the base of the exterior columns are simulated. The change in the axial rigidity is neglected. A triangular shaped static lateral load is applied to the structure. The loading process applied is the same as was the case for the static analysis

described earlier. The secondary P-Δ effect of the axial load is not incorporated in the analysis. It is not the intent of this study to throughly investigate the influence of changing axial load on the dynamic response of the system but merely its significance in the present case.

6.4.1 Effect of Changing Axial Force under Monotonically Increasing Lateral Load.

The effect of changing the axial force in the first story exterior columns is studied first for the increasing lateral load.

The base shear-top story displacement relationship of the structure FW-2 is shown in Fig.6.23. The curves of displacement are obtained by using the layered model (solid line) as well as by using the concentrated spring model (dotted line). The two curves are almost identical primarily because the layered model is applied only to the exterior first story columns. The curve using the layered model shows that the left column yields at the base at an early stage while the center and right columns do not yield at all during the loading process. On the other hand the columns using the concentrated spring model all yield at the same point and at a later stage than the layered model.

The moment-curvature hysteresis loops of the layered section in the layered model are shown in Fig.6.24. Various applied constant axial load curves form the backbone hysteresis loops. They are made up of actual smooth curves rather than idealized piecewise straight lines. The hysteresis loops determined with layered sections at the base of both exterior columns are plotted in the figure. The hysteresis loops

of the layered section shift from one moment-curvature curve with a constant axial force to another moment-curvature curve with a different constant axial force in order to reflect change in axial force. On the hysteresis loop with increasing axial force in the column, a stiffer slope than that used in the concentrated spring model results. The concentrated spring model's primary curve is based on a constant axial force of 4.45 KN. On a hysteresis loop with decreasing axial force in the column, the slope of the hysteresis loop is softer than that of the primary curve and furthermore the slope of the curve becomes negative after yielding occurs. The concentrated spring model's primary curve then positions itself approximately as the mean curve between the stiffer and softer curves. When the layered section takes on a negative stiffness, this is replaced by a slight positive stiffness for computational ease during the analysis of the structure. Therefore a numerical error is introduced in the analysis of the behavior of the structure with the layered model columns.

The loading path is traced on the interaction diagram for the layered section of the exterior column. The loading paths at the base of the two exterior columns are plotted for monotonically increasing lateral load on the structure. These two loading paths take the form shown in Fig.6.25. One is subjected to monotonically increasing axial force superimposed on the dead load, the other is subjected to a monotonically decreasing axial force down from the dead load. In the figure, loading path No.2 for the column section with increasing axial force starts from the Nd=5.5 KN.(dead load). It rises gradually becoming flat when yielding occurs at the ends of the beams. Once the

loading path reaches the yielding line on its moment-axial force interaction diagram, the slope becomes stiffer again until that loading path reaches the ultimate branch of the moment-axial force interaction diagram. At this point the edge of the column section crushes. After this crushing occurs and if still increasing axial load is induced to the section, the column cross section changes into another cross section with the crush portion deleted from the original section. In such a case the loading path turns inside taking on arbitrary slope depending upon the section properties and loading combination. Loading path No.1 for a column section with decreasing axial force also starts from the level Nd=5.5 KN.(dead load). It decreases along a path symmetric about the axis of Nd=5.5 KN., with loading path No.2. Distortion of the curve shown as loading No.1 is probably the result of a small numerical error. Once loading path No.1 reaches the yielding line and the axial force continues to decrease, (this may entail an increase in tension if the axial force has reached into the tensile range.) the loading path begins heading toward the point of the pure tension failure for the cross section.

6.4.2 Effect of Changing Axial Force under One Cycle Loading

The base shear-top story displacement relationship of the structure(Fw-2) under one cycle loading is shown in Fig.6.26. This entire load-displacement relationship is identical for both cases(by the layered model and by the concentrated spring model).

The moment-curvature hysteresis loops of layered sections are shown in Fig.6.27. For the first one quarter cycle of loading, the

curves of No.1 and No.2 are the same as the ones just described for the case of monotonically increasing load. For the next half cycle of loading and unloading, the column layered section of No.1 experiences a snap-through phenomenon. For the structural analysis this phenomenon is modified as shown in Fig.3.11(d). The stiffness of this portion is replaced by a small positive one. After this snap-through phenomenon has occurred, the column section again demonstrates stiffer flexural rigidity. How much depends upon the level of axial force. The column of No.2 on the other side of the structure then experiences similar relationships of a form which appears antisymmetrical about the origin. In order to verify this hysteresis loop, check points are created along its path. The results are illustrated in Fig.6.28. The behavior of the cross section illustrated in the figure shows how the steel and concrete strains in its cross section shift during one cycle loading.

CHAPTER 7

SUMMARY AND CONCLUSIONS

7.1 Summary

The nonlinear analyses of multistory reinforced concrete frame-wall structures subjected to strong motion earthquakes are carried out. The structures used in the investigation are those tested by D.P.Abrams using the University of Illinois Earthquake Simulator[2]. Three mathematical models : the concentrated spring model, the multiple spring model, and the layered model, are presented to represent the inelastic behavior of a reinforced concrete cantilever beam. The nonlinear behavior of these mechanical models is introduced through their material properties. Geometrical nonlinearities are not considered. Hysteresis loops for each model are established. These mechanical models are applied to the 10-story reinforced concrete frame-wall structures of Abrams. The concentrated spring model is used for the frame members whereas the multiple spring model is applied to wall members. The layered model is applied to the first story exterior column members only when the effect of changing axial force is investigated. The structures are first analyzed for static loads. Then the dynamic tests are computed. For dynamic loads, the time-history acceleration input records obtained from the test are used. The computed results are compared with the experimental results. The mechanical models are shown to be useful tools for investigating the behavior of reinforced concrete frame-wall structures under both static and seismic loadings.

7.2 Consclusions

The modeling of reinforced concrete structures to include their inelastic response is a very difficult, complicated problem. But by adopting the simple assumptions and analytical procedures described in this study, a close or reasonably faithful reproduction of the experimental results is obtained. Using more sophisticated material and mechanical models, which necessitates the introduction of additional parameters to define, leads to extra computational effort with but a small improvement in results. It should be kept in mind that the results obtained in this study are for the laboratory test specimens.

The following statements are also added to the conclusions.

1. Inelastic actions of the wall play the major role in controlling the structural response. The multiple spring model shows the detailed inelastic behavior of the wall.

2. Frequencies of the structure decrease considerably during the earthquake motion reflecting a significant reduction of structural component stiffnesses.

3. The mechanical models used in the study : the concentrated spring model for frame members and the multiple spring model for wall members, satisfactorily reproduce the response values and the response waveforms of the specimens.

4. Pinching action of column-beam joints produces only slightly larger displacements and slightly smaller accelerations, and shear forces in the structure since the wall members dominate the behavior of the structure.

5. Reduction of flexural rigidity of the first story exterior columns due to the effect of changing axial load does not significantly alter the overall behavior of this structure. This is again a consequence of the structure being dominated mainly by its wall. The layered model shows the detailed behavior of the inelastic zone of these column members.

6. Even though response-history calculations are very expensive, consuming both time and money, an inelastic response-history

analysis using the concentrated spring model and the multiple spring model produces very detailed information about the response of structures to a particular earthquake. Therefore the response-history approach though expensive is a very effective tool to study the influence of certain quantities on the response.

7. By proper design of the beam members in a frame, yielding in the column members can be minimized. Computed dynamic results demonstrate the adequacy of this design philosophy.

7.3 Recommendations for Further Studies

Some areas of further studies are,

1. Using the mathematical model developed in this study, investigate the influence of variations in the significant parameters.

2. Extend the analysis procedure to include nonlinear geometric effects.

3. Extend the mechanical model to predict both bending failures and shear failures in wall members so that individual and combined effects of inelastic interaction can be assessed.

4. The models presented in this study are limited to plane structures with the makeup of the laboratory test specimen. The mathematical models should be extended to the general case taking account : (a) the effect of slabs, (b) non-uniformly reinforced beams, (c) the effect of torsion, etc.

Before additional analytical progress is made,however, some experimental research is necessary on,

1. Shear deformation characteristics of shear walls.

2. Shear deformation characteristics of beam-column joint panels.

3. Moment-curvature relations and failure criterior for reinforced concrete columns under changing axial load.

4. Load-deflection curves of various types of shear walls: I-beam type, channel type, box type, and circular type, etc.

The further studies described herein will be the next advanced steps to understand the inelastic behavior of reinforced concrete structures.

LIST OF REFERENCES

1. Abrams, D. P., "Measured Hysteresis Relationships for Small-Scale Beams," Civil Engineering Studies, Structural Research Series, No. 432, University of Illinois, Urbana, November 1976.

2. Abrams, D. P., and Sozen, M. A., "Experimental Study of Frame-Wall Interaction in Reinforced Concrete Structures Subjected to Strong Earthquake Motions," Civil Engineering Studies, Structural Research Series, University of Illinois, Urbana (to be published).

3. ACI Committee 442, Title No. 68-11, "Response of Buildings to Lateral Forces."

4. Agrawal, A. B., Jaeger, L. G., and Mufti, A. A., "Crack Propagation and Plasticity of Reinforced Concrete Shear Wall under Monotonic and Cyclic Loading," Conf. on Finite Element Methods in Engr., Adelaide, Australia, December 1976.

5. Aktan, E., Pecknold, D. A. W., and Sozen, M. A., "R/C Column Earthquake Response in Two Dimensions," Journal of the Structural Division, ASCE, Vol. 100, No. ST10, October 1974, pp. 1999-2015.

6. Anderson, J. C., and Townsend, W. H., "Models for RC Frames with Degrading Stiffness," Journal of the Structural Division, ASCE, December 1977.

7. Aoyama, H., "Moment-Curvature Characteristics of Reinforced Concrete Members Subjected to Axial Load and Reveral of Bending," Proceedings of International Symposium on the Flexural Mechanics of Reinforced Concrete, ASCE-ACI, Miami, November 1964, pp. 183-212.

8. Bathe, K. J., and Wilson, E. L., "Stability and Accuracy Analysis of Direct Integration Methods of Earthquake Engineering and Structural Dynamics, Vol. 1, No. 3, January-March 1973, pp. 283-291.

9. Chen, W. F., and Atsuta, T., "Theory of Beam-Columns," Vol. 1, McGraw-Hill, Inc., New York, N.Y., 1976.

10. Clough, R. W., and Benuska, K. L., "Nonlinear Earthquake Behavior of Tall Buildings," Journal of the Engineering Mechanics Division, ASCE, Vol. 93, No. EM3, June 1967, pp. 129-146.

11. Clough, R. W., and Penzien, J., "Dynamics of Structures," McGraw-Hill, Inc., New York, N.Y., 1975.

12. Darwin, D., and Pecknold, D. A. W., "Analysis of RC Shear Panels under Cyclic Loading," Journal of the Structural Division, ASCE, Vol. 102, No. ST2, February 1976, pp. 355-369.

13. Fintel, M., "Handbook of Concrete Engineering," Van Nostrand Reinhold, New York, N.Y., 1974.

14. Gavlin, N. L., "Bond Characteristics of Model Reinforcement," Civil Engineering Studies, Structural Research Series, No. 427, University of Illinois, Urbana, 1976.

15. Giberson, M. F., "The Response of Nonlinear Multi-Story Structures Subjected to Earthquake Excitation," Earthquake Engineering Research Laboratory, California Institute of Technology, Pasadena, 1967.

16. Gurfinkel, G., and Robinson, A., "Determination of Strain Distribution and Curvature in a Reinforced Concrete Section Subjected to Bending Moment and Longitudinal Load," ACI Journal, Title No. 64-37, July 1967.

17. Hand, F. R., Pecknold, D. A., and Schnobrich, W. C., "Nonlinear Layered Analysis of RC Plates and Shells," Journal of the Structural Division, ASCE, Vol. 99, No. ST7, July 1973, pp. 1491-1505.

18. Harrison, H. B., "Computer Methods in Structural Analysis," Prentice-Hall, Inc., Englewood Cliffs, New Jersey, 1973.

19. Hays, C. O., Jr., and Matlock, H., "Nonlinear Discrete Element Analysis of Frames," Journal of the Structural Division, ASCE, Vol. 103, No. ST10, October 1973.

20. Hisada, T., Ohmori, N., and Bessho, S., "Earthquake Design Considerations in Reinforced Concrete Columns," Kajima Institute of Construction Technology, Tokyo, Japan, January 1972.

21. Hognestad, E., "A Study of Combined Bending and Axial Load in Reinforced Concrete Members," University of Illinois Engineering Experimental Station, Bulletin Series No. 399, November 1951, p. 128.

22. Karsan, I. D., and Jirsa, J. O., "Behavior of Concrete under Compressive Loadings," Journal of the Structural Division, ASCE, Vol. 95, No. ST12, December 1969.

23. Karlsson, B. I., Aoyama, H., and Sozen, M. A., "Spirally Reinforced Concrete Columns Subjected to Loading Reversals," Fifth World Conference on Earthquake Engineering, Session 2-D, Rome, Italy, 1973.

24. Kent, D. C., and Park, R., "Flexural Members with Confined Concrete," Journal of the Structural Division, ASCE, Vol. 97, No. ST7, July 1971, pp. 1969-1990.

25. Kreger, M. E., and Abrams, D. P., "Measured Hysteresis Relationships for Small-Scale Beam-Column Joints," Civil Engineering Studies, Structural Research Series, No. 453, University of Illinois, Urbana, August 1978.

26. Kubota, T., "Studies on Strength and Deformation of Reinforced Concrete Flexural Members under Consideration of Bond Stress," Ph.D. Thesis, The Tokyo Metropolitan University, Tokyo, Japan, 1972.

27. Lybas, J. M., and Sozen, M. A., "Effect of Beam Strength and Stiffness on Dynamic Behavior of Reinforced Concrete Coupled Walls," Civil Engineering Studies, Structural Research Series, No. 444, University of Illinois, Urbana, July 1977.

28. McNamara, J. F., "Solution Schemes for Problems of Nonlinear Structural Dynamics," Journal of Pressure Vessel Technology, ASME, May 1974.

29. Montgomery, C. J., and Hall, W. J., "Studies on the Seismic Design of Low-Rise Steel Buildings," Civil Engineering Studies, Structural Research Series, No. 442, University of Illinois, Urbana, July 1977.

30. Muto, K., "Aseismatic Design Analysis of Buildings," Maruzen Syoten, Inc., Tokyo, Japan, 1974.

31. Newmark, N. M., "A Method of Computation for Structural Dynamics," Journal of the Engineering Mechanics Division, Vol. 85, No. EM3, Proc. Paper 2099, July 1959, pp. 67-94.

32. Otani, S., "Inelastic Analysis of R/C Frame Structures," Journal of the Structural Division, ASCE, Vol. 100, No. ST7, July 1974, pp. 1433-1449.

33. Otani, S., "SAKE, A Computer Program for Inelastic Analysis of R/C Frames to Earthquake," Civil Engineering Studies, Structural Research Series, No. 413, University of Illinois, Urbana, November 1974.

34. Otani, S., and Sozen, M. A., "Behavior of Multistory Reinforced Concrete Frames during Earthquakes," Civil Engineering Studies, Structural Research Series, No. 392, University of Illinois, Urbana, November 1972.

35. Padilla-Mora, R., and Schnobrich, W. C., "Nonlinear Response of Framed Structures to Two-Dimensional Earthquake Motion," Civil Engineering Studies, Structural Research Series, No. 408, University of Illinois, Urbana, July 1974.

36. Park, R., and Paulay, T., "Reinforced Concrete Structures," John Wiley & Sons, Inc., New York, N.Y., 1975.

37. Park, R., Kent, D. C., and Sampson, R. A., "Reinforced Concrete Members with Cyclic Loading," Journal of the Structural Division, ASCE, Vol. 98, ST7, July 1972, pp. 1341-1360.

38. Schnobrich, W. C., "Behavior of Reinforced Concrete Structures Predicted by the Finite Element Method," An International Journal, Computers & Structures, Vol. 7, No. 3, June 1977, pp. 365-376.

39. Sinha, B. P., Gerstle, K. H., and Tulin, L. G., "Stress-Strain Relations for Concrete under Cylic Loading," Journal ACI, Proc., Vol. 61, No. 2, February 1964, pp. 195-211.

40. Sozen, M. A., "Hysteresis in Structural Elements," Applied Mechanics in Earthquake Engineering, ASME, AMD, Vol. 8, November 1974, pp. 63-98.

41. Suidan, M., and Schnobrich, W. C., "Finite Element Analysis of Reinforced Concrete," Journal of the Structural Division, ASCE, Vol. 99, No. ST10, Proc. Paper 10081, October 1973, pp. 2109-2122.

42. Takayanagi, T., and Schnobrich, W. C., "Computed Behavior of Reinforced Concrete Coupled Shear Walls," Civil Engineering Studies, Structural Research Series, University of Illinois, Urbana, December 1976.

43. Takeda, T., "Dynamic Analysis of Reinforced Concrete Structures (in Japanese)," Concrete Journal, Japan National Council on Concrete, JANACC, Vol. 12, No. 8, August 1974, pp. 33-41.

44. Takeda, T., Sozen, M. A., and Nielsen, N. N., "Reinforced Concrete Response to Simulated Earthqueks," Journal of the Structural Division, ASCE, Vol. 96, No. ST12, December 1970, pp. 2557-2573.

45. Takizawa, H., "Strong Motion Response Analysis of Reinforced Concrete Buildings (in Japanese)," Concrete Journal, Japan National Council on Concrete, JANACC, Vol. 11, No. 2, February 1973, pp. 10-21.

46. Thomas, K., and Sozen, M. A., "A Study of the Inelastic Rotation Mechanism of Reinforced Concrete Connections," Civil Engineering Studies, Structural Research Series, No. 301, University of Illinois, Urbana, August 1965.

47. Wakabayashi, M., "Behavior of Systems," Panel Papers and Discussions, Proceedings, Sixth World Conference on Earthquake Engineering, Vol. 1, New Delhi, India, 1977.

48. Weeks, G., "Temporal Operators for Nonlinear Structural Dynamics Problems," Journal of the Engineering Mechanics Division, ASCE, Vol. 98, No. EM5, October 1972.

49. Wight, J. K., and Sozen, M. A., "Strength Decay of Reinforced Concrete Columns," Journal of the Structural Division, ASCE, Vol. 101, No. ST5, May 1975, pp. 1053-1065.

50. Wilson, E. L., Farhoomand, J., and Bathe, K. J., "Nonlinear Dynamic Analysis of Complex Structures," Earthquake Engineering and Structural Dynamics, Vol. 1, 1973, pp. 241-252.

51. Yuzugullu, O., and Schnobrich, W. C., "A Numerical Procedure for the Determination of the Behavior of a Shear Wall Frame System," Journal ACI, Proc., Vol. 70, No. 7, July 1973, pp. 474-479.

TABLE 2.1 REINFORCING SCHEDULES FOR THE STRUCTURES OF FW-1 AND FW-2

	FW-1				FW-2			
STORY OR LEVEL	WALLS	BEAMS	COLUMNS (EXT.)	COLUMNS (INT.)	WALLS	BEAMS	COLUMNS (EXT.)	COLUMNS (INT.)
10	2	2	2	3	2	2	2	2
9	2	3	2	3	2	2	2	2
8	2	3	2	2	2	2	2	2
7	2	3	2	2	2	3	2	2
6	2	3	2	2	2	3	2	2
5	4	3	2	2	2	3	2	2
4	4	2	2	2	2	3	2	2
3	4	2	2	2	2	3	3	2
2	8	2	2	2	2	2	3	2
1	8	2	2	2	2	2	3	2

FOR WALLS NUMBER OF NO.2G WIRES PER ONE SIDE OF CROSS SECTION, 1-NO.2G WIRE DIAMETER 6.65 MM.
AREA 34.8 MM**2

FOR BEAMS, COLUMNS NUMBER OF NO.13G WIRES PER FACE
1-NO.13G WIRE DIAMETER 2.34 MM.
AREA 4.29 MM**2

TABLE 5.1 ASSUMED CHARACTERISTICS OF A CANTILEVER BEAM SPECIMEN FOR HYSTERESIS LOOP STUDY (FIG.5.3)

LENGTH (MM.) 152.4

RIGID ZONE (MM.) 25.4

FLEXURAL RIGIDITIES (KN-M.**2) (SHOWN IN FIG.3.4)
SHEAR DEFORMATION INCLUDED
STEEL BAR SLIP INCLUDED

SD1 = 9.57
SD2 = 2.14
SD3 = 0.08

CRACKING MOMENT (KN-M.) 0.03
YIELDING MOMENT (KN-M.) 0.125

LOADING PROCESS (KN.)

CASE 1		CASE 2			
CYCLE	LOAD	CYCLE	LOAD	CYCLE	LOAD
1	1.07	1	0.445	11	1.38
2	-1.16	2	-0.445	12	0.89
3	1.25	3	1.11	13	1.42
4	-1.34	4	-0.89	14	-1.11
5	1.42	5	1.16	15	-0.445
6	-1.51	6	-1.16	16	-1.43
7	1.60	7	1.25	17	1.47
8	-1.69	8	-0.223	18	-1.56
9	1.74	9	1.34	19	1.56
10	0.0	10	-1.38	20	0.0

TABLE 5.2 ASSUMED CHARACTERISTICS OF A BEAM-COLUMN JOINT SPECIMEN FOR LOAD-DISPLACEMENT RELATIONSHIP STUDY (FIG.5.5)

1. MATERIAL PROPERTIES

CONCRETE			
COMPRESSIVE STRENGTH	f'_c	(MPA)	42.4
TENSILE STRENGTH	f_t	(MPA)	3.25
YOUNG MODULUS	E_c	(MPA)	30800
			*(22000)
SHEAR MODULUS	G	(MPA)	13200
STRAIN AT f'_c	ε_o		0.003
AT ULTIMATE	ε_{cu}		0.004
AT f_t	ε_t		0.000105
STEEL REINFORCEMENT			
YIELD STRESS	f_{sy}	(MPA)	356
ULTIMATE STRESS	f_{su}	(MPA)	382
YOUNG MODULUS	E_s	(MPA)	203000
STRAIN AT YIELD	ε_y		0.00175
AT ULTIMATE	ε_{su}		0.07
AT STRAIN HARDENING			0.01

* THE VALUE IN THE ( ) IS PREFERABLE

TABLE 5.2 (CONTINUED)

2. SECTION PROPERTIES

	DIMENSION (MM.)	STEEL (WIRE)	LENGTH (MM.)	RIGID LENGTH (MM.)
BEAM	38.0 X 38.0	2 X 2-NO.13G	152.4	25.4
COLUMN	38.0 X 51.0	2 X 2-NO.13G	114.3	19.1

3. STIFFNESS PROPERTIES

SD = FLECTURAL RIGIDITY (KN-M**2)
SHEAR DEFORMATION INCLUDED
STEEL BAR SLIP INCLUDED
MC = CRACKING MOMENT (KN-M.)
MY = YIELDING MOMENT (KN-M.)

	SD1	SD2	SD3	MC	MY
BEAM	5.68	1.38	0.043	0.031	0.086
COLUMN	9.71	2.25	0.083	0.055	0.122

4. LOADING PROCESS (LOAD INCREMENT *1/50)

CYCLE	LOAD (KN.)
1	1.0
2	0.0
3	-1.0
4	0.0
5	1.0

TABLE 5.3 ASSUMED CHARACTERISTICS OF A CANTILEVER WALL SPECIMEN FOR LOAD-DISPLACEMENT RELATIONSHIP STUDY

1. MATERIAL PROPERTIES

CONCRETE			
COMPRESSIVE STRENGTH	f'_c	(MPA)	33.1
TENSILE STRENGTH	f_t	(MPA)	2.86
YOUNG MODULUS	E_c	(MPA)	27200 *(22000)
SHEAR MODULUS	G	(MPA)	11600
STRAIN AT f'_c	ε_o		0.003
AT ULTIMATE	ε_{cu}		0.004
AT f_t	ε_t		0.000105
STEEL REINFORCEMENT			
YIELD STRESS	f_{sy}	(MPA)	338
ULTIMATE STRESS	f_{su}	(MPA)	386
YOUNG MODULUS	E_s	(MPA)	200000
STRAIN AT YIELD	ε_y		0.00169
AT ULTIMATE	ε_{su}		0.08
AT STRAIN HARDENING			0.01

* THE VALUE IN THE ( ) IS PREFERABLE

TABLE 5.3 (CONTINUED)

2. SECTION PROPERTIES

	DIMENSION (MM.)	STEEL (WIRE)	LENGTH (MM.)
WALL	38.0 X 203.0	2 X 2-NO.2G	686.0

3. STIFFNESS PROPERTIES

SD = FLECTURAL RIGIDITY (KN-M**2.)
SHEAR DEFORMATION INCLUDED
STEEL BAR SLIP INCLUDED
EI = FLEXURAL RIGIDITY (KN-M.**2)
MC = CRACKING MOMENT (KN-M.)
MY = YIELDING MOMENT (KN-M.)

(A) CONCENTRATED SPRING MODEL

	SD1	SD2	SD3	MC	MY
WALL	2097	525	22.2	0.98	4.42

(B) MULTIPLE SPRING MODEL

NUMBER OF ELEMENTS 7
LEGTH OF EACH ELEMENT MM. (FIXED END TO FREE END)
12.7 25.3 63.5 101.8 127.0 177.8 177.8

	EA	GA	EI1	EI2	EI3	MC	MY
EACH WALL ELEMENT	193000	35000	661	204	1.8	0.98	4.42

TABLE 5.3 (CONTINUED)

(C) LAYERED MODEL

LENGTH (MM.)	686.0
LENGTH OF INELASTIC ZONE (MM.)	71.
CROSS-SECTION (MM.)	38.0 X 203.0
NUMBER OF CONCRETE LAYERS	40
" UNCONFINED LAYERS (EACH,TOP AND BOTTOM)	4
WIDTH OF UNCONFINED CONCRETE ON EACH SIDE OF CROSS-SECTION (MM)	5.1
STEEL REINFORCEMENT (TOP AND BOTTOM)	2X2 NO.2G WIRES

STEEL AREA AND DISTANCE FROM THE TOP OF THE CROSS SECTION

	AREA(MM**2)	DISTANCE(MM.)
(1)	70	10.2
(2)	70	193.0

4. LOADING PROCESS (LOAD INCREMENT *1/50)

CYCLE	LOAD (KN.)
1	6.85
2	0.0
3	-6.50
4	0.0
5	7.40
6	0.0
7	-6.50
8	0.0

TABLE 6.1 SUMMARY OF ASSUMED ANALYTICAL CONDITIONS FOR NUMERICAL EXAMPLES

(A) STATIC LOADING

GENERAL CONDITIONS

LOADING SHAPE	TRIANGULAR SHAPE OVER HIGHT
MAXIMUM LOAD AT TOP	4.45 KN.
LOADING INCREMENT	MAXIMUM LOAD *1/50

CASE	TYPE	LOADING CONDITION	TYPE OF CANTILEVER BEAM MODEL	HYSTERESIS MODEL
1	FW-1	MONOTONIC	C, M	1
2	FW-2	MONOTONIC	C, M	1
3	FW-2	MONOTONIC	C, M, L	1
4	FW-2	CYCLIC	C, M, L	1

WHERE

C = CONCENTRATED SPRING MODEL
M = MULTIPLE SPRING MODEL
L = LAYERED MODEL

TABLE 6.1 (CONTINUED)

(B) DYNAMIC LOADING

GENERAL CONDITIONS

DAMPING FACTOR	0.02
TIME INTERVAL, SEC.	0.0004
DURATION TIME, SEC.	3.0
NUMBER OF STEPS	7500

CASE	TYPE	EXPERIMENTAL RUN	MAXIMUM BASE ACC.	TYPE OF CANTILEVER BEAM MODEL	HYSTERESIS MODEL
1	FW-1	RUN-1	0.55G	C, M	1
2	FW-1	RUN-3	2.41G	C, M	1
3	FW-2	RUN-1	0.49G	C, M	1
4	FW-2	RUN-2	0.92G	C, M	1
5	FW-2	RUN-2	0.92G	C, M	2

WHERE

C = CONCENTRATED SPRING MODEL
M = MULTIPLE SPRING MODEL

TABLE 6.2 ASSUMED MATERIAL PROPERTIES FOR FRAME-WALL STRUCTURES

PROPERTIES

CONCRETE

			FW-1	FW-2
COMPRESSIVE STRENGTH	f'_c	(MPA)	33.1	42.1
TENSILE STRENGTH	f_t	(MPA)	2.86	3.24
YOUNG MODULUS	E_c	(MPA)	27200	30700
			*(19300)	*(23000)
SHEAR MODULUS	G	(MPA)	11600	13100
STRAIN AT f'_c	ε_o		0.003	0.003
AT ULTIMATE	ε_{cu}		0.004	0.004
AT f'_t	ε_t		0.000105	0.000105

STEEL REINFORCEMENT

			FW-1 AND FW-2	
			BEAMS COLUMNS	WALLS
YIELD STRESS	f_y	(MPA)	352	338
ULTIMATE STRESS	f_{su}	(MPA)	382	400
YOUNG MODULUS	E_s	(MPA)	200000	200000
STRAIN AT YIELD	ε_y		0.00178	0.00170
STRAIN AT ULTIMATE	ε_{su}		0.07	0.07
STRAIN AT STRAIN HARDENING			0.01	0.002

* THE VALUE IN THE ( ) IS PREFERABLE

TABLE 6.3 CONFIGURATIONS OF THE STRUCTURES FW-1 AND FW-2

1. COMMON PARAMETERS

NO. OF STORIES	10
HEIGHT OF EACH STORY (MM.)	229.
WEIGHT OF EACH STORY (Kg.)	454
BEAM LENGTH (MM.)	305.
" RIGID ZONE LENGTH	25.4
COLUMN LENGTH (MM.)	229.
" RIGID ZONE LENGTH	19.
UNLOADING COEFFICIENT FOR HYSTERESIS RULES	0.5

2. WALL MEMBERS

NO. OF ELEMENTS FOR WALL MEMBERS AND LENGTH OF EACH ELEMENT

		(FROM TOP TO BOTTOM)						
LEVEL	NO.	1	2	3	4	5	6	7
10	2	114.3	114.3					
9	2	114.3	114.3					
8	2	114.3	114.3					
7	3	76.2	76.2	76.2				
6	3	76.2	76.2	76.2				
5	3	76.2	76.2	76.2				
4	3	76.2	76.2	76.2				
3	4	57.2	57.2	57.2	57.0			
2	4	57.2	57.2	57.2	57.0			
1	7	38.1	38.1	38.1	38.1	38.1	25.4	12.7

TABLE 6.4 STIFFNESS PROPERTIES OF CONSTITUENT MEMBERS OF THE STRUCTURES FW-1 AND FW-2

EA = AXIAL RIGIDITY (KN.)
GA = SHEAR RIGIDITY (KN.)
EI = FLEXURAL RIGIDITY (KN-M**2.) SHOWN IN FIG.3.5
SD = " SHOWM IN FIG.3.4 SHEAR DEFORMATION INCLUDED STEEL BAR SLIP INCLUDED
MC = CRACKING MOMENT (KN-M.)
MY = YIELDING MOMENT (KN-M.)

WALL MEMBERS (FW-1)

LEVEL	EA	GA	EI1	EI2	EI3	MC	MY
10	211000.	37600.	726.	242.	2.6	0.76	4.23
9	211000.	37600.	726.	242.	2.6	0.76	4.23
8	211000.	37600.	726.	242.	2.6	0.76	4.23
7	211000.	37600.	726.	242.	2.6	0.76	4.23
6	211000.	37600.	726.	515.	8.6	0.76	7.54
5	211000.	37600.	726.	515.	8.6	0.76	7.54
4	211000.	37600.	726.	717.	12.6	0.76	14.12
3	211000.	37600.	726.	717.	12.6	0.76	14.12
2	211000.	37600.	726.	717.	12.6	0.76	14.12
1	211000.	37600.	726.	717.	12.6	0.76	14.12

BEAM MEMBERS (FW-1)

LEVEL	SD1	SD2	SD3	MC	MY
10	6.51	1.20	0.049	0.026	0.086
9	8.80	1.83	0.098	0.026	0.126
8	8.80	1.83	0.098	0.026	0.126
7	8.80	1.83	0.098	0.026	0.126
6	8.80	1.83	0.098	0.026	0.126
5	8.80	1.83	0.098	0.026	0.126
4	6.51	1.20	0.049	0.026	0.086
3	6.51	1.20	0.049	0.026	0.086
2	6.51	1.20	0.049	0.026	0.086
1	6.51	1.20	0.049	0.026	0.086

TABLE 6.4 (CONTINUED)

EA = AXIAL RIGIDITY (KN.)
GA = SHEAR RIGIDITY (KN.)
SD = FLEXURAL RIGIDITY (KN-M**2.)
SHEAR DEFORMATION INCLUDED
STEEL BAR SLIP INCLUDED
MC = CRACKING MOMENT (KN-M.)
MY = YIELDING MOMENT (KN-M.)

EXTERIOR COLUMN MEMBERS (FW-1)

LEVEL	EA	SD1	SD2	SD3	MC	MY
10	52700.	8.38	1.82	0.060	0.047	0.124
9	52700.	8.38	1.82	0.060	0.047	0.124
8	52700.	9.34	2.23	0.066	0.067	0.158
7	52700.	9.34	2.23	0.066	0.067	0.158
6	52700.	9.34	2.23	0.066	0.067	0.158
5	52700.	9.34	2.23	0.066	0.067	0.158
4	52700.	10.50	2.72	0.080	0.085	0.194
3	52700.	10.50	2.72	0.080	0.085	0.194
2	52700.	10.50	2.72	0.080	0.085	0.194
1	52700.	10.50	2.72	0.080	0.085	0.194

INTERIOR COLUMN MEMBERS (FW-1)

LEVEL	EA	SD1	SD2	SD3	MC	MY
10	52700.	12.64	2.83	0.066	0.047	0.170
9	52700.	12.64	2.83	0.066	0.047	0.170
8	52700.	9.34	2.23	0.066	0.067	0.158
7	52700.	9.34	2.23	0.066	0.067	0.158
6	52700.	9.34	2.23	0.066	0.067	0.158
5	52700.	9.34	2.23	0.066	0.067	0.158
4	52700.	10.50	2.72	0.080	0.085	0.194
3	52700.	10.50	2.72	0.080	0.085	0.194
2	52700.	10.50	2.72	0.080	0.085	0.194
1	52700.	10.50	2.72	0.080	0.085	0.194

TABLE 6.4 (CONTINUED)

EA = AXIAL RIGIDITY (KN.)
GA = SHEAR RIGIDITY (KN.)
EI = FLEXURAL RIGIDITY (KN-M**2)
SHOWN IN FIG.3.5
SD = " SHOWM IN FIG.3.4
SHEAR DEFORMATION INCLUDED
STEEL BAR SLIP INCLUDED
MC = CRACKING MOMENT (KN-M.)
MY = YIELDING MOMENT (KN-M.)

WALL MEMBERS (FW-2)

LEVEL	EA	GA	EI1	EI2	EI3	MC	MY
10	237600.	42270.	818.	263.	2.6	0.85	4.23
9	237600.	42270.	818.	263.	2.6	0.85	4.23
8	237600.	42270.	818.	263.	2.6	0.85	4.23
7	237600.	42270.	818.	263.	2.6	0.85	4.23
6	237600.	42270.	818.	263.	2.6	0.85	4.23
5	237600.	42270.	818.	263.	2.6	0.85	4.23
4	237600.	42270.	818.	263.	2.6	0.85	4.23
3	237600.	42270.	818.	263.	2.6	0.85	4.23
2	237600.	42270.	818.	263.	2.6	0.85	4.23
1	237600.	42270.	818.	263.	2.6	0.85	4.23

BEAM MEMBERS (FW-2)

LEVEL	SD1	SD2	SD3	MC	MY
10	7.18	1.32	0.049	0.029	0.088
9	7.18	1.32	0.049	0.029	0.088
8	7.18	1.32	0.049	0.029	0.088
7	9.57	2.14	0.080	0.029	0.125
6	9.56	2.14	0.080	0.029	0.125
5	9.55	2.14	0.080	0.029	0.125
4	9.54	2.14	0.080	0.029	0.125
3	9.53	2.14	0.080	0.029	0.125
2	7.18	1.32	0.049	0.029	0.088
1	7.18	1.32	0.049	0.029	0.088

TABLE 6.4 (CONTINUED)

EA = AXIAL RIGIDITY (KN.)
GA = SHEAR RIGIDITY (KN.)
SD = FLEXURAL RIGIDITY (KN-M**2)
SHOWN IN FIG.3.4
SHEAR DEFORMATION INCLUDED
STEEL BAR SLIP INCLUDED
MC = CRACKING MOMENT (KN-M.)
MY = YIELDING MOMENT (KN-M.)

EXTERIOR COLUMN MEMBERS (FW-2)

LEVEL	EA	SD1	SD2	SD3	MC	MY
10	59400.	8.93	1.81	0.060	0.053	0.125
9	59400.	8.93	1.81	0.060	0.053	0.125
8	59400.	11.22	2.42	0.103	0.072	0.170
7	59400.	11.22	2.42	0.103	0.072	0.170
6	59400.	11.22	2.42	0.103	0.072	0.170
5	59400.	11.22	2.42	0.103	0.072	0.170
4	59400.	12.83	2.92	0.149	0.090	0.211
3	59400.	16.54	4.23	0.180	0.090	0.211
2	59400.	16.54	4.23	0.180	0.090	0.211
1	59400.	16.54	4.23	0.180	0.090	0.211

INTERIOR COLUMN MEMBERS (FW-2)

LEVEL	EA	SD1	SD2	SD3	MC	MY
10	59400.	8.93	1.81	0.060	0.053	0.125
9	59400.	8.93	1.81	0.060	0.053	0.125
8	59400.	11.22	2.42	0.103	0.072	0.170
7	59400.	11.22	2.42	0.103	0.072	0.170
6	59400.	11.22	2.42	0.103	0.072	0.170
5	59400.	11.22	2.42	0.103	0.072	0.170
4	59400.	12.83	2.92	0.149	0.090	0.211
3	59400.	12.83	2.92	0.149	0.090	0.211
2	59400.	12.83	2.92	0.149	0.090	0.211
1	59400.	12.83	2.92	0.149	0.090	0.211

TABLE 6.5 MODE SHAPES AND FREQUENCIES OF THE STRUCTURES FW-1 AND FW-2

1. FW-1

(A) MODE SHAPE

	BEFORE RUN -			AFTER 0.55G RUN-1			AFTER 2.41G RUN-3		
LEVEL	MODE			MODE			MODE		
	1	2	3	1	2	3	1	2	3
10	1.36	-0.56	0.32	1.43	-0.64	0.33	1.43	-0.65	0.33
9	1.26	-0.33	0.04	1.27	-0.31	-0.01	1.27	-0.31	-0.02
8	1.15	-0.07	-0.20	1.11	0.01	-0.27	1.11	0.02	-0.29
7	1.02	0.17	-0.31	0.94	0.28	-0.34	0.94	0.30	-0.35
6	0.87	0.36	-0.24	0.76	0.46	-0.20	0.77	0.46	-0.18
5	0.70	0.47	-0.03	0.59	0.54	0.05	0.60	0.51	0.08
4	0.52	0.49	0.21	0.42	0.51	0.28	0.44	0.48	0.29
3	0.35	0.40	0.34	0.27	0.40	0.37	0.29	0.38	0.37
2	0.19	0.25	0.30	0.14	0.24	0.31	0.16	0.24	0.31
1	0.06	0.10	0.14	0.04	0.09	0.15	0.06	0.09	0.15

(B) FREQUENCY, HZ

	5.0	17.8	37.0	2.8	11.5	27.8	2.5	10.4	25.3

* MODAL PARTICIPATION FACTORS ARE INCLUDED IN MODE SHAPES

TABLE 6.5 (CONTINUED)

2. FW-2

(A) MODE SHAPE

	BEFORE RUN -			AFTER 0.49G RUN-1			AFTER 0.92G RUN-2		
LEVEL	MODE			MODE			MODE		
	1	2	3	1	2	3	1	2	3
10	1.39	-0.59	0.31	1.41	-0.60	0.29	1.39	-0.57	0.28
9	1.27	-0.32	0.02	1.27	-0.33	0.03	1.27	-0.32	0.03
8	1.13	-0.04	-0.22	1.13	-0.05	-0.18	1.15	-0.08	-0.17
7	0.99	0.20	-0.31	0.98	0.19	-0.28	1.02	0.14	-0.27
6	0.83	0.38	-0.22	0.82	0.38	-0.24	0.88	0.32	-0.23
5	0.66	0.49	0.00	0.66	0.50	-0.06	0.74	0.43	-0.07
4	0.49	0.49	0.22	0.50	0.52	0.15	0.59	0.47	0.14
3	0.33	0.40	0.34	0.35	0.46	0.31	0.43	0.42	0.29
2	0.18	0.25	0.29	0.20	0.32	0.32	0.27	0.30	0.30
1	0.05	0.09	0.14	0.07	0.14	0.18	0.11	0.14	0.17

(B) FREQUENCY, HZ

	5.3	18.3	38.8	2.4	10.4	26.4	2.0	8.8	23.4

* MODAL PARTICIPATION FACTORS ARE INCLUDED IN MODE SHAPES

TABLE 6.6 MAXIMUM RESPONSES OF FRAME-WALL STRUCTURES

(1) ACCELERATION (G.)

STRUCTURE	FW-1	FW-1	FW-2	FW-2	FW-2
RUN	R1	R3	R1	R2	R2,SL
MAX. BASE ACC.	0.55G	2.41G	0.49G	0.92G	0.92G
LEVEL					
10	1.06	1.48	0.68	0.84	0.84
	-1.23	-1.99	-0.68	-1.01	-0.97
9	0.68	0.95	0.55	0.60	0.60
	-0.90	-1.18	-0.52	-0.70	-0.63
8	0.61	0.84	0.49	0.51	0.51
	-0.71	-0.95	-0.42	-0.48	-0.45
7	0.63	0.92	0.48	0.47	0.46
	-0.64	-1.33	-0.42	-0.55	-0.55
6	0.67	1.11	0.46	0.44	0.40
	-0.62	-1.36	-0.40	-0.66	-0.68
5	0.63	1.10	0.42	0.56	0.51
	-0.58	-1.42	-0.44	-0.78	-0.78
4	0.62	1.26	0.37	0.54	0.54
	-0.51	-1.65	-0.45	-0.84	-0.83
3	0.61	1.32	0.31	0.62	0.65
	-0.47	-1.86	-0.44	-0.85	-0.82
2	0.59	1.28	0.33	0.68	0.71
	-0.42	-2.05	-0.42	-0.79	-0.76
1	0.57	1.31	0.36	0.66	0.67
	-0.37	-2.18	-0.44	-0.82	-0.82

SL = HYSTERESIS MODEL 2 USED FOR BEAM-COLUMN JOINTS

TABLE 6.6 (continued)

(2) DISPLACEMENT (MM.)

STRUCTURE	FW-1		FW-1		FW-2		FW-2		
RUN	R1		R3		R1		R2	R2,SL	
MAX. BASE ACC.	0.55G		2.41G		0.49G		0.92G		
LEVEL	C	E	C	E	C	E	C	C	E
10	28.9	28.2	45.7	58.5	23.1	28.4	41.2	43.3	42.8
	-24.3		-42.4		-23.6		-26.1	-33.2	
9	25.6	26.5	41.4	49.9	21.1	25.6	37.1	39.2	39.2
	-21.3		-37.1		-21.1		-23.7	-29.8	
8	22.4	23.8	36.8	41.0	18.8	23.6	32.8	34.9	32.7
	-18.3		-32.0		-18.6		-21.2	-26.3	
7	18.8	20.5	32.0	35.9	16.7	20.6	28.5	30.5	32.0
	-15.2		-26.7		-16.0		-18.6	-22.8	
6	15.3	17.0	26.9	29.4	14.3	17.3	24.0	25.9	27.5
	-12.1		-21.7		-13.3		-15.9	-19.2	
5	11.7	13.5	21.3	22.2	11.7	14.2	19.4	21.1	23.4
	-8.9		-16.8		-10.6		-13.0	-15.6	
4	8.5	9.5	16.2	17.0	9.1	10.7	14.9	16.3	16.2
	-6.4		-12.2		-8.0		-10.0	-12.0	
3	5.3	7.1	11.1	11.9	6.4	8.3	10.4	11.5	14.6
	-4.1		-8.0		-5.5		-7.1	-8.5	
2	2.8	4.1	6.4	7.1	3.9	5.1	6.3	7.0	8.9
	-2.1		-4.4		-3.1		-4.2	-5.1	
1	0.9	2.0	2.4	3.5	1.6	2.3	2.5	2.9	4.7
	-0.6		-1.7		-1.2		-1.6	-2.0	

C = COMPUTED RESPONSE RESULTS
E = EXPERIMENTAL RESPONSE RESULTS[2]
SL = HYSTERESIS MODEL 2 USED FOR BEAM-COLUMN JOINTS

TABLE 6.6 (continued)

(3) RELATIVE DISPLACEMENT (MM.)

STRUCTURE	FW-1	FW-1	FW-2	FW-2	FW-2
RUN	R1	R3	R1	R2	R2,SL
MAX. BASE ACC.	0.55G	2.41G	0.49G	0.92G	0.92G
LEVEL					
10	3.2	4.5	2.1	4.2	4.1
	-3.0	-5.1	-2.5	-2.5	-3.5
9	3.4	4.7	2.2	4.3	4.3
	-3.1	-5.1	-2.5	-2.5	-3.5
8	3.5	4.8	2.3	4.4	4.4
	-3.1	-5.1	-2.6	-2.6	-3.5
7	3.5	5.0	2.4	4.5	4.6
	-3.1	-4.9	-2.6	-2.7	-3.6
6	3.5	5.2	2.5	4.6	4.8
	-3.0	-4.8	-2.7	-2.9	-3.6
5	3.3	5.2	2.6	4.6	4.8
	-2.8	-4.5	-2.6	-3.0	-3.6
4	3.0	4.9	2.7	4.4	4.8
	-2.4	-4.0	-2.5	-3.0	-3.5
3	2.6	4.5	2.6	4.2	4.6
	-2.0	-3.4	-2.3	-2.9	-3.4
2	1.9	3.8	2.3	3.7	4.1
	-1.4	-2.7	-1.9	-2.5	-3.1
1	0.9	2.3	1.6	2.5	2.8
	-0.6	-1.6	-1.2	-1.6	-2.0

TABLE 6.6 (continued)

(4) STORY SHEAR (KN.)

STRUCTURE	FW-1	FW-1	FW-2	FW-2	FW-2
RUN	R1	R3	R1	R2	R2,SL
MAX. BASE ACC.	0.55G	2.41G	0.49G	0.92G	0.92G
LEVEL					
10	4.8	6.6	3.0	3.7	3.7
	-5.4	-8.9	-3.0	-4.5	-4.3
9	7.7	10.5	5.5	6.4	6.4
	-9.4	-13.2	-5.3	-7.6	-7.1
8	9.2	12.7	7.3	8.0	8.0
	-12.0	-15.0	-7.0	-9.4	-8.5
7	10.5	13.9	8.6	9.1	9.1
	-13.1	-16.9	-8.1	-9.8	-8.6
6	12.2	16.4	9.6	10.6	10.5
	-14.8	-15.9	-8.9	-10.3	-9.7
5	14.3	17.5	10.3	11.7	11.6
	-16.2	-18.2	-10.1	-11.5	-10.7
4	16.3	17.8	11.0	12.4	12.3
	-17.2	-20.2	-11.2	-12.3	-11.4
3	17.8	18.8	11.6	13.0	12.9
	-18.0	-21.5	-12.1	-13.1	-12.8
2	18.9	19.7	11.7	13.3	13.2
	-18.7	-22.9	-12.8	-16.0	-15.3
1	19.9	20.4	11.6	13.3	13.2
	-19.0	-27.7	-13.3	-18.7	-17.8

TABLE 6.6 (continued)

(5) WALL SHEAR (KN.)

STRUCTURE	FW-1	FW-1	FW-2	FW-2	FW-2
RUN	R1	R3	R1	R2	R2,SL
MAX. BASE ACC.	0.55G	2.41G	0.49G	0.92G	0.92G
LEVEL					
10	5.0	6.9	4.4	5.7	6.7
	-5.0	-5.3	-3.9	-4.4	-4.3
9	1.5	6.6	1.6	2.6	2.5
	-3.4	-5.8	-1.8	-4.3	-4.9
8	4.0	5.3	1.1	2.5	2.1
	-3.3	-6.9	-1.9	-3.0	-4.0
7	5.2	6.9	2.3	1.8	3.1
	-5.1	-10.6	-0.9	-4.0	-3.3
6	6.5	8.6	2.0	2.8	2.7
	-6.1	-9.0	-2.4	-3.4	-4.3
5	8.8	9.9	7.3	4.1	4.0
	-8.9	-12.4	-3.9	-4.3	-3.6
4	10.7	12.6	3.7	3.3	3.4
	-13.1	-13.9	-4.1	-4.6	-5.4
3	12.1	13.6	4.7	6.6	6.5
	-13.7	-15.7	-5.3	-5.9	-8.3
2	13.4	15.0	6.3	7.0	7.1
	-14.6	-18.1	-7.8	-11.4	-9.8
1	16.3	14.4	7.8	7.0	7.1
	-15.1	-22.9	-5.8	-8.3	-6.3

TABLE 6.6 (continued)

(6) OVERTURNING MOMENT (KN-M.)

STRUCTURE	FW-1	FW-1	FW-2	FW-2	FW-2
RUN	R1	R3	R1	R2	R2,SL
MAX. BASE ACC.	0.55G	2.41G	0.49G	0.92G	0.92G
LEVEL					
10	1.1	1.5	0.7	0.9	0.9
	-1.2	-2.0	-0.7	-1.0	-1.0
9	2.9	3.8	1.9	2.3	2.3
	-3.4	-5.0	-1.9	-2.8	-2.6
8	4.9	6.7	3.6	4.2	4.2
	-6.1	-8.1	-3.5	-4.9	-4.5
7	7.1	9.7	5.6	6.1	6.1
	-9.1	-11.1	-5.3	-7.2	-6.5
6	9.3	12.7	7.7	8.1	8.1
	-12.1	-14.7	-7.3	-9.3	-8.2
5	12.2	15.7	9.8	10.5	10.3
	-15.2	-17.5	-9.3	-11.0	-10.1
4	15.3	19.5	12.2	13.2	13.0
	-18.9	-20.0	-11.3	-13.1	-12.6
3	18.5	23.1	14.7	15.9	15.8
	-22.6	-24.1	-13.9	-15.8	-15.1
2	22.8	26.8	17.1	18.8	18.7
	-26.5	-28.3	-16.7	-18.6	-17.8
1	27.3	31.3	19.5	21.7	21.7
	-30.3	-33.7	-19.8	-21.5	-20.6

TABLE 6.7 PROPERTIES OF LAYERED MODEL USED FOR THE STRUCTURE FW-2

1. MATERIAL PROPERTIES ASSUMED (COLUMN IN FW-2) ARE TABULATED IN TABLE 6.2

2. SECTION PROPERTIES

LENGTH (MM.)	114.5
LENGTH OF INELASTIC ZONE (MM.)	25.4
CROSS-SECTION (MM.)	38.0 X 51.0
NUMBER OF CONCRETE LAYERS	20
" UNCONFINED LAYERS (EACH, TOP AND BOTTOM)	4
WIDTH OF UNCONFINED CONCRETE ON EACH SIDE OF CROSS-SECTION (MM)	7.6
STEEL REINFORCEMENT (TOP AND BOTTOM)	3-NO.13G WIRES

STEEL AREA AND DISTANCE FROM THE TOP OF THE CROSS SECTION

	AREA(MM**2)	DISTANCE(MM.)
(1)	12.8	7.6
(2)	12.8	43.2

3. LOADING PROCESS (KN.) (VALUES OF TOP LATERAL FORCE IN TRIANGULAR LOAD SHAPE)

CYCLE	1	2	3	4	5
CASE A	3.56				
CASE B.	2.67	0.0	-2.67	0.0	2.67

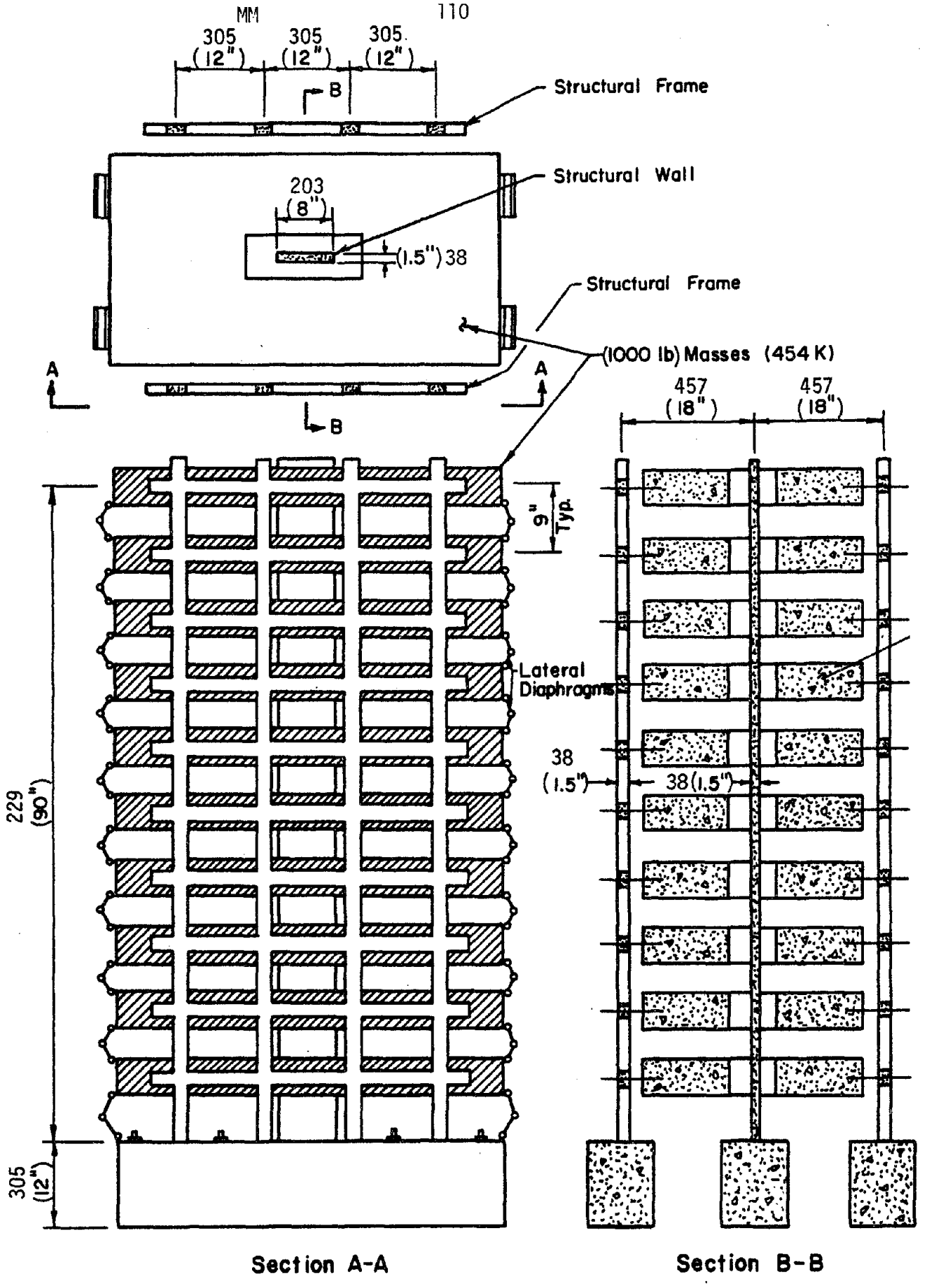

FIG. 2.1 REINFORCED CONCRETE FRAME-WALL TEST STRUCTURE

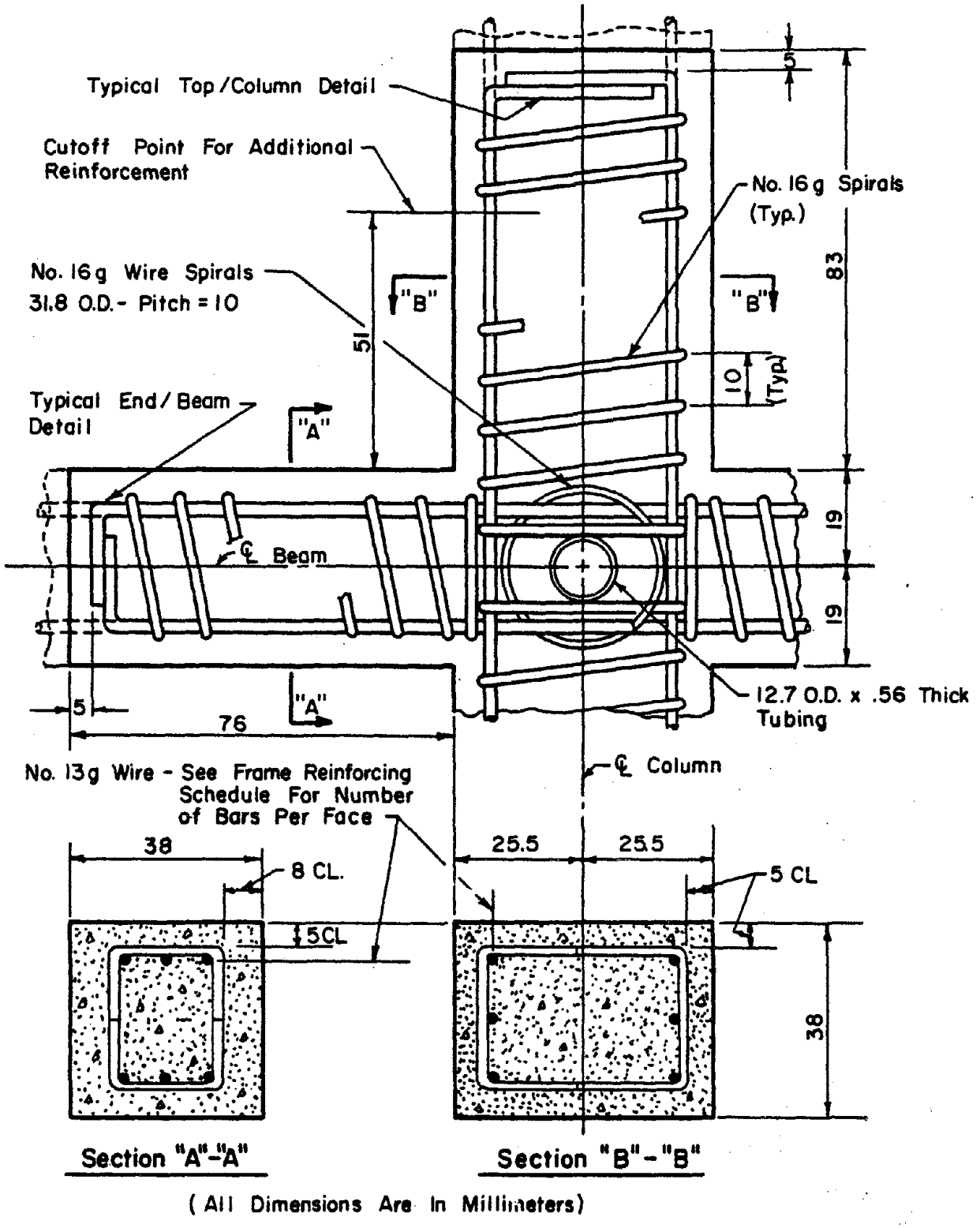

FIG. 2.2 REINFORCEMENT DETAILS OF STRUCTURAL COMPONENTS

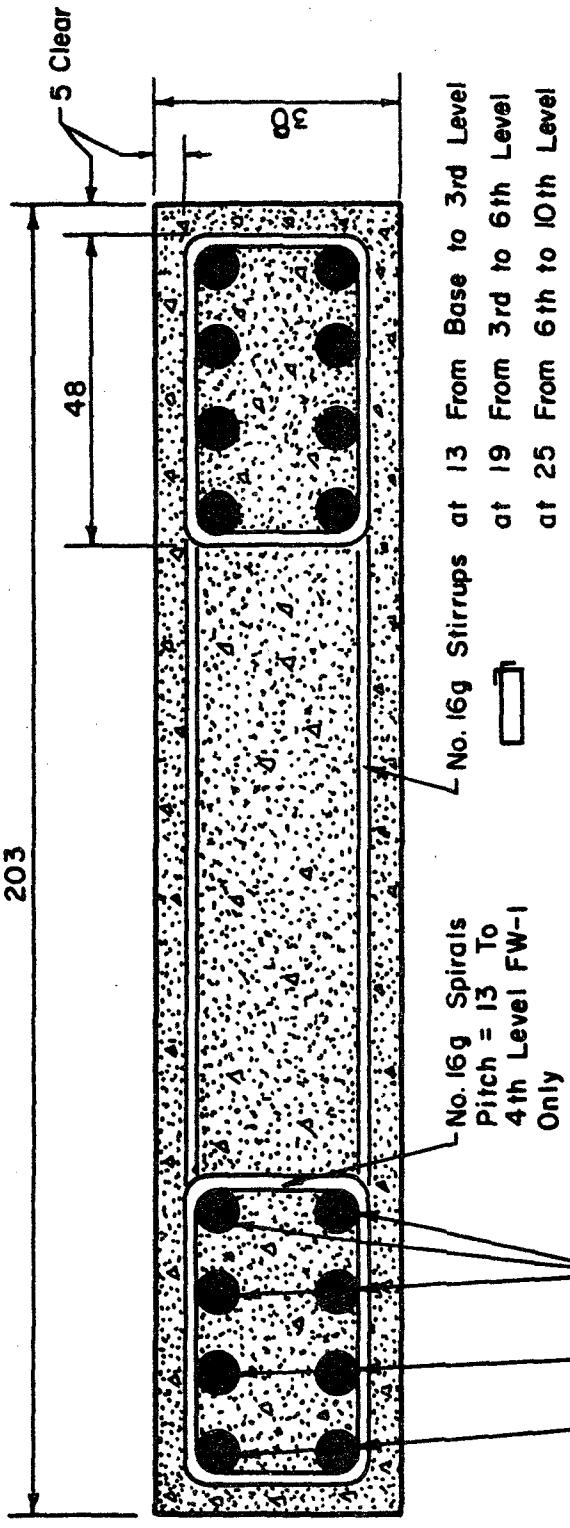

FIG. 2.2 (continued)

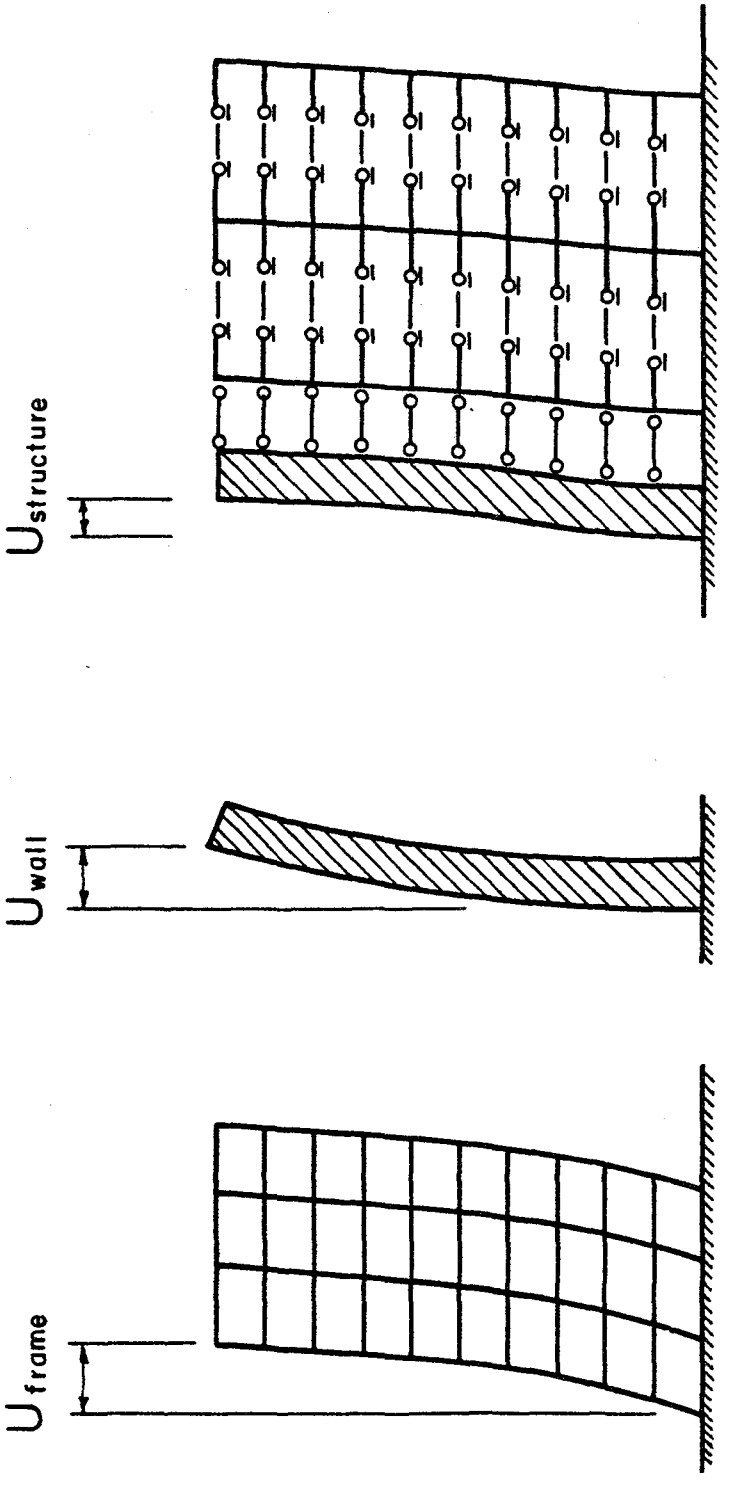

FIG. 2.3 DEFORMATION MODES OF FRAME-WALL STRUCTURES

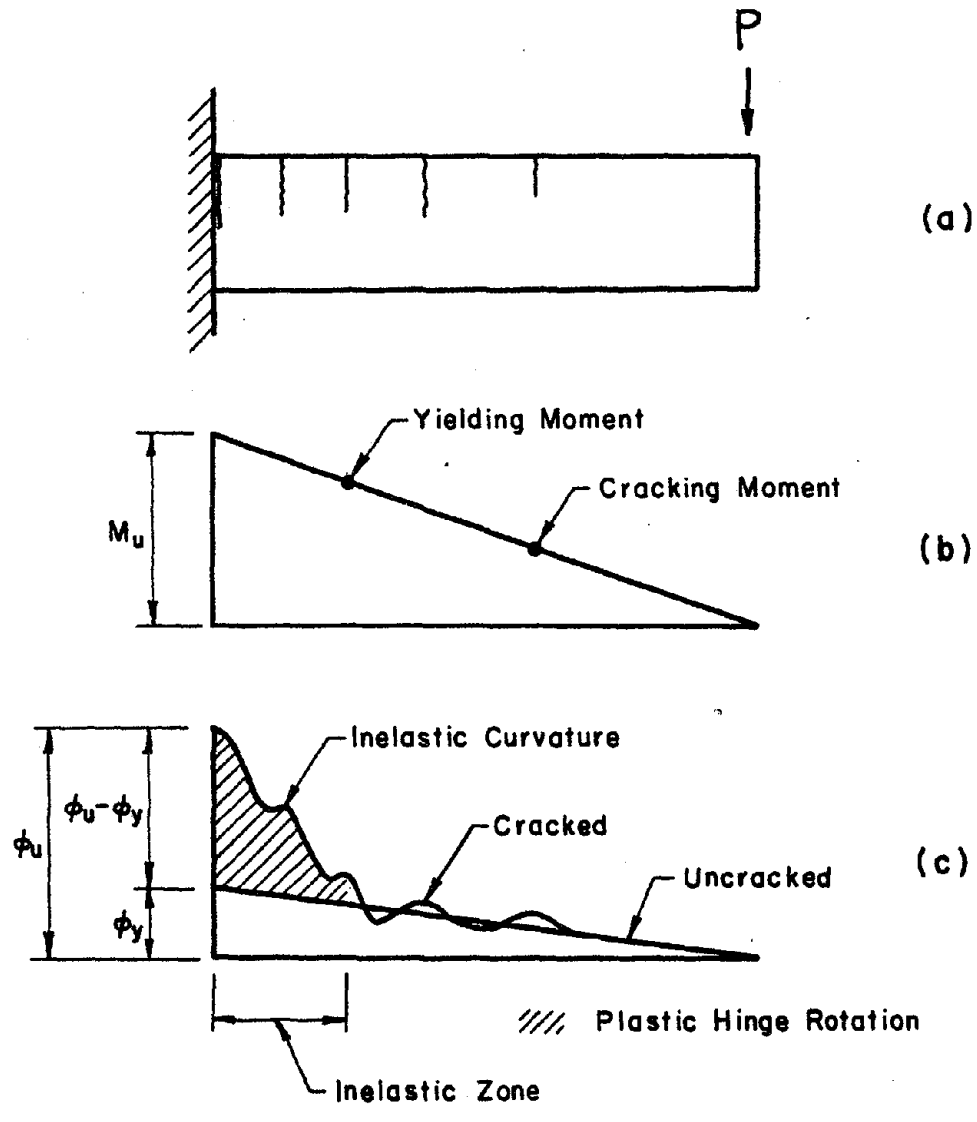

(a) Cantilever Beam
(b) Bending Moment Diagram
(c) Curvature Diagram

ϕ_y = Curvature Due To Elastic Deformation

ϕ_u = Curvature Due To Plastic Deformation

FIG. 2.4 CURVATURE DISTRIBUTION ALONG A CANTILEVER BEAM [36]

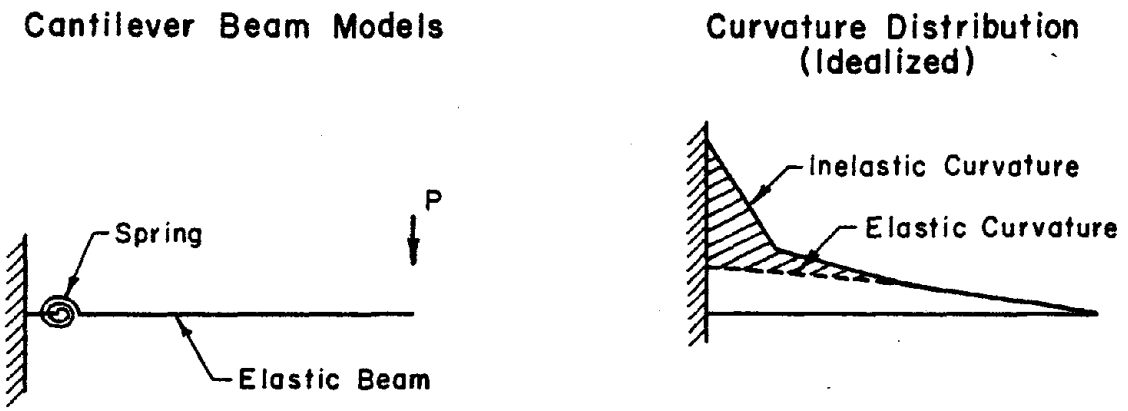

(a) Concentrated Spring Model

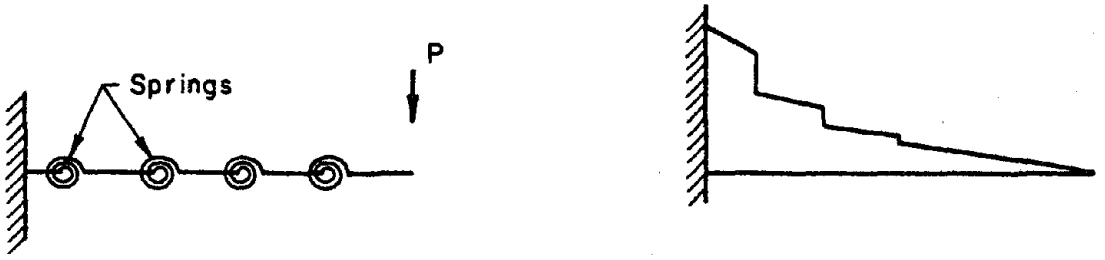

(b) Multiple Spring Model

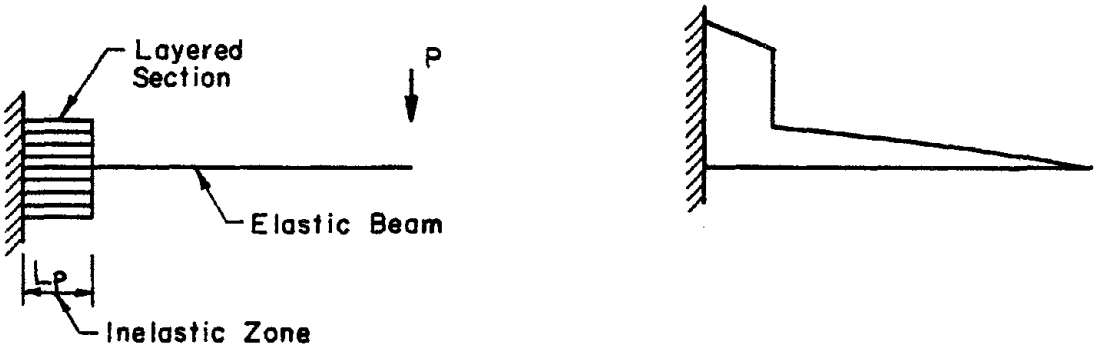

(c) Layered Model

FIG. 2.5 MECHANICAL MODELS USED IN INVESTIGATION

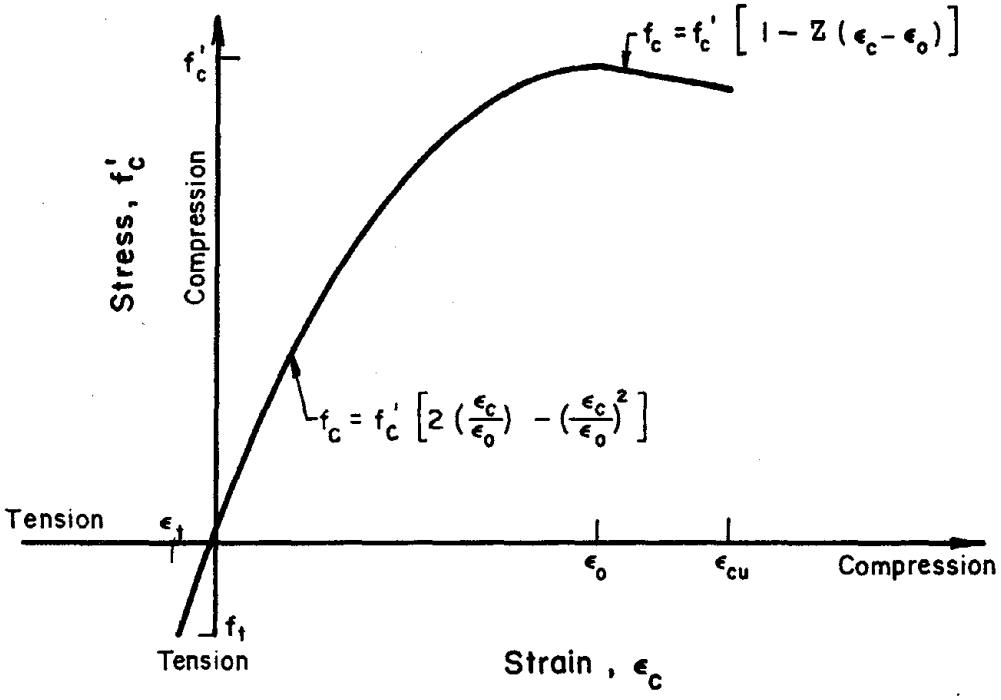

(a) Concrete

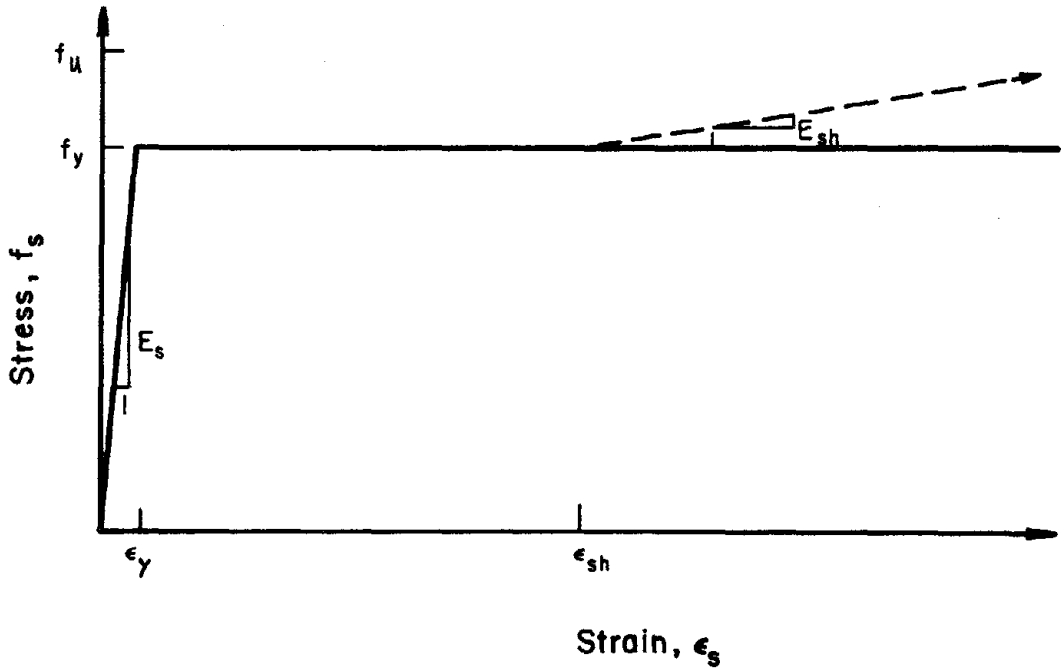

(b) Steel

FIG. 3.1 IDEALIZED STRESS-STRAIN RELATIONSHIPS FOR CONCRETE AND STEEL FOR THE CONCENTRATED SPRING AND MULTIPLE SPRING MODELS

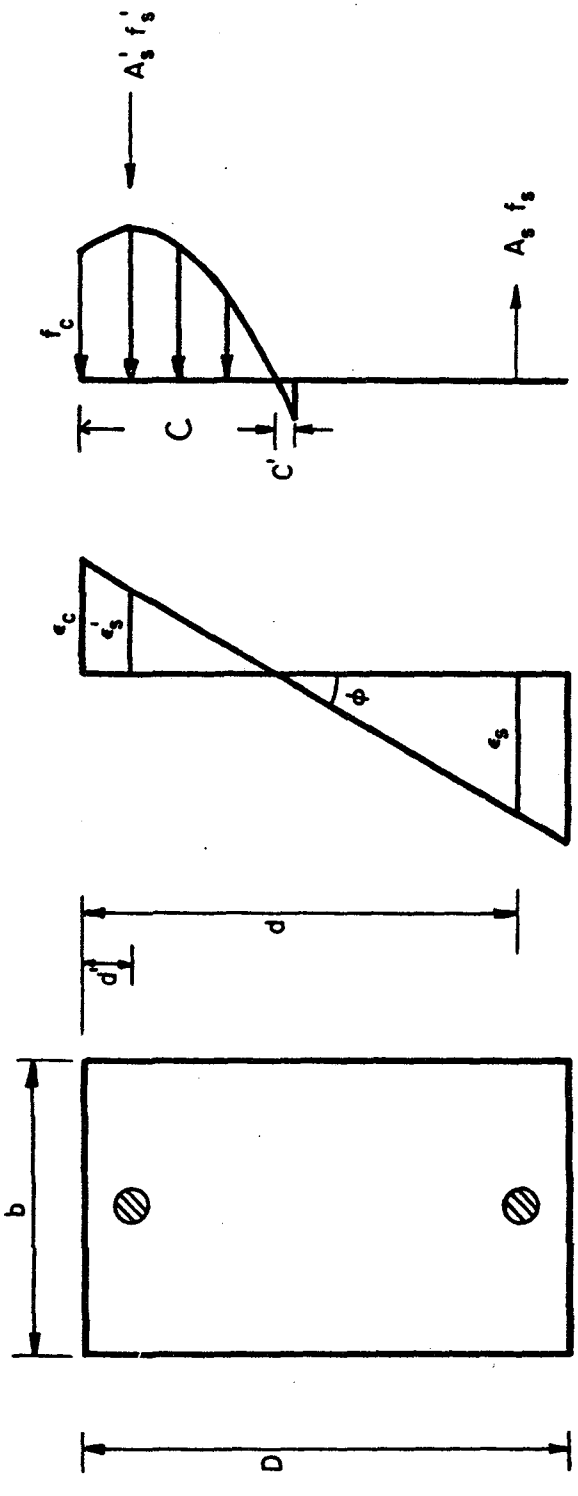

FIG. 3.2 DISTRIBUTIONS OF STRESS AND STRAIN OVER A CROSS SECTION

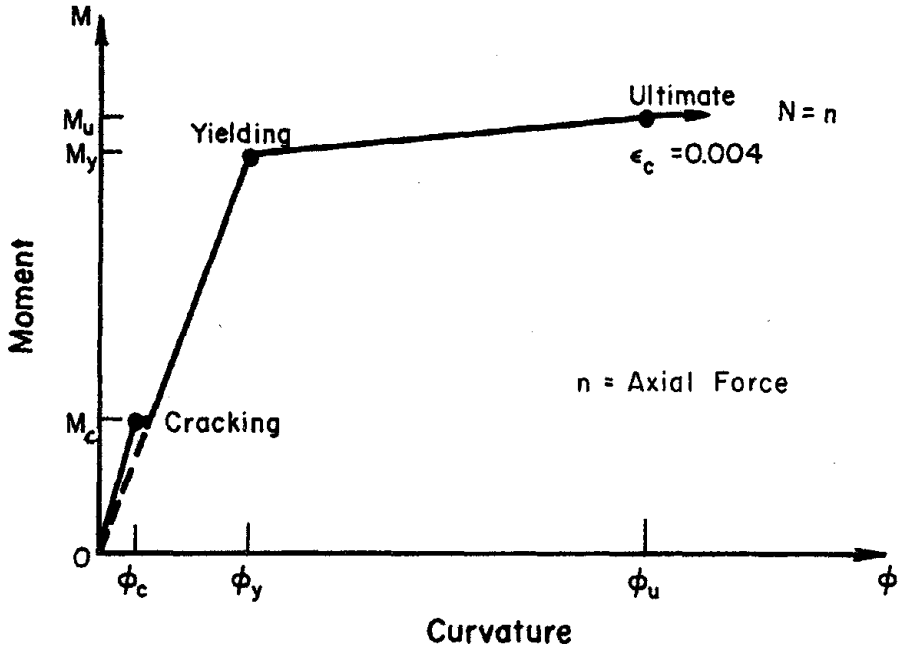

FIG. 3.3 IDEALIZED MOMENT-CURVATURE RELATIONSHIP USED FOR THE CONCENTRATED SPRING MODEL

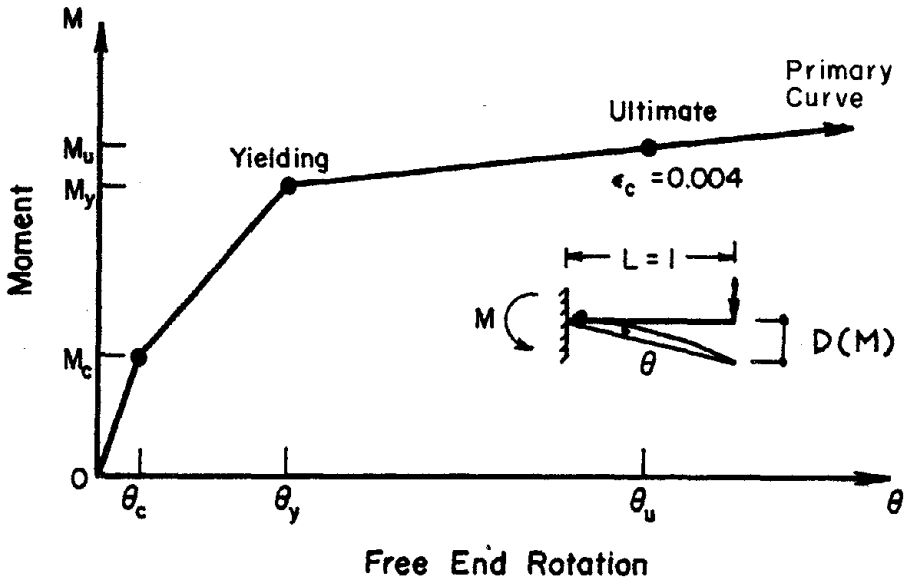

FIG. 3.4 IDEALIZED MOMENT-ROTATION RELATIONSHIP USED FOR THE CONCENTRATED SPRING MODEL

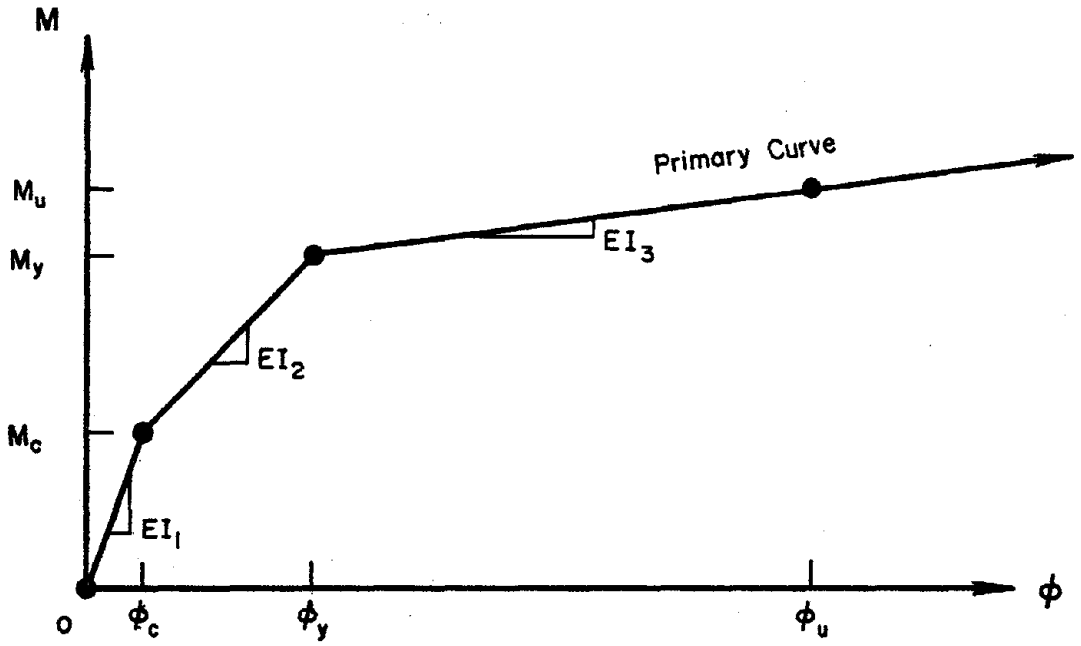

FIG. 3.5 IDEALIZED MOMENT-CURVATURE RELATIONSHIP FOR EACH SPRING OF THE MULTIPLE SPRING MODEL

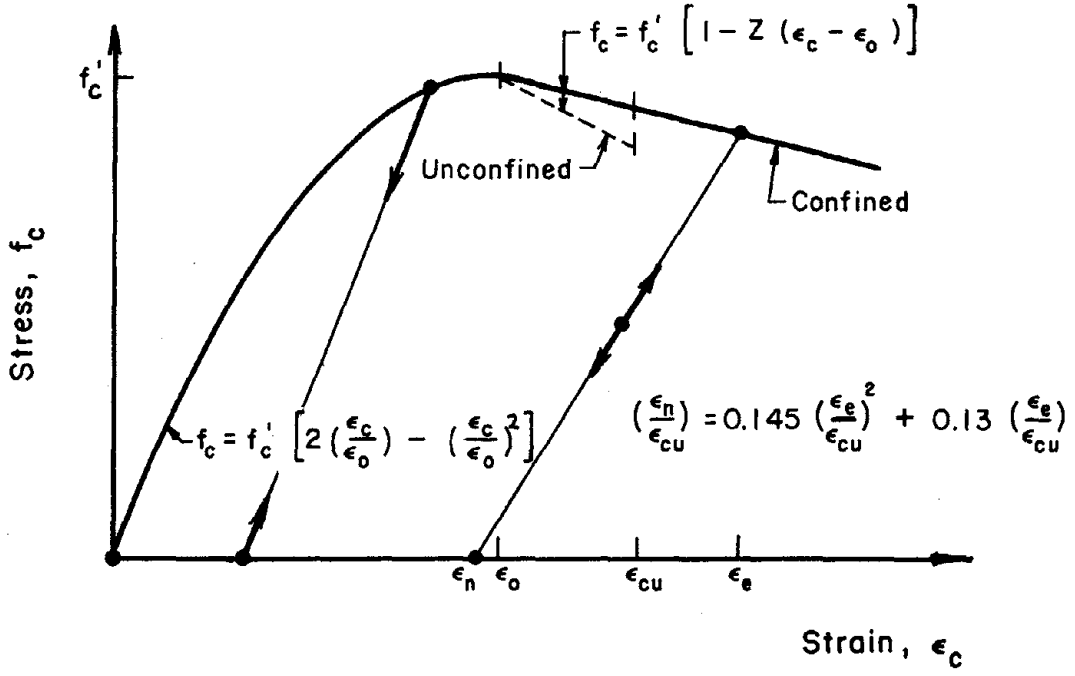

(a) Concrete

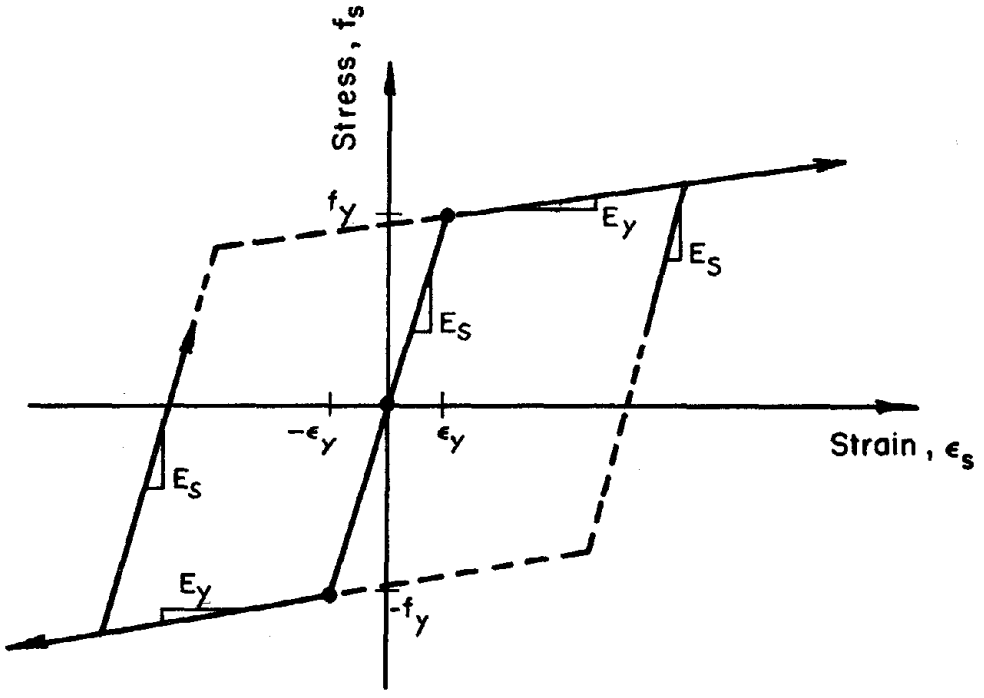

(b) Steel

FIG. 3.6 IDEALIZED STRESS-STRAIN RELATIONSHIPS USED WITH THE LAYERED MODEL

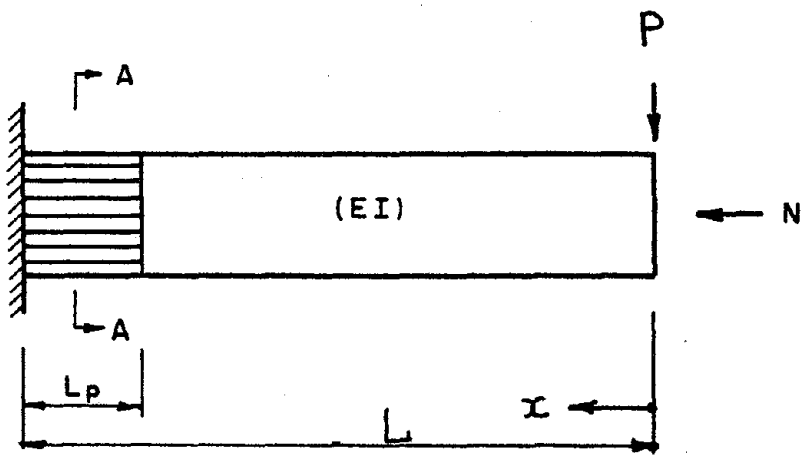

A Layered Model

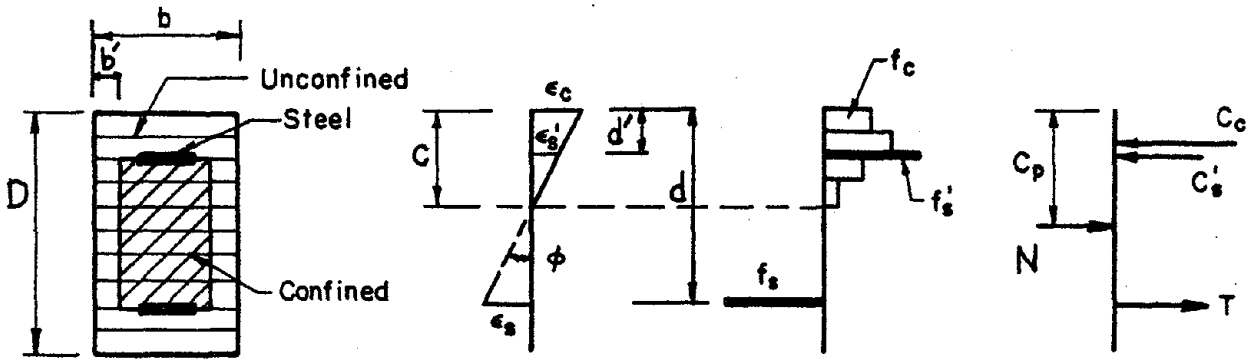

(a) Idealized A-A Section

(b) Imposed Strains

(c) Element Stresses

(d) Resultant Forces

FIG. 3.7 DISTRIBUTIONS OF STRESS AND STRAIN OVER A CROSS SECTION OF THE LAYERED MODEL

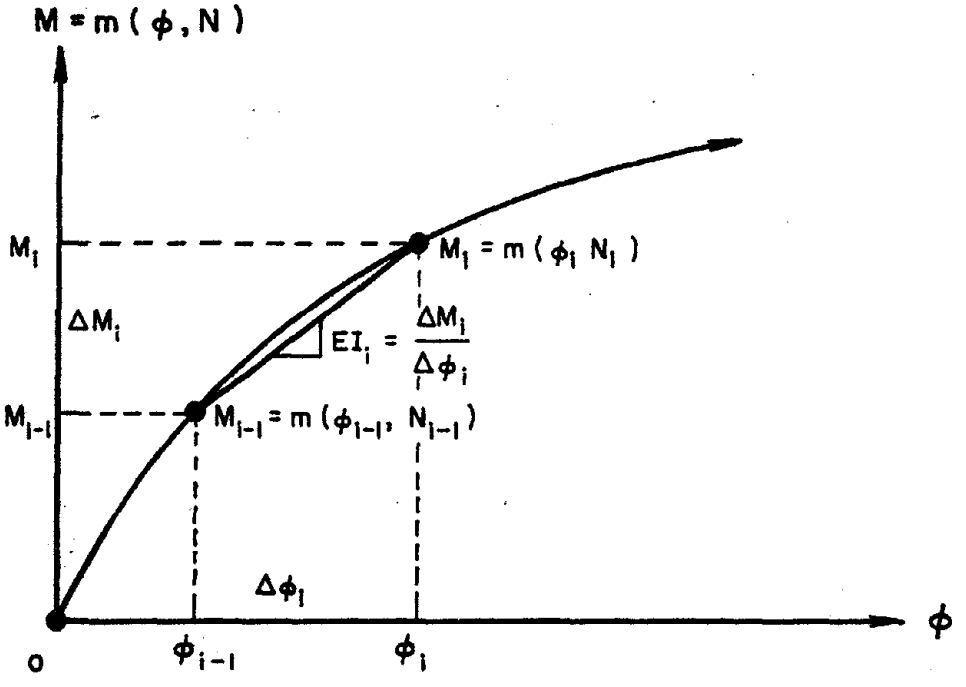

FIG. 3.8 INSTANTANEOUS MOMENT-CURVATURE RELATIONSHIPS FOR THE LAYERED SECTION OF THE LAYERED MODEL

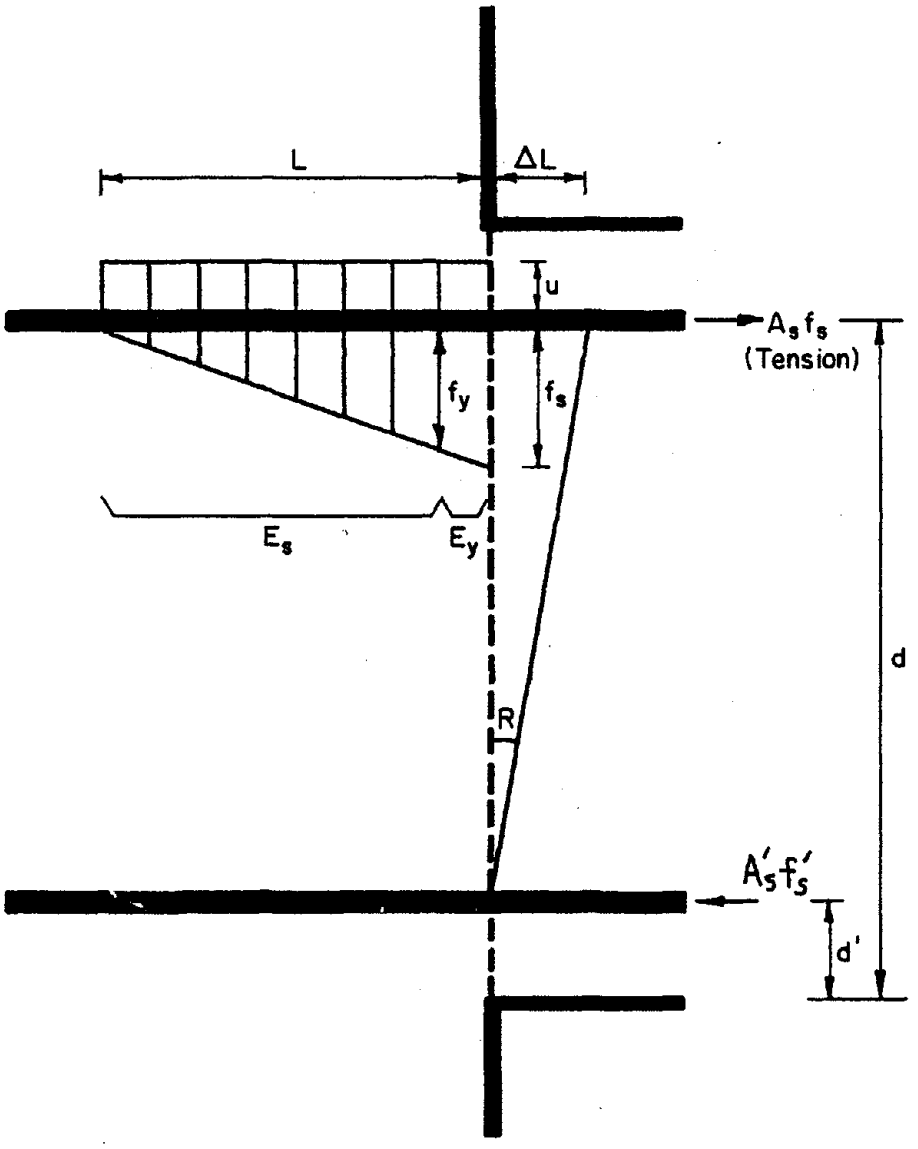

FIG. 3.9 BOND SLIP MECHANISM

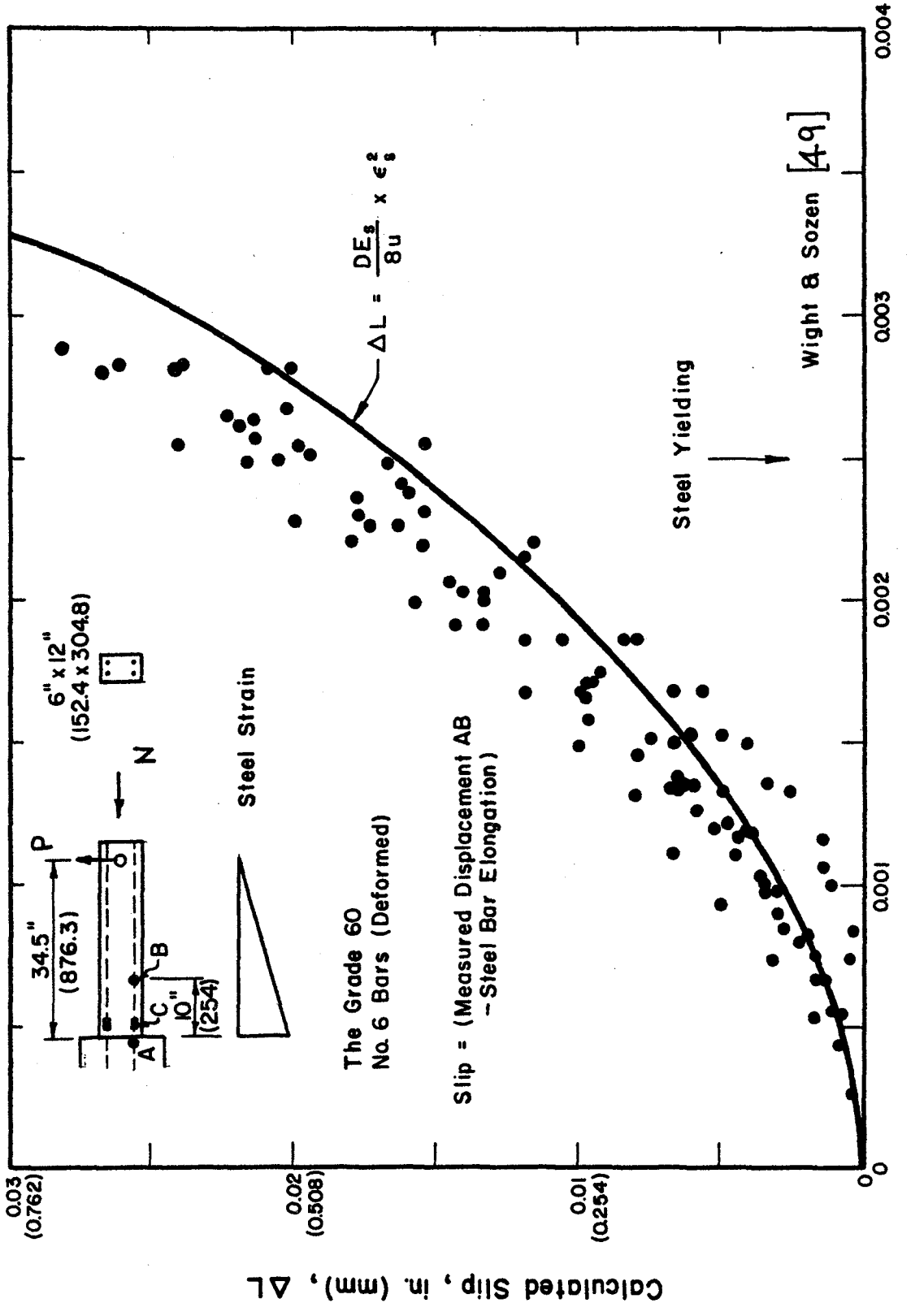

FIG. 3.10 COMPARISON OF COMPUTED BOND SLIP WITH EXPERIMENTAL DATA

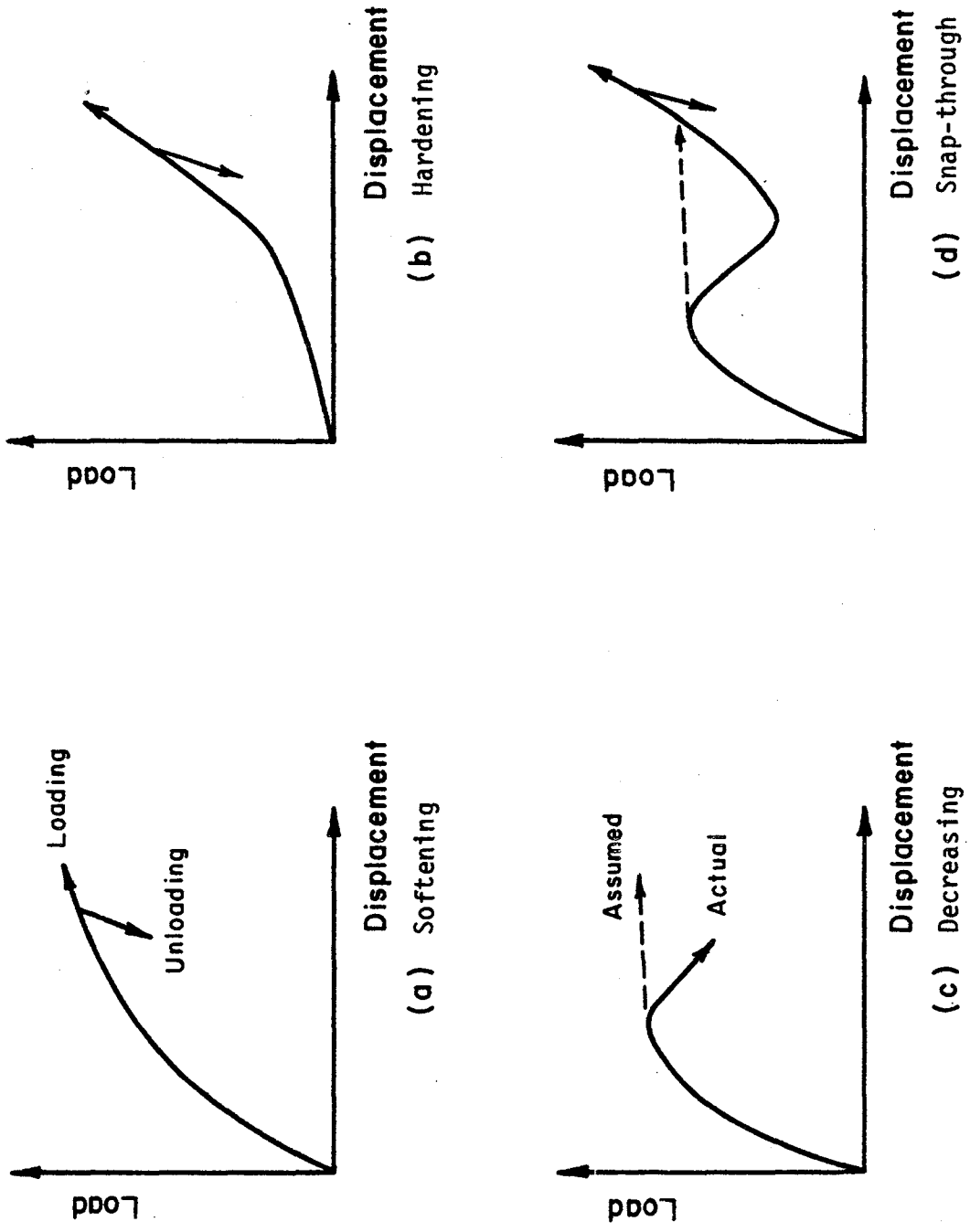

FIG. 3.11 TYPICAL LOAD-DISPLACEMENT CURVES FOR INELASTIC ANALYSIS

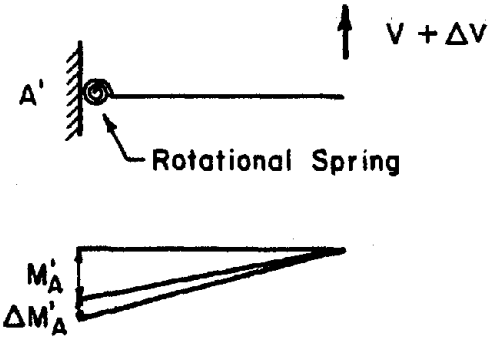

a) Concentrated Spring Model

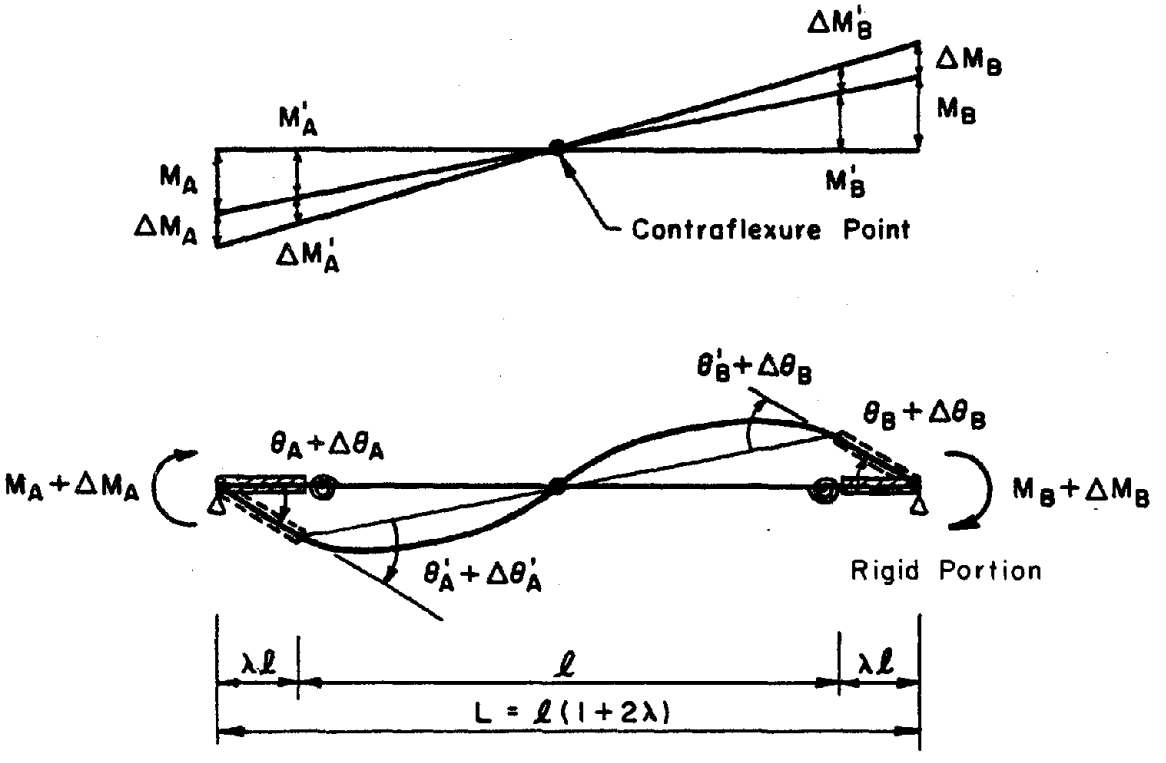

b) Equivalent Simple Beam Model

FIG. 4.1 DEFORMED SHAPES OF A CONCENTRATED SPRING MODEL AND AN EQUIVALENT SIMPLE BEAM MODEL

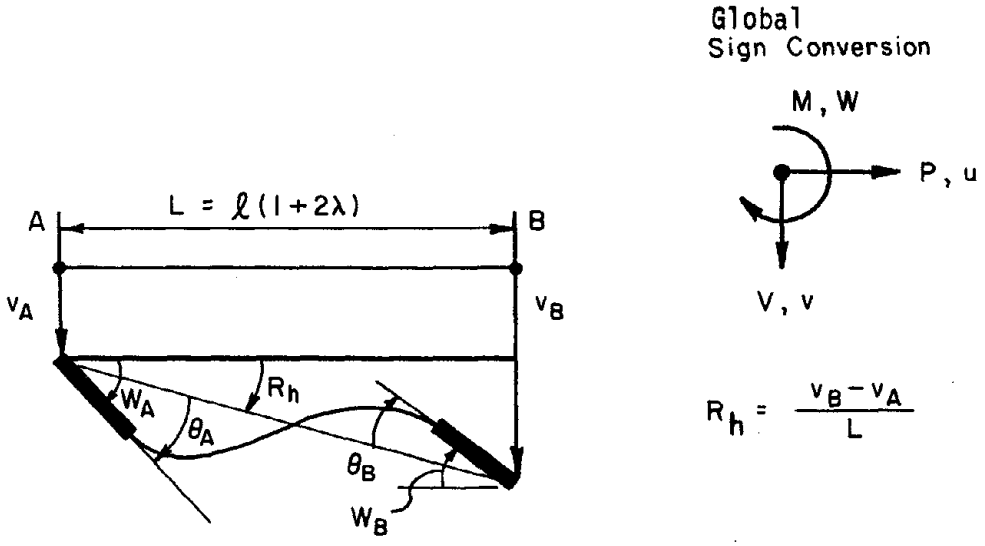

a) A Horizontal Member

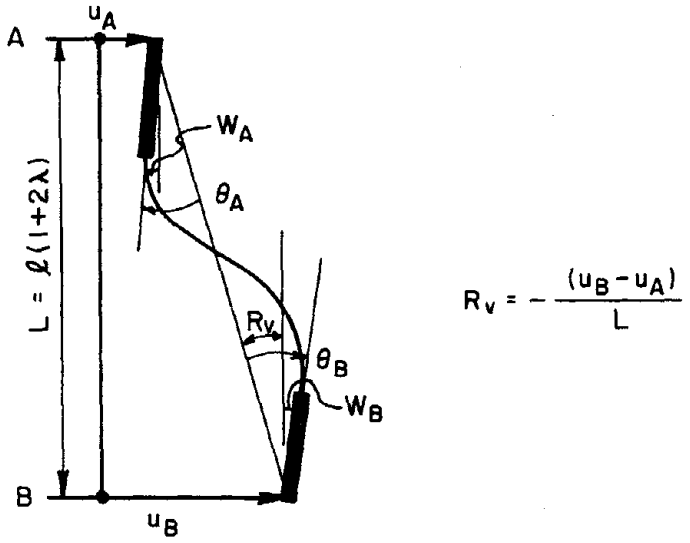

b) A Vertical Member

FIG. 4.2 TYPICAL MEMBERS IN GLOBAL COORDINATES SYSTEM

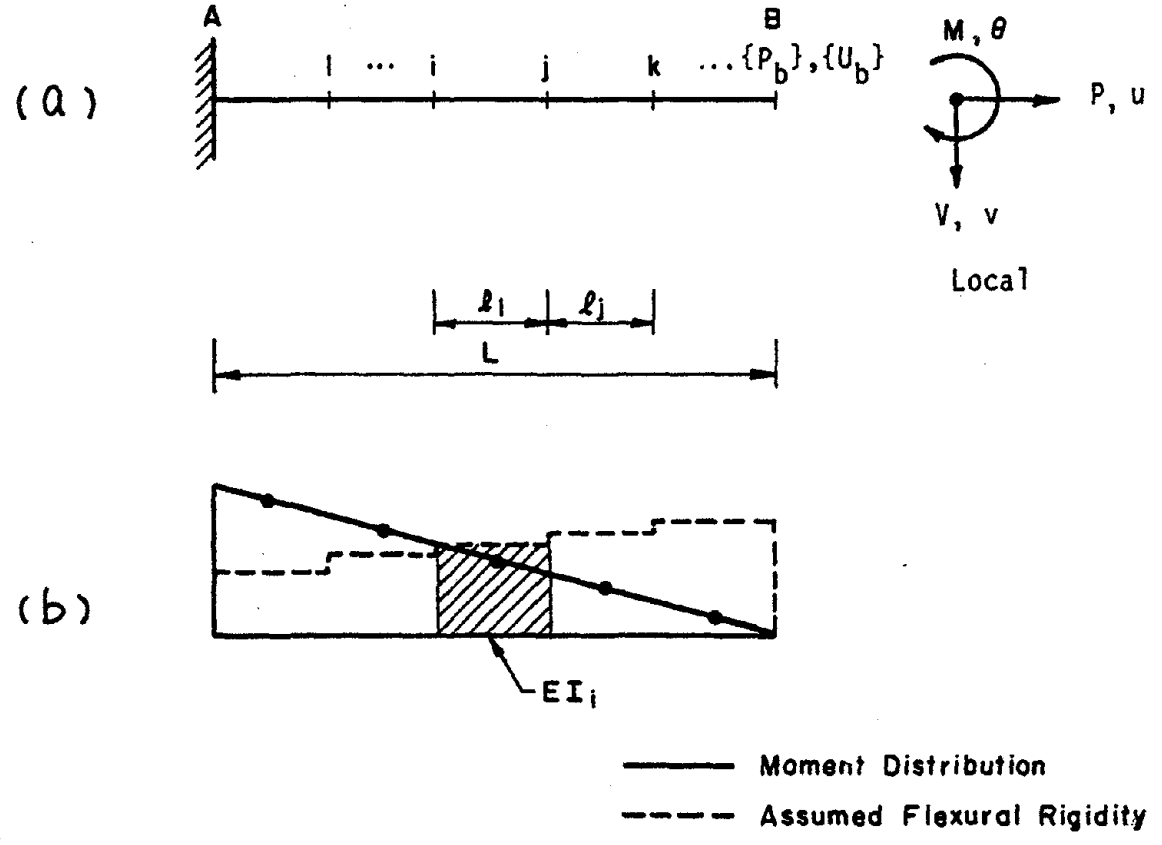

FIG. 4.3 MULTIPLE SPRING MODEL

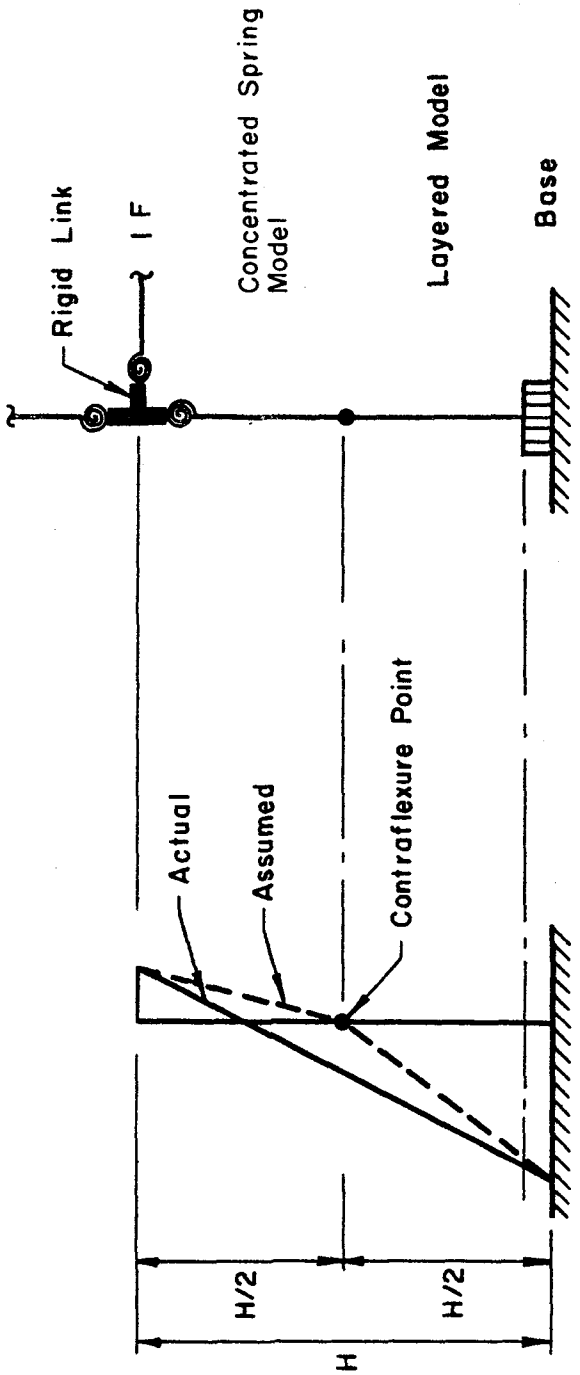

(a) Moment Distribution (b) 1st Story Column

FIG. 4.4 APPLICATION OF THE LAYERED MODEL TO 1ST STORY EXTERIOR COLUMNS

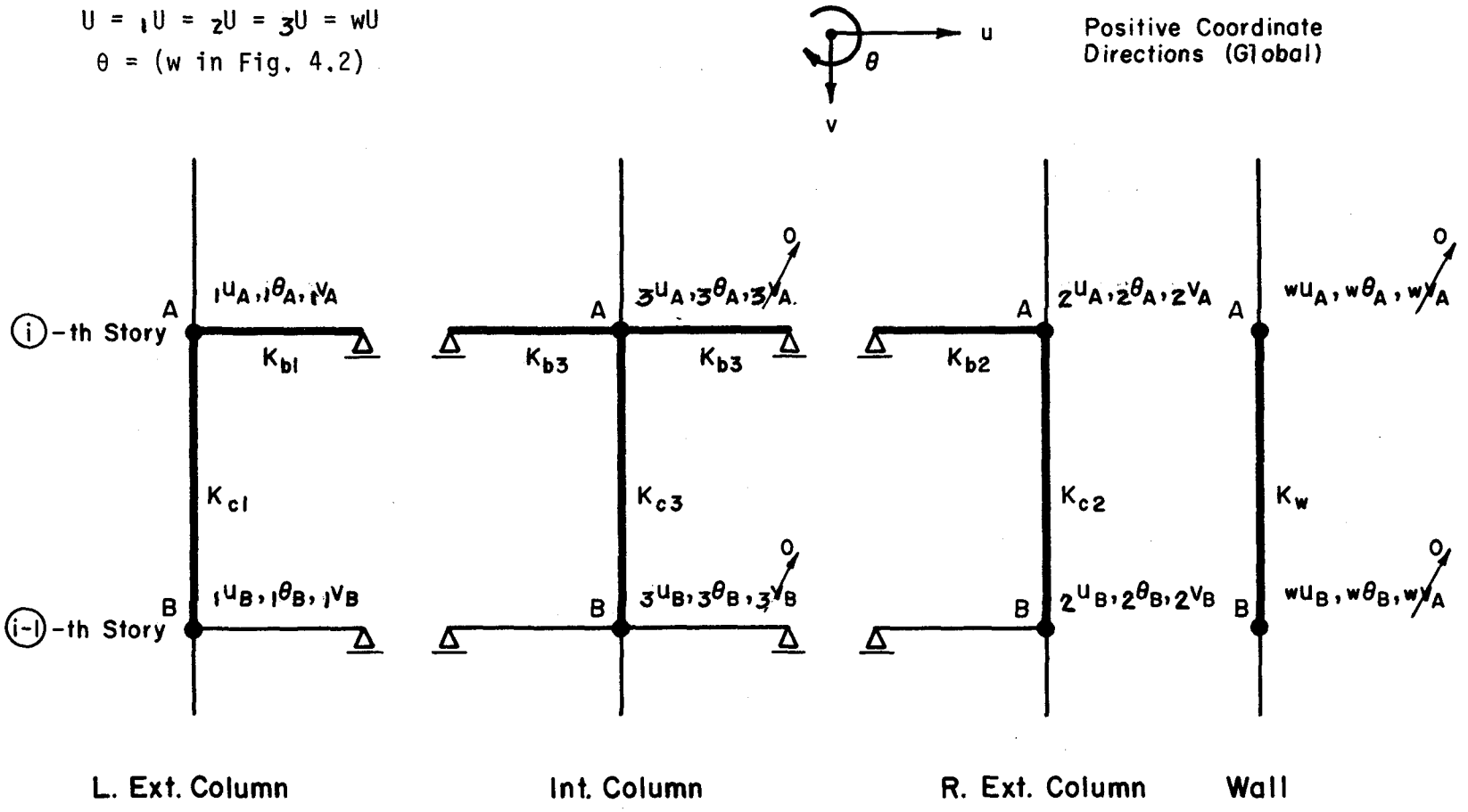

FIG. 4.5 GLOBAL COORDINATES: DISPLACEMENTS OF THE i-th AND i-1-th STORIES OF THE STRUCTURE

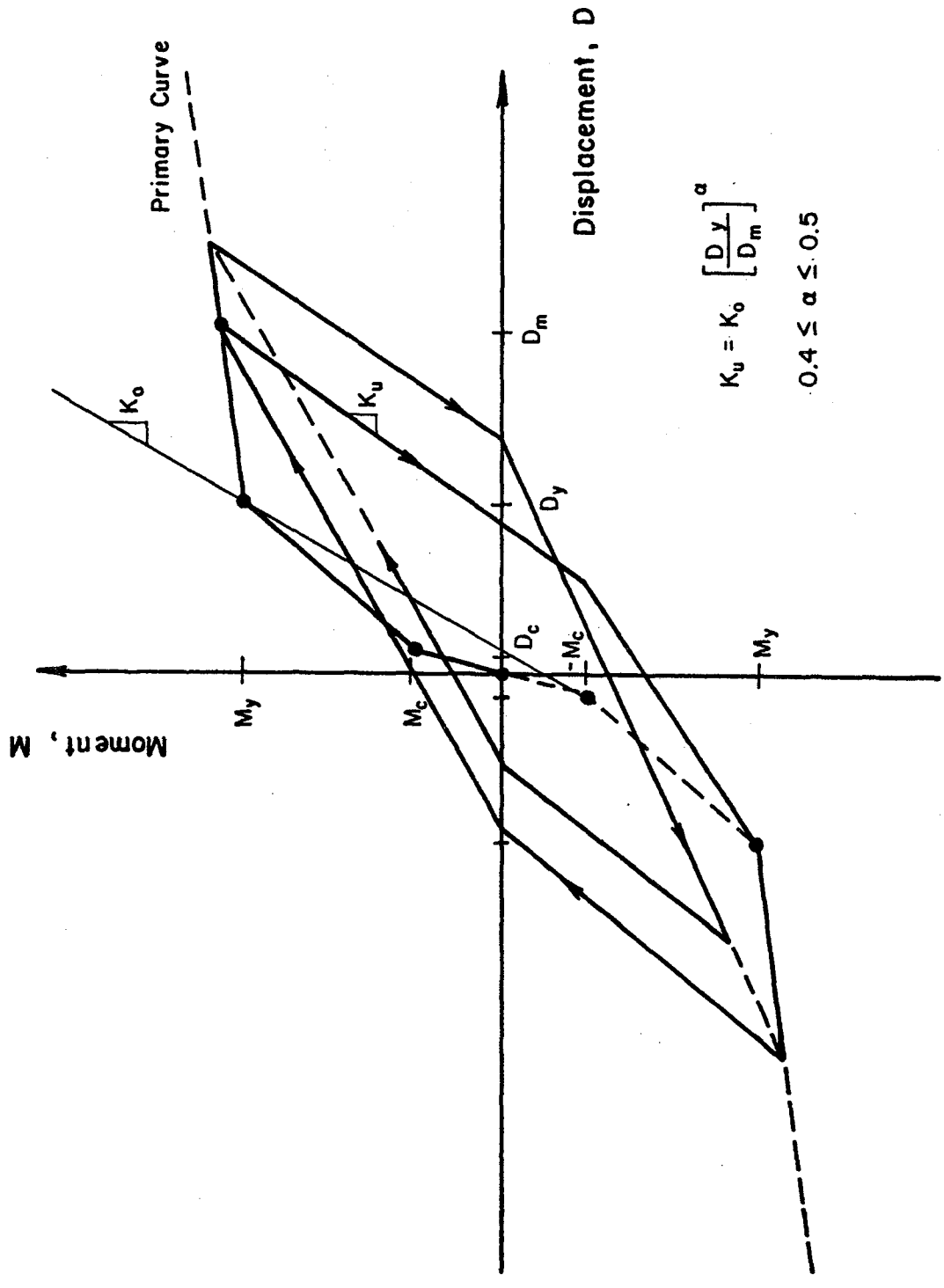

FIG. 5.1 HYSTERESIS MODEL 1 (TAKEDA MODEL)

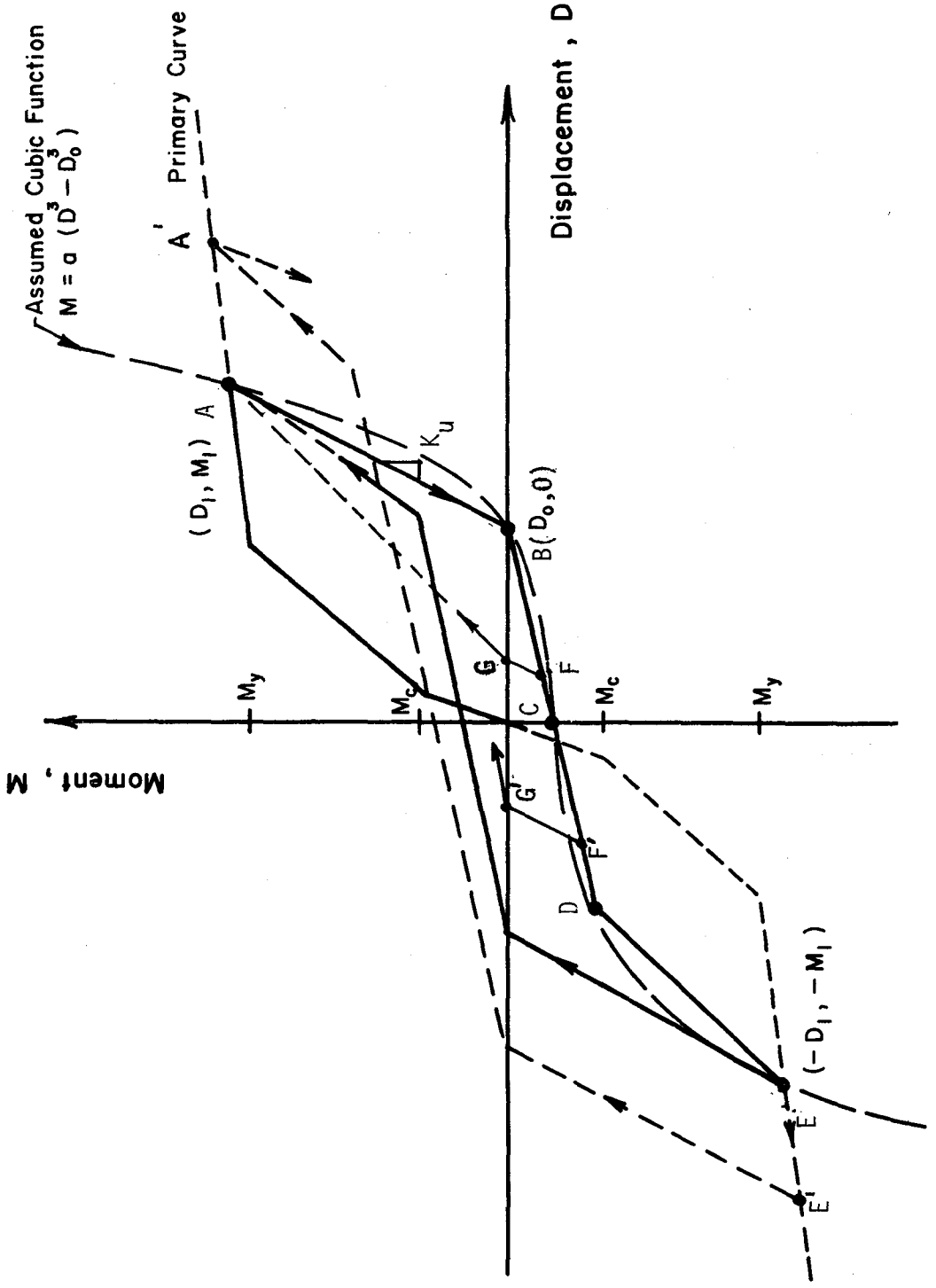

FIG. 5.2 HYSTERESIS MODEL 2

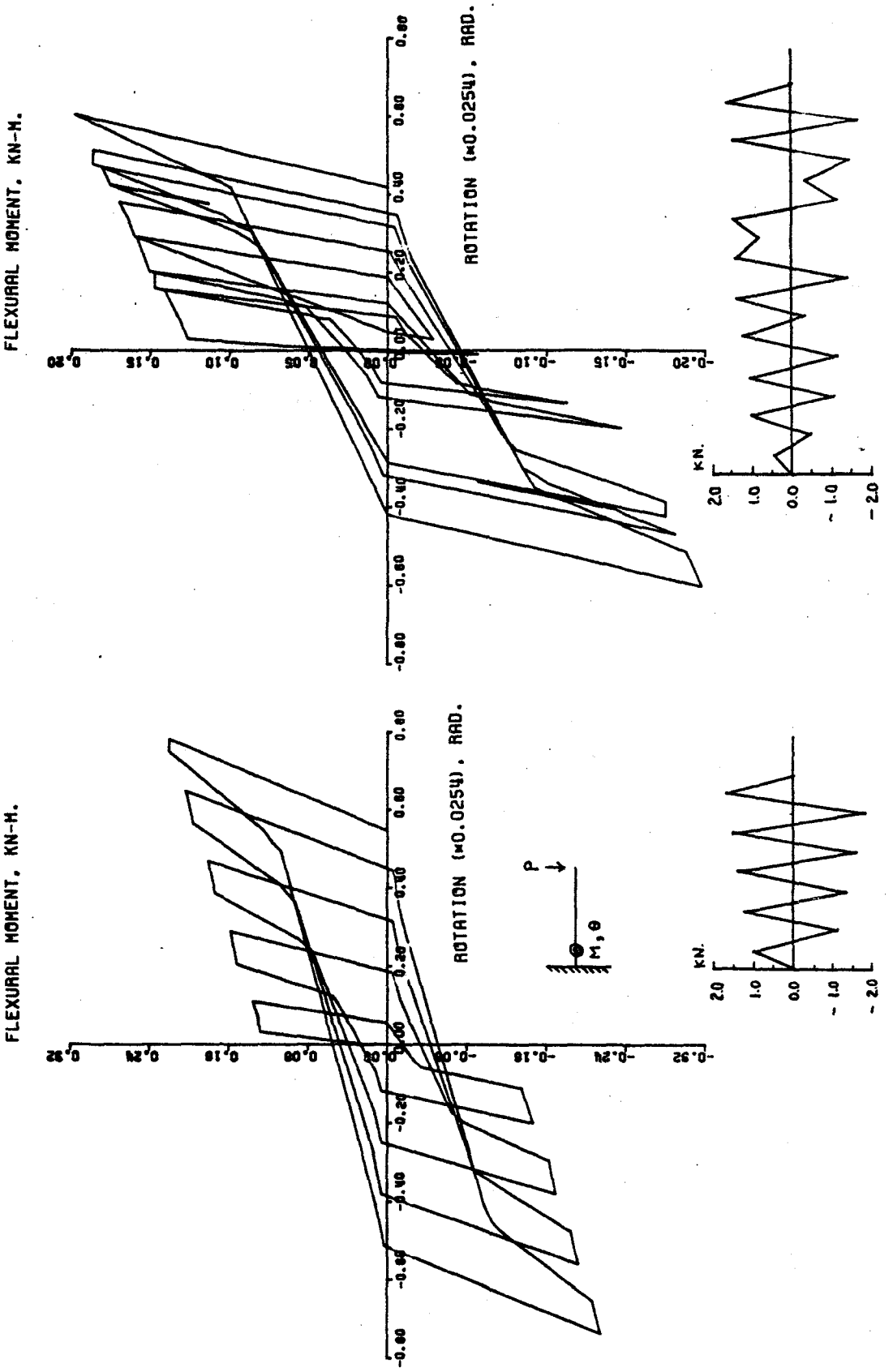

FIG. 5.3 COMPUTED MOMENT-ROTATION RELATIONSHIPS OF A CANTILEVER BEAM USING HYSTERESIS MODEL 2

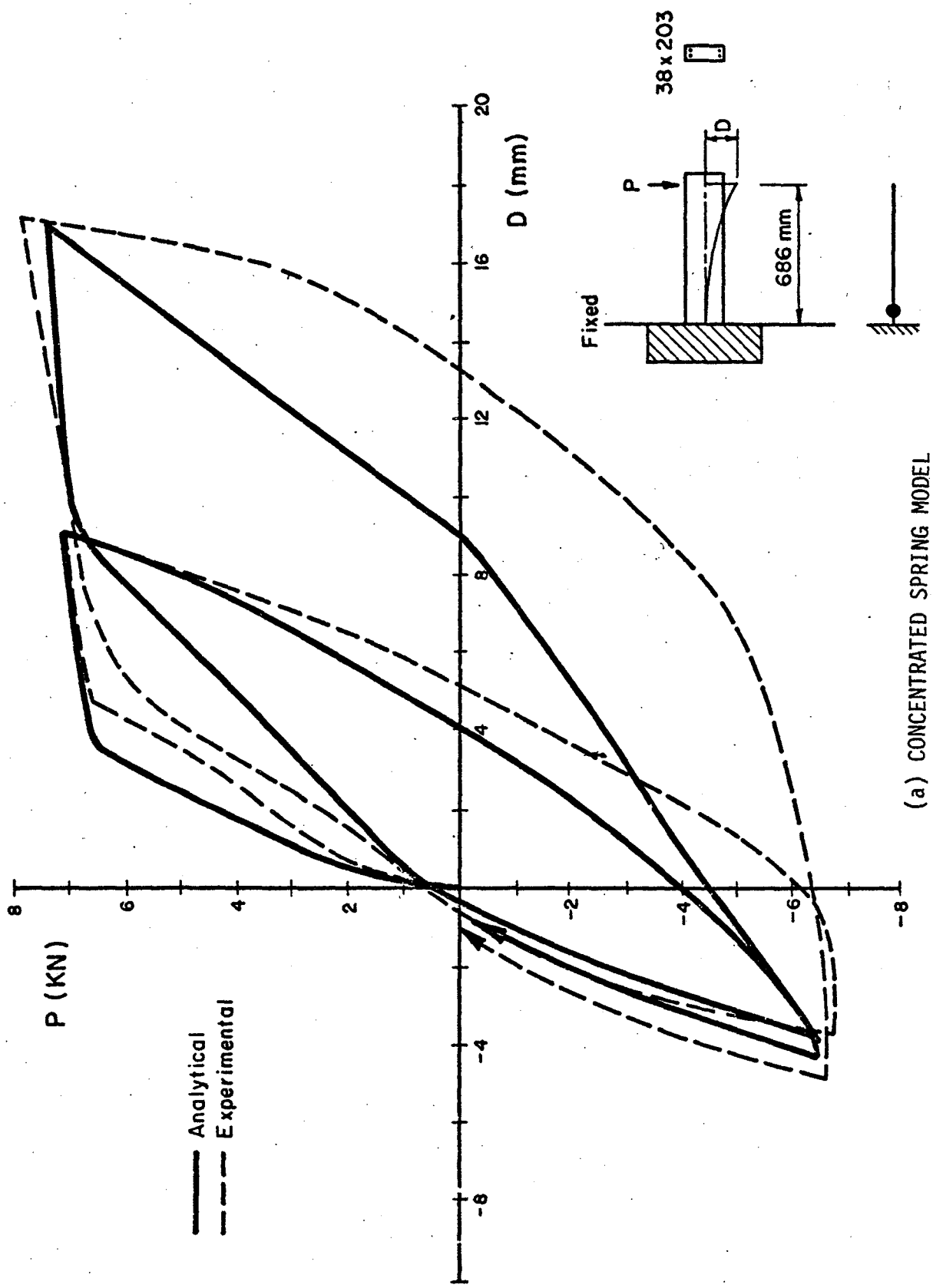

(a) CONCENTRATED SPRING MODEL

FIG. 5.4 FORCE-DISPLACEMENT RELATIONSHIPS OF A CANTILEVER BEAM

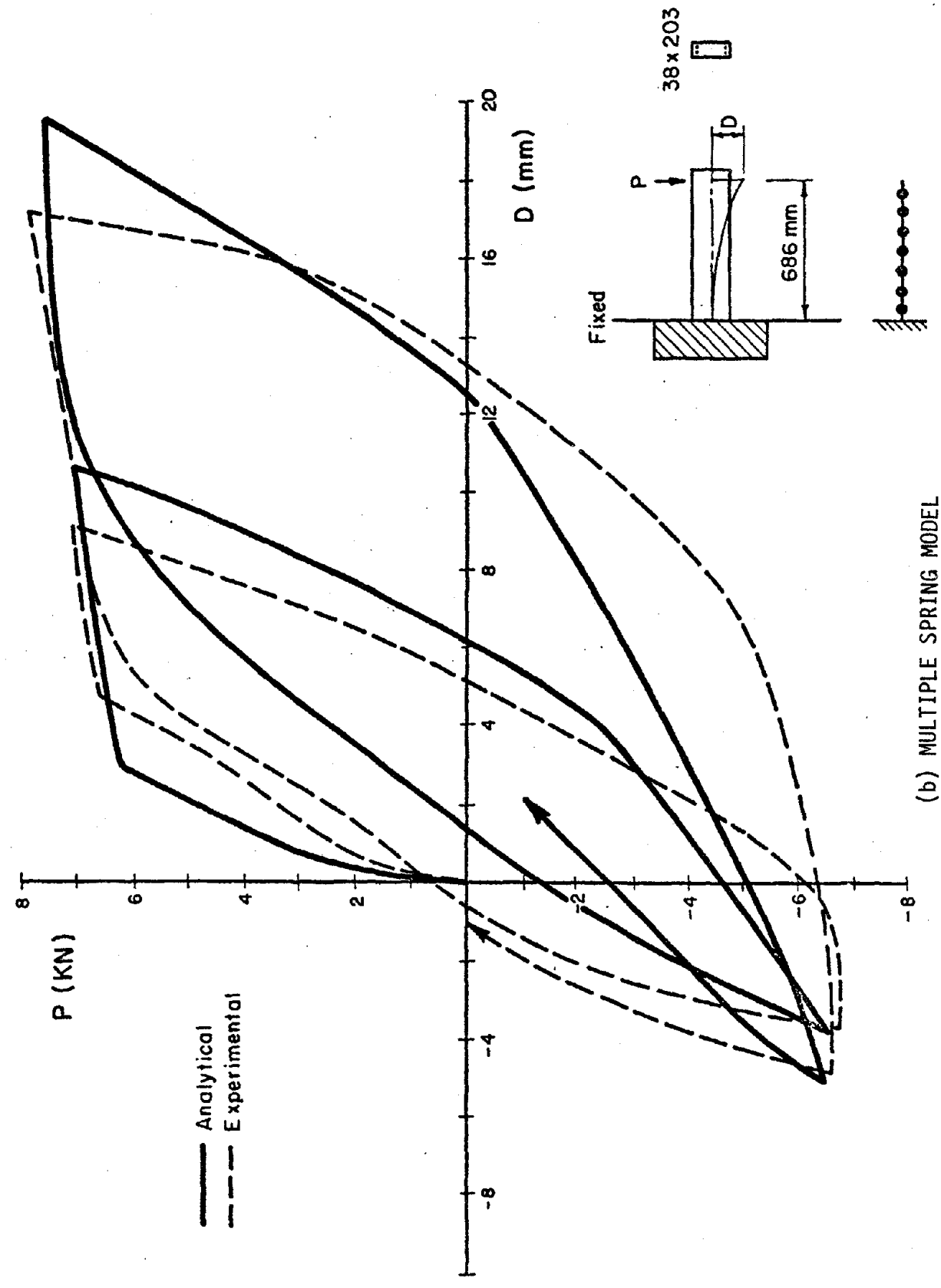

(b) MULTIPLE SPRING MODEL

FIG. 5.4 (continued)

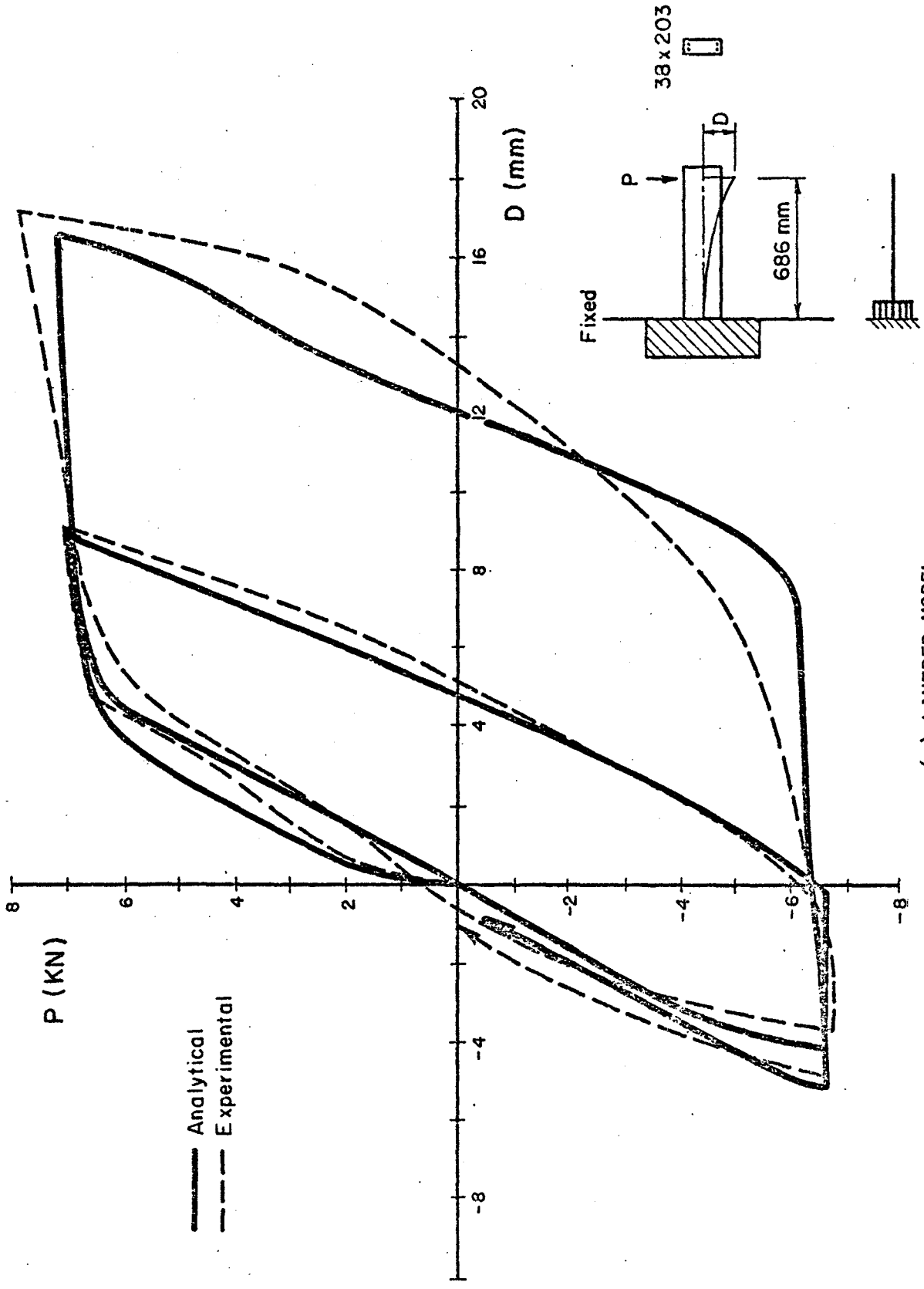

(c) LAYERED MODEL

FIG. 5.4 (continued)

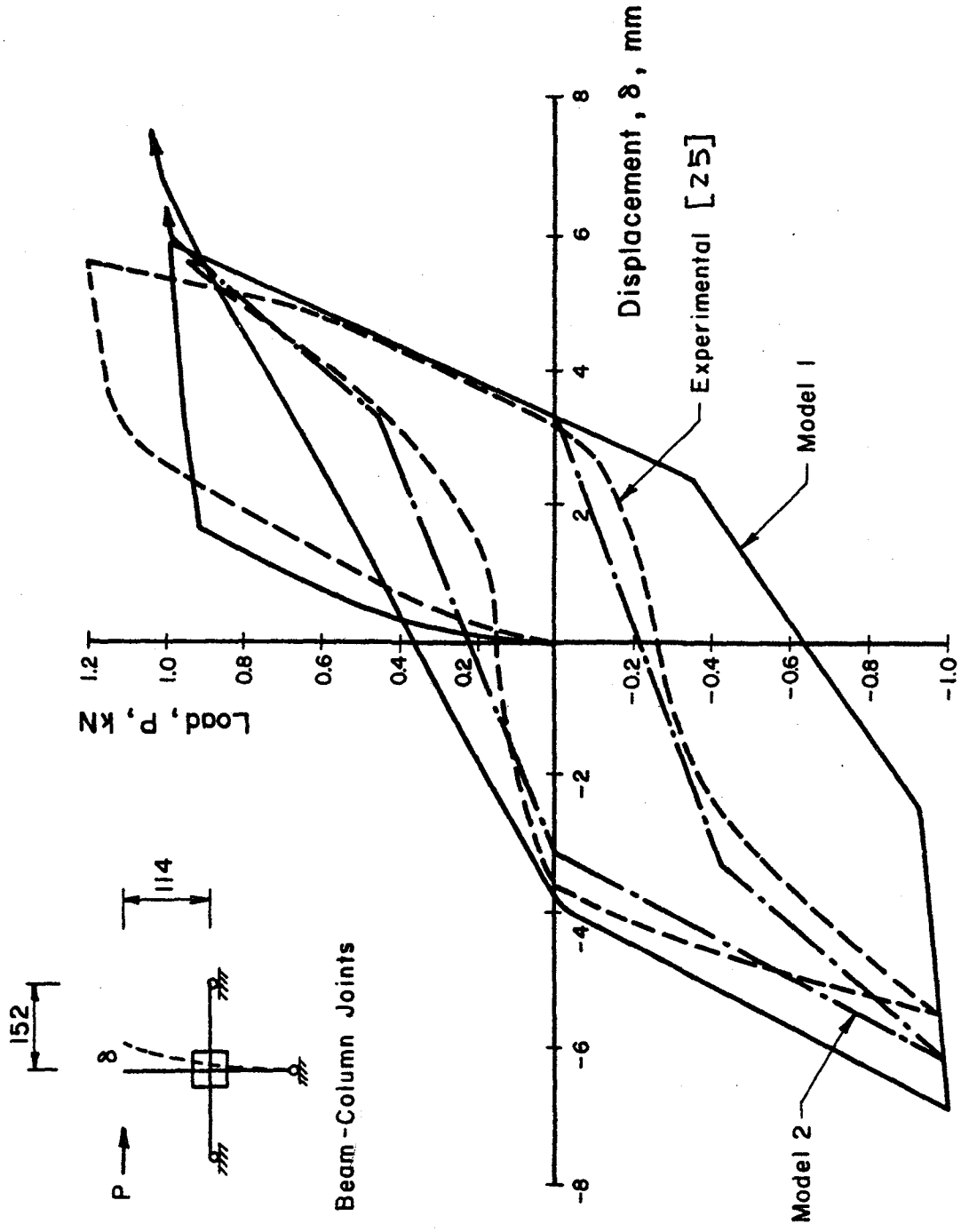

FIG. 5.5 FORCE-DISPLACEMENT RELATIONSHIPS OF BEAM-COLUMN JOINTS

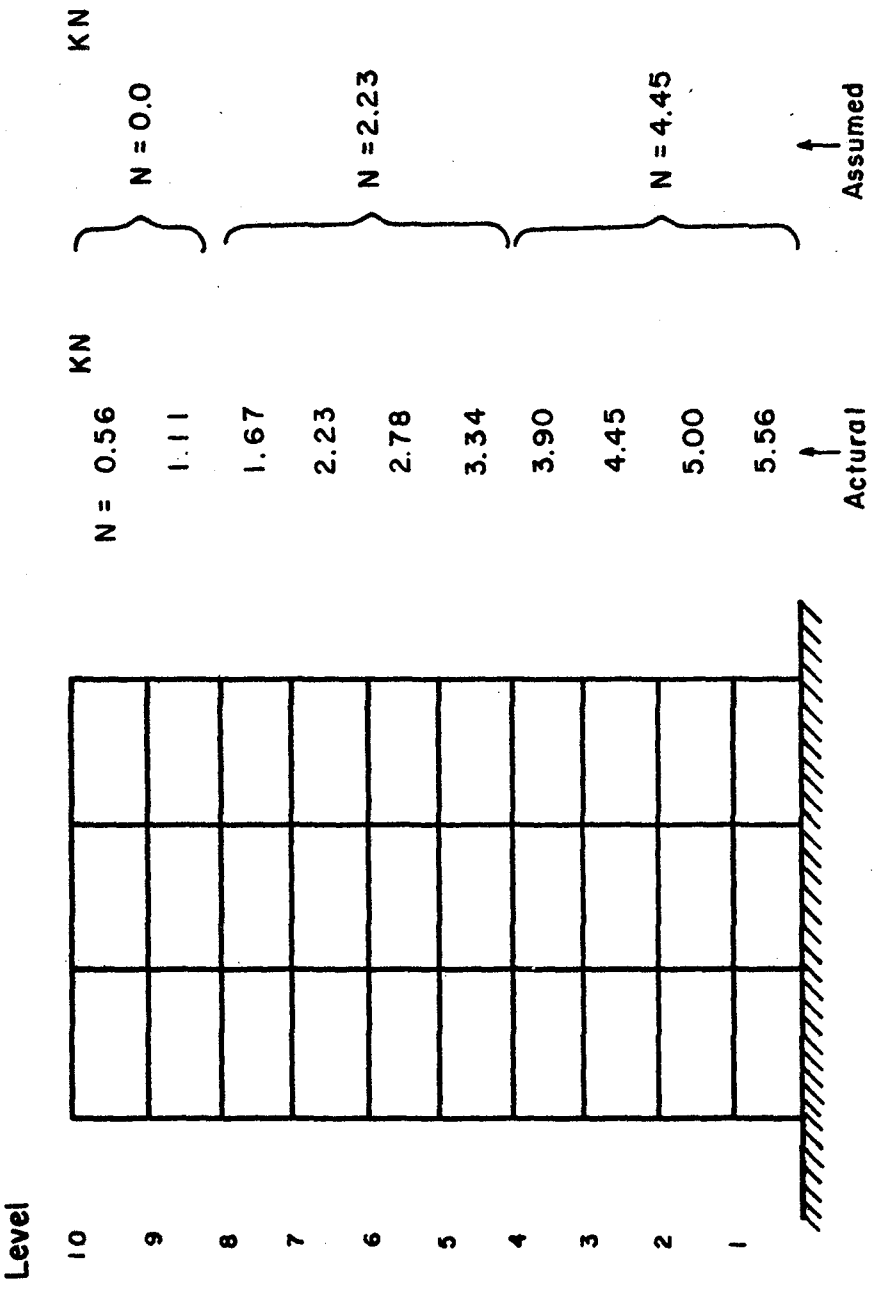

FIG. 5.6 ASSUMED AXIAL LOADS USED IN COLUMN MEMBERS WHEN ESTABLISHING HYSTERESIS RULES

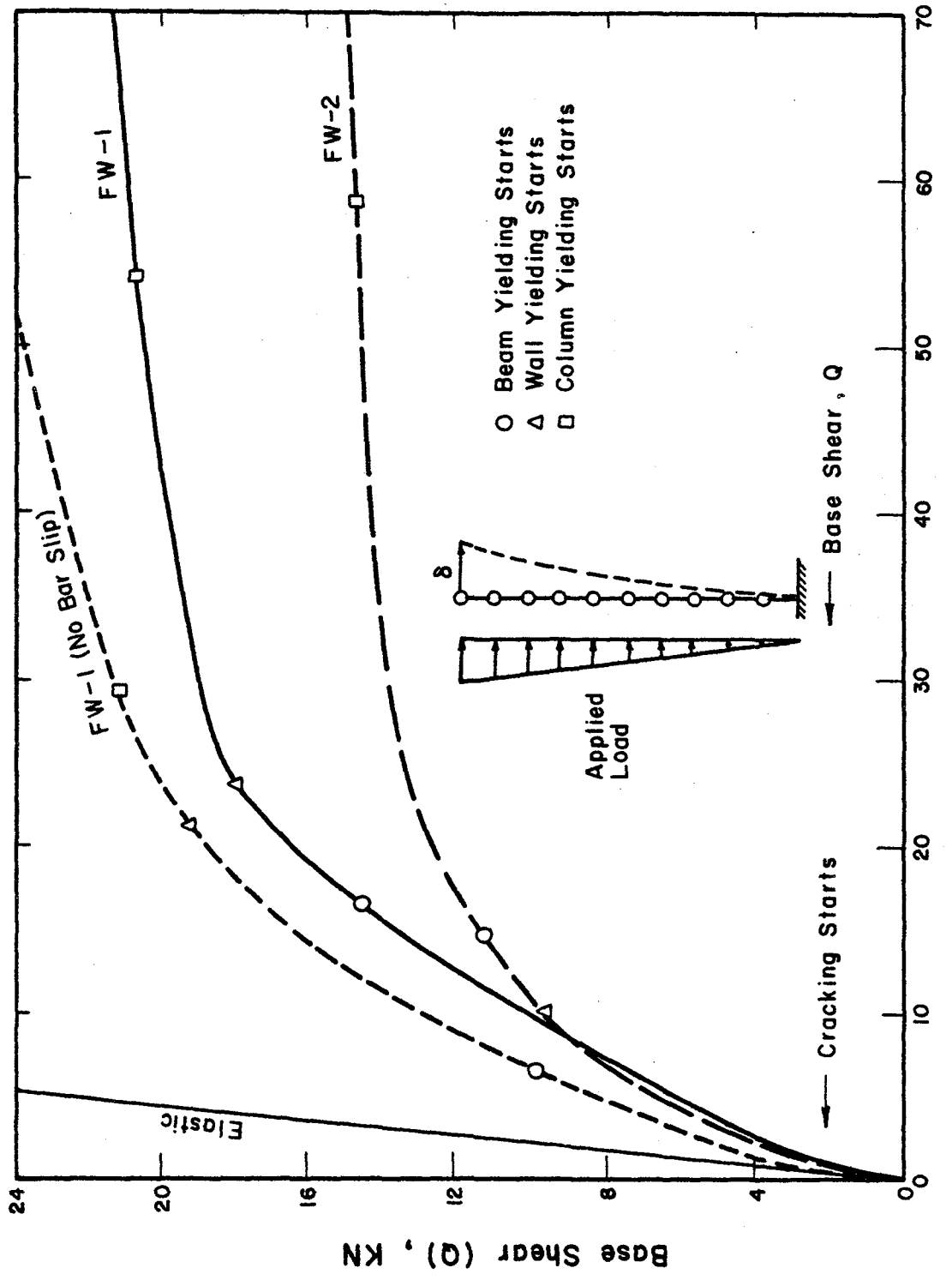

FIG. 6.1 BASE SHEAR-TOP DISPLACEMENT RELATIONSHIPS OF THE STRUCTURES UNDER MONOTONICALLY INCREASING EXTERNAL LOAD

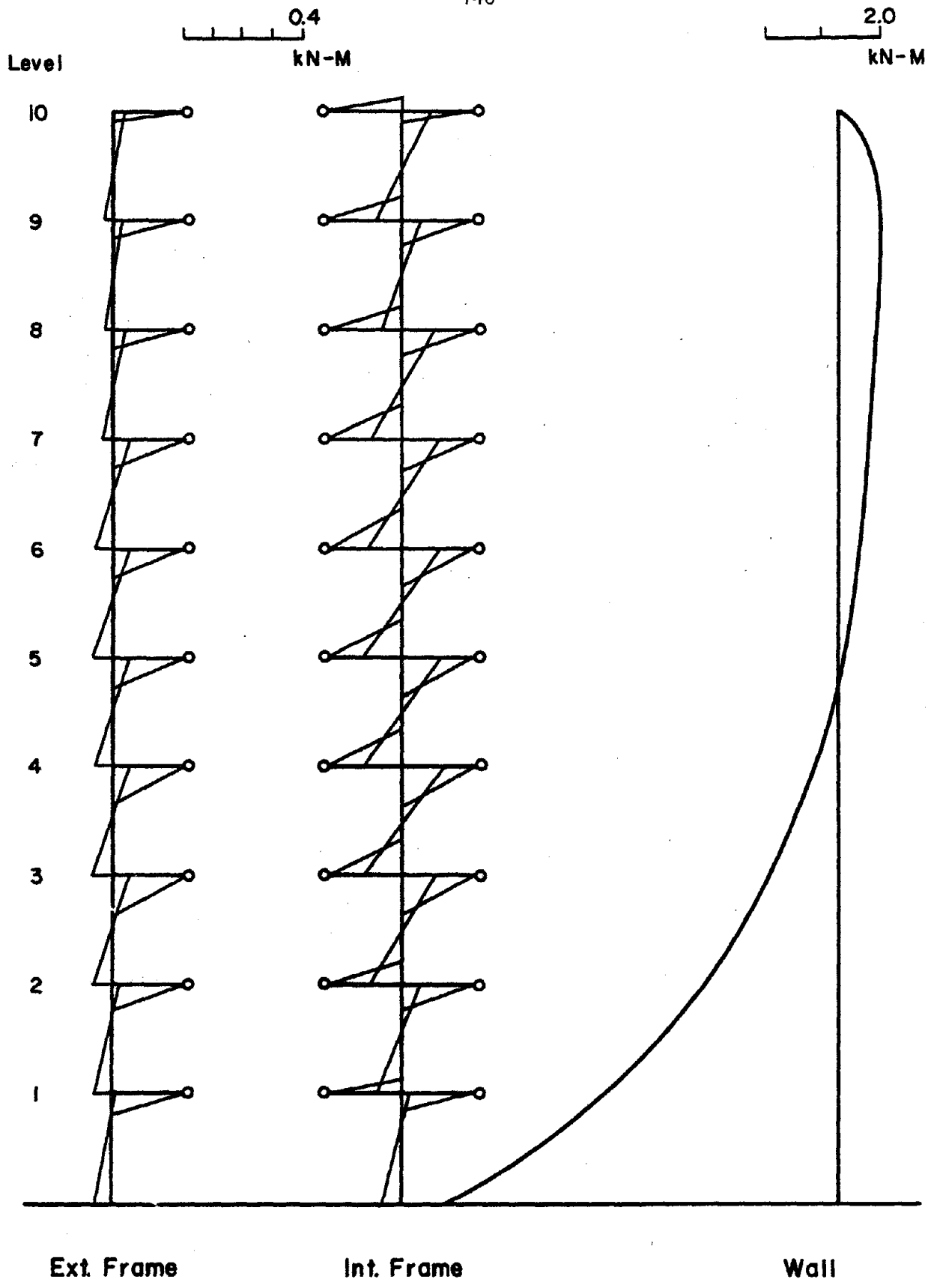

(a) Elastic

FIG. 6.2 MOMENT DISTRIBUTION PATTERNS AT THE COLLAPSE LOAD (FW-2)

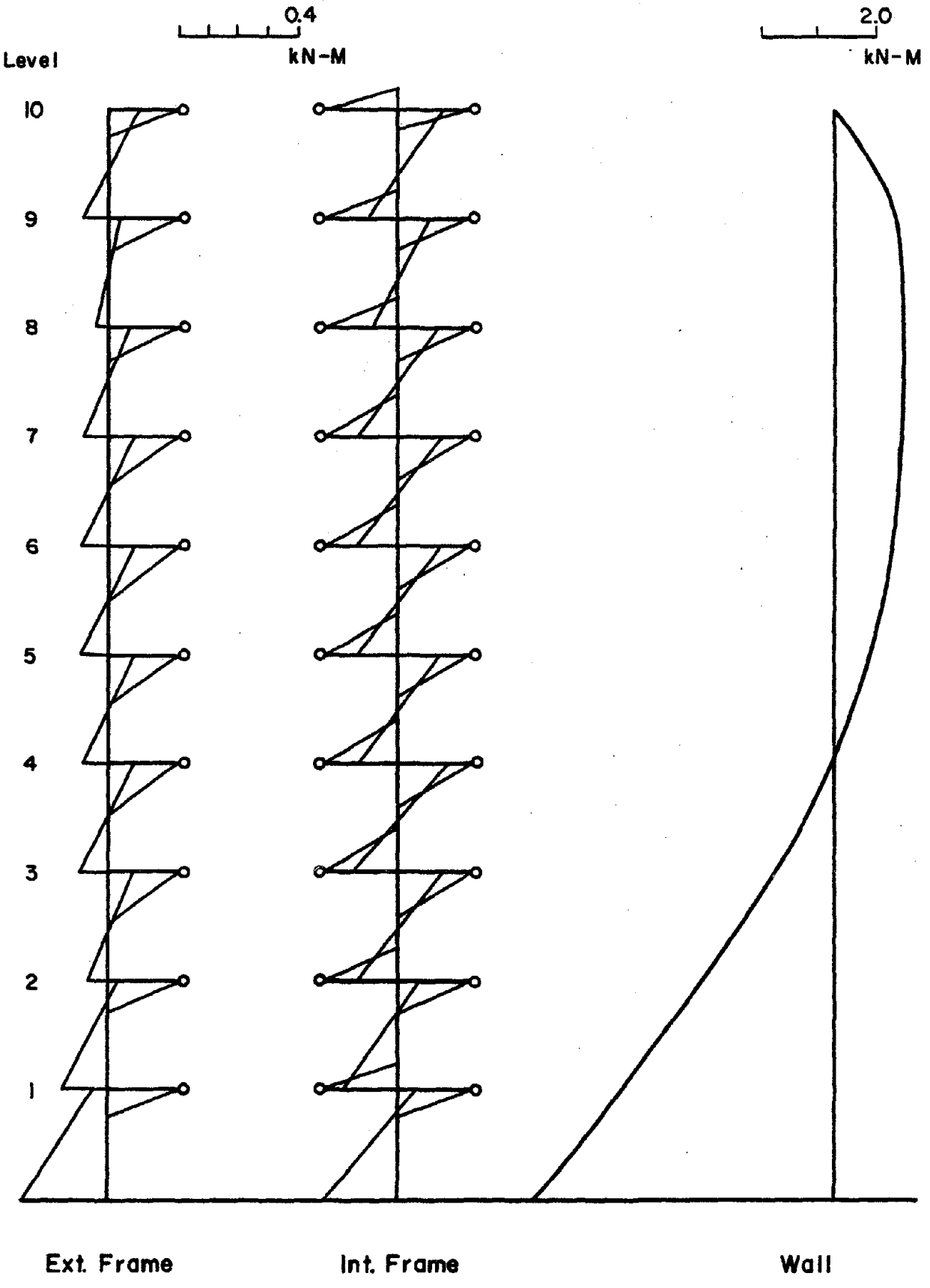

(b) Inelastic

FIG. 6.2 (continued)

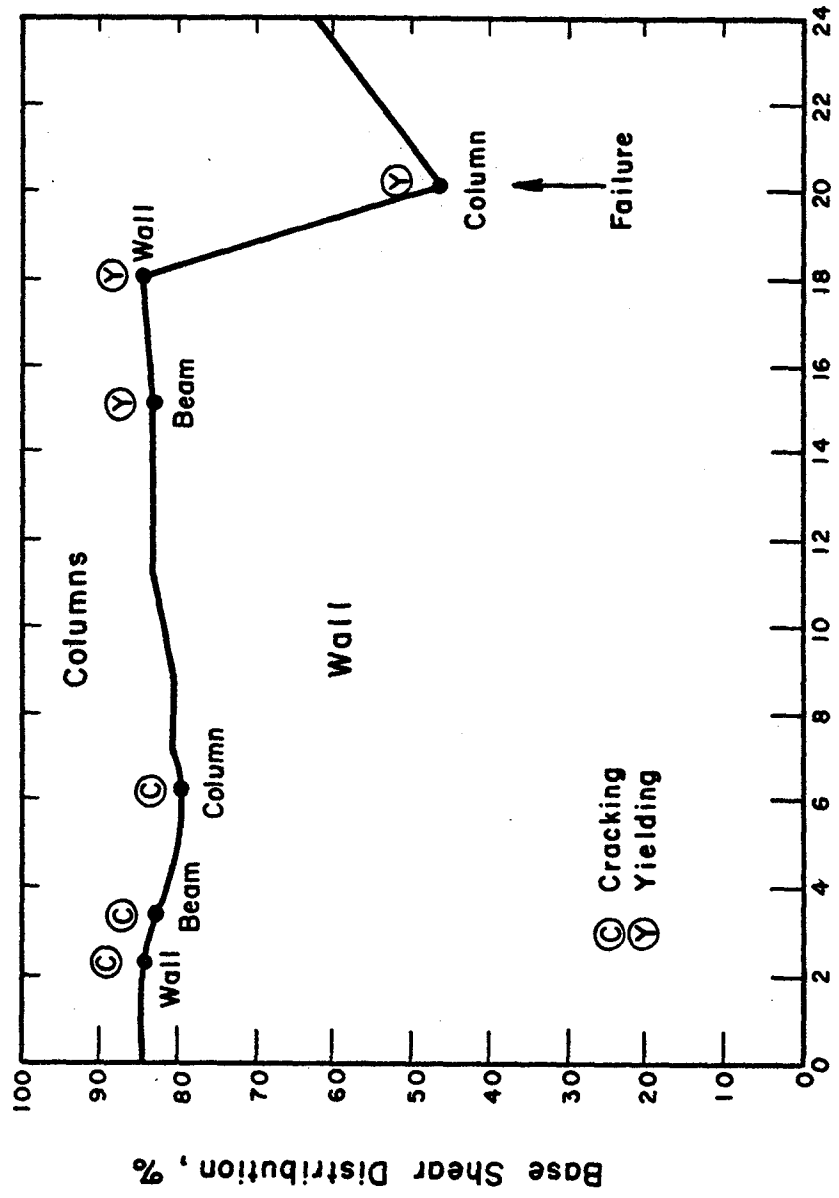

FIG. 6.3 REDISTRIBUTION OF BASE SHEAR BETWEEN WALL AND COLUMNS OF STRUCTURE FW-1 UNDER MONOTONICALLY INCREASING LOAD

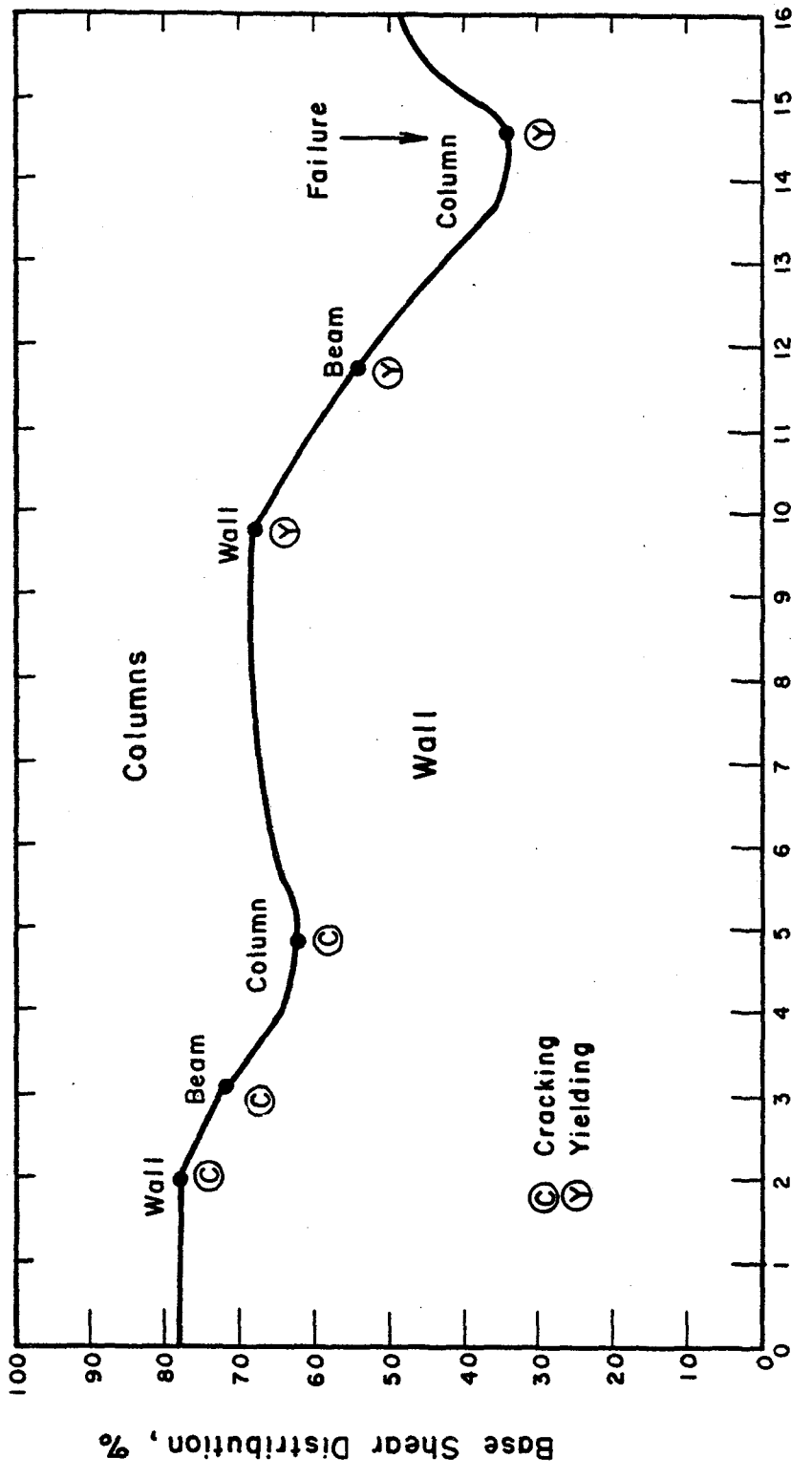

FIG. 6.4 REDISTRIBUTION OF BASE SHEAR BETWEEN WALL AND COLUMNS OF STRUCTURE FW-2 UNDER MONOTONICALLY INCREASING LOAD

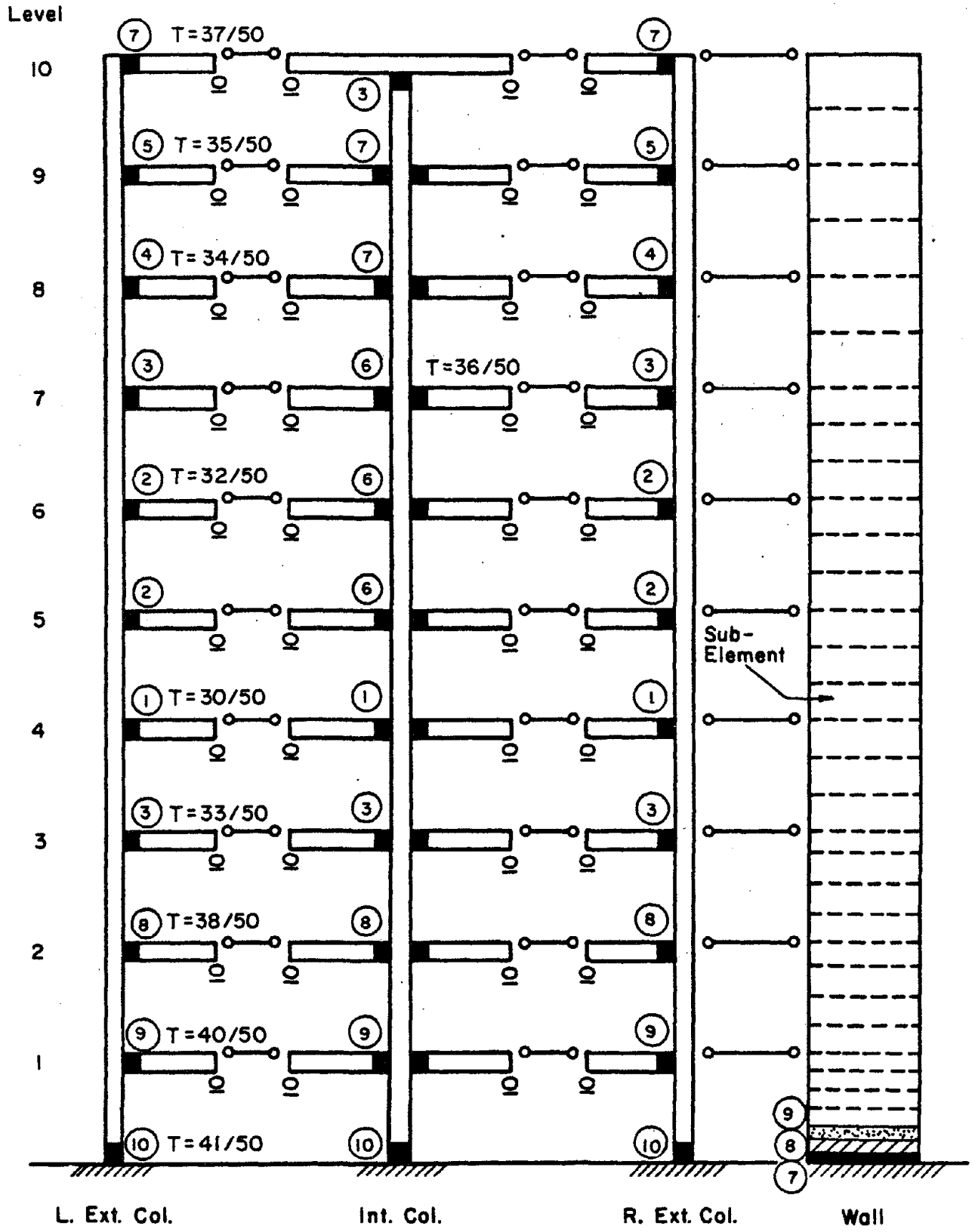

FIG. 6.5 COLLAPSE MECHANISM FOR STRUCTURE FW-1 UNDER STATIC TRIANGULAR LATERAL LOADING

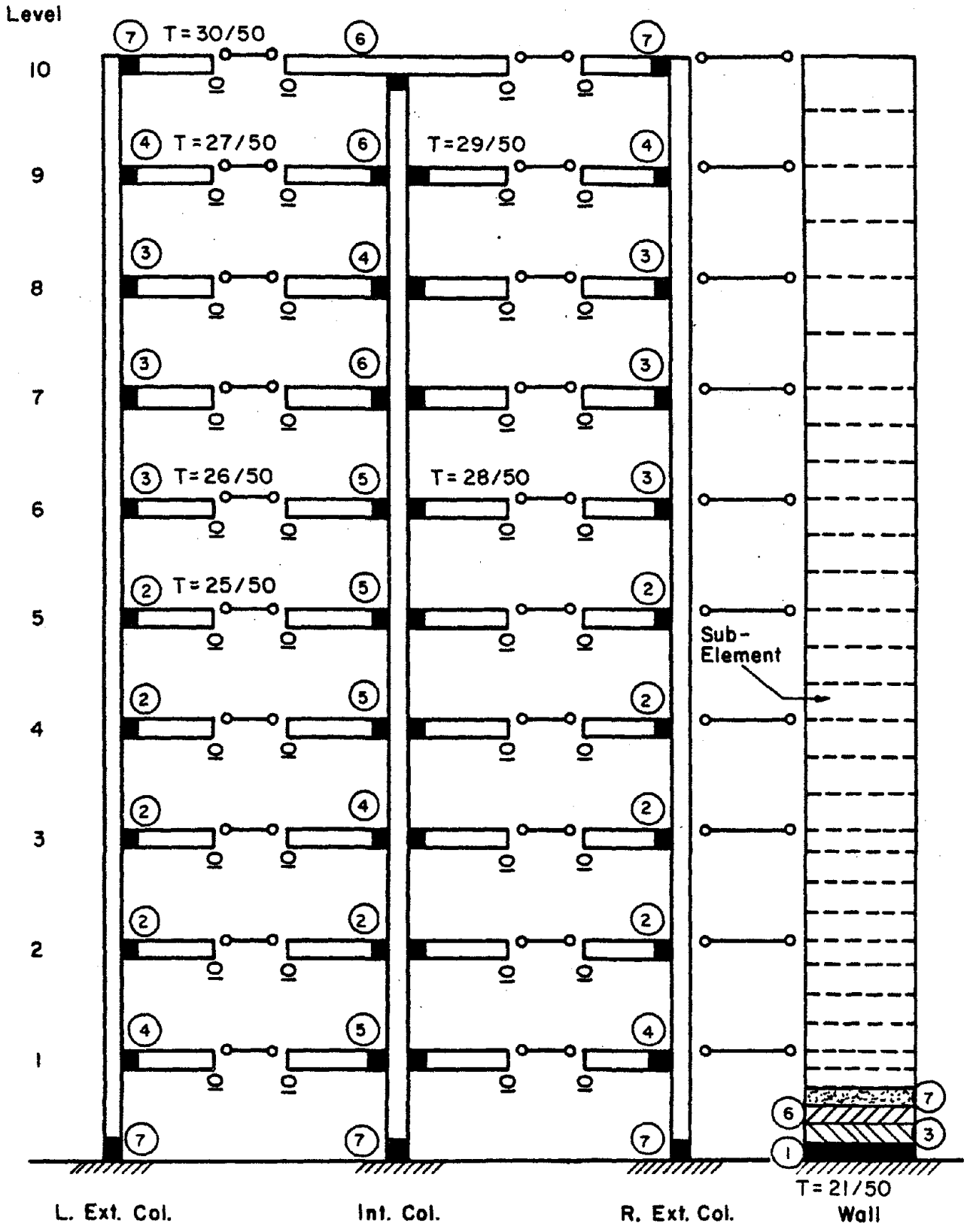

FIG. 6.6 COLLAPSE MECHANISM FOR STRUCTURE FW-2 UNDER STATIC TRIANGULAR LATERAL LOADING

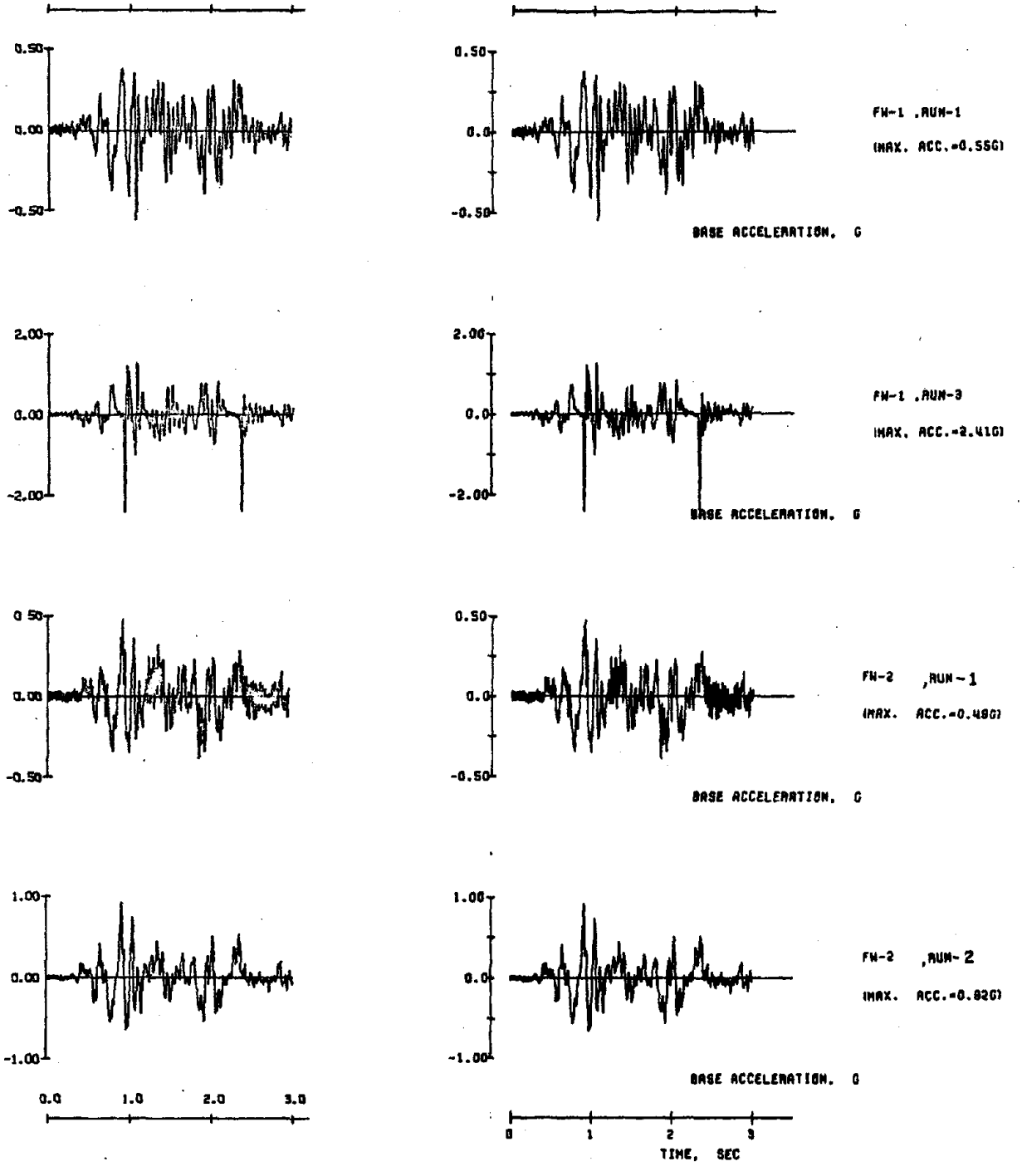

(Observed) (Used)

FIG. 6.7 BASE ACCELERATION WAVEFORMS AS OBSERVED IN TESTS AND COMPARISON WITH THOSE USED FOR RESPONSE ANALYSIS

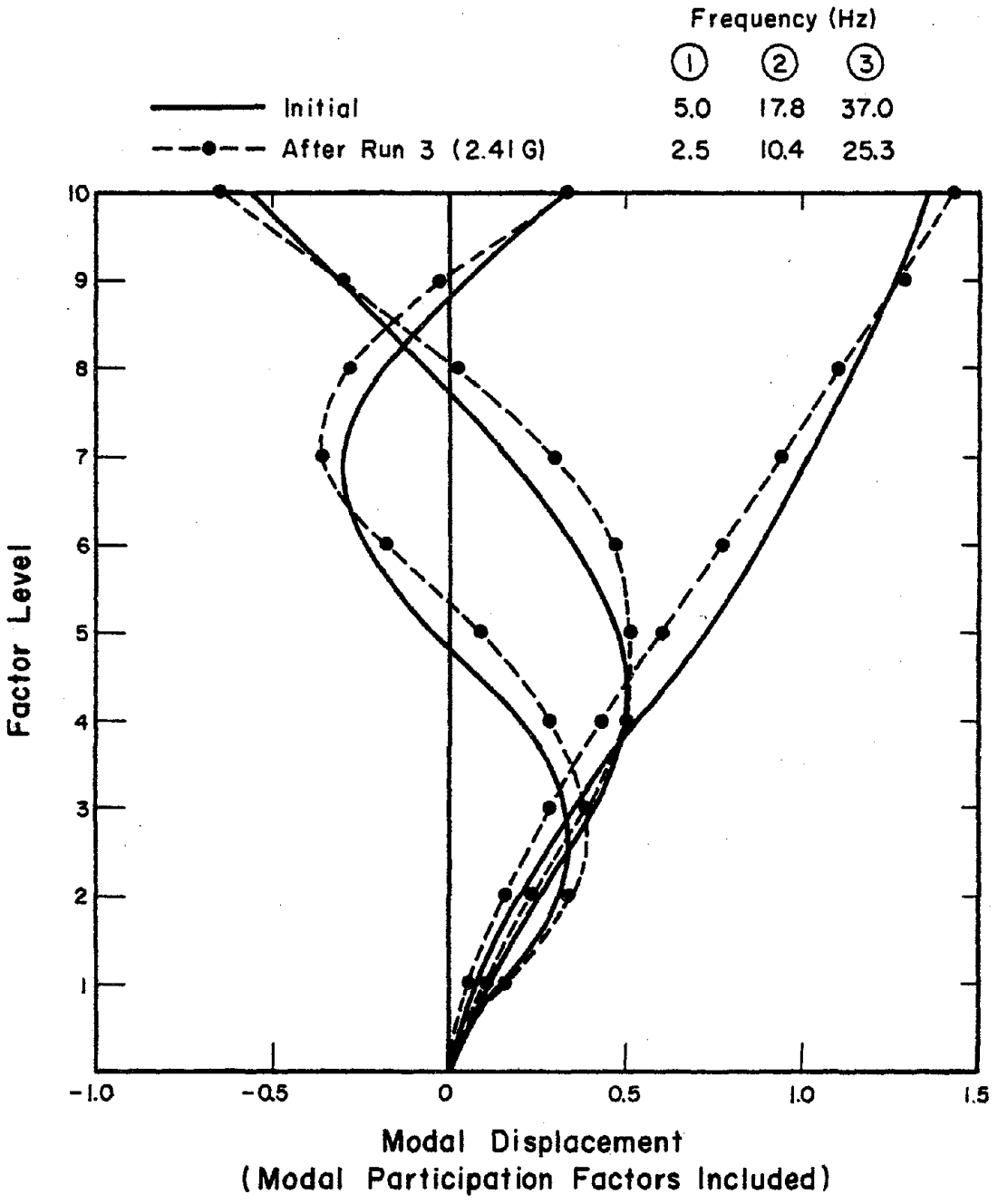

FIG. 6.8 MODE SHAPES OF STRUCTURE FW-1

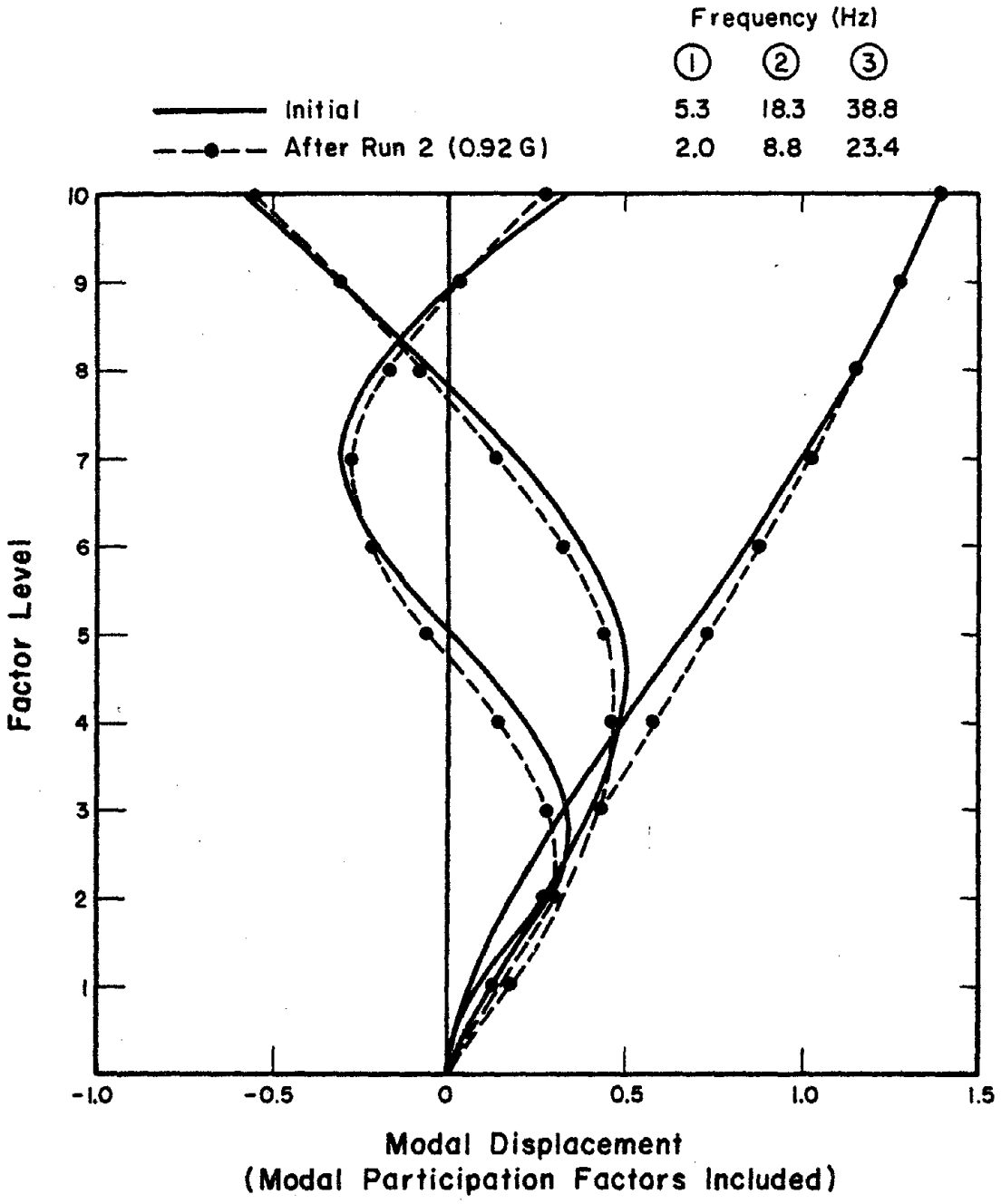

FIG. 6.9 MODE SHAPES OF STRUCTURE FW-2

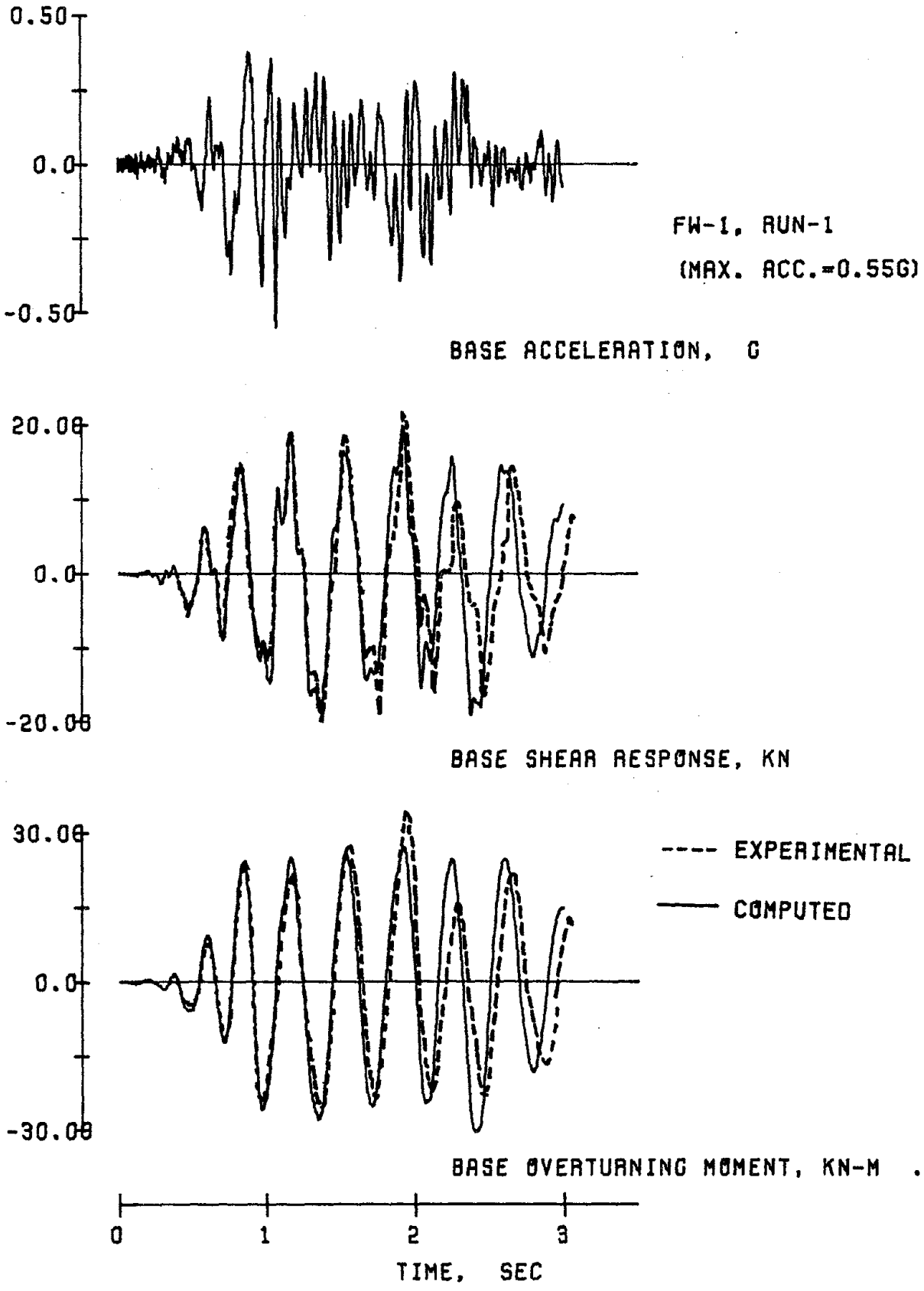

FIG. 6.10 RESPONSE WAVEFORMS FOR STRUCTURE FW-1, RUN-1

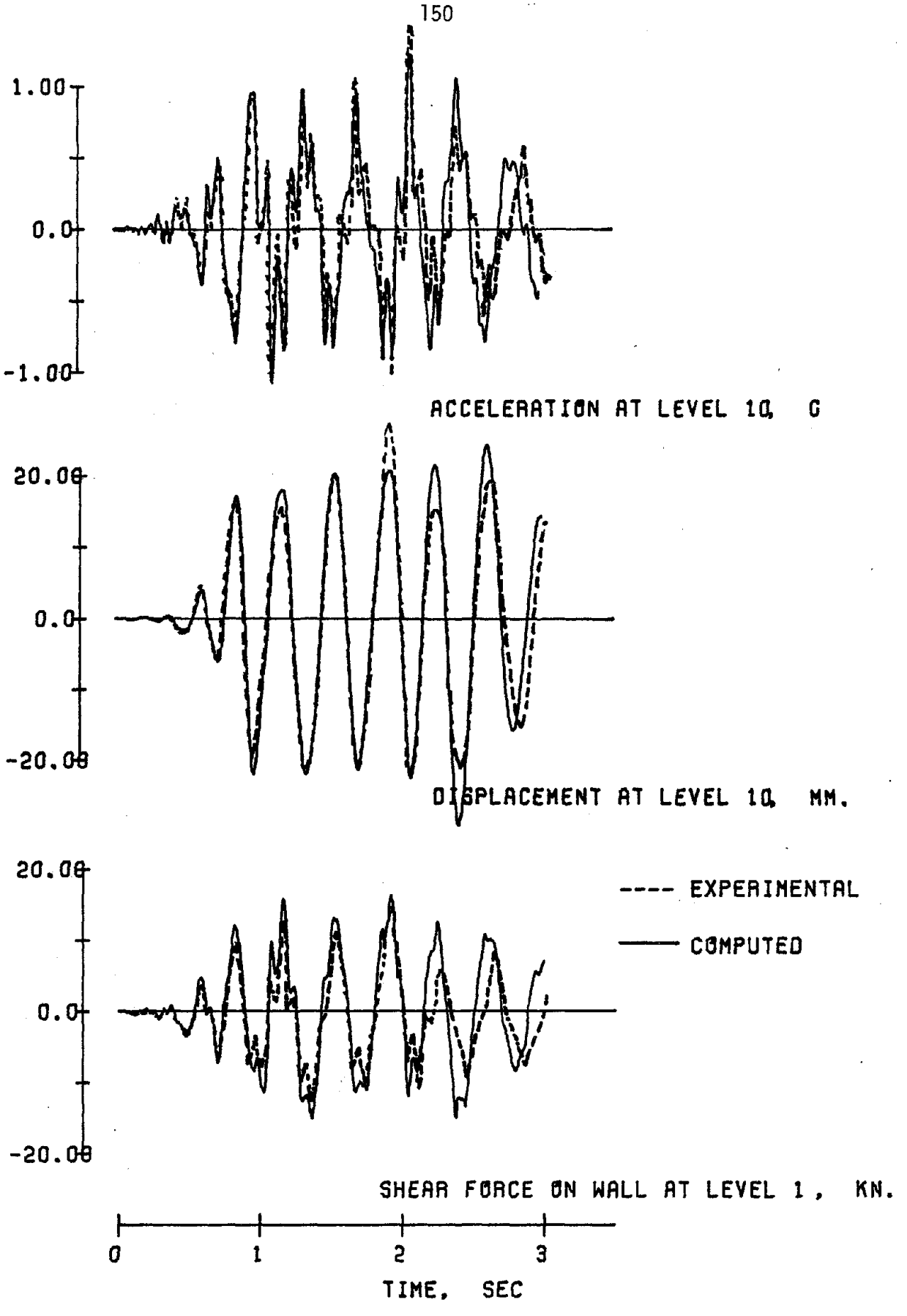

FIG. 6.10 (continued) STRUCTURE FW-1, RUN 1

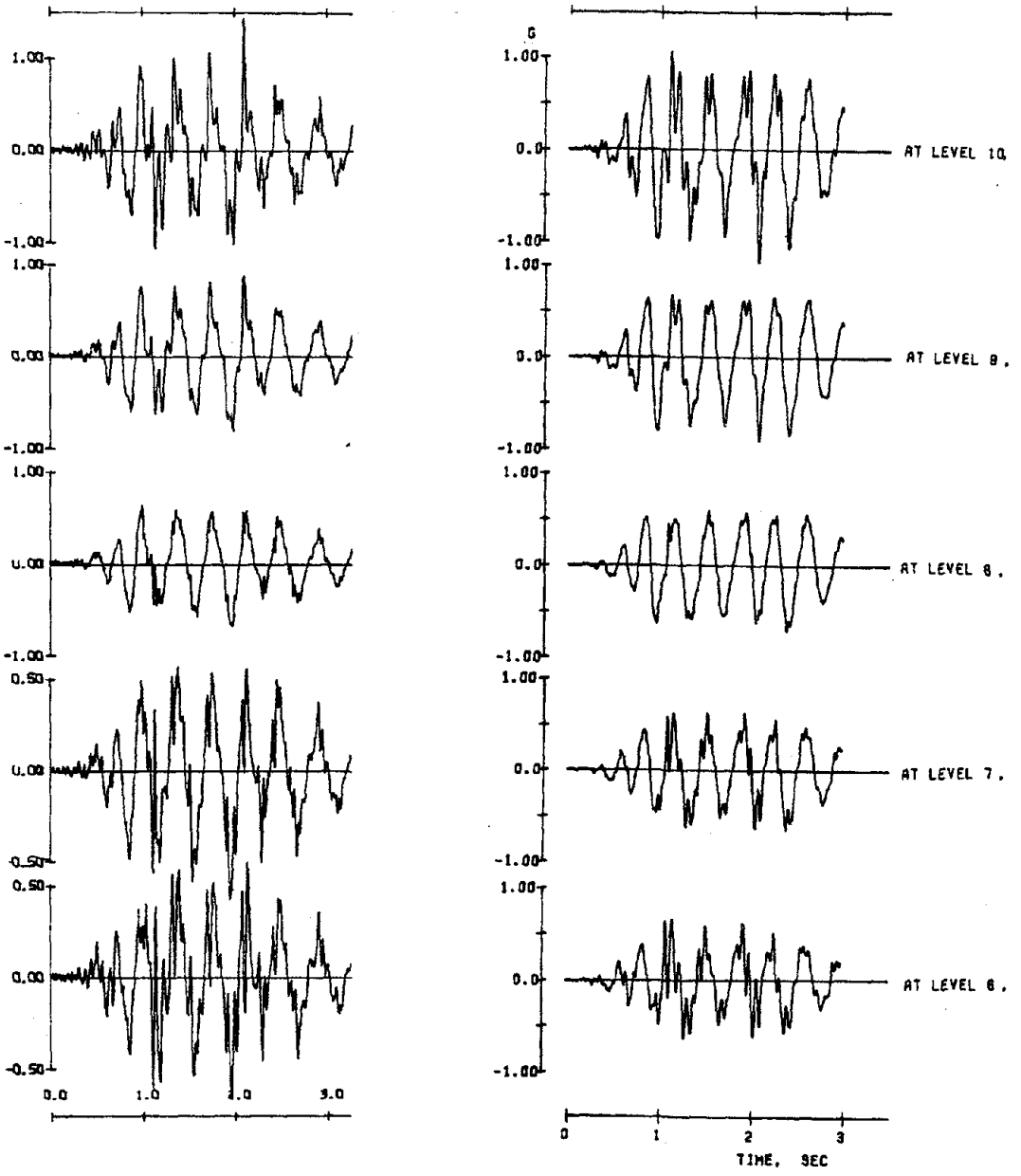

ACCELERATION FOR STRUCTURE FW-1, RUN-1

FIG. 6.10 (continued)

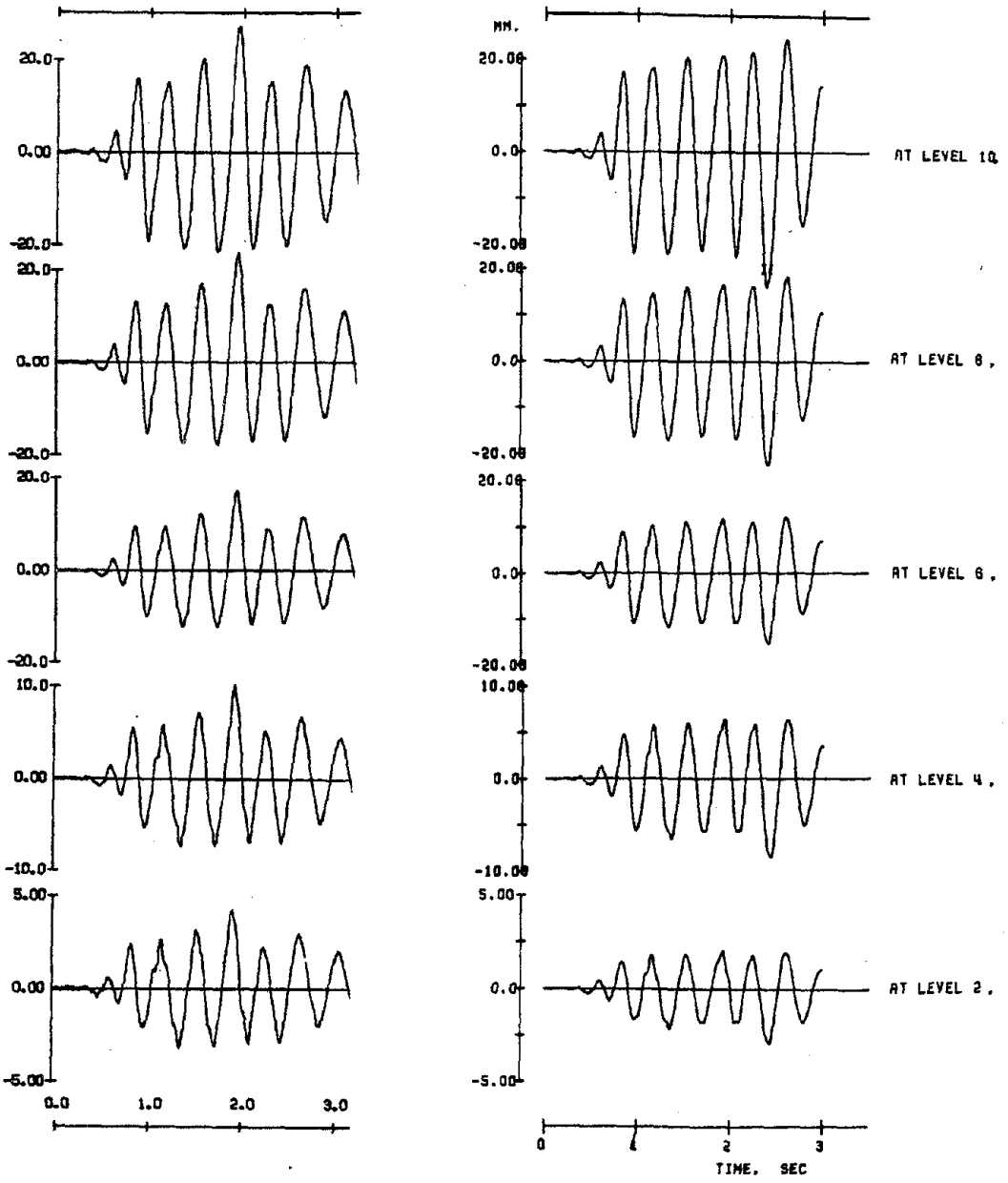

DISPLACEMENT FOR STRUCTURE FW-1, RUN-1

FIG. 6.10 (continued)

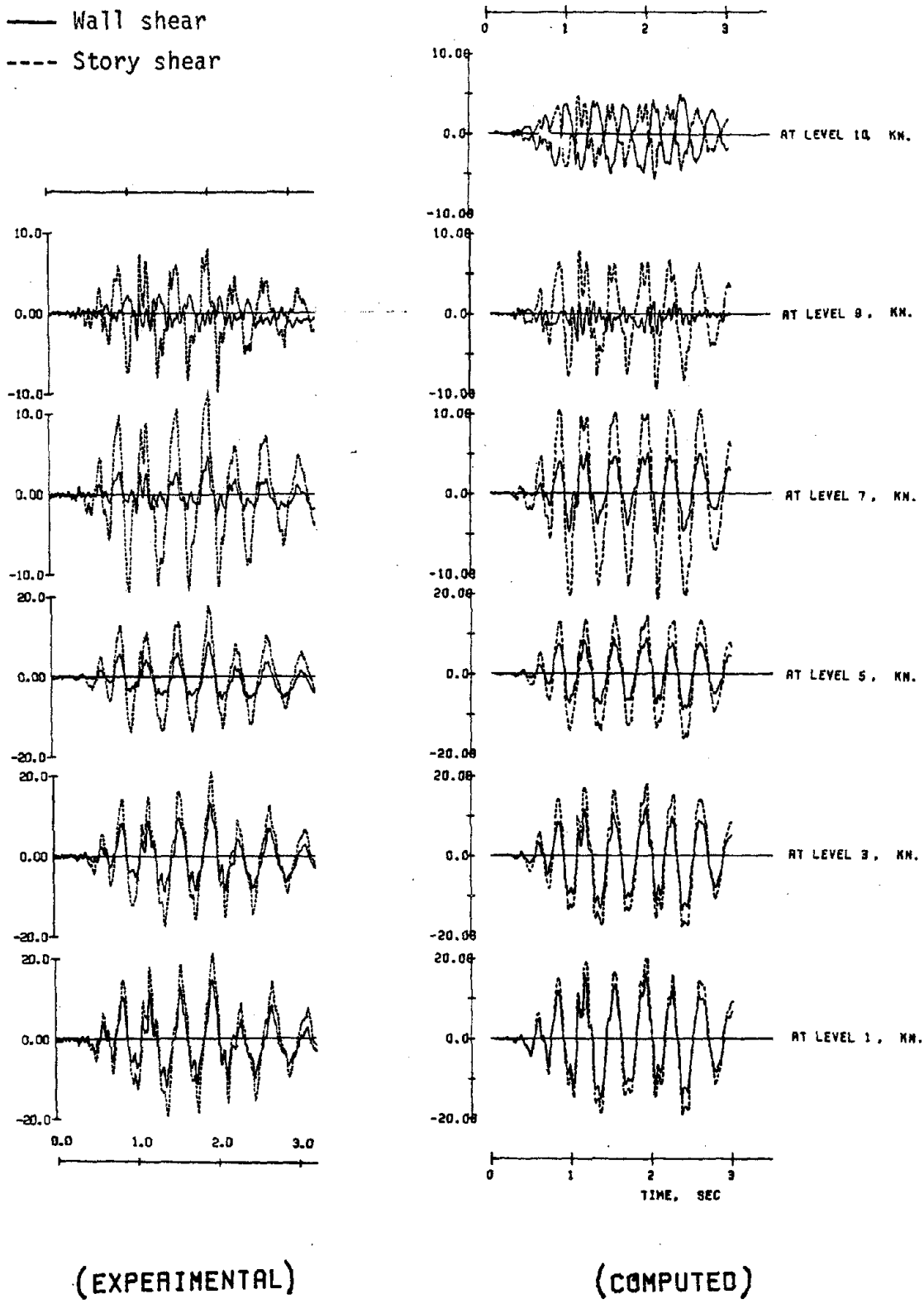

SHEAR FORCE FOR STRUCTURE FW-1, RUN-1

FIG. 6.10 (continued)

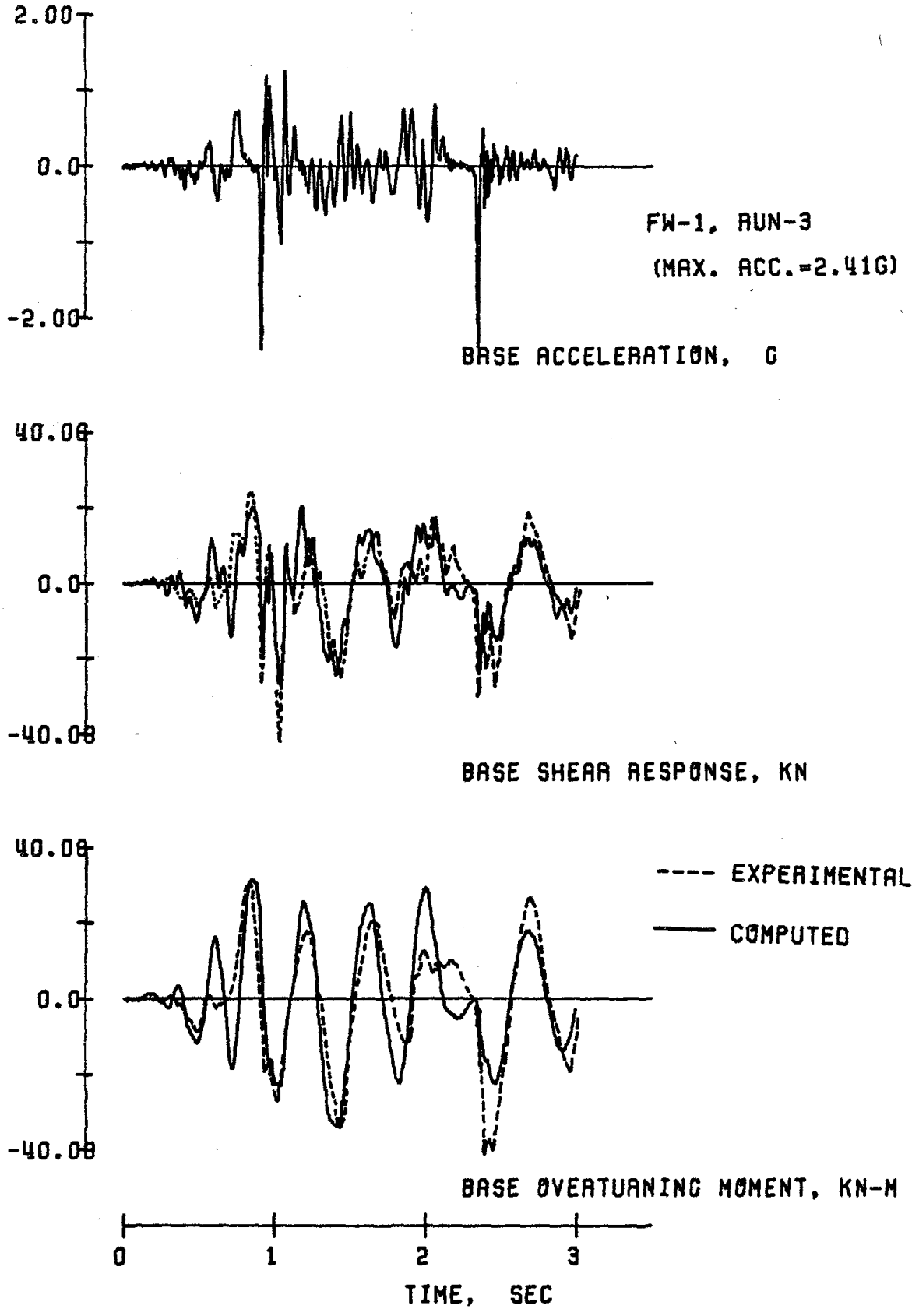

FIG. 6.11 RESPONSE WAVEFORMS FOR STRUCTURE FW-1, RUN-3

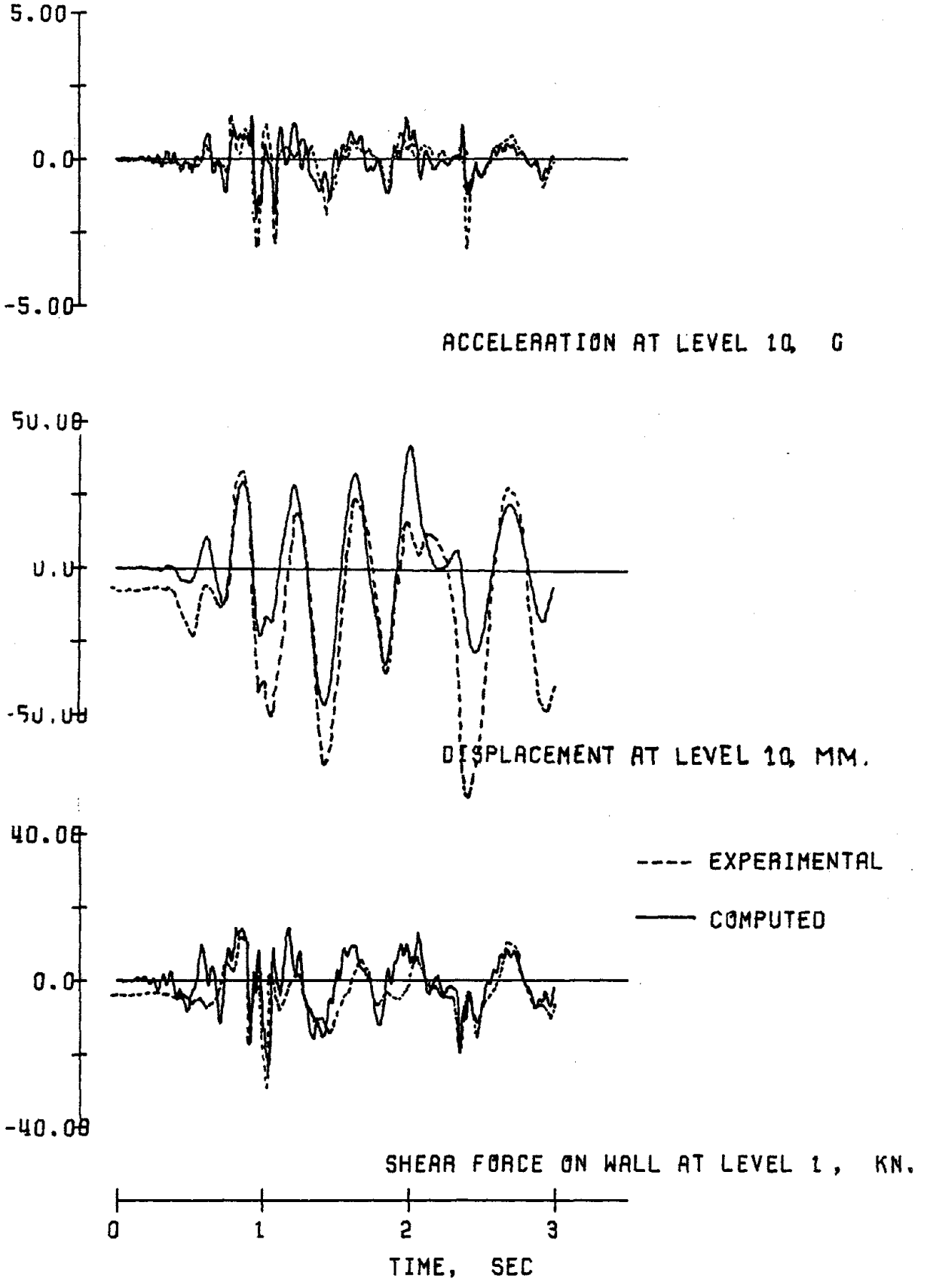

STRUCTURE FW-1, RUN-3

FIG. 6.11 (continued)

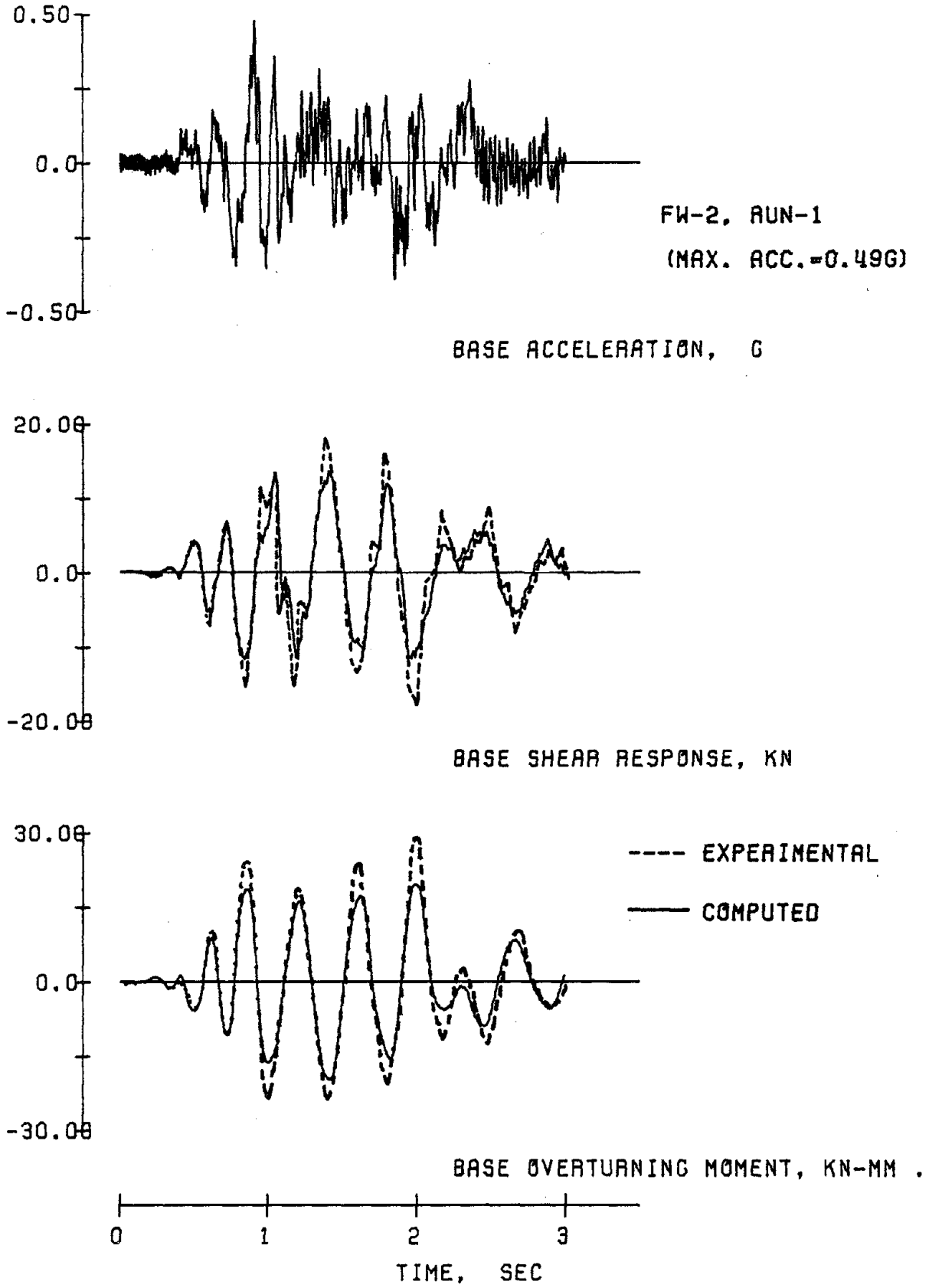

FIG. 6.12 RESPONSE WAVEFORMS FOR STRUCTURE FW-2, RUN-1

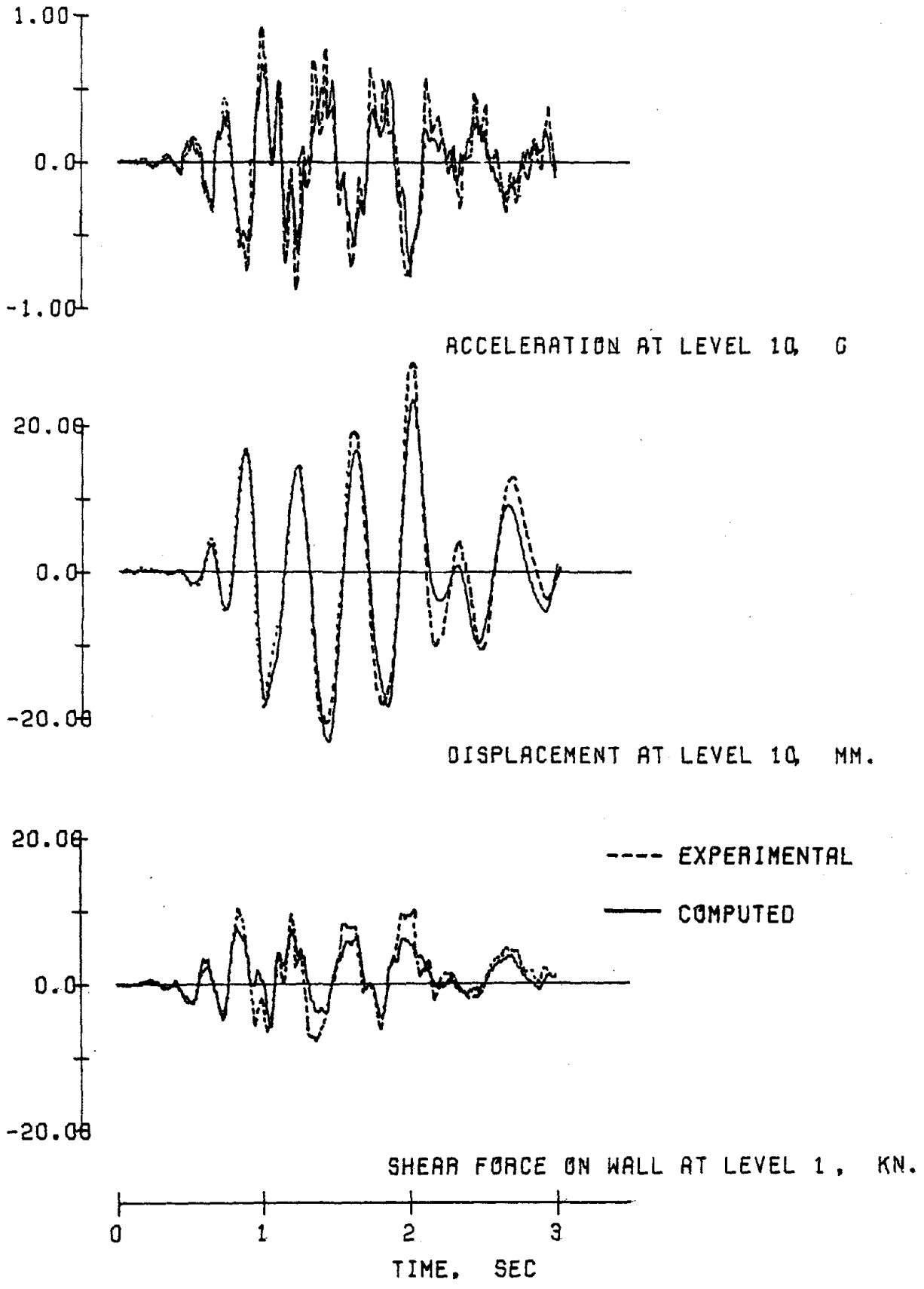

STRUCTURE FW-2, RUN-1

FIG. 6.12 (continued)

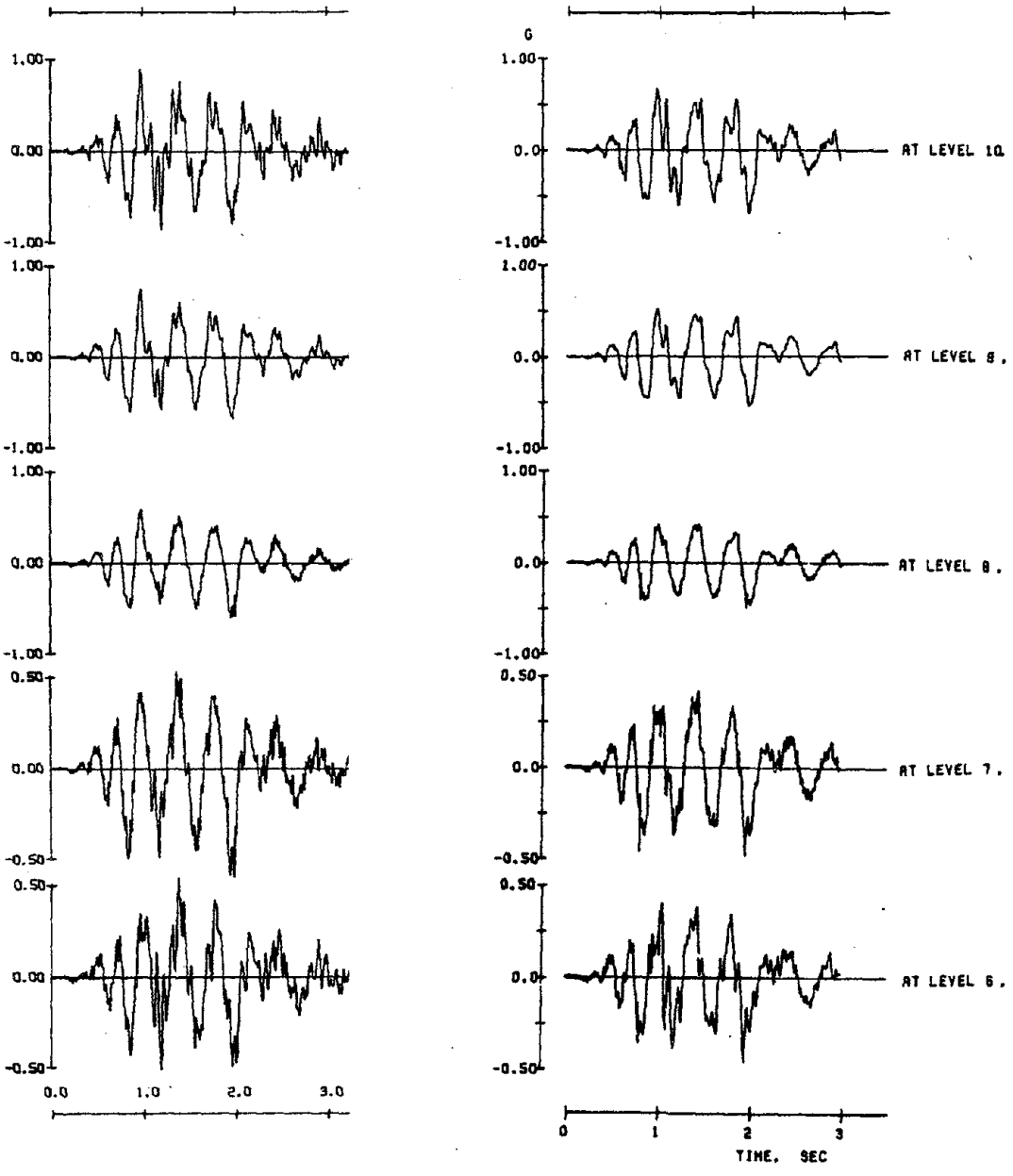

ACCELERATION FOR STRUCTURE FW-2, RUN-1

FIG. 6.12 (continued)

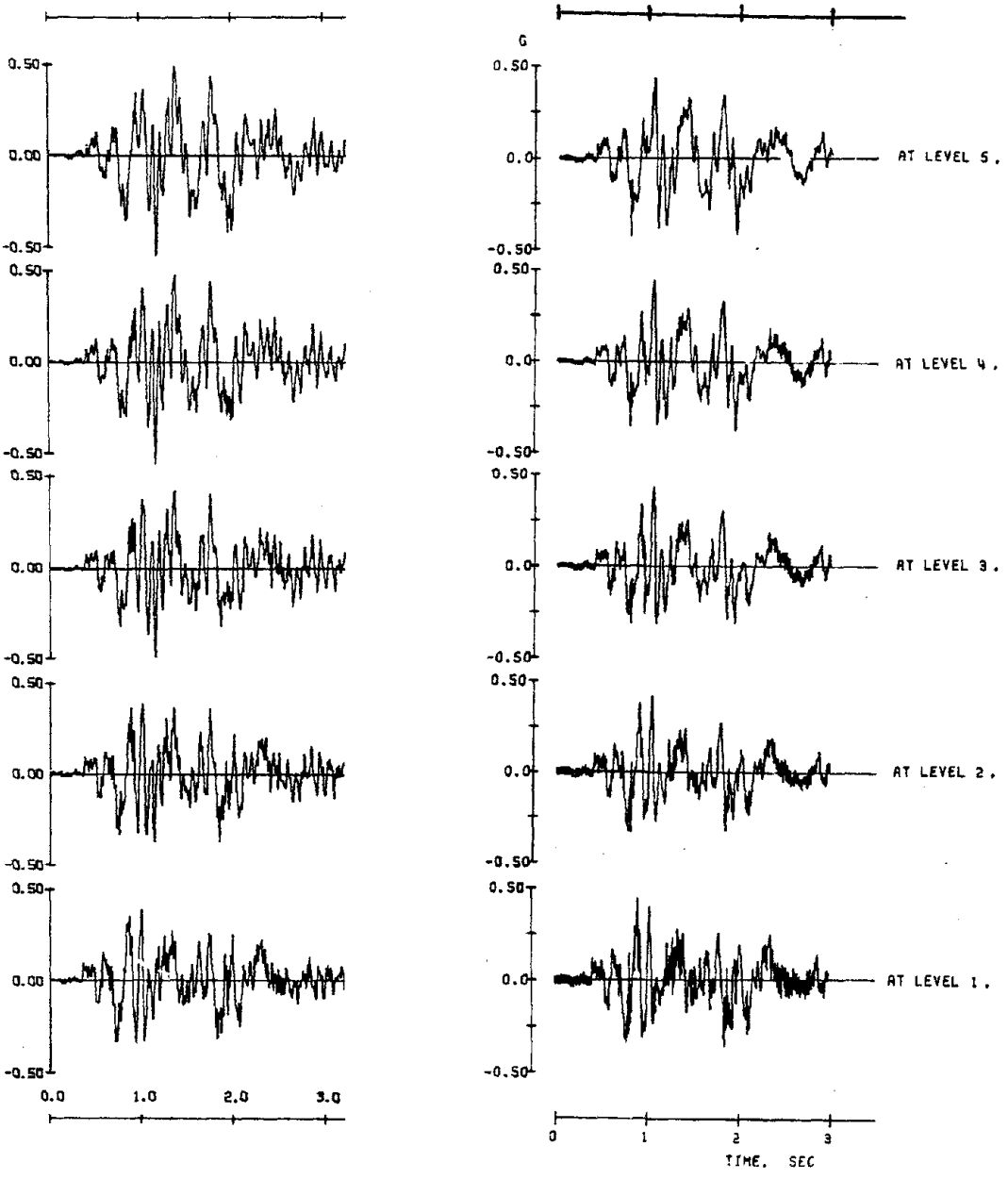

(EXPERIMENTAL) (COMPUTED)

ACCELERATIONS FOR STRUCTURE FW-2, RUN-1

FIG. 6.12 (continued)

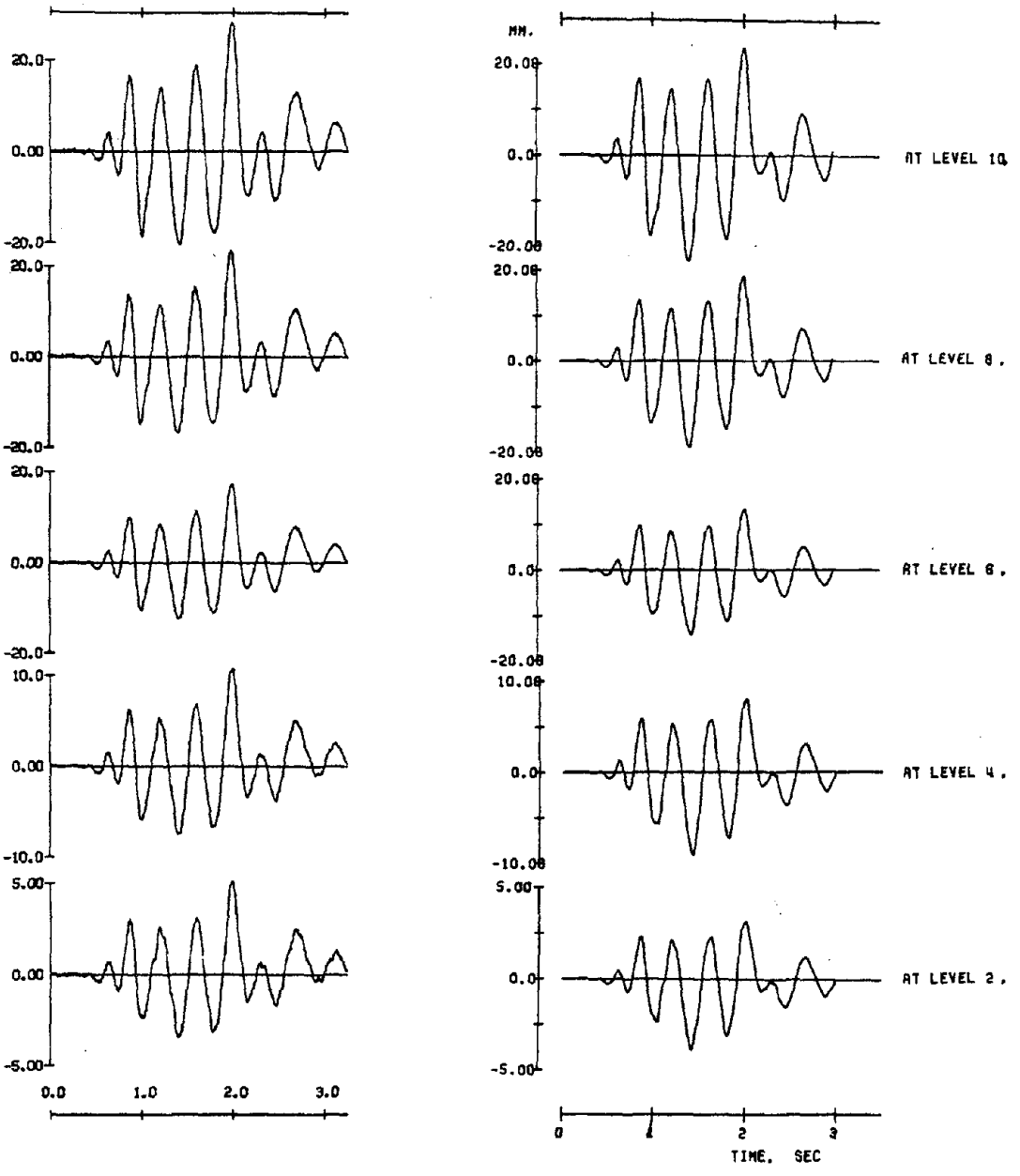

(EXPERIMENTAL) (COMPUTED)

DISPLACEMENTS FOR STRUCTURE FW-2, RUN-1

FIG. 6.12 (continued)

—— Wall shear

---- Story shear

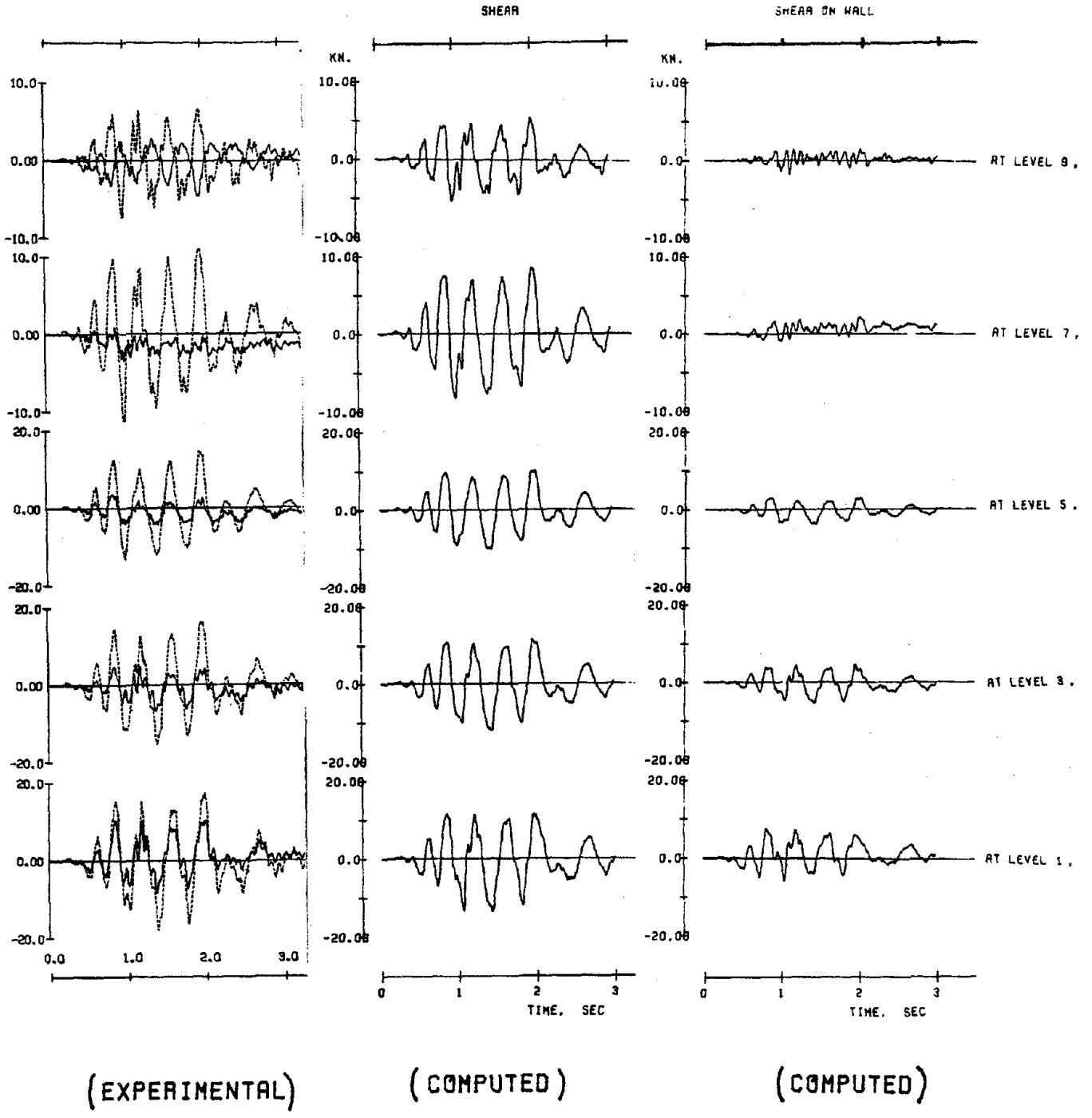

SHEAR FORCES FOR STRUCTURE FW-2, RUN-1

FIG. 6.12 (continued)

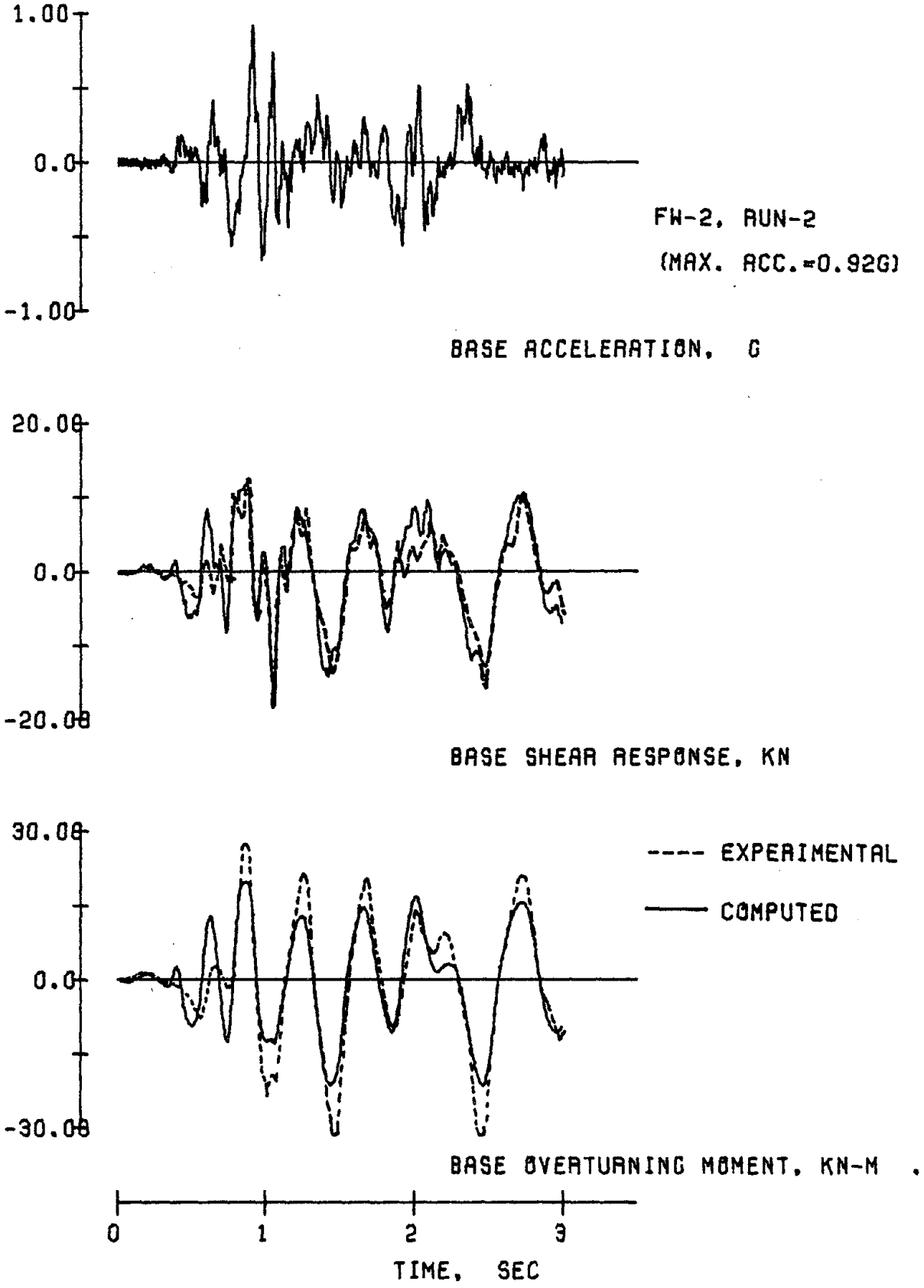

FIG. 6.13 RESPONSE WAVEFORMS FOR STRUCTURE FW-2, RUN-2

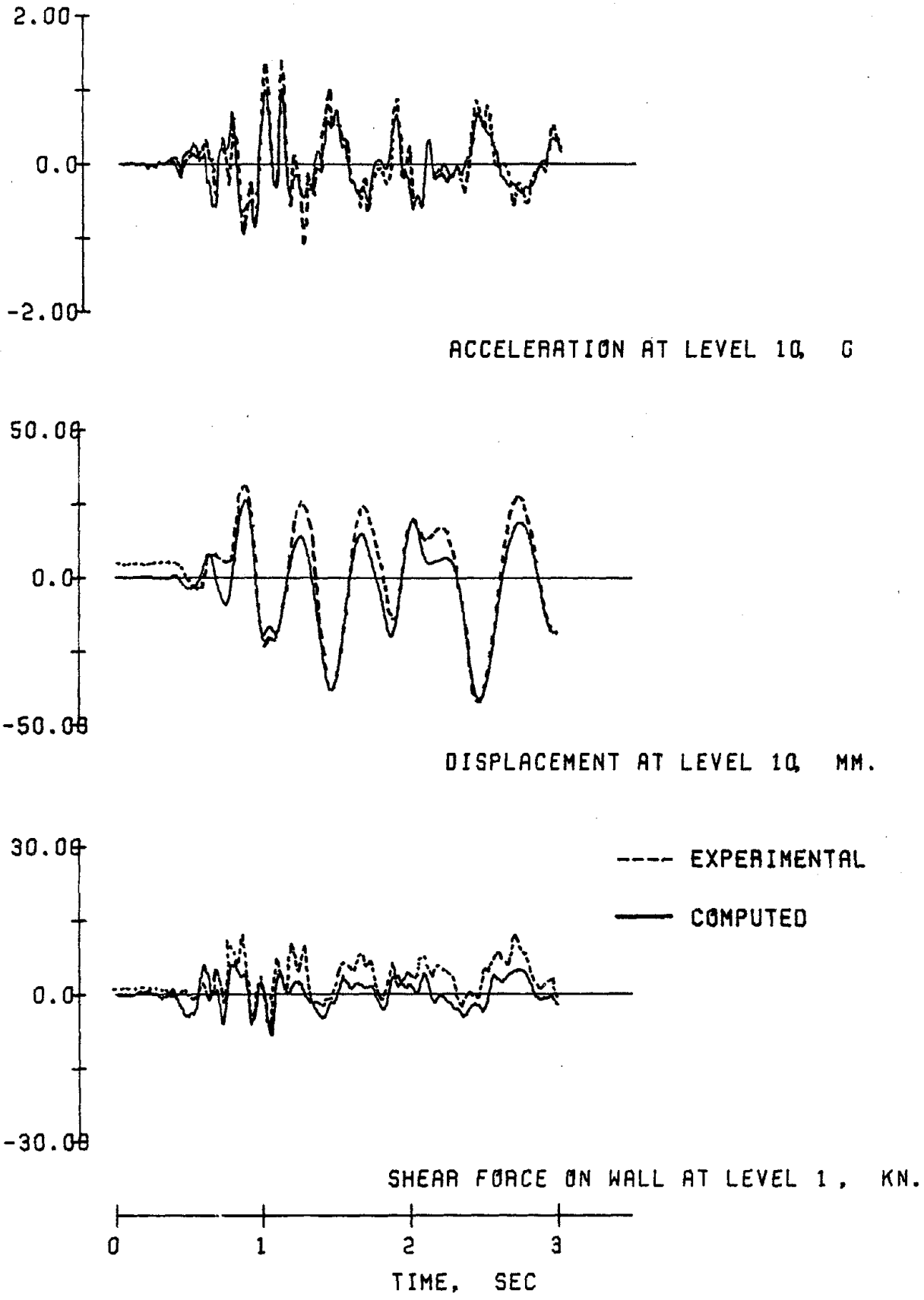

STRUCTURE FW-2, RUN-2

FIG. 6.13 (continued)

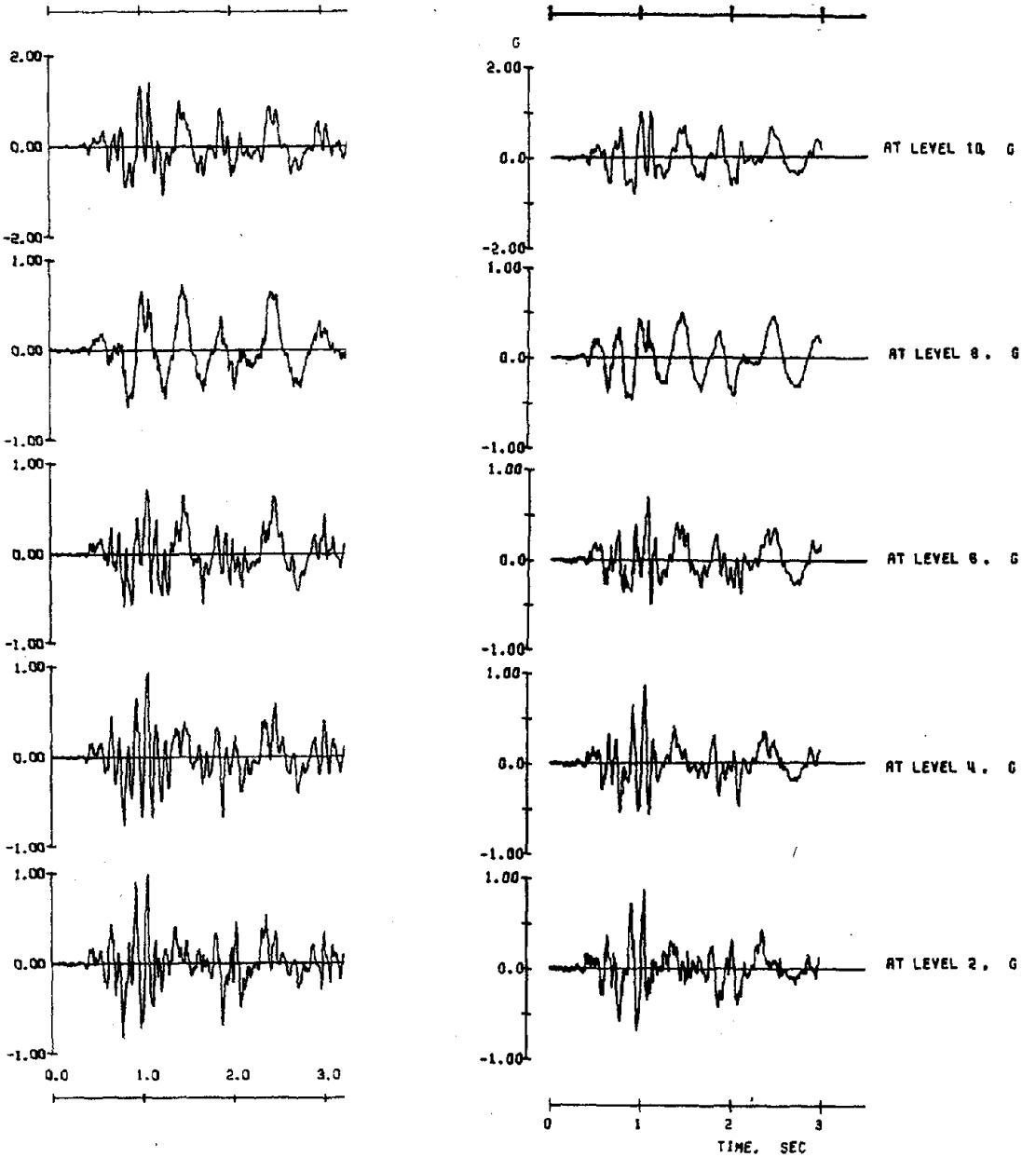

ACCELERATIONS FOR STRUCTURE FW-2, RUN-2

FIG. 6.13 (continued)

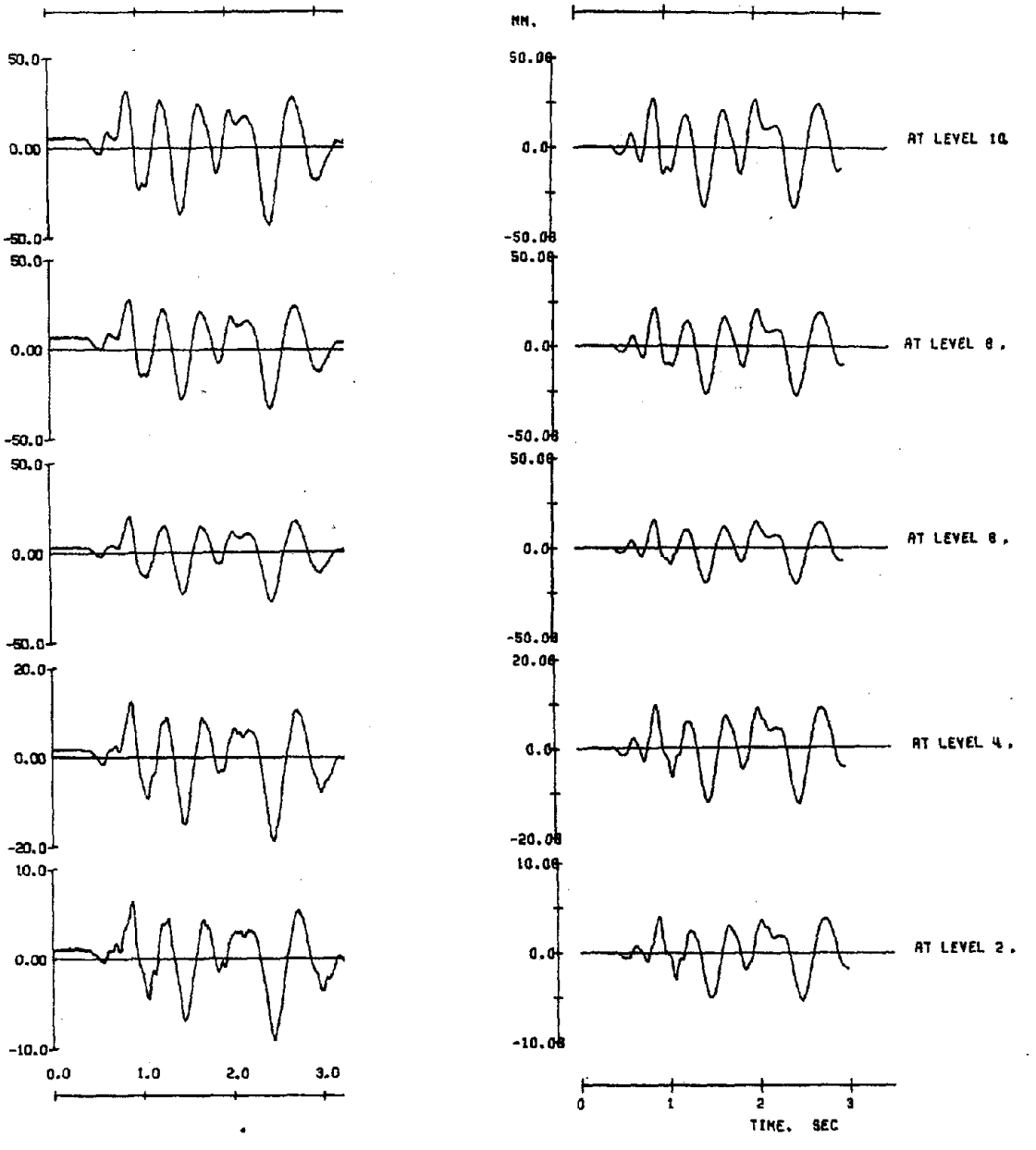

(EXPERIMENTAL) (COMPUTED)

DISPLACEMENTS FOR STRUCTURE FW-2, RUN-2

FIG. 6.13 (continued)

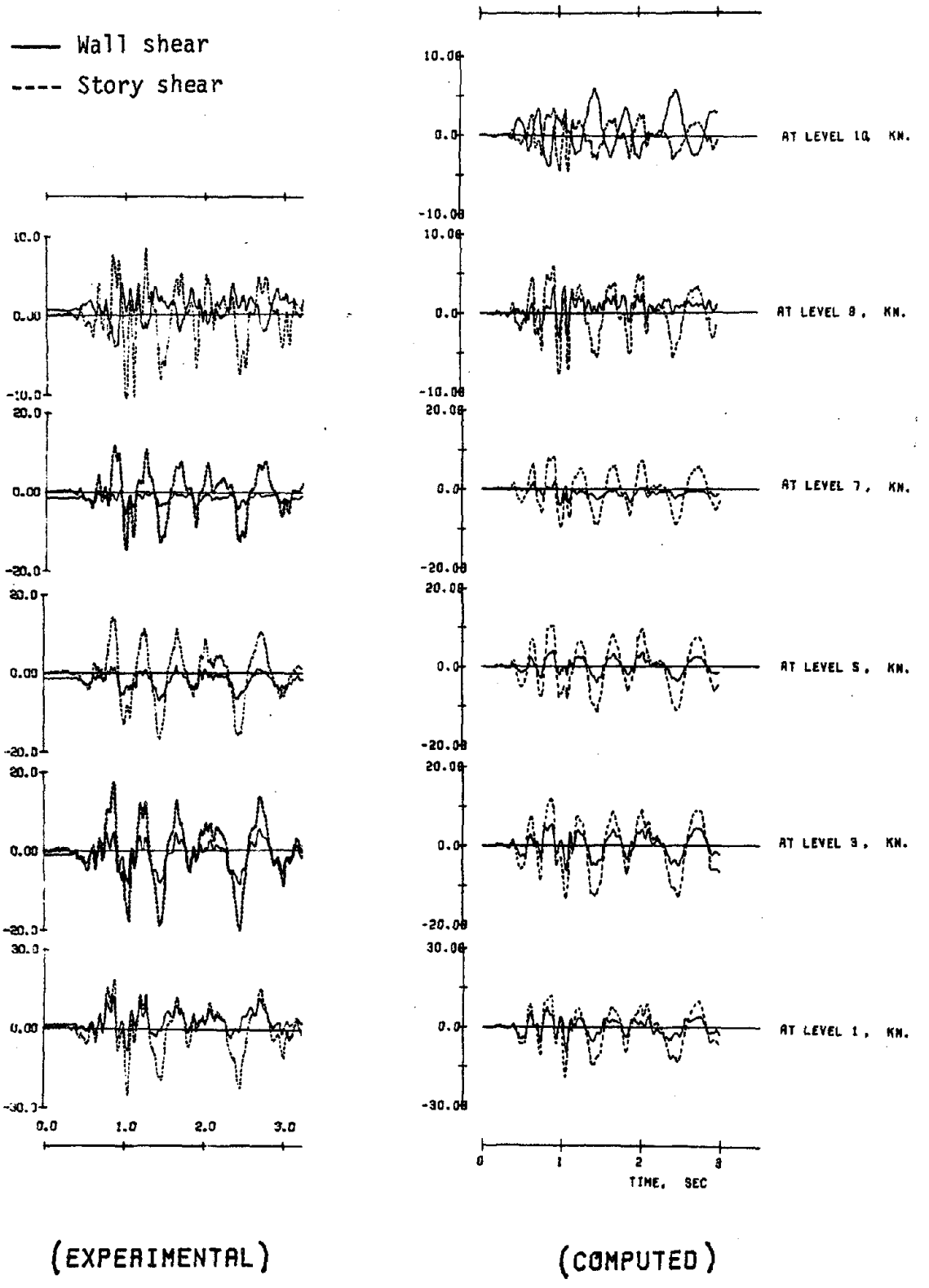

SHEAR FORCES FOR STRUCTURE FW-2, RUN-2

FIG. 6.13 (continued)

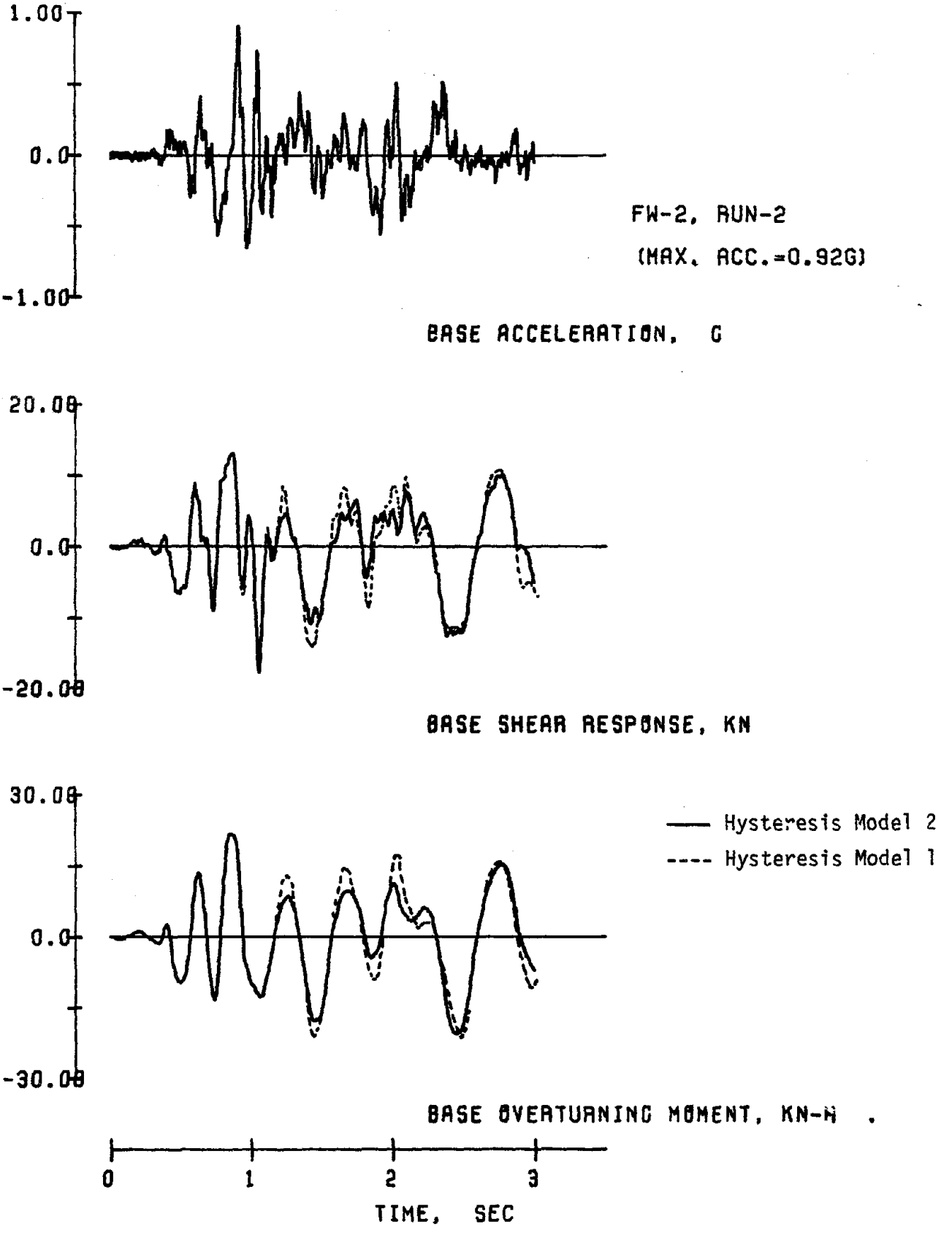

FIG. 6.14 RESPONSE WAVEFORMS FOR STRUCTURE FW-2, RUN-2 USING HYSTERESIS MODELS 1 AND 2

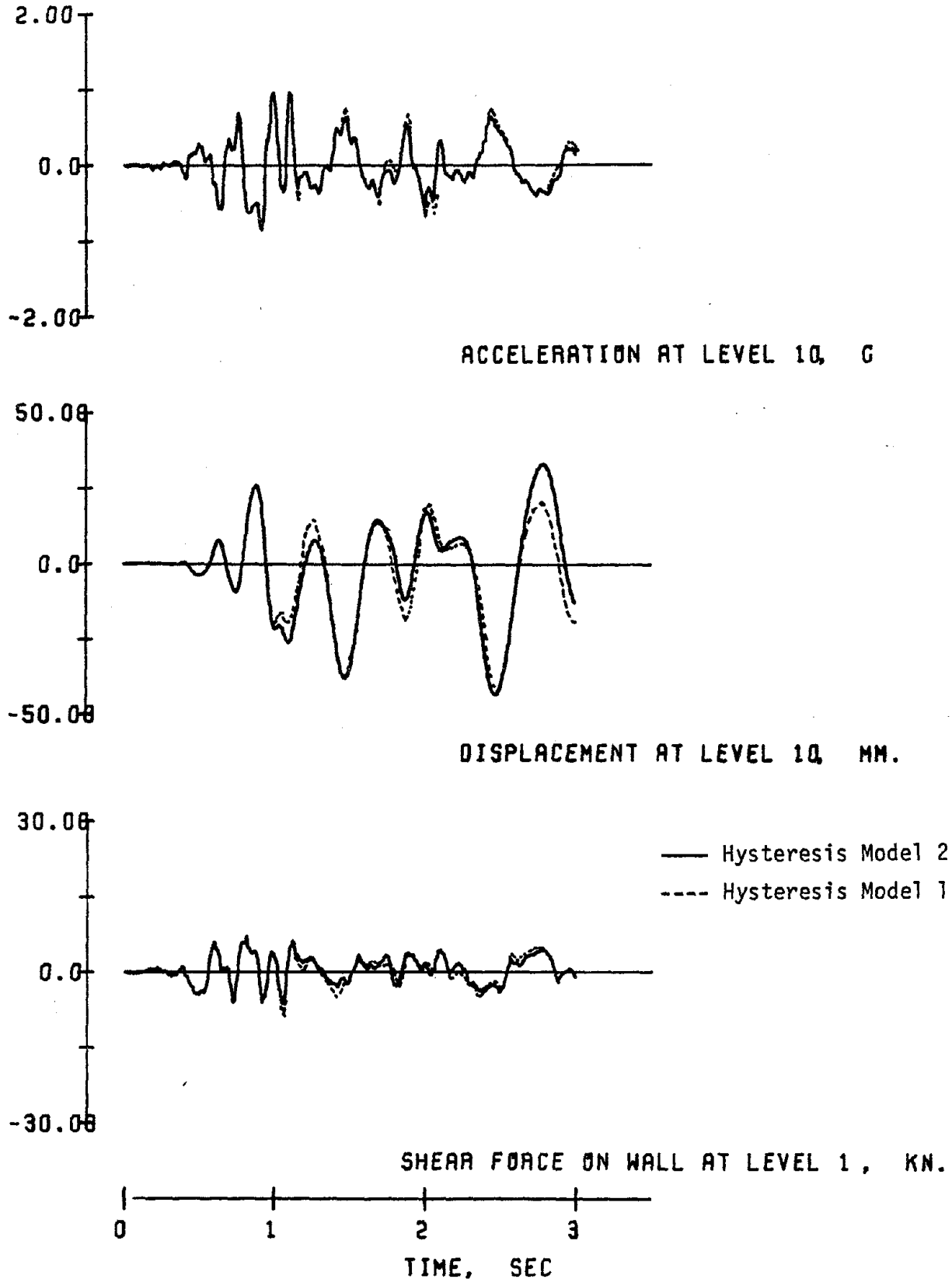

FIG. 6.14 (continued)

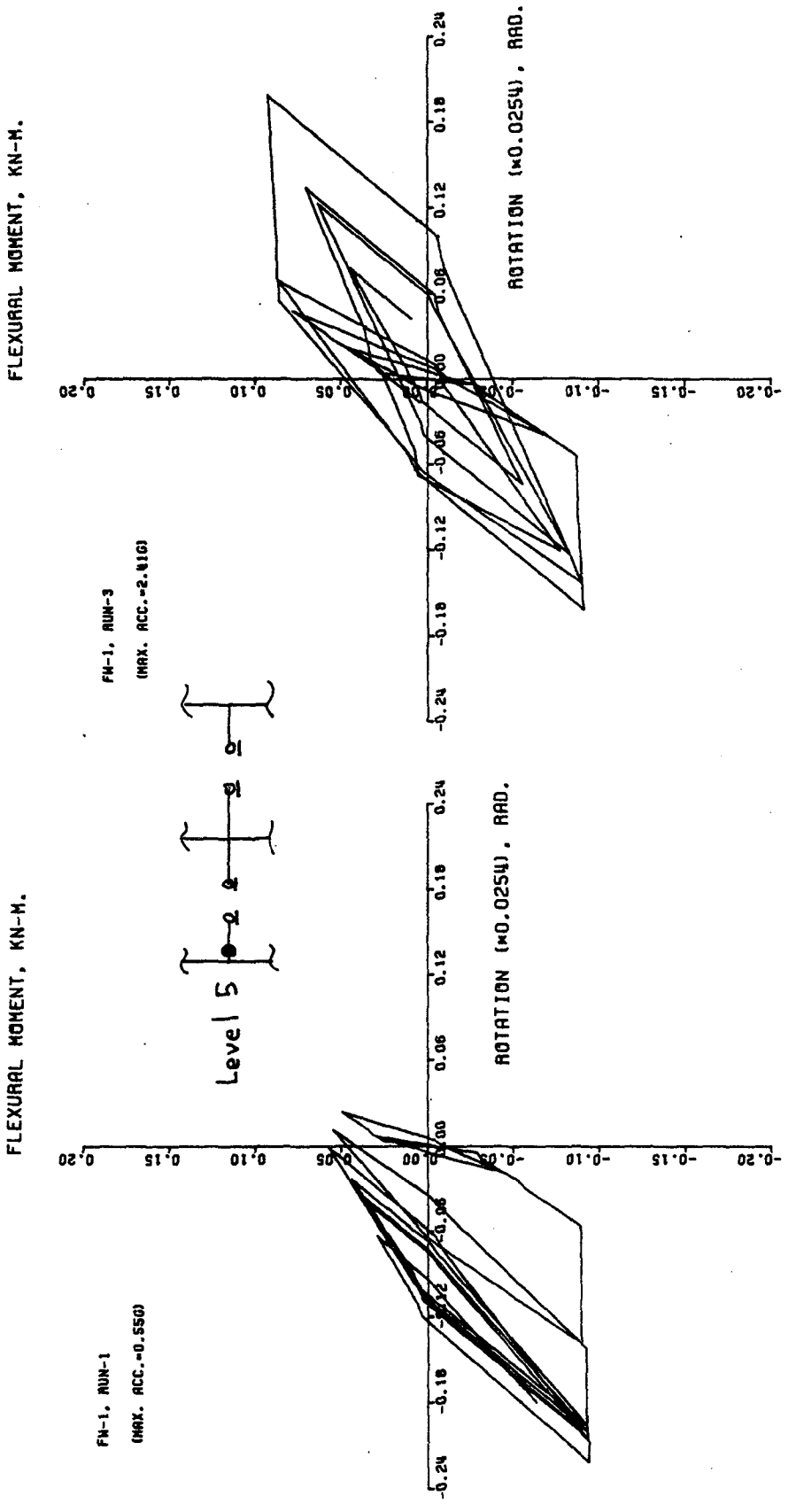

FIG. 6.15 MOMENT-ROTATION RELATIONSHIPS OF THE FLEXURAL SPRING AT THE 5TH LEVEL LEFT EXTERIOR BEAM

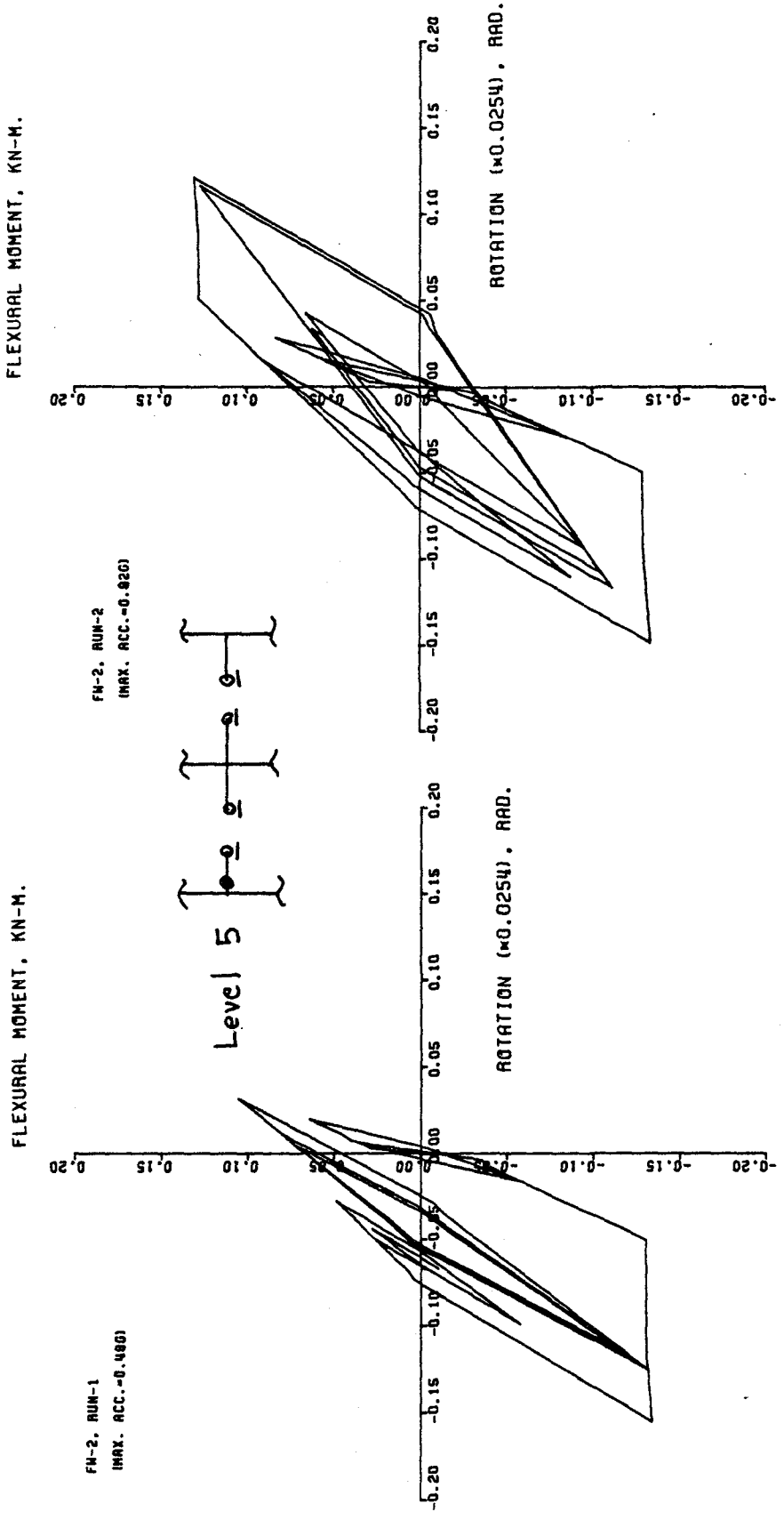

FIG. 6.15 (continued)

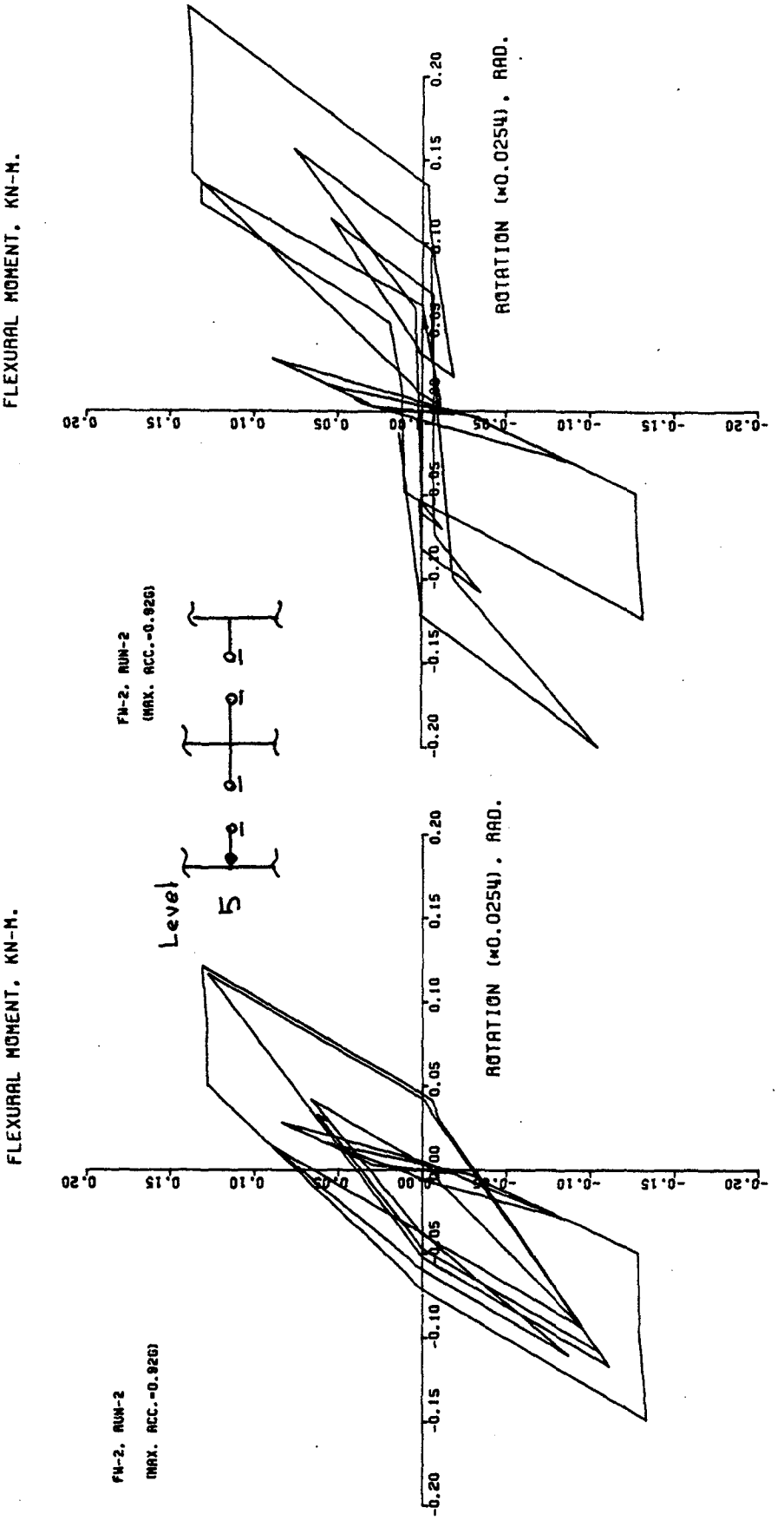

FIG. 6.16 MOMENT-ROTATION RELATIONSHIPS OF THE FLEXURAL SPRING USING HYSTERESIS MODELS 1 AND 2 AT THE 5TH LEVEL LEFT EXTERIOR BEAM

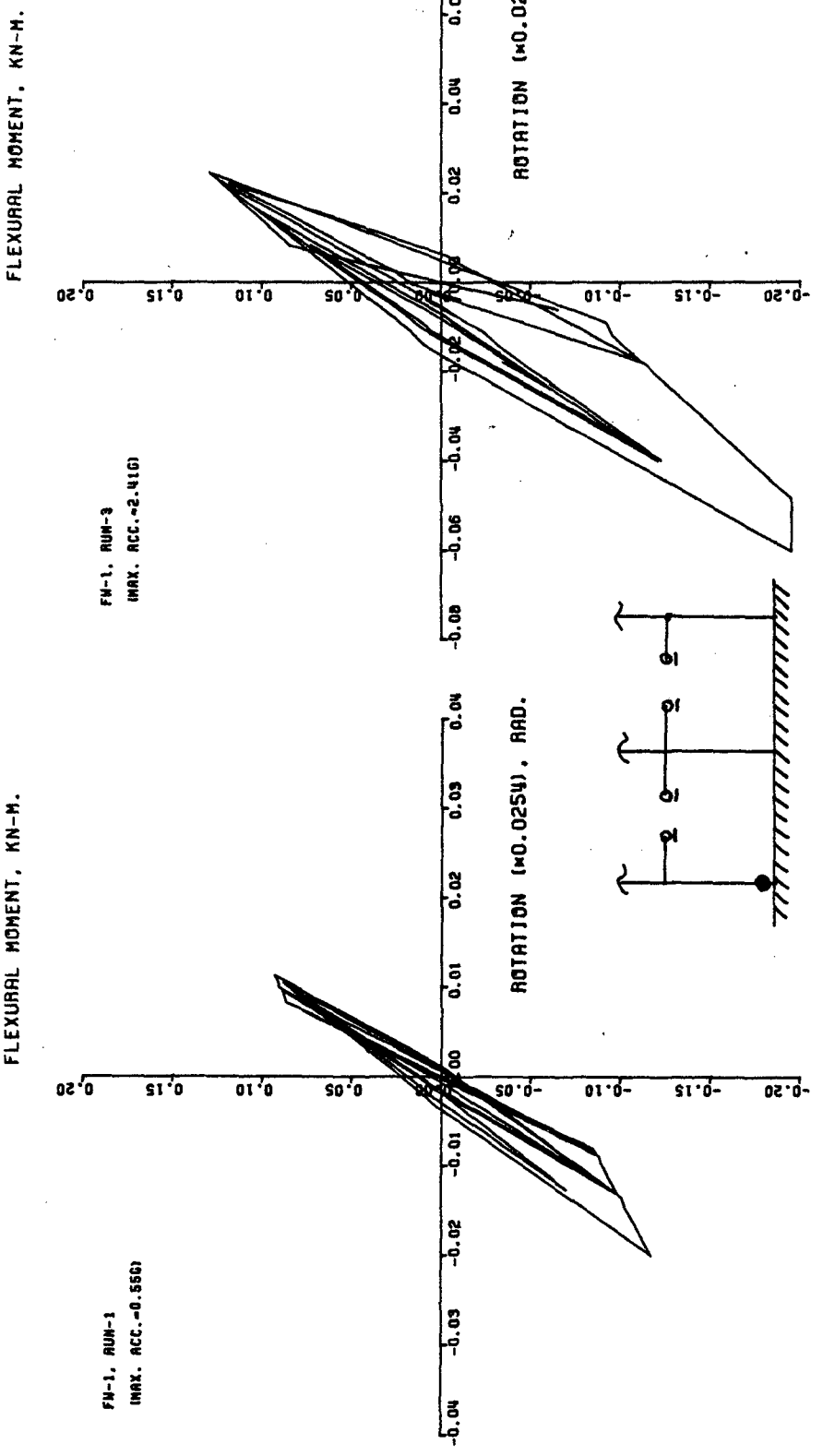

FIG. 6.17 MOMENT-ROTATION RELATIONSHIPS OF A FLEXURAL SPRING AT THE BASE OF THE LEFT COLUMN

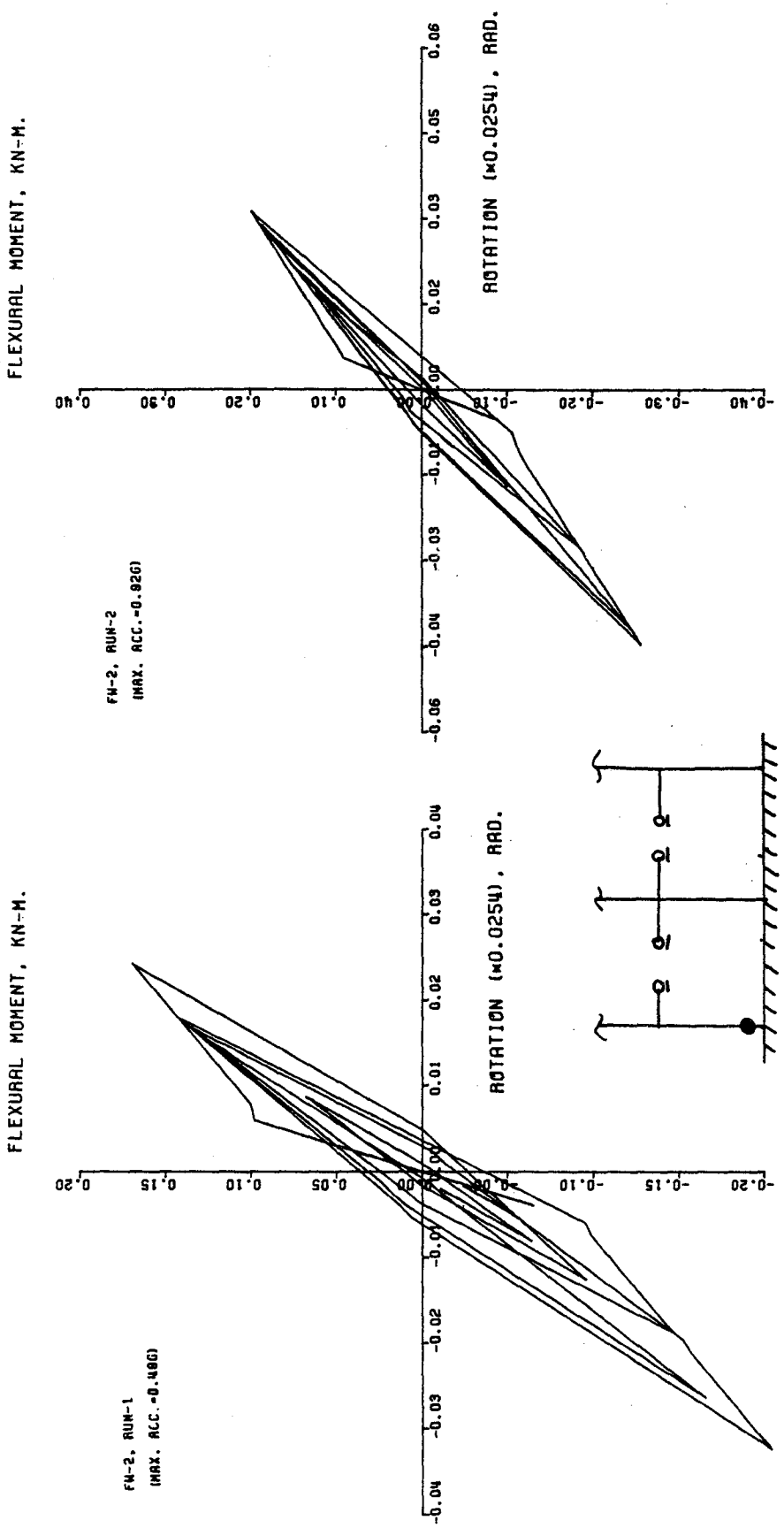

FIG. 6.17 (continued)

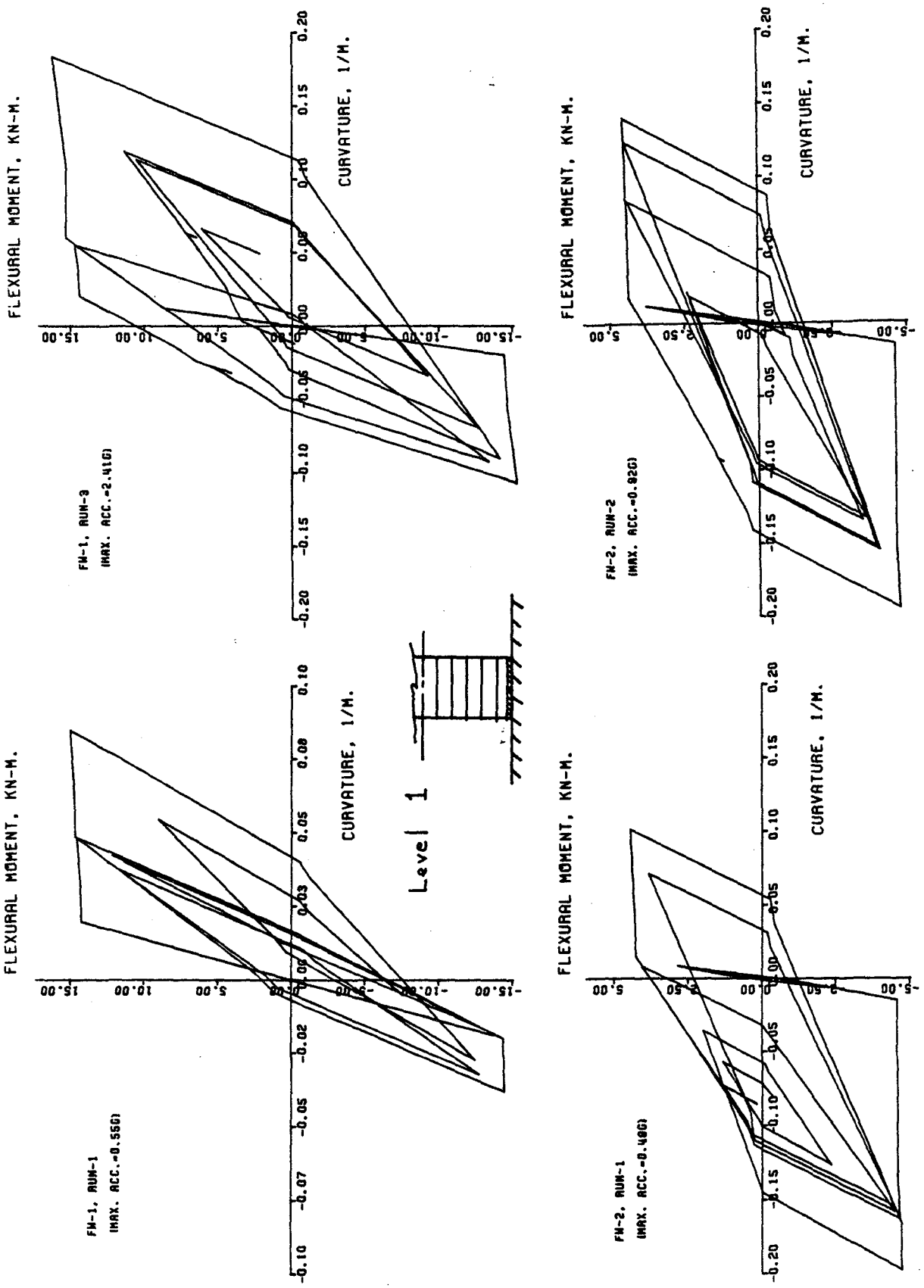

FIG. 6.18 MOMENT-CURVATURE RELATIONSHIPS OF THE FLEXURAL SPRING AT THE BASE ELEMENT OF THE WALL

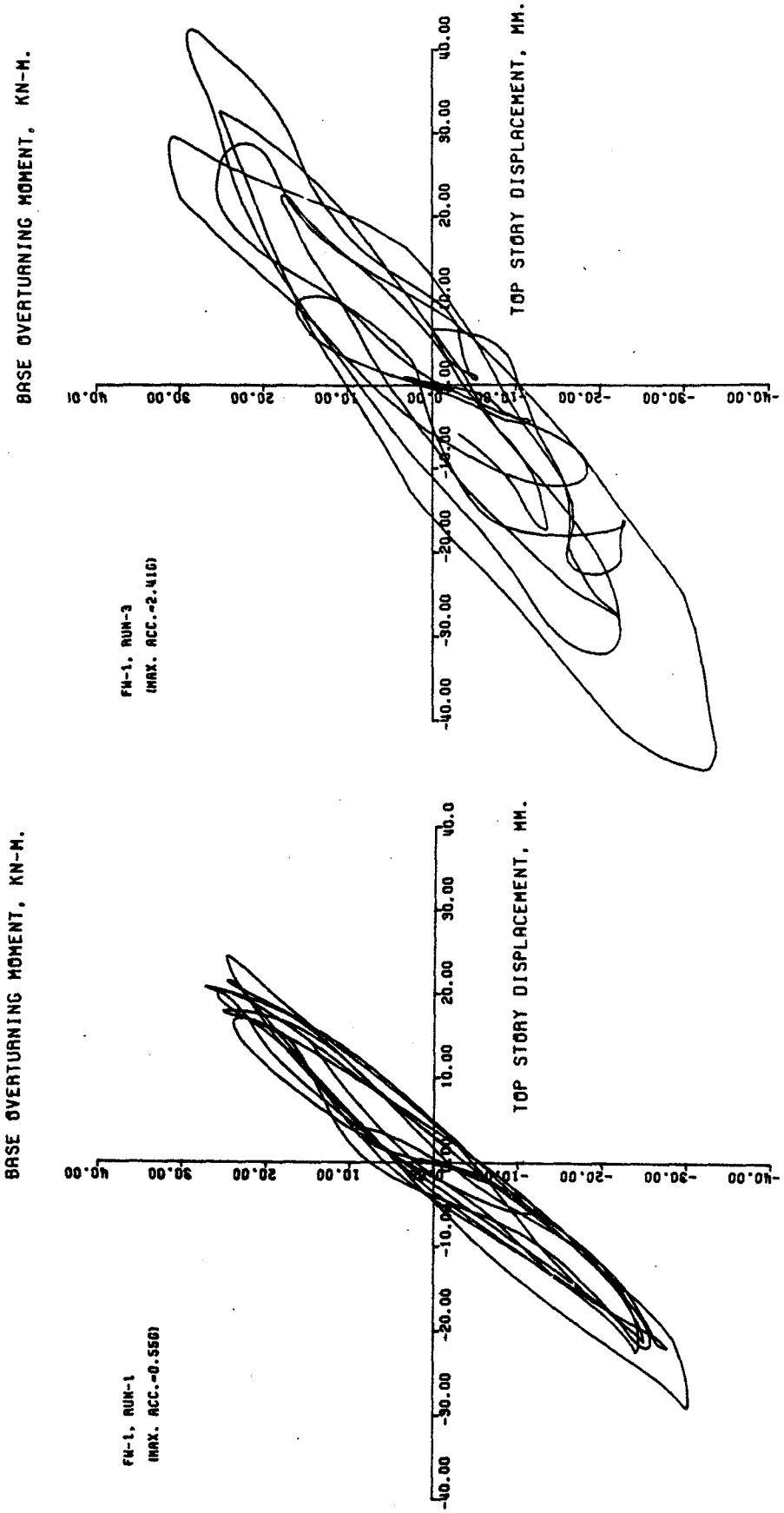

FIG. 6.19 BASE OVERTURNING MOMENT VS. TOP-STORY DISPLACEMENT RELATIONSHIPS OF THE STRUCTURES

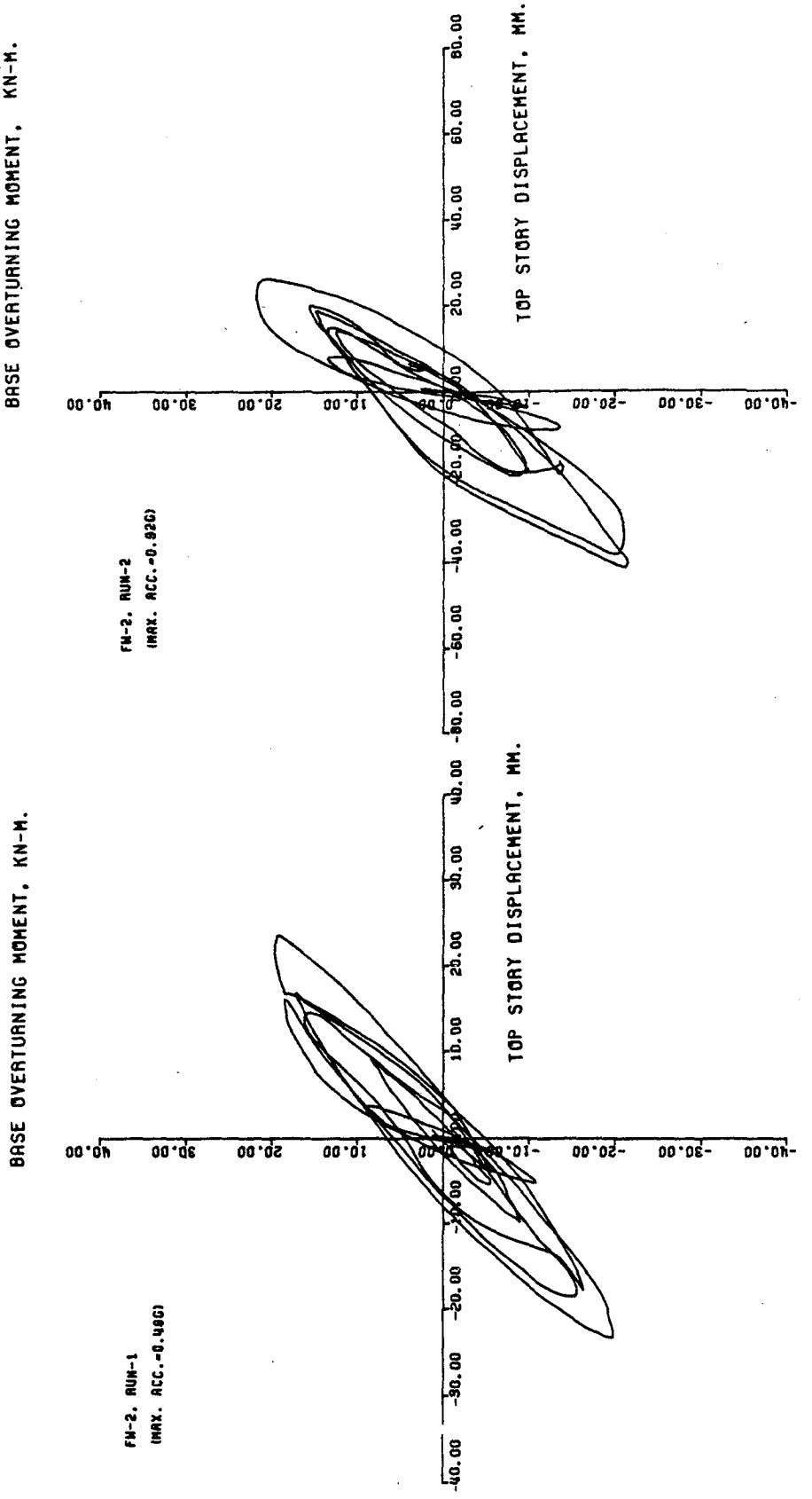

FIG. 6.19 (continued)

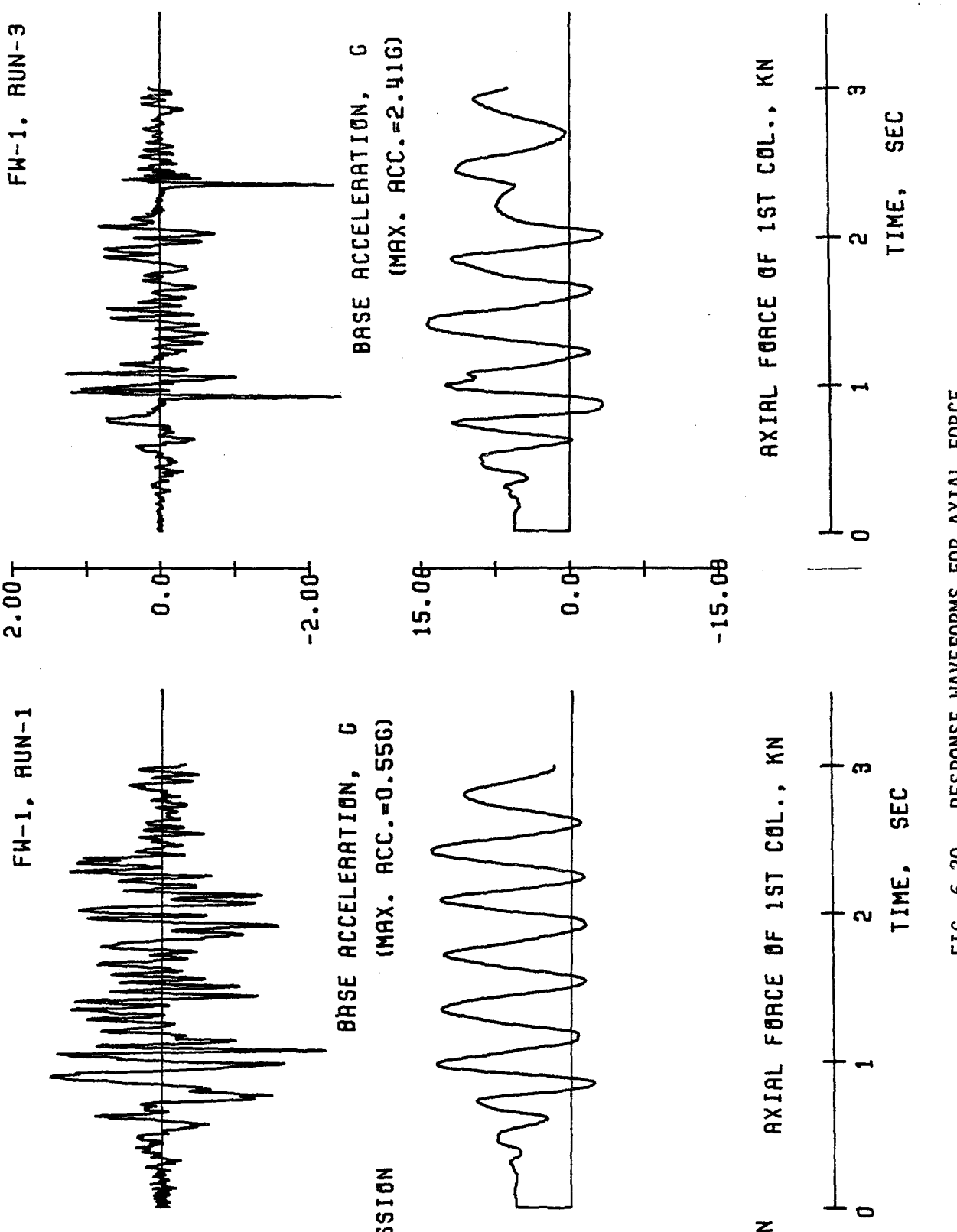

FIG. 6.20 RESPONSE WAVEFORMS FOR AXIAL FORCE AT THE BASE OF THE LEFT COLUMN

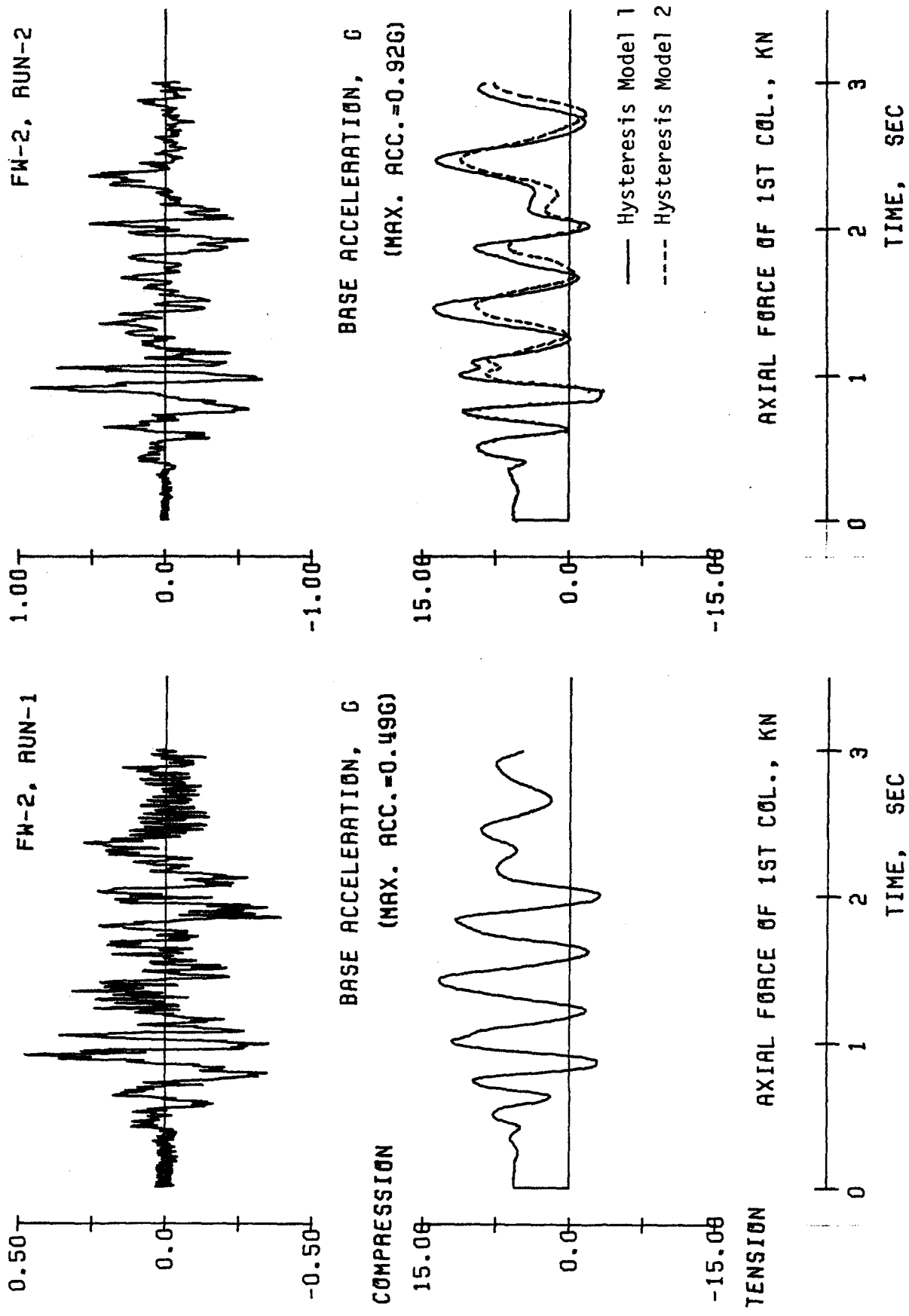

FIG. 6.20 (continued)

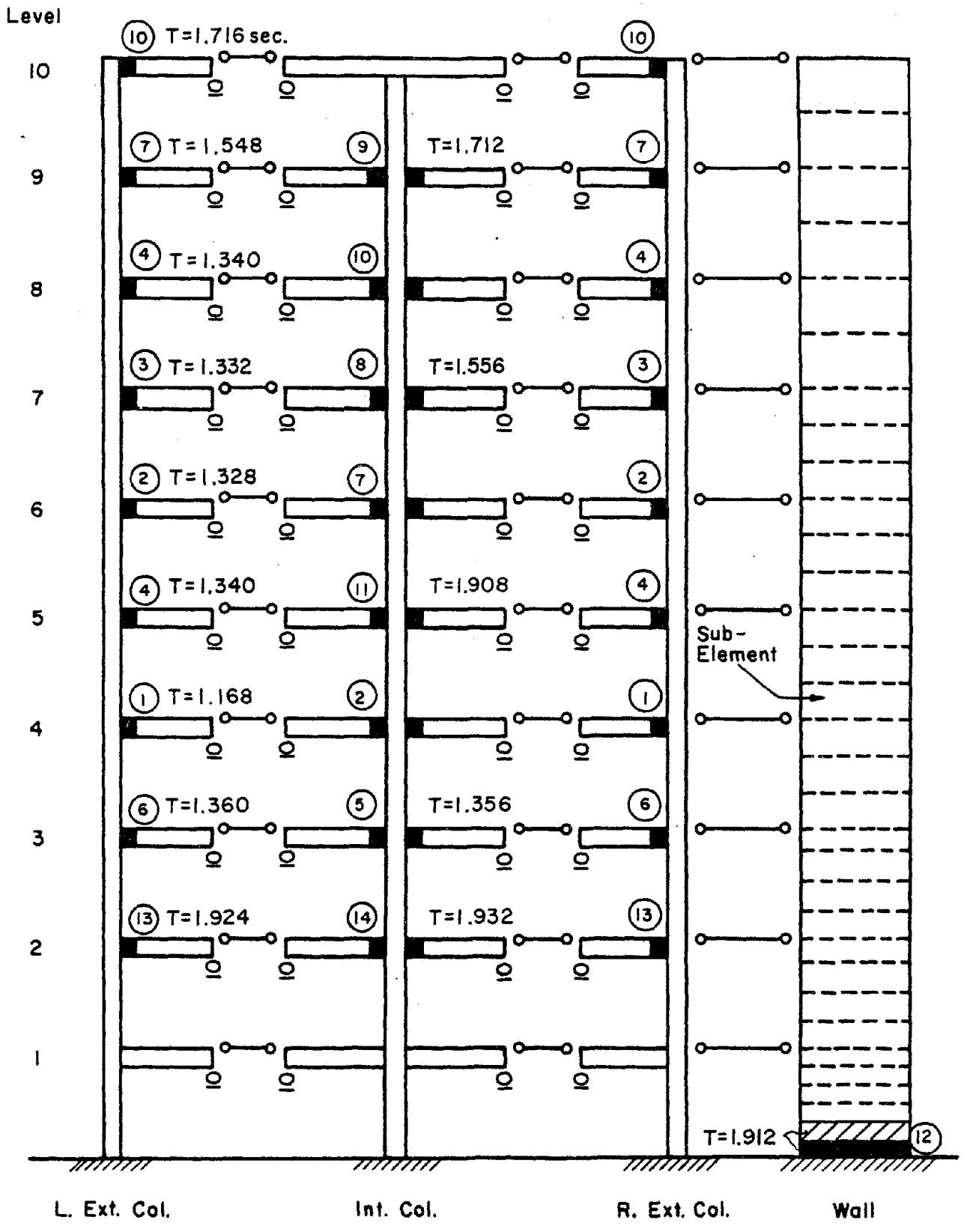

FIG. 6.21 COMPUTED STRUCTURAL YIELD PATTERNS
(STRUCTURE FW-1, RUN-1)

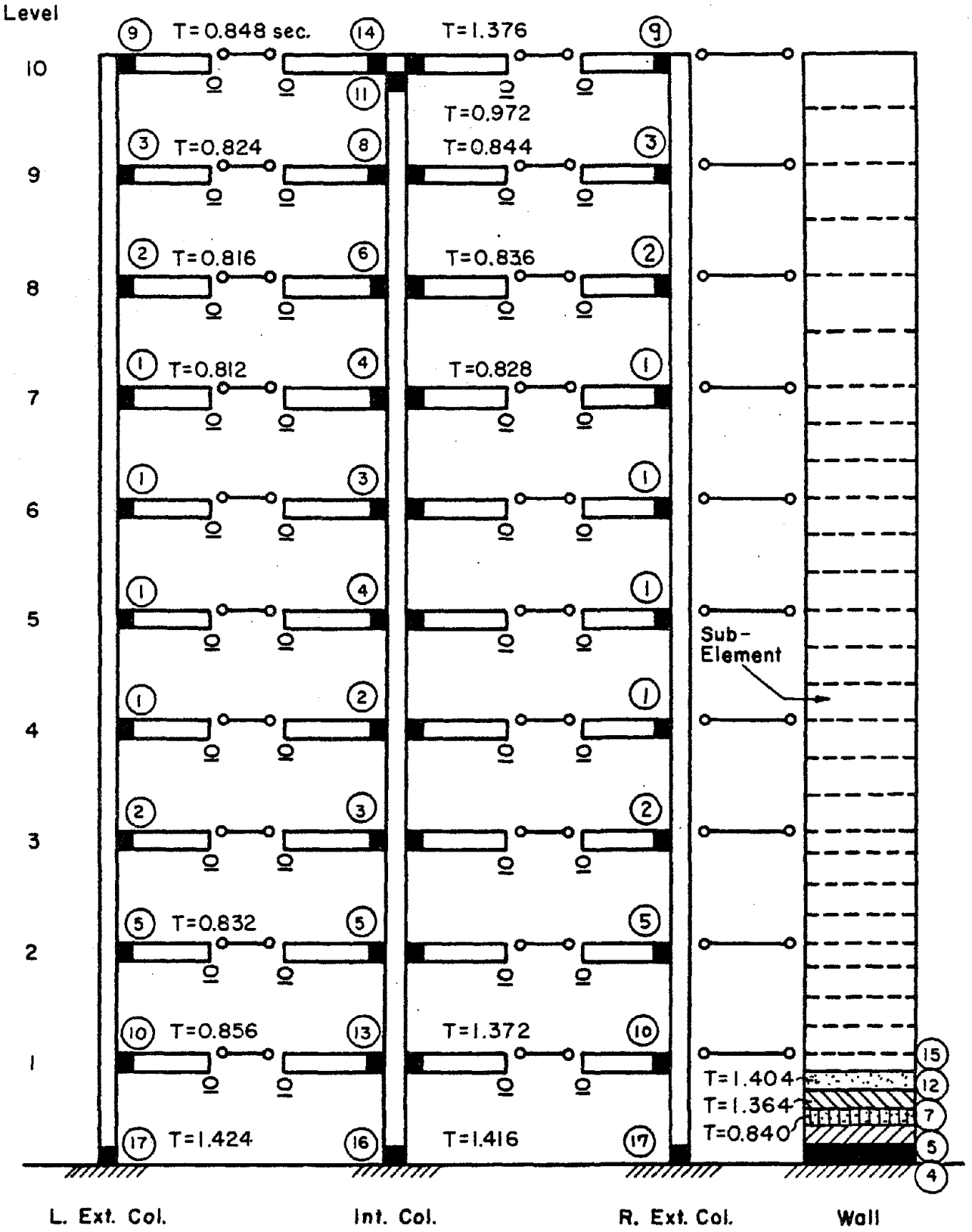

STRUCTURE FW-1, RUN-3

FIG. 6.21 (continued)

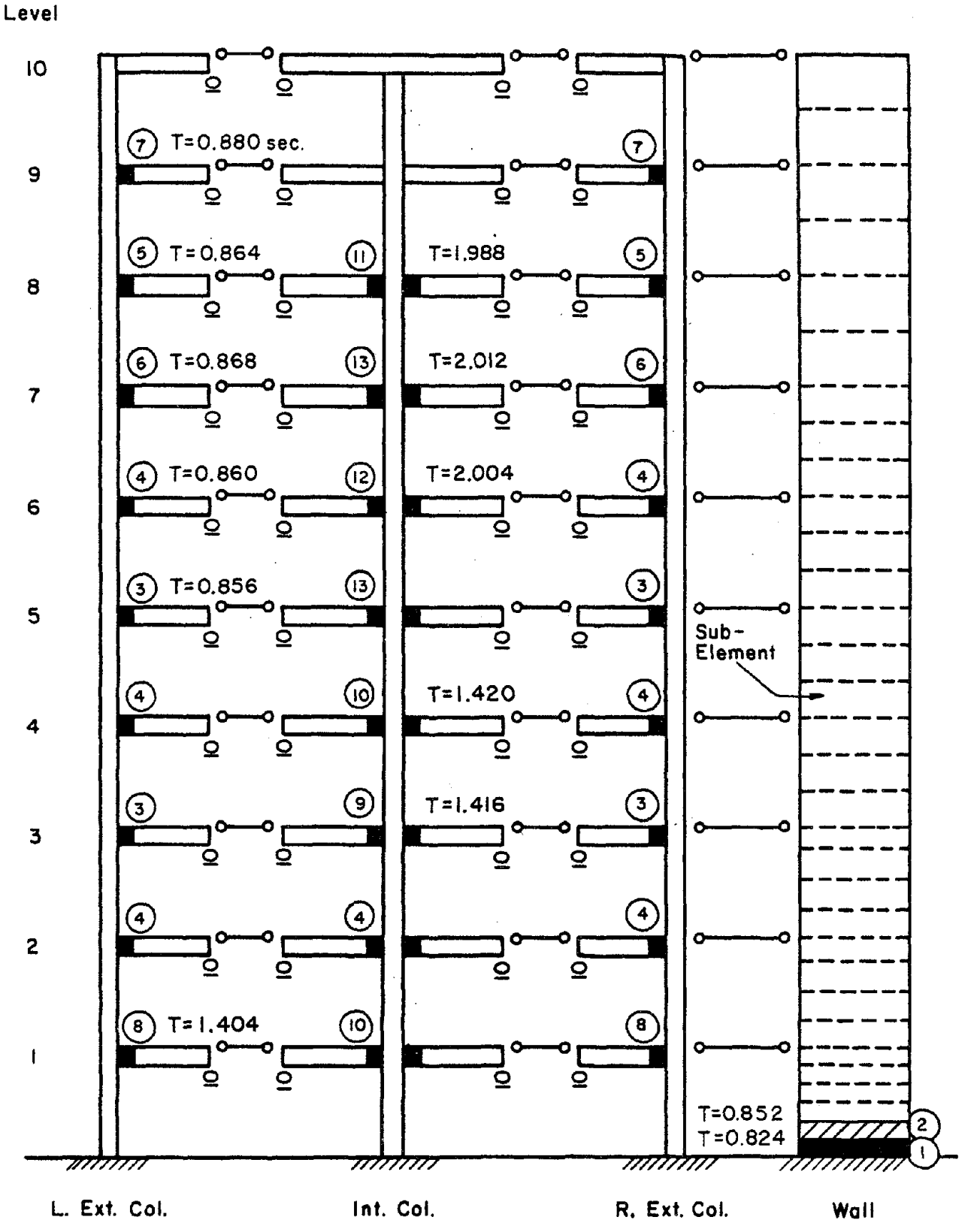

STRUCTURE FW-2, RUN-1

FIG. 6.21 (continued)

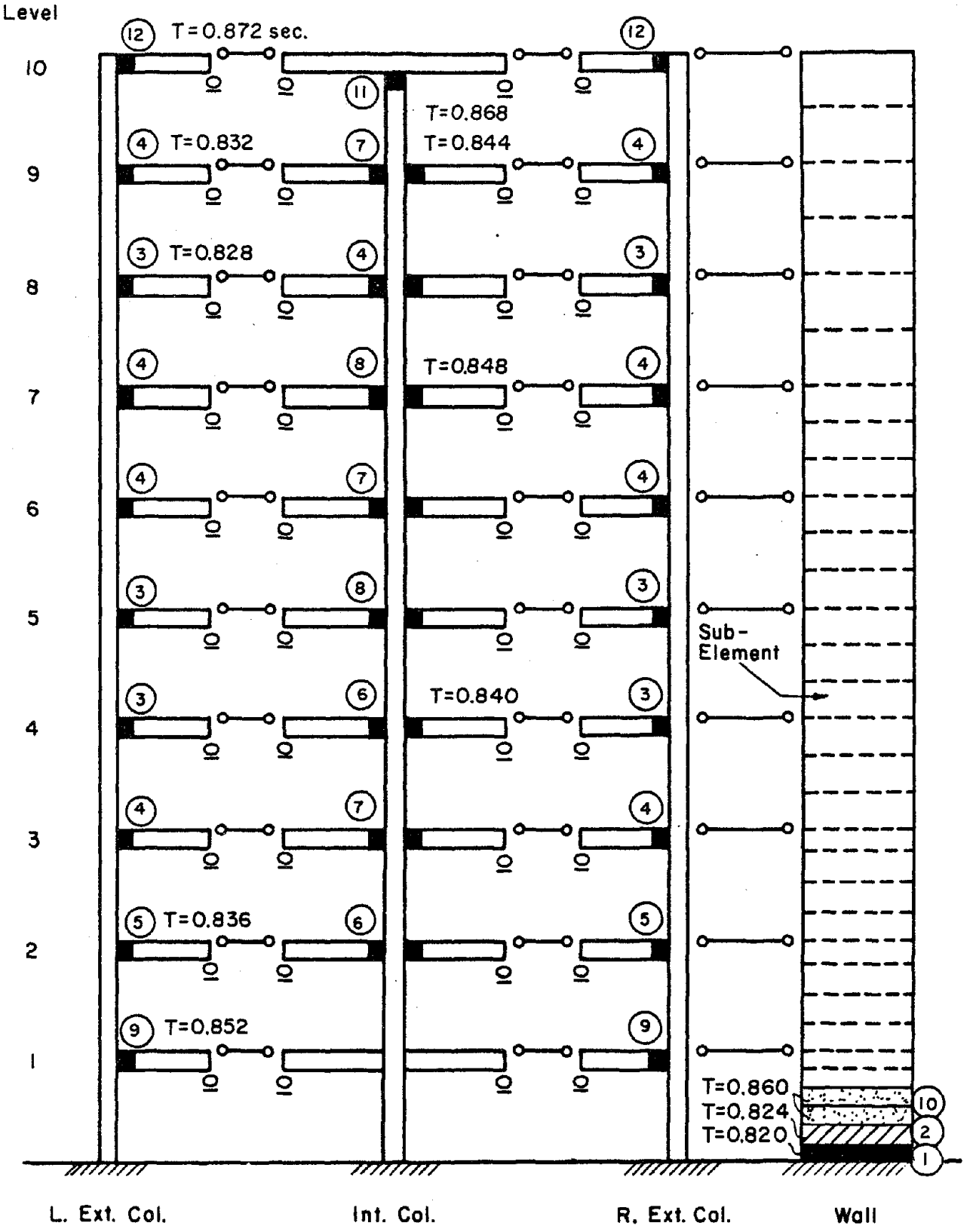

STRUCTURE FW-2, RUN-2

FIG. 6.21 (continued)

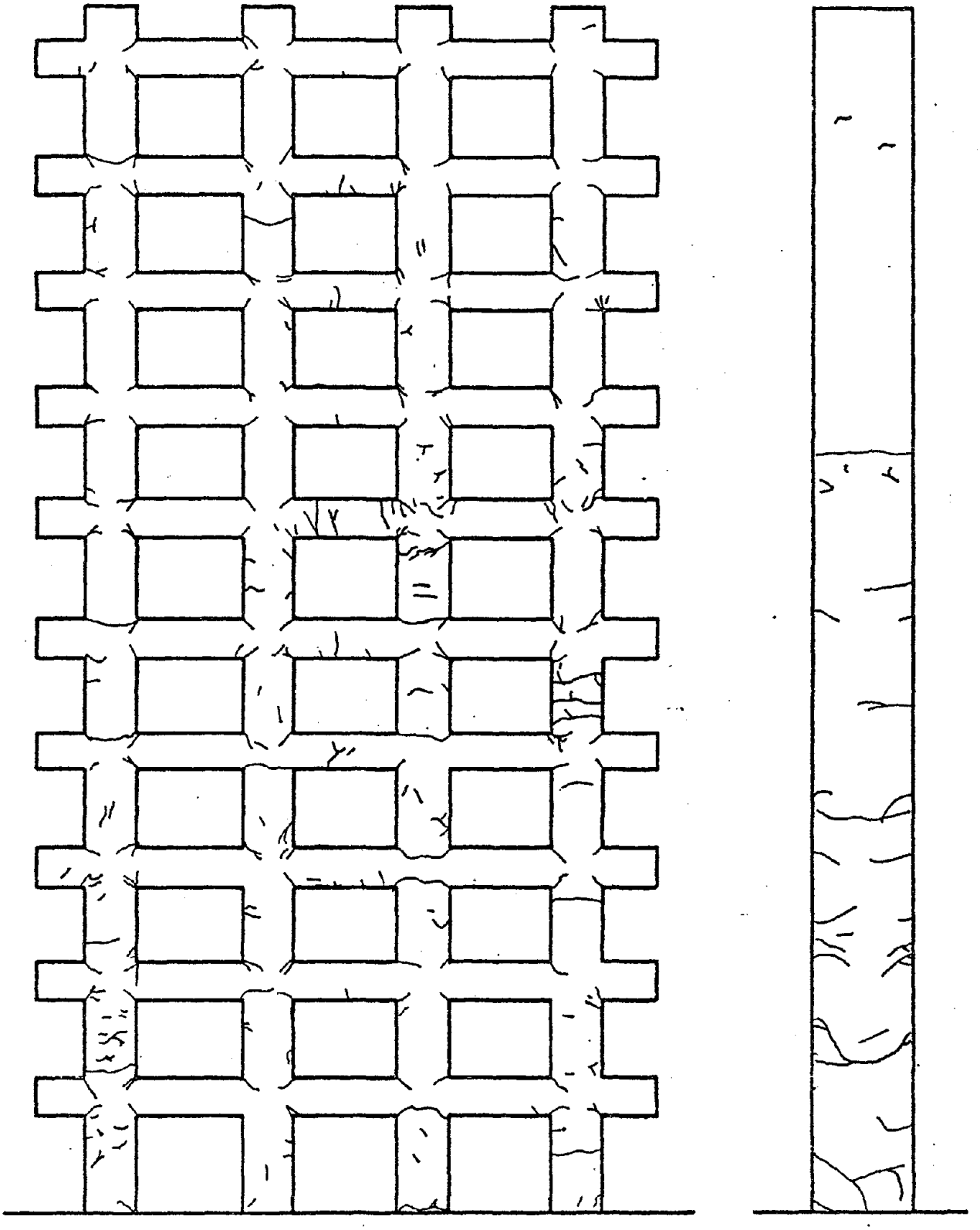

(Not To Scale)

Abrams & Sozen [2]

FIG. 6.22 OBSERVED CRACK PATTERNS IN STRUCTURE FW-2, RUN-2

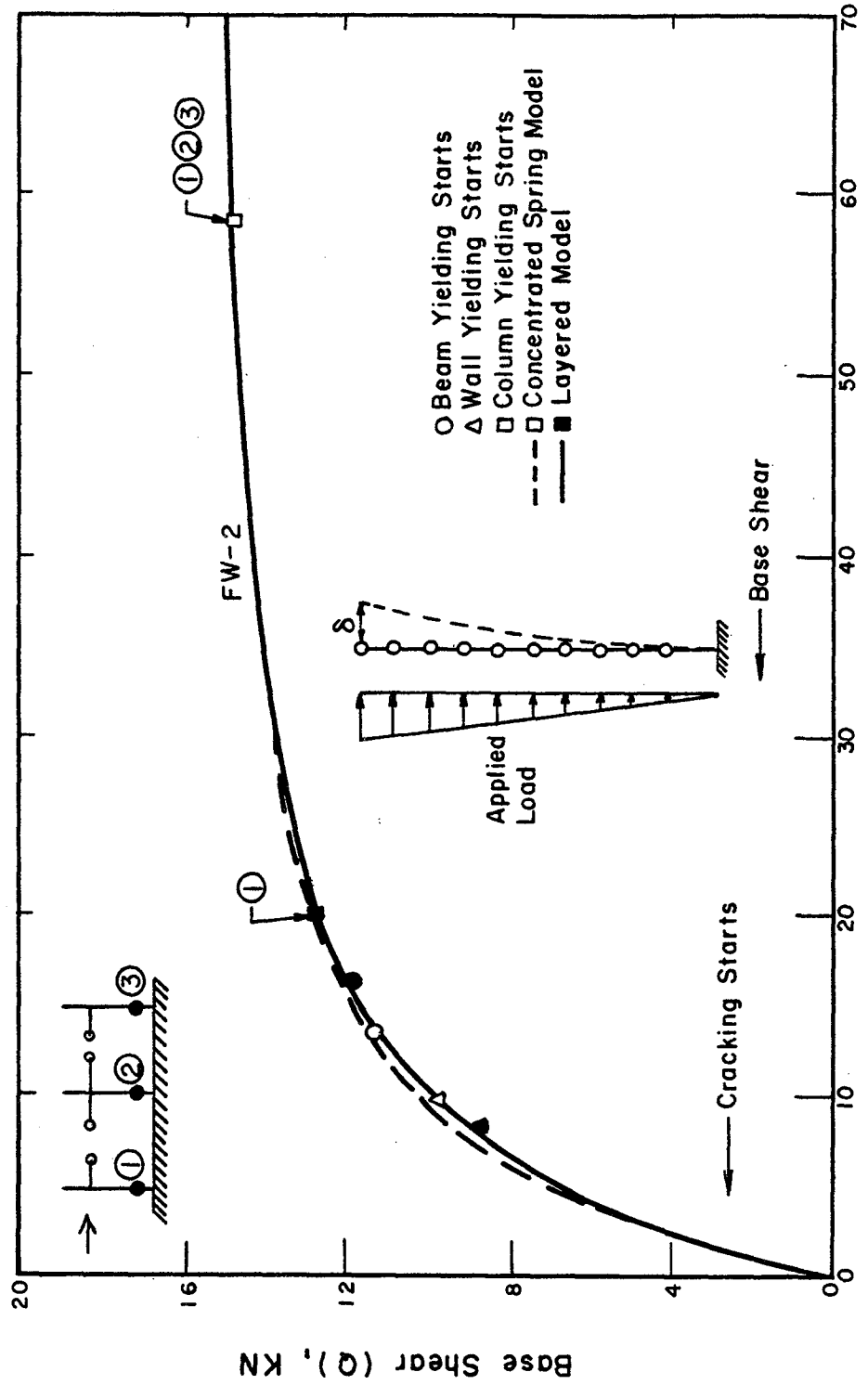

FIG. 6.23 BASE SHEAR VS. TOP-STORY DISPLACEMENT RELATIONSHIPS OF STRUCTURE FW-2 USING CONCENTRATED SPRING MODEL AND LAYERED MODEL

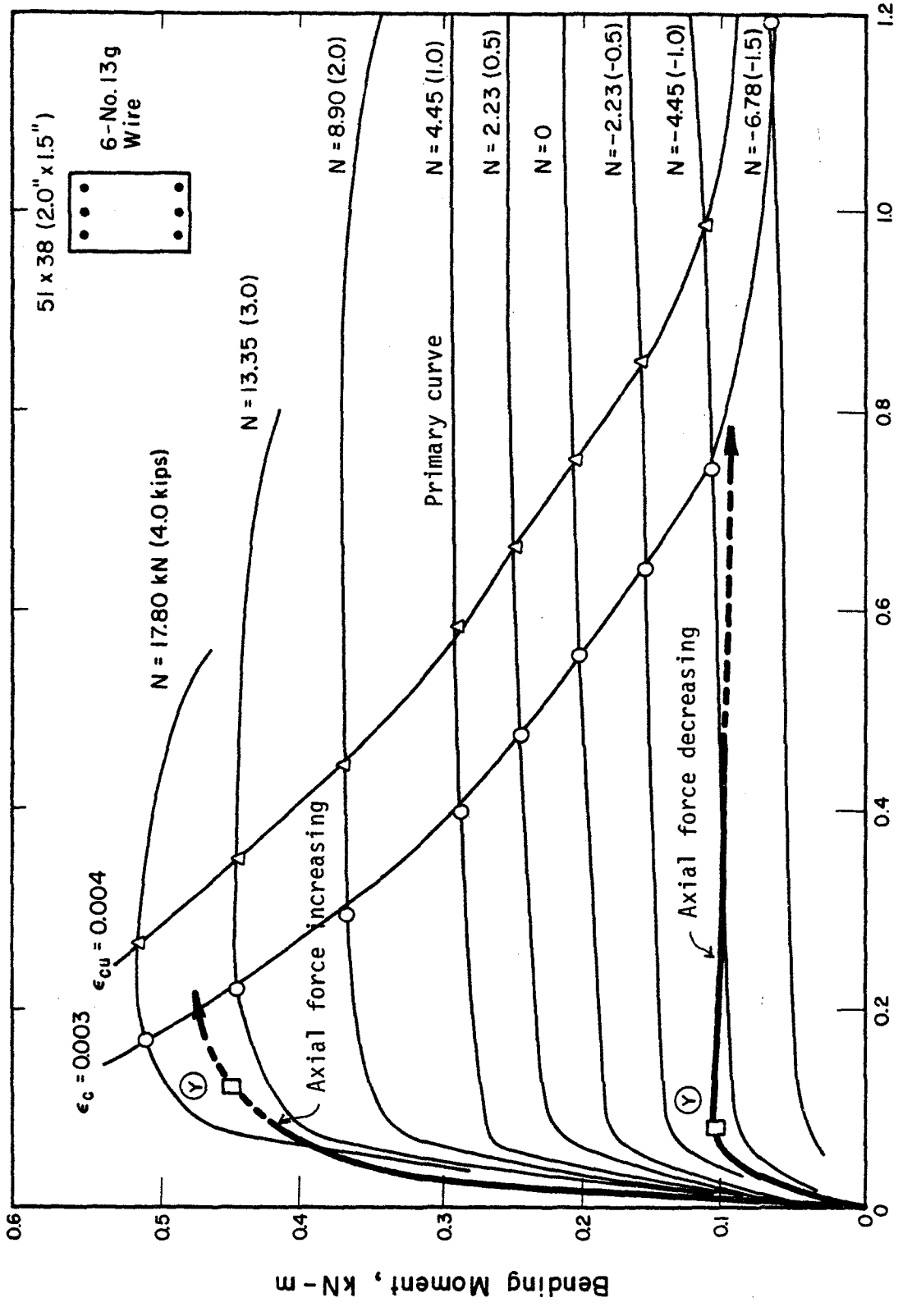

FIG. 6.24 MOMENT-CURVATURE RELATIONSHIPS OF THE LAYERED SECTION AT THE BASE OF THE COLUMNS

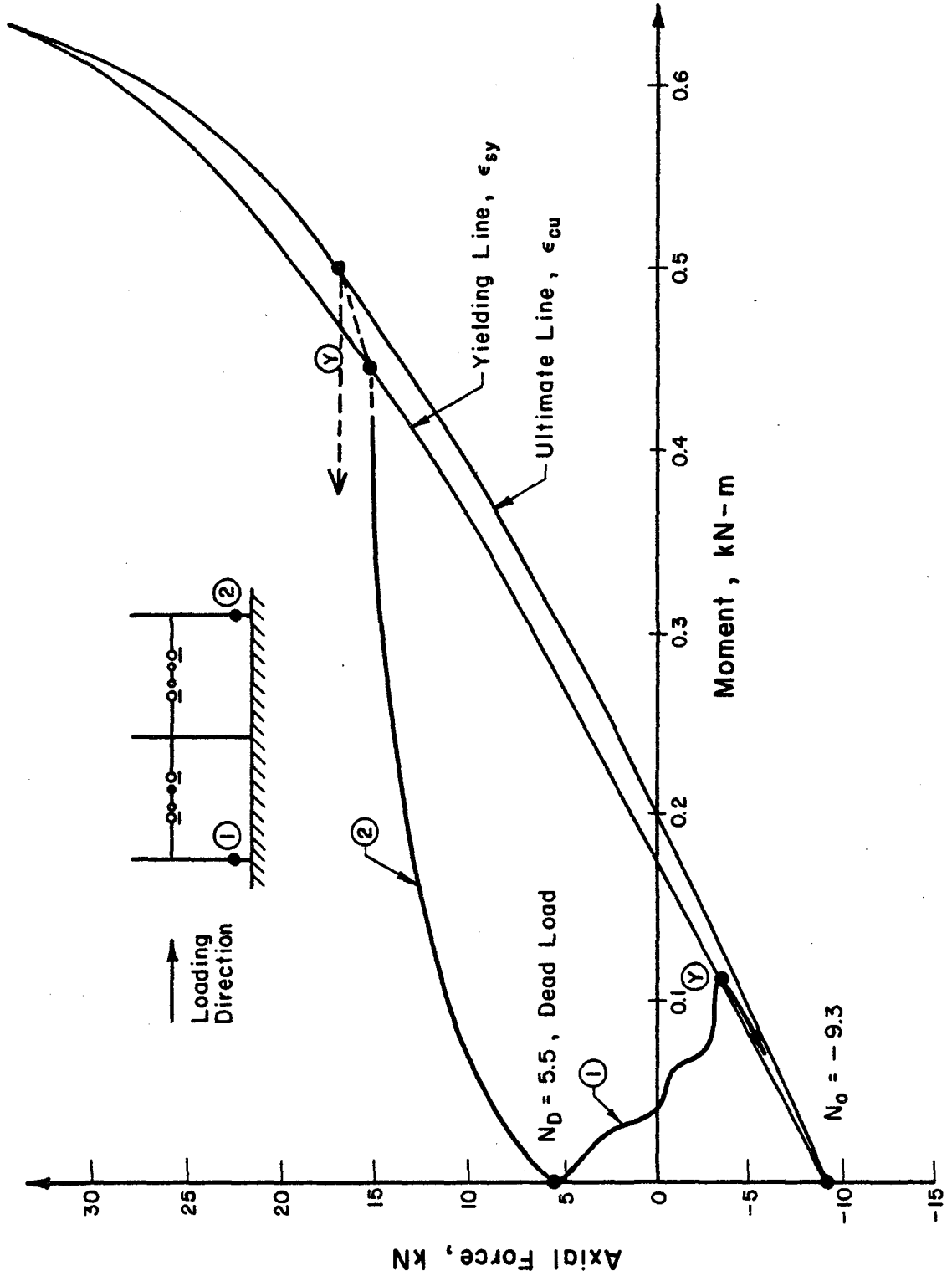

FIG. 6.25 LOADING PATH AT THE BASE OF THE EXTERIOR COLUMNS

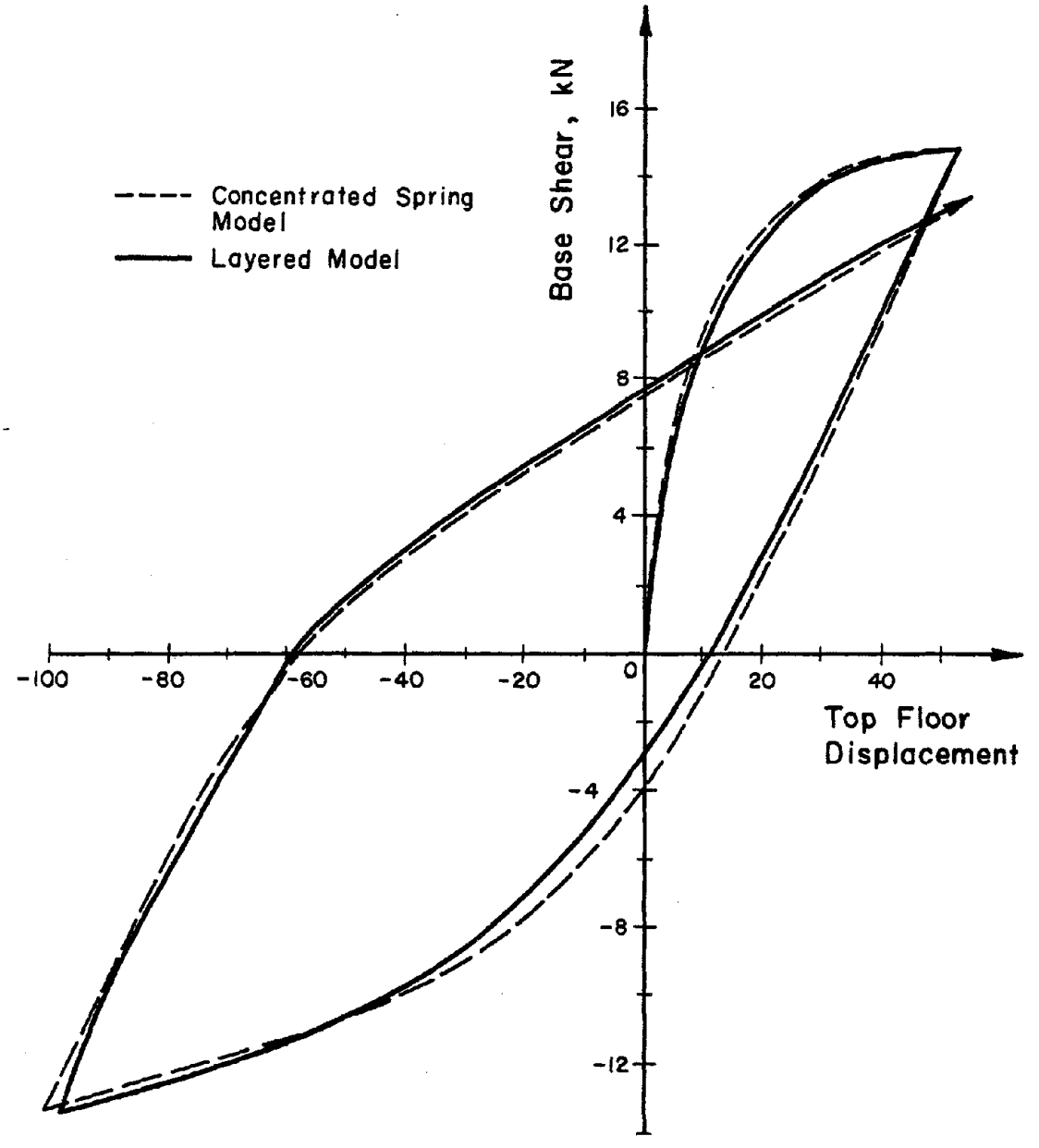

FIG. 6.26 BASE SHEAR VS. TOP-STORY DISPLACEMENT RELATIONSHIPS OF STRUCTURE FW-2 USING CONCENTRATED SPRING MODEL AND LAYERED MODEL FOR SINGLE CYCLE OF LOADING

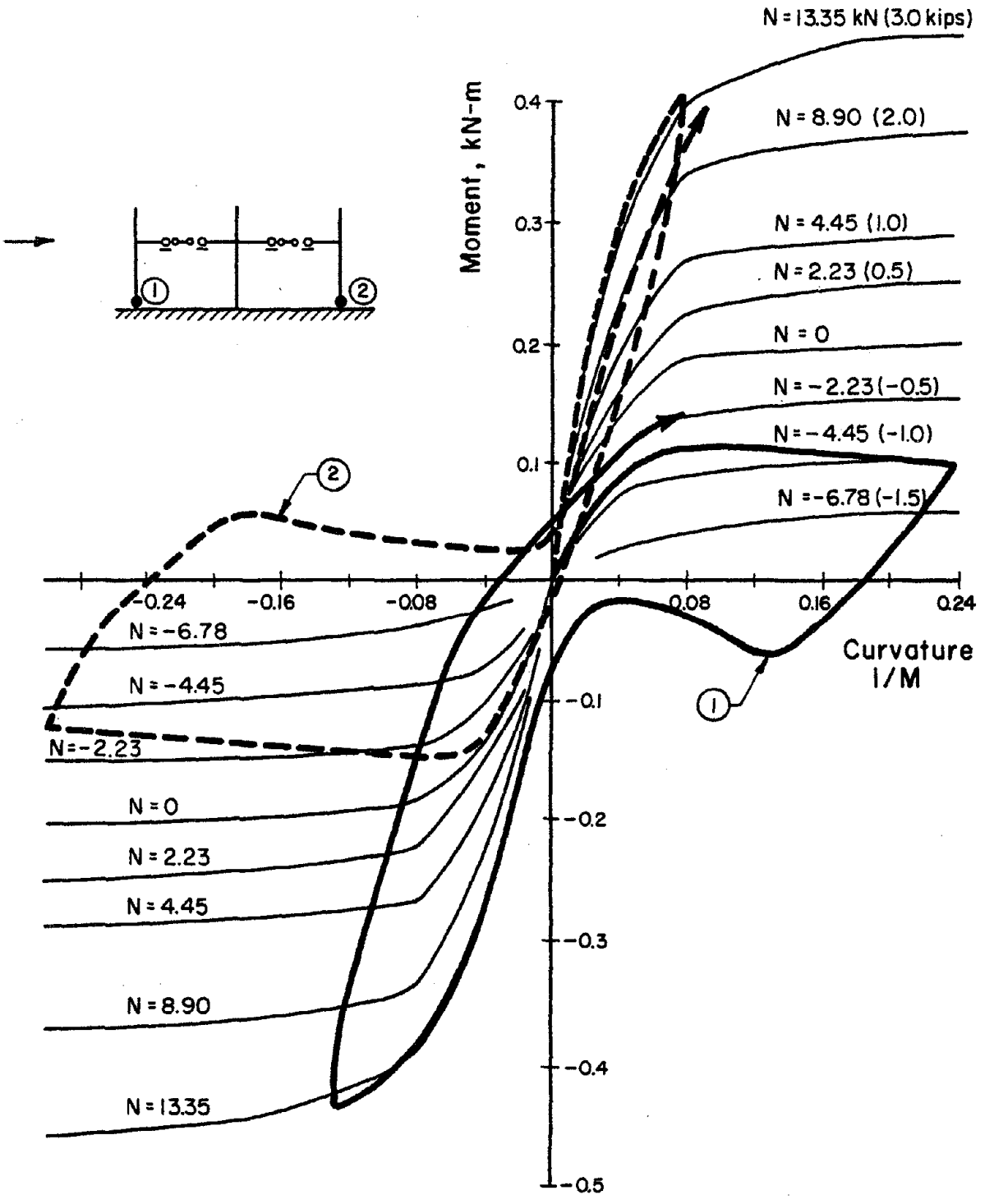

FIG. 6.27 MOMENT-CURVATURE RELATIONSHIPS OF THE LAYERED SECTION AT THE BASE OF THE COLUMNS FOR SINGLE CYCLE OF LOADING

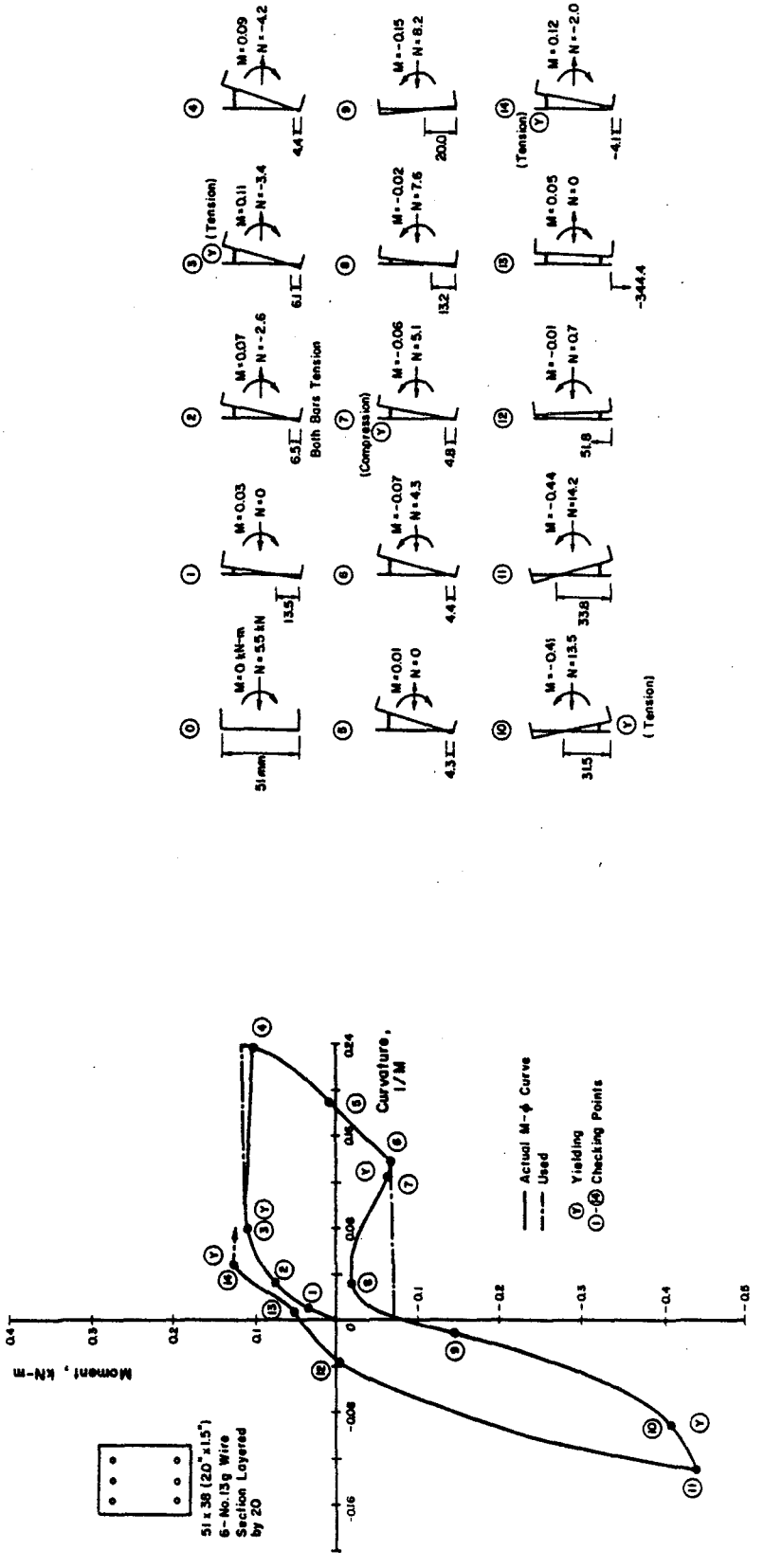

FIG. 6.28 BEHAVIOR OF THE LAYERED SECTION AT THE BASE OF THE COLUMNS FOR SINGLE CYCLE OF LOADING

APPENDIX A

DETAILS OF STIFFNESS MATRICES

A.1 Frame Member Stiffnesses

A.1.1 Local Coordinates

$$\begin{Bmatrix} M'_A \\ M'_B \\ N' \end{Bmatrix} = \begin{bmatrix} K_{11} & K_{12} & 0 \\ K_{21} & K_{22} & 0 \\ 0 & 0 & K_{33} \end{bmatrix} \begin{Bmatrix} \theta'_A \\ \theta'_B \\ \varepsilon' \end{Bmatrix}$$

A.1.2 Global Coordinates

$$\begin{Bmatrix} P_A \\ V_A \\ M_A \\ P_B \\ V_B \\ M_B \end{Bmatrix} = K_m \begin{Bmatrix} u_A \\ v_A \\ w_A \\ u_B \\ v_B \\ w_B \end{Bmatrix}$$

A.1.3 Column Members

$$K_m = K_{c_j} = \left[\begin{array}{ccc:ccc} {}_jC_1 & 0 & -{}_jC_2 & -{}_jC_1 & 0 & -{}_jC_4 \\ & {}_jC_0 & 0 & 0 & -{}_jC_0 & 0 \\ & & {}_jC_3 & {}_jC_2 & 0 & {}_jC_5 \\ \hdashline & & & {}_jC_1 & 0 & {}_jC_4 \\ & & & & {}_jC_0 & 0 \\ & & & & & {}_jC_6 \end{array}\right]$$

$$(j = 1, \sim 3)$$

where

$$\Sigma K = K_{11} + K_{12} + K_{21} + K_{22}$$

$$_jC_0 = K_{33}$$

$$_jC_1 = \frac{1}{\ell^2}\,\Sigma K$$

$$_jC_2 = \frac{1}{\ell}\,(K_{11} + K_{21}) + \frac{\lambda}{\ell}\,\Sigma K$$

$$_jC_3 = K_{11} + 2\lambda(K_{11} + K_{12}) + \lambda^2\Sigma K$$

$$_jC_4 = \frac{1}{\ell}\,(K_{12} + K_{22}) + \frac{\lambda}{\ell}\,\Sigma K$$

$$_jC_5 = K_{12} + \lambda\Sigma K + \lambda^2\Sigma K$$

$$_jC_6 = K_{22} + 2\lambda(K_{12} + K_{22}) + \lambda^2\Sigma K$$

A.1.4 Beam Members (Fixed-Hinged Members)

$$\begin{Bmatrix} V_A \\ M_A \end{Bmatrix} = K_m \begin{Bmatrix} v_A \\ w_A \end{Bmatrix}$$

$$K_m = K_{b_j} = \begin{bmatrix} {}_jb_1 & {}_jb_2 \\ {}_jb_2 & {}_jb_3 \end{bmatrix} \qquad \text{for } j = 1, 2$$

$$K_m = K_{b_3} = 2 \cdot \begin{Bmatrix} {}_3b_2 \\ {}_3b_3 \end{Bmatrix} \qquad \text{for } j = 3$$

$$v_A = 0$$

where

$$_jb_1 = K_{11}/\ell^2$$

$$_jb_2 = \frac{K_{11}}{\ell}\,(1 + \lambda)$$

$$_jb_3 = K_{11}(1 + \lambda)^2$$

A.2 Wall Member Stiffness

A.2.1 Local Coordinates

$$K_{bb} = F_{ab}^{-1} = \begin{bmatrix} K_1 & 0 & 0 \\ 0 & K_2 & K_3 \\ 0 & K_3 & K_4 \end{bmatrix}$$

A.2.2 Global Coordinates

$$K_m = K_w = \begin{bmatrix} W_1 & 0 & -W_2 & -W_1 & 0 & -W_4 \\ & W_0 & 0 & 0 & -W_0 & 0 \\ & & W_3 & W_2 & 0 & W_5 \\ & & & W_1 & 0 & W_4 \\ & \text{Sym.} & & & W_0 & 0 \\ & & & & & W_6 \end{bmatrix}$$

(W_0 is neglected in this study)

where

$W_0 = K_1$

$W_1 = K_2$

$W_2 = LK_2 - K_3$

$W_3 = K_2L^2 - 2K_3L + K_4$

$W_4 = K_3$

$W_5 = LK_3 - K_4$

$W_6 = K_4$

A.3 Connectivity Matrix, [A]

		Frame Vertical Displacement and Rotation										Wall Rotation		Story Horiz. Displ.	
		ith story					i-1th story					i	i-1	i	i-1
		$1^{v}A$	$1^{\theta}A$	$2^{v}A$	$2^{\theta}A$	$3^{\theta}A$	$1^{v}B$	$1^{\theta}B$	$2^{v}B$	$2^{\theta}B$	$3^{\theta}B$	$w^{\theta}A$	$w^{\theta}B$	u_A	u_B
K_{c_1}	P_A													1	
	V_A	1													
	M_A		1												
	P_B														1
	V_B								1						
	M_B									1					
K_{c_2}	P_A													1	
	V_A			1											
	M_A				1										
	P_B														1
	V_B								1						
	M_B									1					
K_{c_3}	P_A													1	
	M_A					1									
	P_B														1
	M_B										1				
K_{b_1}	V_A	1													
	M_A		1												
K_{b_2}	V_A			1											
	M_A				1										
K_{b_3}	M_A					1									
K_w	P_A													1	
	M_A											1			
	P_B														1
	M_B												1		

A.4 Story Stiffness Matrix, K_i

$$\begin{Bmatrix} {}^{1}V_A \\ {}^{1}M_A \\ {}^{2}V_A \\ {}^{2}M_A \\ {}^{3}M_A \\ \hline {}^{1}V_B \\ {}^{1}M_B \\ {}^{2}V_B \\ {}^{2}M_B \\ {}^{3}M_B \\ \hline {}^{w}M_A \\ {}^{w}M_B \\ \hline P_A \\ P_B \end{Bmatrix} = K_i \begin{Bmatrix} {}^{1}v_A \\ {}^{1}\theta_A \\ {}^{2}v_A \\ {}^{2}\theta_A \\ {}^{3}\theta_A \\ \hline {}^{1}v_B \\ {}^{1}\theta_B \\ {}^{2}v_B \\ {}^{2}\theta_B \\ {}^{3}\theta_B \\ \hline {}^{w}\theta_A \\ {}^{w}\theta_B \\ \hline u_A \\ u_B \end{Bmatrix}, \quad (i = 10 \sim 1)$$

(Fig. 4.5)

$$K_i = \left[\begin{array}{cc:cc:cc} {}_{i}S_1 & {}_{i}S_2 & 0 & 0 & -{}_{i}R_1 & {}_{i}R_1 \\ & {}_{i}S_3 & 0 & 0 & -{}_{i}R_2 & {}_{i}R_2 \\ \hdashline & & {}_{i}W_3 & {}_{i}W_5 & -{}_{i}W_2 & {}_{i}W_2 \\ & & & {}_{i}W_6 & -{}_{i}W_4 & {}_{i}W_4 \\ \hdashline & \text{Sym.} & & & {}_{i}T_1 & -{}_{i}T_1 \\ & & & & & {}_{i}T_1 \end{array}\right]$$

14 x 14

where

$$ {}_iS_1 = \begin{bmatrix} {}_1C_0 + {}_1b_1 & {}_1b_2 & 0 & 0 & 0 \\ & {}_1C_3 + {}_1b_3 & 0 & 0 & 0 \\ & & {}_2C_0 + {}_2b_1 & -{}_2b_2 & 0 \\ & & & {}_2C_3 + {}_2b_3 & 0 \\ \text{Sym.} & & & & {}_3C_3 + 2\cdot{}_3b_3 \end{bmatrix} $$

$$ {}_iS_2 = \begin{bmatrix} -{}_1C_0 & 0 & 0 & 0 & 0 \\ & {}_1C_5 & 0 & 0 & 0 \\ & & -{}_2C_0 & 0 & 0 \\ & & & {}_2C_5 & 0 \\ \text{Sym.} & & & & {}_3C_5 \end{bmatrix}, \quad {}_iS_3 = \begin{bmatrix} {}_1C_0 & 0 & 0 & 0 & 0 \\ & {}_1C_6 & 0 & 0 & 0 \\ & & {}_2C_0 & 0 & 0 \\ & & & {}_2C_6 & 0 \\ \text{Sym.} & & & & {}_3C_6 \end{bmatrix} $$

$$ {}_iR_1 = \begin{Bmatrix} 0 \\ {}_1C_2 \\ 0 \\ {}_2C_2 \\ {}_3C_2 \end{Bmatrix}, \quad {}_iR_2 = \begin{Bmatrix} 0 \\ {}_1C_4 \\ 0 \\ {}_2C_4 \\ {}_3C_4 \end{Bmatrix} $$

$$ {}_iT_1 = ({}_1C_1 + {}_2C_1 + {}_3C_1 + w_1) $$

$$ {}_iW_n = W_n $$

A.5 Structural Stiffness Matrix

A.5.1 General Expression

$$\begin{Bmatrix} F_F \\ F_w \\ F_H \end{Bmatrix} = \underset{70 \times 70}{\begin{bmatrix} A_1 & 0 & R_1 \\ 0 & A_2 & R_2 \\ R_1^T & R_2^T & E \end{bmatrix}} \begin{Bmatrix} D_F \\ D_w \\ D_H \end{Bmatrix}$$

where

$$\{F_F\} = \{{}_fF_i\} = \begin{Bmatrix} {}^1V_i \\ {}^1M_i \\ {}^2V_i \\ {}^2M_i \\ {}^3M_i \end{Bmatrix}, \quad \{D_F\} = \{{}_fD_i\} = \begin{Bmatrix} {}^1v_i \\ {}^1\theta_i \\ {}^2v_i \\ {}^2\theta_i \\ {}^3\theta_i \end{Bmatrix}$$

$$\{F_w\} = \{{}_wF_i\} = \{{}_wM_i\}$$

$$\{D_w\} = \{{}_wD_i\} = \{{}_w\theta_i\}$$

$$\{F_H\} = \{{}_hF_i\} = \{{}_hP_i\}$$

$$\{D_H\} = \{{}_hD_i\} = \{{}_hu_i\}$$

$$(i = 10 \sim 1)$$

A.5.2 $[A_1]$, (50 x 50)

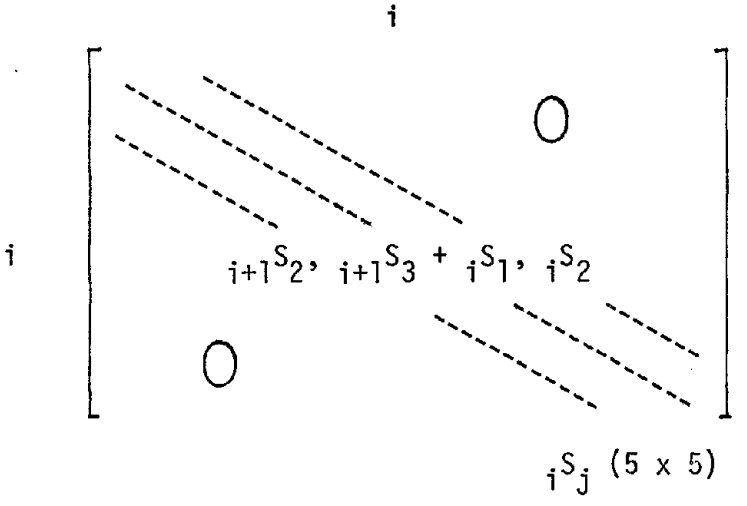

A.5.3 $[A_2]$, (10 x 10)

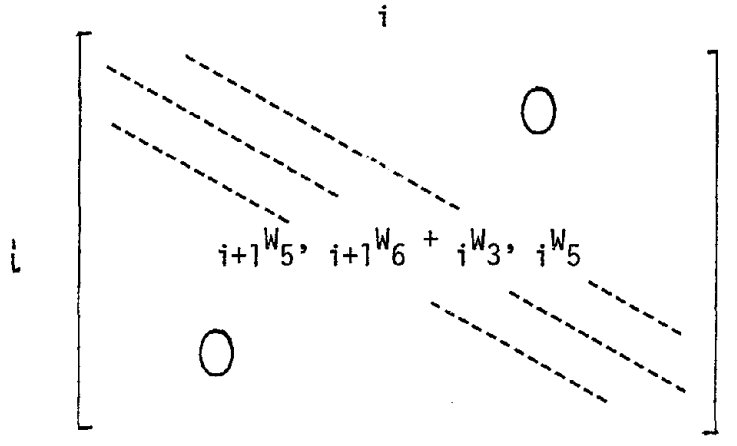

A.5.4 $[R_1]$, (50 x 10)

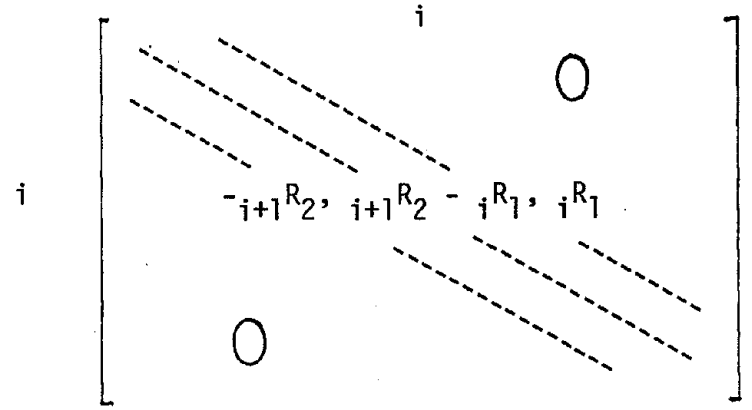

${}_iR_j = (5 \times 1)$

A.5.5 $[R_2]$, (10 x 10)

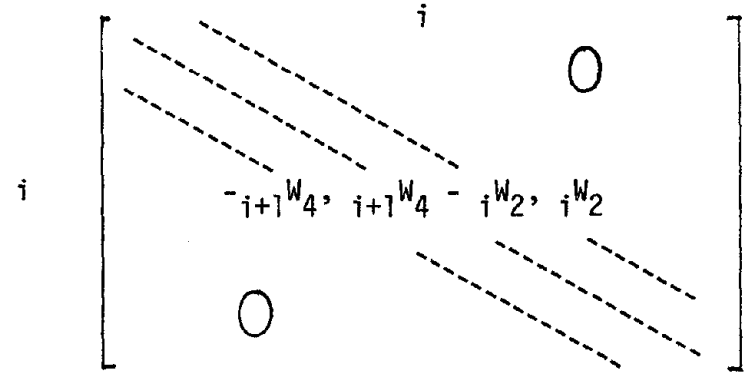

A.5.6 $[E]$, (10 x 10)

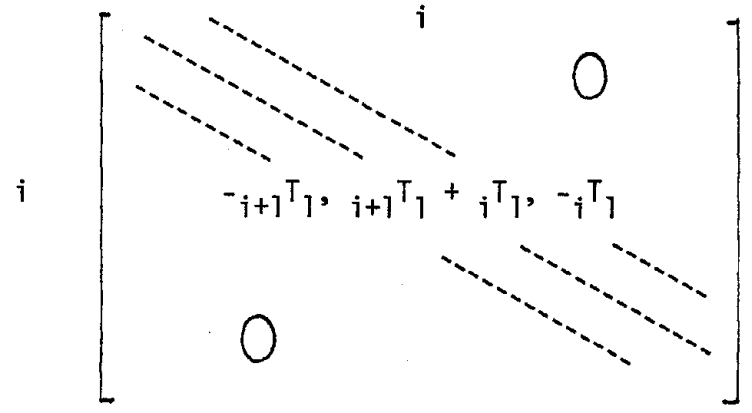

APPENDIX B

COMPUTER PROGRAM FOR NONLINEAR RESPONSE ANALYSIS OF REINFORCED CONCRETE FRAME-WALL STRUCTURES

The computer program is developed for nonlinear analysis of reinforced concrete frame-wall structures subjected to static and dynamic loadings.

The program can be used to obtain frequencies and mode shapes of the structure. Both elastic analysis and inelastic analysis of either static or dynamic loadings can be performed. The method of analysis is described in Chapter 4. The program is written in the FORTRAN IV computer language on the CYBER 175 computer furnished by the Digital Computer Laboratory of the University of Illinois. The size of the structure that can be analyzed can be increased by appropriate changes in the dimensioning statements. But at this stage, the program is applicable to structures in the form of 10-story regular rectangular plane frame-wall systems with an isolated shear wall. The total core space required for the program is approximately 111500B CM STORAGE in addition to temporary disk space in which calculated response values are stored. It took approximately 100 CP SECOND EXECUTION TIME on the CYBER 175 computer for the program to complete a response analysis of this 10-story structure subjected to 3.0 seconds of base motion at a 0.0004 second integration time interval (with calculating new stiffness of the structure at every ten times, 0.004 second).

The flow diagram of the computer program for nonlinear response analysis of reinforced concrete frame-wall systems is shown in Fig. B.1.

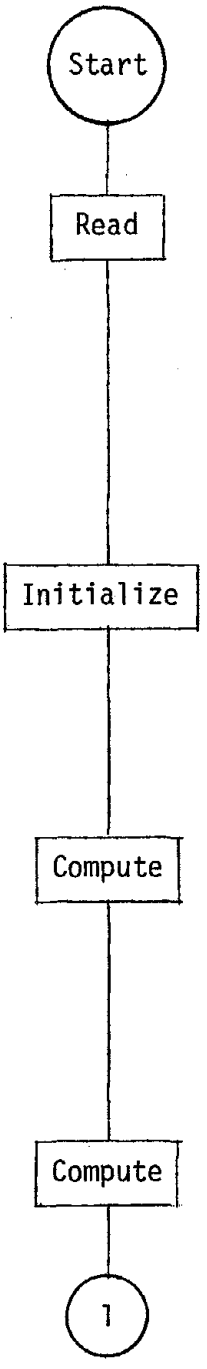

Material Properties
Structural Geometries
Stiffness Properties of Members
Coefficients of Hysteresis Rules

All Variables

Initial Member Stiffness Matrices, K_{bj}, K_{cj}, K_w
Initial Story Stiffness Matrices, K_i
Initial Structural Stiffness Matrix

Reduce Initial Structural Stiffness Matrix, K_H

FIG. B.1 FLOW DIAGRAM OF COMPUTER PROGRAM FOR NONLINEAR RESPONSE ANALYSIS OF REINFORCED CONCRETE FRAME-WALL SYSTEMS

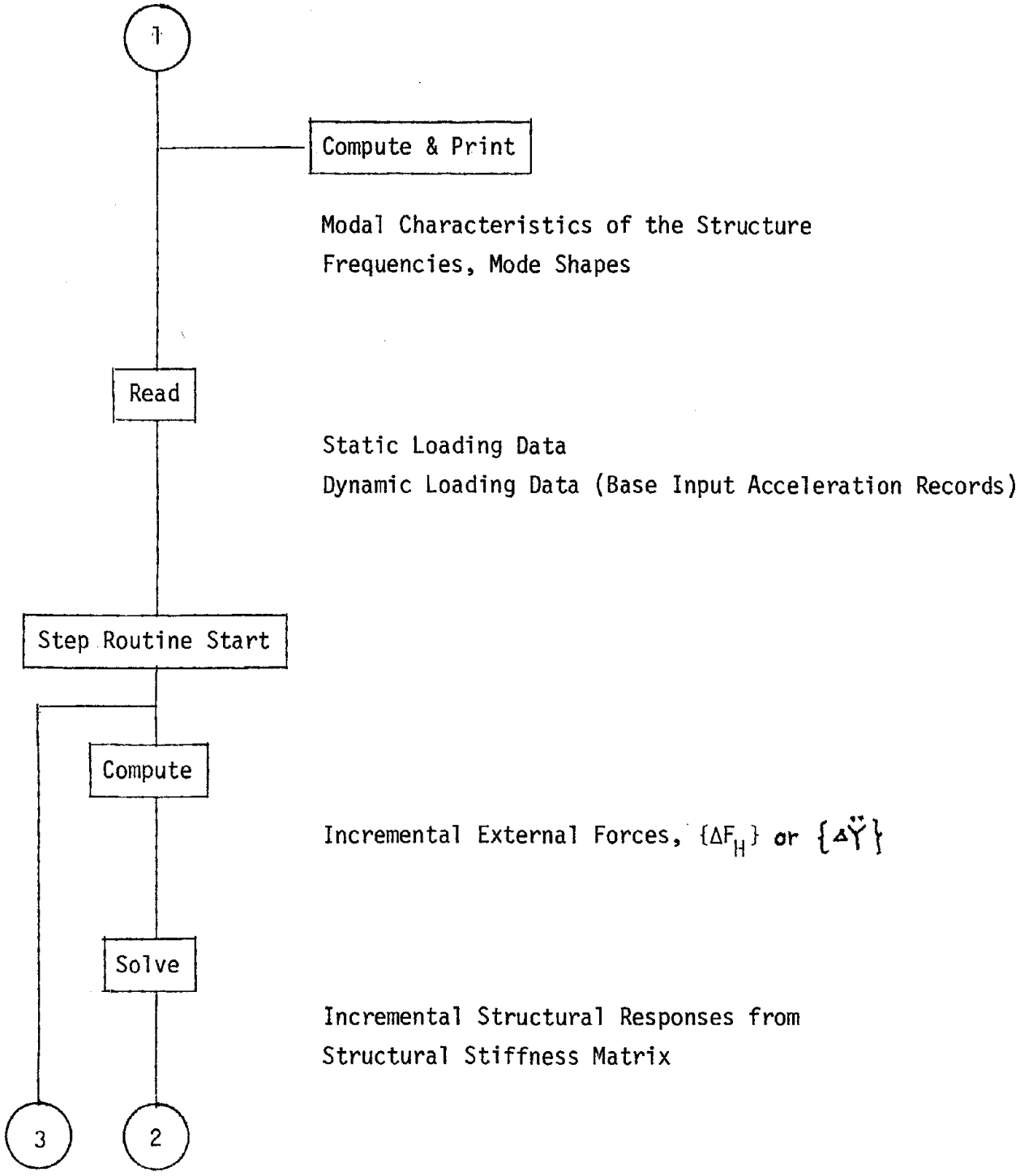

FIG. B.1 (continued)

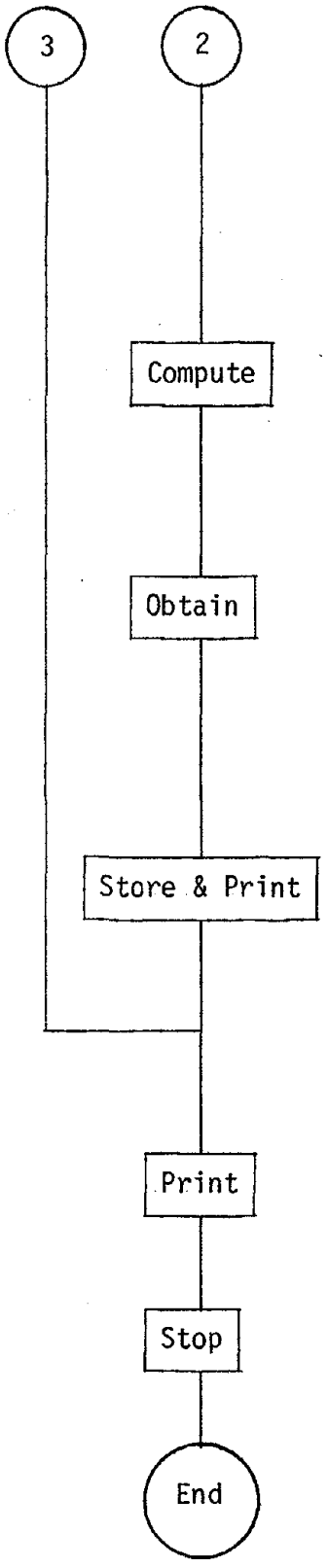

Static Case

$$\{\Delta D_H\} = |K_H|^{-1}\{\Delta F_H\}$$

Dynamic case (equations of motion)

$$\{\Delta X\} = [A]^{-1}\{B\}$$

Incremental and Total Member Forces
Incremental and Total Member Displacements

New Stiffnesses for Beam, Column and Wall Members
Based on Hysteresis Rules
New Reduced Structural Stiffness Matrix

In Disk

Structural Response Values
Member Forces and Member Displacements

Maximum and Minimum Structural
Response Values

FIG. B.1 (continued)

APPENDIX C

NOTATION

All symbols used in the text are defined when they are first introduced. For convenience, they have been listed below.

a = coefficient in the hysteresis model 2, or constant (=0.5) in the hysteresis rule

A = area of a cross section

$[A]$ = dynamic stiffness matrix, or connectivity matrix

A_s = area of tensile reinforcement

A'_s = area of compressive reinforcement

b = width of the cross section

$\{B\}$ = dynamic load matrix

c = depth of the neutral axis

c' = distance from the neutral axis to the point of the maximum tensile stress of concrete

C_1, C_2 = coefficients for damping matrix

$[C]$ = transformation matrix from local to global coordinates, or damping matrix, or instantaneous damping matrix which is evaluated at the end of previous step

C_c = concrete compression force

C'_s = steel compression force

C_p = distance from extreme compression fiber to the centroid of axial load

d = distance from extreme compressive fiber to the center of tensile reinforcement

d' = distance from extreme compressive fiber to the center of compressive reinforcement

D = total depth of a section, or diameter of a reinforcing bar, or displacement variable in the hysteresis moel 2

D_c = cracking displacement of the unit length of a cantilever beam

D_m = maximam deflection attained in the direction of loading in the hysteresis rule

D_o = displacement value on the x coordinate which is obtained by using the slope K_u in the hysteresis model 2

D_y = yielding deflection in the hysteresis rule

$\{D_F\}$, $\{D_W\}$ = displacement vector (except of holizontal displacement) of frame term, wall term in the structural stiffness matrix, respectively

$\{D_H\}$ = horizontal displacement vector

$D(M)$ = free end displacement of a cantilever beam

E_{ij} = transformation matrix of an element ij of the multiple spring model

E_s = modulus of elasticity of steel

E_{sh} = modulus to define stiffness in strain hardening range of steel

E_y = inelastic modulus of reinforcement after yielding

EA = axial rigidity of a section

EI = initial flexural rigidity

EI_1, EI_2, EI_3 = flexural rigidity of before cracking, from cracking to yielding, and after yielding ,respectively

EI_i = instantaneous flexural rigidity of a layered section

EI_y = ratio of flexural rigidity after yielding to before yielding

f_c = stress of concrete

f'_c = compressive uniaxial strength of concrete

f_L = instantaneous rotational flexibility

f_{en} = concrete stress at which concrete strain is ε_e

f_t = tensile strength of concrete

f_s = stress of steel, or stress of tensile reinforcement

f'_s = stress of compressive reinforcement

f_y = yield stress of steel

f_u = ultimate stress of steel

$f(M)$ = rotational flexibility resulting from bond slip, inelastic action over the beam length ℓ

$f_b(M)$ = flexibility due to bond slippage

$[f]$ = flexibility matrix of a cantilever beam

$[F_{ab}]$ = flexibility matrix of a cantilever beam ab

$[F_{ij}]$ = flexibility matrix of an element ij of the multiple spring model

$[F_M]$ = horizontal force vector of a structure

$[F_F]$, $[F_w]$ = force vector of frame term, wall term, respectively

$[F]$ = instantaneous flexibility matrix

GA = elastic shear rigidity of a section

GA_i = shear rigidity of i element

I_g = moment of inertia of a gross section

K_o = primary slope of system in the hysteresis rule

K_u = new unloading slope in the hysteresis rule

K_m = member stiffness matrix in global coordinates

K_{cj}, K_{bj}, K_w = column, beam, and wall member stiffness matrices, respectively

$[K_H]$ = reduced structural stiffness matrix of size, number of stories by number of stories

K_i = story stiffness matrix

ℓ = length of a flexible element in a simple beam

ℓ_k = length of subelement k of the multiple spring model

L = length of a beam, or development length of bond stress, or length of a cantilever beam

ΔL = elongation of reinforcing steel

L_p = length of the inelastic zone of the layered model

m_i = lumped mass at the story i

$m(\phi_i, N_i)$ = bending moment function in the layered model

M = bending moment, or moment variable in the hysteresis model 2

M_c, M_y, M_u = cracking, yielding, and ultimate moment(moment at concrete strain equal to 0.004), respectively

ΔM_A = incremental moment at the fixed end of a cantilever beam

$\Delta M'_A, \Delta M'_B$ = incremental moments at the ends of a flexible line element of a simple beam

$\Delta M_A, \Delta M_B$ = incremental end moments of a member, or incremental joint moments in global coordinates

$[M]$ = diagonal mass matrix

n = number of story

N = axial load acting on a section

ΔN = incremental axial force

$\{\Delta P_b\}$, $\{P_b\}$ = incremental applied force vector, applied force vector at the tip of a cantilever beam, respectively

ΔP_A, ΔP_B = incremental horizontal forces in global coordinates

$R(M)$ = rotation due to reinforcements slip at the fixed end of a cantilever beam at which moment of M is developed

SD_i = instantaneous stiffness of the concentrated spring model of unit length

T = steel tension force, or transformation matrix

T_i = i-th period of a structure

Δt = time interval

u = average bond stress

Δu_A, Δu_B = incremental lateral displacement in global coordinates

$\{\Delta U_b\}$, $\{U_b\}$ = incremental displacement vector, displacement vector at the tip of a cantilever beam, respectively

ΔV_A, ΔV_B = incremental vertical forces in global coordinates

Δv_A, Δv_B = incremental vertical displacement in global coordinates

Δw_A, Δw_B, $\Delta\theta_A$, $\Delta\theta_B$ = incremental joint rotation in global coordinates

$\{\dot{x}\}$, $\{\ddot{x}\}$ = relative story velocity and acceleration vector at the end of previous step, respectively

$\{\Delta x\}$, $\{\Delta\dot{x}\}$, $\{\Delta\ddot{x}\}$ = relative incremental story displacement, volocity, and acceleration vector, respectively

$\{\Delta\ddot{Y}\}$ = incremental base acceleration vector

y_t = distance from neutral axis of a section to extreme fiber in tension

Z = constant which defines the descending slope of the stress-strain curve of concrete

α = reduction facter for shear rigidity (=0.5)

β = constant of the Newmark β method

λC = distance from extreme compression fiber to centroid of concrete compression force

ε = axial strain of a section

$\Delta\varepsilon$ = incremental axial strain

ε_c = strain of concrete

ε_{cu} = concrete strain of 0.004

ε_e = concrete strain on the envelope curve

ε_n = concrete plastic strain

$\varepsilon_o, \varepsilon_t, \varepsilon_y, \varepsilon_u$ = concrete strain at which f'_c, f_t, f_y, and f_u are attained, respectively

ε_{sh} = steel strain at which strain hardening of steel commences

ε_s = steel strain or tensile steel strain

ε'_s = compressive steel strain

θ, $\Delta\theta$ = rotation, incremental rotation of a cantilever beam, respectively

$\Delta\theta'_A, \Delta\theta'_B, \Delta\theta_A, \Delta\theta_B$ = incremental rotations at the ends of a flexible line element, at the supported joints of a simple beam, respectively

$\{\Delta\theta\}$ = incremental joint rotation vector

λ = ratio of the length of a rigid portion to that of a flexible element for a simple beam

λ_k = damping factor of the k-th mode

ϕ = curvature

ϕ_c, ϕ_y, ϕ_u = curvature at cracking, yielding, and ultimate, respectively

ϕ_i = incremental curvature

w_k = circular frequency of the k-th mode